Astrocytic modulation of neuronal network oscillations

Alba Bellot-Saez

Western Sydney University, School of Medicine

The MARCS Institute for Brain, Behaviour and Development

Biomedical Engineering and Neuromorphic Systems Research Program

A thesis submitted in fulfilment of the requirements for the degree of

Doctor of Philosophy

2019

Supervisor: Dr. Yossi Buskila

Co-supervisors: Dr. Morven A. Cameron and Professor John W. Morley

Dedicated to my family,
for their never-ending support.

Statement of Authentication

The work presented in this thesis is, to the best of my knowledge and belief, original except as acknowledged in the text. I hereby declare that I have not submitted this material, either in full or in part, for a degree at this or any other institution.

Alba Bellot-Saez

June 2019

Acknowledgments

I wish to express my honest gratitude to my mentor and primary supervisor, Dr. Yossi Buskila, who has opened my mind to the understanding of the real significance of the role of astrocytes within brain networks. I truly appreciate the time dedicated in reading my long emails, as well as the constant guidance provided throughout my candidature. I am also grateful to my co-supervisors, Dr. Morven A. Cameron and Professor John W. Morley for their moral support and advice anytime I needed. I want to thank Ashleigh Deschamps and Nikola Mills for their always cheerful work in the Animal Facility. A huge THANK YOU to all the members from the e-phys lab, including Sindy Kueh, Orsola Kékesi, Check Ying Tan, Victor Pérez Fernández and Winston Seah, for their help and support during our "Electrophysiology and Cheese" meetings and, most importantly, for their unconditional friendship that will last long beyond the end of this thesis.

I also extend my deepest gratitude to all my colleagues from the BENS group and the MARCS Institute, namely professor André van Schaik, associate professor Paul Breen and Dr. Gaetano Gargiulo, for their fruitful discussions and their applied engineering skills in building both the Braincubator™ (PaYo Scientific PTY LTD) and the differential amplifier used in my thesis experiments. Special thanks to Ram K. Singh and Dr. Gregory Cohen for their patience and dedication provided anytime I had troubles in programming with MATLAB (MathWorks).

Personally, I could not have completed this work without the support of my partner and roomie, Victor Pérez Fernández, which I deeply thank for anything in particular and for everything that really matters in life, including all the frustrating but passionate hours spent with Illustrator and Photoshop. Last but not least, I could not be grateful enough for all the courage and the tireless support my beloved friends and family members provided me all the way through (more than 15.000 km apart) until the end of the Ph.D. candidature completion.

Table of Contents

List of tables

List of figures

CHAPTER 1: General introduction

CHAPTER 2: Astrocytic modulation of cortical oscillations

CHAPTER 3: Quantitative determination and detection of extracellular K^+ alterations

CHAPTER 4: Neuromodulation of astrocytic K^+ clearance

APPENDIX: Figures

List of abbreviations

5-HT	5-Hidroxytryptamine, serotonin
ABP	actin-binding protein
AC	adenylyl cyclase
ACh	acetylcholine
aCSF	artificial cerebrospinal fluid
AD	Alzheimer's Disease
ALS	amyotrophic lateral sclerosis
AMPA	α-amino-3-hydroxy-5-methyl-4-isoxazolepropionic acid
APG	asante potassium green
AQP-4	aquaporin 4
ATP	adenosine triphosphate
Ba^{2+}	barium
$BaCl_2$	barium chloride
BDNF	brain-derived neurotrophic factor
BOLD	blood oxygen level-dependent
Ca^{2+}	calcium
$[Ca^{2+}]_i$	intracellular calcium concentration
cAMP	3',5'-cyclic adenosine monophosphate
CCD	charge-coupled device
CICR	calcium-induced-calcium-release
CNS	central nervous system
CP	cortical plate

CREB	cAMP response element-binding
Cx	connexin
DA	dopamine
DAG	D-1,2-Diacilglicerol
DB-1	double-barrelled K^+-selective microelectrodes with small tips of ~1 µm
DB-3	double-barrelled K^+-selective microelectrodes with big tips of ~3 µm
DIC	differential interference contrast
DMDCS	dimethyldichlorosilane
EEG	electroencephalography
EGTA	ethylene glycol-bis(β-aminoethyl ether)-N,N,N′,N′-tetraacetic acid
EPSPs	excitatory postsynaptic potentials
ER	endoplasmic reticulum
fMRI	functional magnetic resonance imaging
f_R	resonance frequency
FRET	Förster resonance energy transfer
FWHA	full width at half amplitude
GABA	gamma-aminobutyric acid
GFAP	glial fibrillary acidic protein
GFP	green fluorescent protein
GJ	gap junction
GLT-1	glutamate transporter 1
GNR	glia to neuron ratio
GPCR	G protein-coupled receptor

GTP	guanosine-5'-triphosphate
HCN	hyperpolarization-activated cyclic nucleotide-gated channel
HD	Huntington's Disease
HEPES	4-(2- hydroxyethyl)-1-piperazineethanesulfonic acid
HMDS	hexamethyldisilazane
Hz	hertz
$\boldsymbol{I_h}$	hyperpolarization-activated inward current
$\mathbf{IP_3}$	inositol 1,4,5-triphosphate
IPG	ion potassium green
IPSPs	inhibitory postsynaptic potentials
IZ	intermediate zone
$\mathbf{K^+}$	potassium
$\mathbf{[K^+]_o}$	extracellular potassium concentration
$\mathbf{[K^+]_i}$	intracellular potassium concentration
KCl	potassium chloride
$\mathbf{K_{ir}}$	inward rectifying potassium channel
KO	knock-out
LFP	local field potential
M1	primary motor cortex
MEG	magnetoencephalography
$\mathbf{Mg^{2+}}$	magnesium
mGluRs	metabotropic glutamate receptors
MS	multiple sclerosis

MSI	magnetic source imaging
MUA	multi-unit activity
MZ	marginal zone
Na^+	sodium
NA	numerical aperture
NCX	Na^+/Ca^{2+} exchanger
NE	noradrenaline
NG2	neural/glial antigen 2
NKA	Na^+-K^+ ATPase pump
NKCC	Na^+-K^+-$2Cl^-$ cotransporter
NMDA	N-methyl-D-aspartate receptor
NREM	non-rapid eye movement
OCT3	organic cation transporter 3
OPCs	oligodendrocyte progenitor cells
PBFI	potassium-binding benzofuran isophthalate
PIP_2	phosphatidylinositol 4,5-biphosphate
PKA	protein kinase A
PKC	protein kinase C
PLA_2	phospholipase A_2
PLC	phospholipase C
PSD	power spectrum density
REM	rapid eye movement
RGCs	radial glial cells

R_{in}	input resistance
RMP	resting membrane potential
ROI	region of interest
rTMS	repetitive transcranial magnetic stimulation
S1	primary somatosensory cortex
SB	single-barrelled K^+-selective microelectrode
SR101	sulforhodamine 101
SSRI	selective serotonin reuptake inhibitor
SVZ	subventricular zone
SWHA	spike width at half amplitude
SWS	slow wave sleep
τ	membrane time constant
tACS	transcranial alternating current stimulation
TMCS	trimethylchlorosilane
TMSDMA	dimethyltrimethylsilylamine
TTX	tetrodoxin
UV	ultraviolet
VGCCs	voltage-gated calcium channels
V_k	Nernst potential for potassium
V_m	equilibrium membrane potential
VSDI	voltage-sensitive dye imaging
VZ	ventricular zone
ZAP	impedance amplitude profile

Publications

The following publications have arisen from the work conducted in this thesis.

Publications contained in the thesis:

1. Bellot-Saez A, Kékesi O, Morley JW, Buskila Y. Astrocytic modulation of neuronal excitability through K^+ spatial buffering. Neurosci. Biobehav. Rev. 77:87-97, 2017.
2. Bellot-Saez A, Cohen G, van Schaik A, Ooi L, Morley JW, Buskila Y. Astrocytic modulation of cortical oscillations. Sci. Rep. 8(1): 11565, 2018.
3. Bellot-Saez A, Morley JW, Buskila Y. Neuromodulation of astrocytic K^+ clearance. Under preparation, 2019.

Other published manuscripts:

4. Cameron MA, Kékesi O, Morley JW, Bellot-Saez A, Kueh S, Breen P, van Schaik A, Tapson J, Buskila Y. Prolonged incubation of acute neuronal tissue for electrophysiology and calcium-imaging. J. Vis. Exp. (120): 1-6, 2017.
5. Buskila Y, Kékesi O, Bellot-Saez A, Seah W, Berg T, Trpceski M, Yerbury JJ, Ooi L. Dynamic interplay between H-current and M-current mediates motoneurons hyperexcitability in amyotrophic lateral sclerosis. Cell. Death. Dis. 10(4): 310, 2019.

Abstract

The synchronization of the neuron's membrane potential results in the emergence of neuronal oscillations at multiple frequencies that serve distinct physiological functions (e.g. facilitation of synaptic plasticity) and correlate with different behavioural states (e.g. sleep, wakefulness, attention). It has been postulated that at least ten distinct mechanisms are required to cover the large frequency range of neuronal oscillations in the cortex, including variations in the concentration of extracellular neurotransmitters and ions, as well as changes in cellular excitability. However, the mechanism that gears the transition between different oscillatory frequencies is still unknown. Over the past decade, astrocytes have been the focus of much research, mainly due to (1) their close association with synapses forming what is known today as the "tripartite synapse", which allows them to bidirectionally interact with neurons and modulate synaptic transmission; (2) their syncytium-like activity, as they are electrically coupled via gap junctions and actively communicate through Ca^{2+} waves; and (3) their ability to regulate neuronal excitability via glutamate uptake and tight control of the extracellular K^+ levels via a process termed K^+ clearance.

In this thesis we hypothesized that astrocytes, in addition to their role as modulators of neuronal excitability, also act as "network managers" that can modulate the overall network oscillatory activity within their spatial domain. To do so, it is proposed that astrocytes fine-tune their K^+ clearance capabilities to affect neuronal intrinsic excitability properties and synchronization with other neurons, thus mediating the **transitions** between neuronal network oscillations at different frequencies. To validate or reject this hypothesis I have investigated the potential role of astrocytes in modulating cortical oscillations at both cellular and network levels, aiming at answering three main research questions:

a) what is the impact of alterations in astrocytic K^+ clearance mechanisms on cortical networks oscillatory dynamics? b) what specific neuronal properties underlying the generation of neuronal oscillations are affected as a result of impairments in the astrocytic K^+ clearance process? and c) what are the bidirectional mechanisms between neurons and astrocytes (i.e. neuromodulators) that specifically affect the K^+ clearance process to modulate the network activity output?

In the first experimental chapter I used electrophysiological recordings and pharmacological manipulations to dissect the contribution of the different astrocytic K^+ clearance mechanisms to the modulation of neuronal network oscillations at multiple frequencies. A key finding was that alterations in membrane properties of layer V pyramidal neurons strongly correlated with the network behaviour following impairments in astrocytic K^+ clearance capabilities, depicted as enhanced excitability underlying the amplification of high-frequency oscillations, especially within the beta and gamma range. The second experimental chapter describes a combinatorial approach based on K^+-selective microelectrode recordings and optical imaging of K^+ ions used to quantitatively determine extracellular K^+ changes and to follow the spatiotemporal distribution of K^+ ions under both physiological and altered K^+ clearance conditions, which affected the K^+ clearance rate. The impact of different neuromodulators on astrocytic function is discussed in the third experimental chapter. Using extracellular K^+ recordings and Ca^{2+} imaging I found that some neuromodulators act specifically on astrocytic receptors to affect both K^+ clearance mechanisms and Ca^{2+} signalling, as evidenced by reduced K^+ clearance rates and altered evoked Ca^{2+} signals.

Overall, this thesis provides new insights regarding the impact of astrocytic K^+ clearance mechanisms on modulating neuronal properties at both cellular and network levels, which in turn imposes alterations on neuronal oscillations that are associated with different behavioural states.

CHAPTER 1:

GENERAL INTRODUCTION

"Like the entomologist hunting for brightly coloured butterflies, my attention was drawn to the flower garden of the grey matter, which contained cells with delicate and elegant forms, the mysterious butterflies of the soul, the beating of whose wings may someday (who knows?) clarify the secret of mental life."

—Santiago Ramón y Cajal

1.1 Neuronal oscillations

In the central nervous system (CNS), neurons communicate via electrochemical signals (i.e. action potentials), which leads to the flow of ionic currents through synaptic contacts[1]. At the network level, the synchronization of the neuron's electrical activity gives rise to rhythmic voltage fluctuations travelling across brain regions, known as neuronal oscillations or brain waves[2]. Neuronal oscillations can be modulated in space and time and are affected by the dynamic interplay between neuronal connectivity patterns, as well as intrinsic circuit and cellular membrane properties (e.g. physical architecture, axonal speed conduction, synaptic delays)[3,4,5]. At the cellular level, these synchronous oscillations fluctuate between two main states, known as "Up states" and "Down states", which occur in the neocortex both *in vitro* and *in vivo*[3]. Whereas Down states refer to resting activity and membrane hyperpolarization, Up states are associated with neuronal depolarization and firing of bursts of action potentials[6].

Importantly, Up states occurring within spatially organized cortical ensembles have been postulated to interact with each other to produce a temporal window for neuronal network communication and coordination[7]. This network coherence is essential for several sensory and motor processes, as well as for cognitive flexibility (i.e. attention, memory)[8,9], thereby playing a fundamental role in the brain's basic functions.

1.1.1 Significance of neuronal oscillations to brain function

Emerging technologies during the past decades led to the description of multiple neuronal oscillations displaying different electrophysiological and connectivity properties across brain areas (e.g. neocortex, thalamus, hippocampus)[10]. Using power spectrum analysis, investigators identified that neuronal oscillations fluctuate within specific frequency bands, ranging from very slow (<0.01 hertz, Hz) to ultra-fast (>1,000 Hz) oscillations, mediated by at least ten different mechanisms[11]. Whereas fast oscillators are more localized within a restricted neural volume[12], slow oscillations typically involve large synchronous membrane voltage fluctuations in wider brain areas[13]. Furthermore, these network dynamics and connectivity patterns change according to behaviour, with some frequency bands being associated with sleep, while other frequencies predominate during arousal or conscious states[14,15,16] (Table 1.1).

In addition, the fact that neuronal oscillations and their behavioural correlates are preserved throughout evolution (e.g. human, macaque, cat, rabbit, rat)[17,18,19,20,21] suggests that they exert relevant physiological roles, potentially by means of mediating synchronization across neuronal ensembles to efficiently coordinate and propagate synaptic information at the network level. Hence, oscillatory frequency bands represent groups of neuronal oscillations acting as individual entities that act similarly during particular brain fucntions[22].

	Delta - δ	Theta - θ	Alpha - α	Beta - β	Gamma- γ
Frequency:	1-4 Hz	4-10 Hz	8-12 Hz	12-30 Hz	>30 Hz
EEG traces:	 23	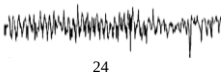 24	 25	 26	 27
Brain area:	Neocortex, Thalamus, Basal ganglia[28,29]	Hippocampus, Dentate gyrus, Entorhinal cortex, Cingulate cortex, Amygdala[30,31,32,33,34]	Neocortex, Thalamus[35,36,37]	Neocortex, Olfactory bulb, Striatum, Dentate gyrus, Thalamus, Hippocampus [26,38,39,40]	Neocortex, Olfactory bulb, Hippocampus[41,42, 43]
Rhythm generators:	1) Interplay between the low threshold Ca^{2+} transient current (I_t) and the hyperpolarization activated cation current (I_h) in thalamocortical neurons[44,45] 2) NMDAR-driven networks of intrinsically bursting cortical neurons in response to depolarization[46,47,48] 3) Increase in K^+ conductance leading to hyperpolarization[49] 4) Neuron-glia interactions to regulate extracellular K^+ through Ca^{2+} waves[50,51 ,52]	1) Interplay between somatic IPSPs (GABAergic neurons in the medial septum) and dendritic EPSPs (performant path) from CA1 pyramidal neurons[31,53,54] 2) ACh-mediated modulation of glutamate release from CA3 collaterals[55] 3) Amplification of membrane resonance and subthreshold oscillations by slow inward K^+ currents in cerebellar granule cells or dendritic Ca^{2+} spikes following activation of NMDAR on CA1 pyramidal neurons[31,56,57] 4) ACh-induced Ca^{2+} release from internal stores (IP_3) in astrocytes[58]	1) Ca^{2+} T-channel-mediated tuning of local cortical networks via GABAergic inhibition of thalamic transmission[59,60] 2) Thalamic gap junction-mediated synchronization of local high-threshold bursting neurons in the lateral geniculate nucleus[19,61] 3) Corticotropin releasing hormone-binding protein-mediated activation of locus coeruleus neuronal firing properties that influence thalamic neurons[62,63,64]	1) Glutamatergic excitation, gap junction-mediated communication between layer V intrinsically bursting cell compartments and M-type K^+ current in the association cortex[65] 2) ACh-mediated modulation and synaptic interactions between layer V pyramidal neurons and low-threshold spiking interneurons in the primary auditory cortex[66] 3) Thalamic or cortical projections in extrastriate area V4 independent of bottom-up V1 drive[67]	1) Excitation of interneural networks via NMDAR and IPSPs kinetics in CA1[68] and ACh-mediated modulation via non-NMDAR in CA3[69] 2) Modulation via gap junctions in cortical layer II/III or via glutamatergic excitation in layer IV[70] 3) Elevations in astrocytic cytosolic Ca^{2+} levels leading to glutamate release[71] 4) AMPAR, $GABA_AR$ and gap junction-related modulation following elevations in extracellular K^+ leading to neurotransmitter release[72,73,74]
Brain functions:	a) Slow wave sleep[75] and deep NREM sleep[76] b) Signal detection and decision making[77,78] c) Memory consolidation[76,79] d) Concentration, motivation and focused attention[80,81,82] e) Facilitation of interlaminar interactions in the cortex to control synaptic rescaling[48]	a) REM sleep[58,83] b) Selective attention, arousal, orienting and voluntary control of movement[77,84,85] c) Modulation of synaptic strength and coordination of phase coding of active neuronal ensembles [86,87] d) Episodic memory, word integration and environmental encoding[88,89,90]	a) Drowsiness and relaxation[91,92] b) Sensory function, movement and visual perceptual framing [84,93,94] c) Task engagement, speed of working memory and cognitive performance[88,95,96,97]	a) Resting and motor tasks[15,92,98] b) Responses to olfactory and visual stimuli [26,99,100] c) Top-down attention and working memory allocation[9,101,102,103]	a) Focused attention and motor task execution[15,92] b) Responses to evoked auditory and visual stimuli[104] c) Facilitation of neuronal communication and efficient cognitive processing[105,106] d) Spatial working and recognition memory[71,107]

Table 1.1 Significance of neuronal network oscillations in the CNS.

Indeed, previous studies have postulated that different oscillation frequencies either compete with each other or cooperate in a specific manner to participate in distinct physiological processes (e.g. bias of input selection, temporal linkage of neurons into assemblies or facilitation of synaptic plasticity)[108,109], which importantly correlate with specific behaviours (e.g. sleep, learning)[2,76], thereby becoming a fundamental tool for both clinical diagnosis and brain research (Table 1.1).

1.1.1.1 Behavioural correlates of neuronal oscillations

Despite lacking a universal consensus on the frequency ranges breakdown[10,110], it is well established that mammalian cortical neurons form behavioural state-dependent oscillating networks that are traditionally classified by characteristics of amplitude and broad frequency bands, including delta (~1-4 Hz), theta (~4-10 Hz), alpha (~8-12 Hz), beta (~12-30 Hz) and gamma (>30 Hz) oscillations[2,11], as shown in Table 1.1.

Delta (δ) oscillations are low frequency fluctuations typically ranging from ~1-4 Hz and are found in brain areas such as the neocortex, thalamus and basal ganglia. These brain waves are predominant during physiological brain states, including sleep (i.e. Slow Wave Sleep, SWS; non-rapid eye movement, NREM, phases 3 and 4)[48,76], as well as in pathology (i.e. coma)[92,111]. According to their low frequency profile, delta oscillations involve large neuronal populations spreading over wide brain regions (e.g. frontal lobes), which are typically active during the performance of mental operations (e.g. calculation, semantics)[81,112] and attention to a specific stimulus, likely mediated via the inhibitory modulation of neuronal networks involved in the processing of other stimuli at different locations[82].

Theta (θ) oscillations range from ~4 to 10 Hz and have been observed in the hippocampus, dentate gyrus, medial septum, amygdala, as well as in different cortical areas (e.g. entorhinal, cingulate

and frontal cortices)[30,31,32,33,34]. These sinusoidal oscillations arise during voluntary control of movement, arousal and rapid eye movement (REM) sleep[24,31], and have been suggested to play a part in memory processes[113] and during inhibitory tasks subserving executive functions[114].

Alpha (α) waves (~8-12 Hz) were the first to be recorded from the human scalp by Berger[25] and are found in both the neocortex and thalamus. They have been associated with drowsiness, relaxation and information processing in response to sensory (e.g. visual) stimuli[92,115]. In addition, alpha rhythms show an inverse relationship with memory and attention, likely reflecting functional inhibition of these cognitive processes[116,117].

Beta (β) oscillations are high frequency oscillations within ~12-30 Hz and are predominant in the neocortex, thalamus, olfactory bulb, striatum, dentate gyrus and hippocampus. The power of these oscillations increases in sensorimotor areas in subjects performing motor tasks, such as muscle contraction[118,119], but attenuated during voluntary movement of body parts or imagined actions[120], thereby being classically associated with an "idling" or resting state[98]. More recent studies postulated that rather than representing lack of movement, beta oscillations may be necessary for the active maintenance of the current cognitive state or *status quo* requiring sensorimotor interaction[121], by impairing neuronal processing related to new movements[122,123].

Similar to beta oscillations, **gamma (γ)** rhythms are considered high frequency oscillations (~30-80 Hz), typically recorded from the neocortex, olfactory bulb and hippocampus, which play a fundamental role in conscious perception[124,125]. Intriguingly, gamma oscillations have been suggested to balance the mainly excitatory connectivity between pyramidal cells with inhibition during activated states of the cortex that occur when performing a specific task[126]. Therefore, gamma oscillations are correlated with motor and high cognitive functions, such as selective

attention[8], as well as memory formation[127], storage[128] and retrieval[129].

Previous studies also showed the presence of sleep spindles reflecting bursts of neuronal oscillatory activity during NREM sleep within the alpha and beta bands (~12-18 Hz)[130], as well as fast (80-200 Hz, "ripples") and ultra-fast oscillations, up to 600 Hz, in both the hippocampus and cortex[131,132]. Interestingly, neuronal oscillations interact across different frequency bands to modulate each other and engage with specific beahviours[2,10]. For instance, transient coupling between theta and gamma bands has been previously reported to be important for activity coordination in distributed neocortical areas during cognitive processing[105], as well as for synaptic plasticity in both the entorhinal cortex and the hippocampus of freely behaving rats[106]. Furthermore, phase relations between regions are diverse and can be modulated by sensory and motor experiences[133], thereby adding more complexity in deciphering how brain waves coordinate to subserve important functions in both the developing and mature human brains.

1.1.1.2 Mechanisms underpinning neuronal oscillations

Neuronal oscillations show a linear progression on a natural logarithmic scale with little overlap, which led Penttonen and Buzsáki (2003)[11] to postulate that at least ten distinct and independent mechanisms are required to cover the large frequency range of cortical network oscillations, and it has been reported that some frequency oscillations are driven by multiple mechanisms[2,108]. Some of the suggested mechanisms affecting individual neuronal activity underlying the generation of network oscillations are summarized in Table 1.1, and most of them include reciprocal interactions between excitatory and inhibitory mechanisms[92] or changes in cellular excitability[70,134]. The latter is often associated with alterations in extracellular ions (e.g. Ca^{2+}) and the hyperpolarization-activated inward current (I_h)[135], which can regulate intrinsic membrane properties[136], as well as the strength and frequency of network oscillations[137].

In particular, neurons consist of inherent membrane resonance and frequency preference properties[138] that allow them to act as resonators or transient oscillators and to select inputs within certain subthreshold frequencies (e.g. theta)[139]. This oscillatory behaviour at multiple frequencies depends on the accurate combination of both low-pass (i.e. passive leak conductance, membrane capacitance) and high-pass (i.e. open probability of voltage-gated channels activated close to the resting membrane potential, RMP)[2] filtering properties, which endow neurons with a wide repertoire to respond faster and more efficiently to spike trains or fast inputs[140]. Therefore, alterations in membrane conductance or potential along the somatodendritic compartments result in differential tuning of the resonant response in cell types (e.g. interneurons *vs* pyramidal cells), which is essential for sculpting the functionality of a neuronal network[141].

In this regard, changes in the concentration of extracellular ions (e.g. K^+, Mg^{2+}, Ca^{2+}) have been recently shown to allow switching between behavioural states, including sleep and arousal *in vivo*[142], indicating that cellular mechanisms particularly affecting the ionic composition of the extracellular space are powerful tools to modulate brain states. Accordingly, K^+ channels play a crucial role in determining the overall network excitability by limiting depolarizing inputs and have been suggested to affect the generation of neuronal oscillations at multiple frequencies[2]. For instance, an early modelling study showed that slow repolarizing K^+ currents are required for the bursting and resonant behaviour at theta frequencies in cerebellar granule cells, by inducing delayed repolarization to terminate the oscillatory Up state amplified by a persistent Na^+ current[56].

In line with these results, activation of K^+ currents *in vivo* has been associated with enhanced spike timing precision at gamma frequencies in both pyramidal and basket cells in the hippocampus[143], as well as with lower frequency oscillations in the delta range[49].

Importantly, neuromodulators have been associated with network oscillations and found to affect the concentration of extracellular ions, including the extracellular K^+ concentration ($[K^+]_o$)[142], as well as slow K^+ conductances in neurons from different brain regions[144,145]. Among the different neuromodulators, acetylcholine (ACh) appears to be the common denominator for most frequency bands (Table 1.1) and as such takes part in brain states involving intercommunication between brain regions, including consciousness, memory formation and attention[146,147]. Indeed, previous studies reported on a role for the cholinergic system in blocking K^+ conductances related to delta oscillations leading to cortical arousal[49,148]. In the hippocampus, activation of medial septal cholinergic inputs led to the generation of high frequency oscillations within ~40 Hz *in vitro*[69], as well as enhanced theta oscillations, by attenuating sharp wave ripples and slow oscillations *in vivo*[55].

Interestingly, different regions within the same brain area may display alternate generators of brain waves oscillating within the same frequency range, as beta oscillations in layer V of the primary auditory cortex are generated via cholinergic stimulation, whereas tonic glutamatergic excitation has been reported to be the underlying mechanism in layer V of the association cortex[66]. These observations support the involvement of ACh in mediating temporal interactions between cortical regions within a single frequency range that could facilitate the assembly of neuronal ensembles[7,149].

However, the fact that neuronal oscillations participate in spatial integration across distant brain regions[2], which occurs over time scales greater than direct synaptic transmission, suggests that other mechanisms involving non-neuronal cells (i.e. glia) are likely to play a role in modulating neuronal oscillations at the network level (Table 1.1)[52,58,71].

Altogether these studies suggest that the degree of neuronal network synchrony and coherence is strongly regulated by distinct cellular mechanisms that become active or inactive to meet behavioural demands. Although many processes have been suggested to impact on the generation and modulation of neuronal oscillations, the mechanisms that gear the transition between different oscillatory frequencies in the cortex, to allow environmental adaptation and thus survival, are still unknown.

1.1.2 Methods to measure neuronal oscillations

Electrical potentials are the result of the difference in voltage between two locations in the brain. These alterations in neuronal membrane voltage can be detected and monitored with high temporal and spatial resolution, thereby allowing the study of different neurophysiological aspects involved in the communication and computation of neuronal oscillations at the network level[17,108,150].

Almost 80 years ago, Hans Berger, a physician, neuro-psychiatrist and an autodidact in neurophysiology, was one of the first to record spontaneous electrical activity from the brain of dogs and cats using a new technique he termed **electroencephalography (EEG)**[151]. Since then he focused on optimizing his experimental methods to study "fluctuations in electrical current which are present at all times and which may be recorded from the surface of the cerebral cortex"[152]. His pioneering work allowed him to measure electrical potentials directly from the cortical surface, thus discovering the first types of brain waves (i.e. alpha) and their physiological role in both health and disease[25].

Today there are several tools that have been extensively applied to monitor brain activity. Here I will summarize the advantages and caveats that some of the most frequently used methods offer to explore the oscillatory behaviour of neuronal networks.

1.1.2.1 Extracellular recordings

Following the development of EEG recordings, researchers improved this technique to allow direct measurements of network oscillations from the subdural region using grid electrodes placed on the cortical surface (electrocorticogram, ECoG)[153], or even deeper inside the brain tissue with small-sized electrodes to measure **local field potentials (LFPs)**, also known as intracranial EEGs[154,155].

LFPs are electrophysiological signals obtained by the summed electric current flowing across local neuronal populations. The LFP signal is low-pass filtered, typically within the range of 100-300 Hz[156], which removes the action potential component, mainly associated with fast fluctuations, and passes the lower frequency signal, believed to represent slow oscillating currents, including synchronized synaptic potentials[157], afterpotentials of somatodendritic spikes[158] and voltage-gated membrane oscillations[57]. Previous experiments based on extracellular recordings with conventional electrodes have been able to capture changes in cortical network dynamics as LFPs with high temporal resolution[159,160]. Interestingly, LFPs in the rodent olfactory bulb have been reported to follow respiratory rhythms during specific brain states (e.g. wakefulness, REM sleep)[161]. Additionally, LFP recordings from neocortical columns in the barrel cortex have revealed that layers V-VI are directly activated by thalamocortical projections, in opposition to the previous conception that sensory information propagates first through layer IV, then to layer II/III and finally to layers V-VI, which further suggests that layer IV is not a mandatory distribution hub for cortical activity[162].

Together, these studies indicate that LFP recordings are a powerful tool able to provide valuable information about the state of a whole network that cannot be obtained at present using intracellular recordings[2,163].

1.1.2.2 Functional imaging

Other techniques that have been widely used to study neuronal oscillations include the **magnetoencephalography (MEG)**, a non-invasive approach that measures magnetic fields generated by the electrical activity of synchronized neurons outside the skull, without the need of attaching electrodes to the scalp[164]. Unlike EEG, the MEG signal typically reflects intracellular currents with higher spatiotemporal resolution, as magnetic fields pass through the scalp and skull without any distortion[165]. Furthermore, MEG is more sensitive to superficial cortical activity, due to the more pronounced decay of magnetic fields as a function of distance, thereby being currently used in the surgical treatment of epilepsy[166]. Despite the improved resolution, MEG is not an accurate method to obtain information about cortical circuits nor the underlying mechanisms giving rise to neuronal oscillations[2].

To achieve structural detail, as well as neurophysiological data, MEG is typically combined with **functional magnetic resonance imaging (fMRI)** as "magnetic source imaging" (MSI). fMRI is based on the detection of magnetic resonance energy from parts within a volume of tissue containing different amounts of water[2]. The hydrogen atoms of water representing magnetic dipoles are misaligned when a radio frequency pulse of energy is applied[2]. After direct application of "receiver oil" on the head, the energy emitted by these atoms going back to their original position generates contrast, which reflects the blood oxygen level, as well as cerebral blood flow and volume[167,168], a mechanism that was first described in the 90's as "blood oxygen level-dependent (BOLD)" contrast[169,170,171]. Importantly, fMRI allows the study of the neuronal organization into networks and the visualization of dynamic connectivity patterns within different brain structures located in distant areas, both under normal physiology[172,173] and pathology[174,175].

In addition, several groups have provided evidence that the BOLD signal used in fMRI can indirectly measure neuronal firing or multi-unit activity (MUA)[176,177,178], typically inferred from field recordings (e.g. intrinsic oscillations; excitatory postsynaptic potentials, EPSPs; inhibitory postsynaptic potentials, IPSPs; action potentials)[179,180]. However, this analogy needs to be carefully revised, as the BOLD signal mainly reflects astrocytic function supporting neuronal activity (e.g. glutamate uptake during neurotransmission)[178], although the precise contribution of astrocytes and other glial cells to the BOLD signal remains dubious.

1.1.2.3 Optical imaging

Optical imaging techniques allow the simultaneous recording from multiple brain regions, which is useful for studying groups of neurons that are active during different behaviours[181,182]. In particular, **voltage-sensitive dye imaging (VSDI)** or extrinsic optical imaging is typically used for visualizing the overall network activity from different brain areas at both high spatial (down to 20-50 µm) and temporal resolutions (down to milliseconds)[183,184,185].

VSDI is based on the action of extrinsic dyes, which bind to the external surface of cellular membranes (i.e. neurons and glial cells). Several dyes have been commercialized over the past decade, including absorption dyes (e.g. RH-155, NK3630)[186,187], fluorescent red dyes (e.g. RH-414, RH-795, JPW-1114, DI-4-ANEPPS, DI-2-ANEPEQ)[12,188,189,190,191], and longer-wavelength fluorescent blue dyes (e.g. RH-1691, RH-1692, RH-1838)[192,193,194]. Following dye excitation with the appropriate wavelength, a molecular rearrangement occurs allowing the instantaneous emission of light, thereby transforming voltage signals into optical signals that are proportional to changes in the stained membrane potential and can be detected using a high-resolution fast-speed camera (i.e. charge-coupled device, CCD)[195,196].

However, this technique has several limitations, most of them associated with the dye size itself, which limits its penetration depth into the cortex (~400-800 μm), typically corresponding to superficial layers[192,197,198]. Consequently, extracellular staining is restricted by the excess of inactive dye, which does not carry the signal but contributes to resting fluorescence[199]. As a consequence, over the past decades several studies have focused on optimizing VSDI recordings in different animal models, mainly by increasing the illumination and reducing the noise of the system[196,198,199]. Yet incrementing the brightness often leads to phototoxicity or photodamage associated with excited state reactions (e.g. disruptive oxygen free radicals) and can easily compromise the integrity of the membrane leading to reduced LFP and VSDI signals and eventually cell death[200], which are probably the reasons why VSDI has been lagging behind other optical techniques, such as Ca^{2+} imaging[201].

Other technologies focus on directly modulating neuronal oscillations rather than monitoring the brain oscillatory activity while engaged in a specific task. These include pharmacological neuromodulation, as well as repetitive transcranial magnetic stimulation (rTMS)[202,203] or transcranial alternating current stimulation (tACS)[204,205], which offer the advantage of assessing the causality of neuronal oscillations to cognitive processes. Together, the combinations of different approaches (e.g. VSDI or Ca^{2+} imaging with LFP recordings or fMRI) and computational models have the power to better characterize biological confounding events and provide new insights into the processes occurring from single cells to neuronal network oscillations[199,206,207,208].

1.2 Glia: passive or active components in the cortex?

The human brain contains two major cell populations, neurons and glia, which were originally observed using rudimentary microscopes more than 150 years ago[209,210,211,212].

However, due to technical limitations of histological methods, together with poor microscopic resolution, glial cells and neurons were initially considered as a single anatomical unit[213,214]. Advances in electrophysiology and biochemistry allowed the first descriptions of non-nervous cells (i.e. glia) as structural independent entities[215,216] and further showed that while neurons are electrically excitable and capable of discharging short voltage pulses known as action potentials[217], glial cells are not. This observation led to the common assumption that glia are passive cells that essentially provide connective[218,219] and nutritional support to neurons[220].

At the beginning of the 20th century, several studies provided evidence that the "glue" in the CNS was actually composed of different classes of glia, based on differences in morphology, function and brain location, including both microglial and macroglial cells (i.e. oligodendrocytes, astrocytes)[221,222]. **Microglia** are part of the immune system and survey the brain for damage and infection, engulfing dead cells and debris[223,224]. Microglial cells have also been implicated in synaptic remodelling by phagocytic mechanisms during normal brain function and become activated in many neurodegenerative diseases (e.g. Alzheimer's Disease, AD)[225,226]. Despite being first described in 1899 as "mesoglia" derived from the mesoderm[227], the formal identification of **oligodendrocytes** and their relation to myelin was demonstrated two decades later[228,229]. Notably, this lipid-rich membrane or myelin sheath enwraps axons and induces clustering of ion channels at nodes of Ranvier, thereby enhancing conduction velocity, which is essential for rapid electrical communication between neurons and their targets[230]. Thus, oligodendrocyte dysfunction leads to demyelination, which occurs in pathological states (e.g. multiple sclerosis, MS)[231]. Another macroglial cell type known as **NG2-glia** or "polydendrocytes" were identified by their expression of the Neural/Glial antigen 2 (NG2) chondroitin sulphate proteoglycan[232,233].

NG2-glia are progenitor cells that eventually give rise to oligodendrocytes (also named oligodendrocyte progenitor cells, OPCs) and play a role in the formation of synapses[234]. Finally, **astrocytes** are polarized, star-shaped glial cells[235] that were initially classified according to their anatomic location and morphological differences appreciated by Golgi staining[236], as fibrous astrocytes of the white matter and protoplasmic astrocytes of the grey matter[237,238]. Similar to rodents and primates, human fibrous astrocytes are larger in diameter compared to protoplasmic astrocytes and possess fewer processes[239] that are straighter and radially orientated[240], establishing contact with nodes of Ranvier of myelinated axons[241,242,243]. On the other hand, human protoplasmic astrocytes are in closer proximity with neuronal cell bodies[244] and possess highly branched processes spanning symmetrically ~100-200 μm from the soma[245], thereby increasing the cortical volume and synaptic density covered by a particular astrocyte[246].

1.2.1 Glia during cortical development

Except for the microglia, which enters the brain from the blood circulation early in an organism's development[222], gliogenesis of astrocytes and oligodendrocytes shares a common origin with neuronal cells in the cortex[247,248].

In early stages of cortical development, neuroepithelial precursor cells from the neuroectoderm in the transient proliferative embryonic zone, known as ventricular zone (VZ), give rise to radial glial cells (RGCs) that form bipolar radial fibers between VZ and the pial surface in the cortex[249,250]. Proliferative RGCs are neural stem cells that divide to form neuronal progenitors or migrating pyramidal neurons, which traverse the subventricular (SVZ) and intermediate (IZ) zones, while migrating along the long RGCs processes to reach their final destinations in the distant cortex or cortical plate (CP; Figure 1.1)[251,252,253].

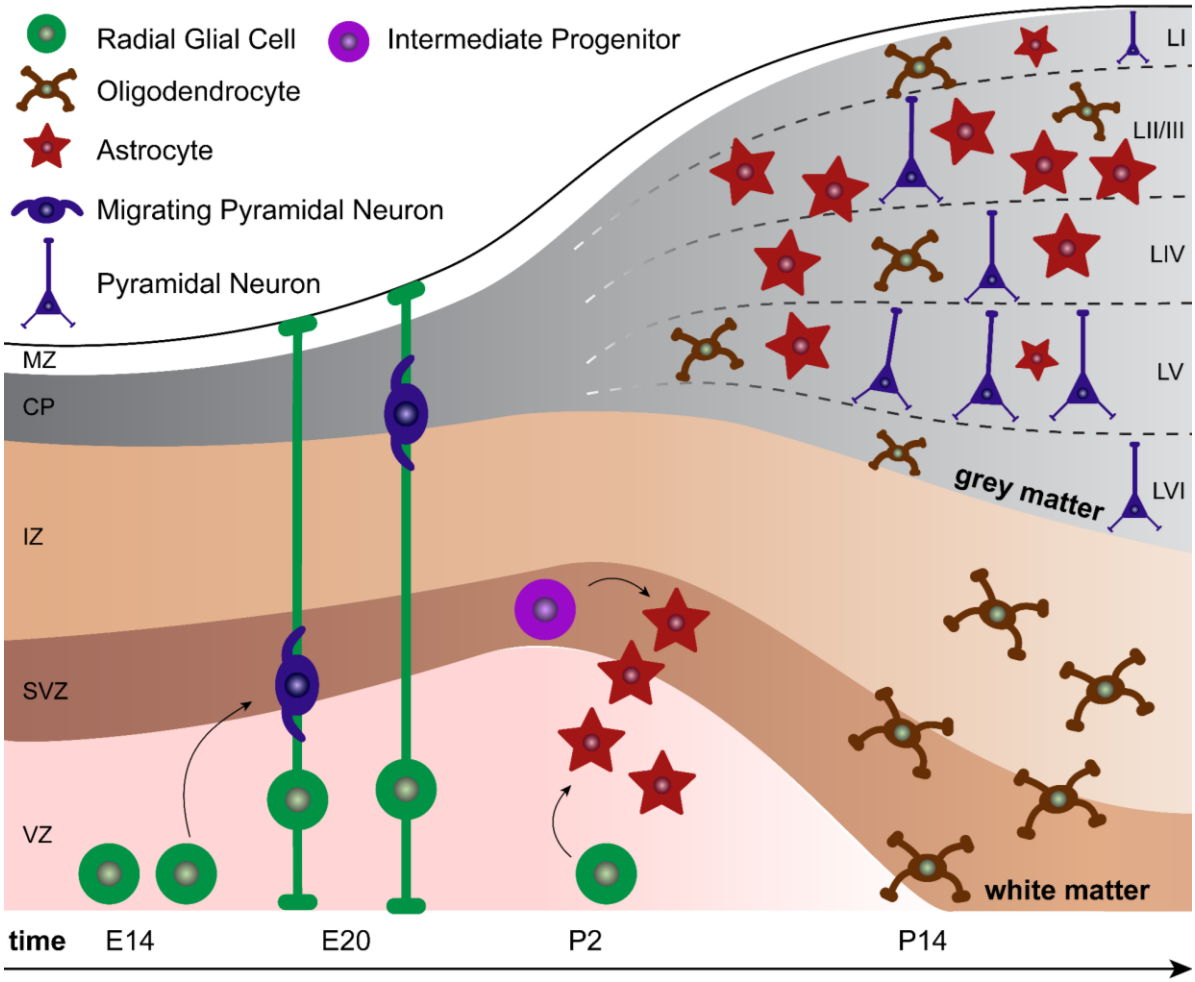

Figure 1.1 Neurogenesis and gliogenesis in the developing cerebral cortex. Schematic illustration showing the development of neurons and glial cells in the rodent cortex. Neurogenesis peaks at embryonic day 14 (E14). Radial glial cells divide to form premature pyramidal neurons that migrate along their processes to reach their final destination in the CP where mature pyramidal neurons will form an inside-out six-layered structure. Astrogenesis starts at postnatal day 2 (P2) from radial glial cells in the VZ or from intermediate progenitors located in the SVZ. Oligodendrocyte generation occurs at later stages in development (P14). *MZ: marginal zone; CP: cortical plate; IZ: intermediate zone; SVZ: subventricular zone; VZ: ventricular zone*

Cohorts of new-born projection or pyramidal neurons generated early during development will eventually occupy a relatively narrow area within the mature cortex[254] and each generation of postmitotic neurons will bypass the previous one, thereby forming the characteristic six-layered cortical structure[255,256], starting from layer VI up to layer II, a phenomenon known as "inside-out gradient of neurogenesis"[257], while layer I originates from the marginal zone (MZ) of the developing CP[258] (Figure 1.1).

Once all neurons have migrated and positioned in their corresponding layers without replacement[259], astrogenesis and oligodendrogenesis commence at later stages in the embryonic development (Figure 1.1). As RGCs mature, most give rise to typical star-shaped astrocytes during the perinatal period in different brain areas including the cortex, hippocampus, striatum, brain stem and hypothalamus[260,261]. Others might remain as specialized radial glia (i.e. Müller glia in the retina[262], Bergmann glia in the cerebellum[263], pituicytes in the neurohypophysis[264]), thus contributing to the heterogeneity of the astrocytic lineage that likely displays different gene expression patterns and functions[265,266].

In addition, grey and white matter astrocytes, as well as oligodendrocytes can originate from intermediate progenitors derived from radial glia located in the neonatal SVZ (i.e. tanycytes at the base of the third ventricle; Figure 1.1)[267,268]. However, some studies suggest that protoplasmic astrocytes may have additional origins, as Zhu *et al.* (2008)[269] showed that they could also arise from NG2-glia in the grey matter of the ventrolateral forebrain at postnatal stages[270], as NG2-glia share similar stellate morphology to astrocytes[271], as well as widespread distribution throughout the CNS, being associated with specific network functions[272]. Altogether, RGCs play key roles during cortical development, not only acting as progenitor cells that give rise to both neurons and glia, but also as a scaffold for the cortical architecture and migrating neurons. Furthermore, despite sharing a common origin with neurons, glial cells are created through different pathways, which might help explain their developmental diversification even within the same brain region.

1.2.2 The glia to neuron ratio conundrum

Glial cells are present in all organisms with a CNS, from early invertebrates (e.g. C. elegans, Drosophila) to humans, with astrocytes the most ancient cell type[273,274].

Despite being conserved during evolution in terms of morphology and size, the proportion of glial cells with respect to neurons, the **glia (G) to neuron (N) ratio (GNR = G/N)**[275], or glial index as originally proposed by Friede in 1954[276], was historically assumed to increase according to the animal's brain or body size[277,278] and along the phylogenetic scale[279], due to observations that neuronal density decreased with increasing cortical volume[280], with humans displaying a GNR of 10:1[281,282,283].

However, the heterogeneity of glial and neuronal cell body densities in different brain areas (e.g. white *vs* grey matter)[284], together with the lack of specific and robust molecular markers for identifying glial subtypes led to controversial results in animal models, such as rodents[285] or primates[286]. For instance, Terry *et al.* (1987)[287], using a semiautomated image-analysis method, provided evidence that while neocortical neuronal density decreases with age, the number of glia increases. Two decades later, another group revealed varying numbers of total glial cells in the human cortex depending on the age, as well as on gender differences[288]. Using a stereological counting technique, they further showed that not all glial subtypes increase with age, as previously reported[287]. In fact, they observed that while the population of oligodendrocytes was correlated with neuronal loss during aging, the number of astrocytes remained constant. These studies claim for the importance of the counting technique when quantifying neurons and glia in different brain structures, rather than in the whole brain[289].

In 2005, the development of the "isotropic fractionator" method by Herculano-Houzel and Lent[290], derived from the "direct enumeration" method[291], which consists of homogenizing fixed brain tissue into a homogeneous suspension of isolated cell nuclei that are counted as total neuronal or non-neuronal cells (i.e. NeuN positive *vs* negative respectively), enabled a more systematic determination of the GNR across different species in both healthy and diseased brains.

Compared to previous stereological methods, this non-stereological counting technique is faster (~24 hours), less time-consuming and can be applied for the quantitative measurement of cells either in whole brain or within brain structures independent of brain volume, both in normal physiology and pathology[292]. Using this technique, more recent studies showed that the human brain contains equal numbers of neurons and non-neuronal cells[293]. This observation was already supported by previous histological data showing a GNR of ~0.99[294,295] and similar glial densities in primates and other mammals[296], thereby demystifying the widespread notion that the GNR uniformly scales with brain size. Instead, the GNR has been negatively correlated with neuronal density across brain structures and species[297,298], with decreased neuronal densities, indicative of larger neurons, related to higher GNRs.

These observations suggest that (1) the heterogeneity in the GNR is likely due to a variation in neuronal densities and that (2) GNRs increase as a function of neuronal size. Hence, several studies proposed that species evolved increased GNRs to support the higher energetic and metabolic demands of larger neurons[278,283], as initially proposed[277]. However, later estimations of the average metabolic cost or glucose usage per neuron, based on total neuronal and non-neuronal cell numbers counted using the isotropic fractionator method, revealed that brain metabolism is best correlated with the total number of neurons, rather than brain mass or neuronal density, leading to the hypothesis that each neuron possesses a "fixed energy budget" that is independent of its size[299]. As a consequence, other groups raised alternative explanations regarding the increased number of glial cells per neuron as they become larger, including a potential role in effective K^+ removal following neuronal activity especially in thicker tissues, such as the cerebral cortex[300].

Furthermore, the increased functional competence of the adult human brain has been linked to the greater architectural complexity and pleomorphism of neocortical protoplasmic astrocytes.

Indeed, protoplasmic astrocytes in humans are typically located in layers II-VI and display different properties compared to rodent astrocytes[301], as supported by observations that human neocortical astrocytes are 2.6-fold larger in diameter, increase their processes by 10-fold to reach further distances, and propagate Ca^{2+} waves significantly faster than rodent astrocytes[240].

Despite some dissimilarities observed throughout evolution, the overall stability of both structural and electrophysiological properties in glial cells across species suggests that they perform fundamental roles in brain physiology. Therefore, future studies should consider reciprocal functional and metabolic interactions between glial cells and neurons to better characterize their real contribution to brain function.

1.2.3 Astrocytes under the spotlight

In the 19th century, Ramón y Cajal proposed the insulation theory, probably the first proposition claiming that astrocytes, rather than acting as simple supporting cells, were directly involved in modulating neuronal activity by isolating neighbouring neurons[302].

In support of this view, Cajal further revealed that "the neuroglia is abundant where intercellular connections are numerous and complicated, not due to the existence of contacts, but rather to regulate and control them, in such a manner that each protoplasmic expansion is in an intimate relationship with only a particular group of nerve terminal branches"[303] and "intended perhaps to produce hormones associated with the brain activity"[216]. These early considerations suggested that astrocytes are strategically located close to synapses, which allow them to critically regulate the overall network function, as proposed previously[304,305].

Today, glial cells are no longer considered a homogenous population exerting supporting roles in the brain, but instead, studies in the past decades revealed essential contributions of glial cells[270], in particular of astrocytes due to their close association with synapses, to many physiological brain functions, including synaptogenesis[306], metabolic coupling[307], nitrosative regulation of synaptic release in the neocortex[308], synaptic transmission[309] and plasticity[310].

1.2.3.1 GFAP and the actin cytoskeleton

The architecture of protoplasmic astrocytes changes during brain development and according to molecular and gene expression patterns, which supports their physiological role[265,266]. The astrocytic morphology is mainly composed of the actin cytoskeleton and intermediate filaments[311], including vimentin in early stages of cortical development, which is progressively replaced by the glial fibrillary acidic protein (GFAP) in differentiated astrocytes[312,313]. However, despite being extensively used as an intracellular specific marker of mature astrocytes[314], several studies have shown that not all astrocytes express GFAP[315], not all cells expressing GFAP are astrocytes[316] and that GFAP immunostaining does not reveal the complete extent of the astrocytic domain in rodents[246], as it is often not detectable in the cell body nor in the finest astrocytic processes[317].

Over the past decades, several research groups have demonstrated the importance of the actin cytoskeleton and intermediate filaments in modulating astrocytic morphology both in physiological and pathological conditions (e.g. neuroinflammation)[318]. For instance, Hanley and colleagues (2013)[319] showed that astrocytes require high activation of the Arp2/3 complex, an actin-binding protein (ABP), to maintain and modulate their typical stellate morphology. Palladin, another ABP expressed predominantly in cortical astrocytes, is upregulated in response to brain injury[320], thus supporting its role in actin assembly and shape remodelling during neuroinflammation.

Whereas some studies using transgenic knock-out (KO) mice showed that GFAP is not necessary to support physiological astrocytic development, morphology or function[321], others found that GFAP is essential in pathological processes, such as reactive astrogliosis[317,322], which may lead to the formation of glial scars with permanent tissue rearrangement[323]. In addition, overexpression of GFAP has been associated with morphological alterations (e.g. hypertrophy of astrocytic processes)[324], loss of astrocytic domain organization[325], impaired neuronal-astrocytic interactions[326] and neurodegenerative disorders (e.g. Alexander's disease)[327,328].

1.2.3.2 Astrocytic channels, receptors, pumps and co-transporters

Protoplasmic astrocytes show a diverse expression of receptors, ion channels, pumps (i.e. ATPase) and cotransporters in different brain areas (e.g. hippocampus, cortex, brain stem, thalamus)[270,329] that allow them to dynamically interact with neurons through several pathways[330,331,332]. Electrophysiological studies together with molecular genetic approaches have shown that cortical astrocytes express both ligand-gated and G protein-coupled receptors (GPCRs), such as N-methyl-D-aspartate (NMDA) receptors[333] and α-amino-3-hydroxy-5-methyl-4-isoxazolepropionic acid (AMPA) receptors[334]. Moreover, astrocytes express receptors for most neurotransmitters and neuromodulators, including metabotropic glutamate receptors (mGluRs)[335], purinergic P2Y adenosine triphosphate (ATP) receptors[336], gamma-aminobutyric acid (GABA) receptors[337], as well as receptors for ACh[338,339], Serotonin (5-Hidroxytryptamine, 5-HT)[340], Histamine[341], Noradrenaline (NE)[342,343] and Dopamine (DA)[344], coupled to second messenger systems.

Notably, astrocytes are characterized by a relatively more hyperpolarized RMP compared to neurons, typically ranging from -70 mV to -80 mV[345,346].

Pharmacological studies in genetically engineered mice found that Ba^{2+}-sensitive, weakly inward rectifying K^+ (K_{ir}) channels, which are highly expressed at synapses and astrocytic end-feet, were crucial in setting the negative RMP in cortical astrocytes[347,348]. Indeed, loss of functional K_{ir} channels has been associated with neurological diseases (e.g. epilepsy[349,350]; amyotrophic lateral sclerosis, ALS[351]; AD[352]; Huntington's Disease, HD[353]; retinal degeneration[354]; malignant gliomas[355]), supporting their physiological value in the CNS.

Other ion channels, like L-type Ca^{2+} channels, were initially identified in cortical astrocytes *in vitro*[356] and later confirmed *in situ*[357]. Despite the existence of voltage-gated Na^+ channels, which has been demonstrated in astrocytic cultures[358] and in brain slices from different brain regions (e.g. corpus callosum, spinal cord, hippocampus)[359,360,361], the functional expression of these channels in cortical astrocytes *in vivo* still has to be confirmed[362]. Aside from channels, ions can cross astroglial membranes through exchangers (e.g. Na^+/Ca^{2+} exchanger, NCX)[304,363], pumps (e.g. Na^+/K^+ ATPase, NKA)[364,365] and transporters (e.g. Na^+-K^+-$2Cl^-$ cotransporter, NKCC)[366,367], which are also expressed in astrocytes. Altogether, astrocytes express various K^+, as well as other ion channels displaying regional differences and specific subcellular distributions.

1.2.3.3 Bidirectional interactions between neurons and astrocytes

In 1895, Cajal proposed that astrocytes exert a major role in modulating brain function during different behavioural states (e.g. sleep, wakefulness)[302]. More than a century later, with the development of new tools, including the patch-clamp technique, as well as the confocal and multi-photon fluorescence imaging methods[190,368], the initial observations by Ramón y Cajal about astrocytes as potential modulators of the brain circuitry are gaining more support.

Despite lacking the ability to fire action potentials, astrocytes possess numerous metabotropic receptors coupled to second messenger systems that allow their communication with neurons, as well as with other astrocytes mainly via **Ca^{2+} signals**[369,370]. Astrocytic Ca^{2+} signals can occur both independently of neuronal activity or following neurotransmitter release, and include intrinsic Ca^{2+} oscillations within individual cells and Ca^{2+} waves that propagate from one cell to another[371,372]. Interestingly, spontaneous Ca^{2+} oscillations differ between cortical layers *in vivo*, being more frequent and asynchronous in astrocytes from layer I compared to layer II/III, suggesting functional network segregation imposed by astrocytic function[373]. Similarly, computational modelling showed that the propagation of astrocytic Ca^{2+} waves is highly variable between brain regions depending on the topology of the astrocytic network, with short-distance connections favouring spreading of Ca^{2+} waves over wider areas[374]. In addition, several studies have provided evidence that astrocytes respond to different neuronally released neurotransmitters and neuromodulators (e.g. ACh, 5-HT, Histamine, NE, DA) by eliciting Ca^{2+} elevations that trigger signalling cascades (e.g. Ca^{2+}-dependent phosphatidylinositol-phospholipase C, PLC, pathway), leading to regulated increases in the intracellular or extracellular concentrations of ions (e.g. Na^{+}, Ca^{2+}, K^{+}) and gliotransmitter release (e.g. ATP, glutamate, adenosine, D-serine)[338,375,376,377,378,379]. For instance, activation of these receptors in astrocytes leads to PLC-mediated hydrolyzation of phosphatidylinositol 4,5-biphosphate (PIP_2), resulting in the formation of inositol 1,4,5-triphosphate (IP_3) and release of diacylglycerol (DAG) in the cytosol[380]. Finally, IP_3 binds to its receptor on the endoplasmic reticulum (ER) leading to Ca^{2+} release from internal stores[381] (Figure 1.2). Furthermore, elevations in the intracellular Ca^{2+} concentration ($[Ca^{2+}]_i$) stimulate the IP_3 receptor, hence promoting bigger increases in $[Ca^{2+}]_i$ until excessive levels inhibit the IP_3 receptor, a process known as "Calcium-Induced-Calcium-Release" (CICR)[382].

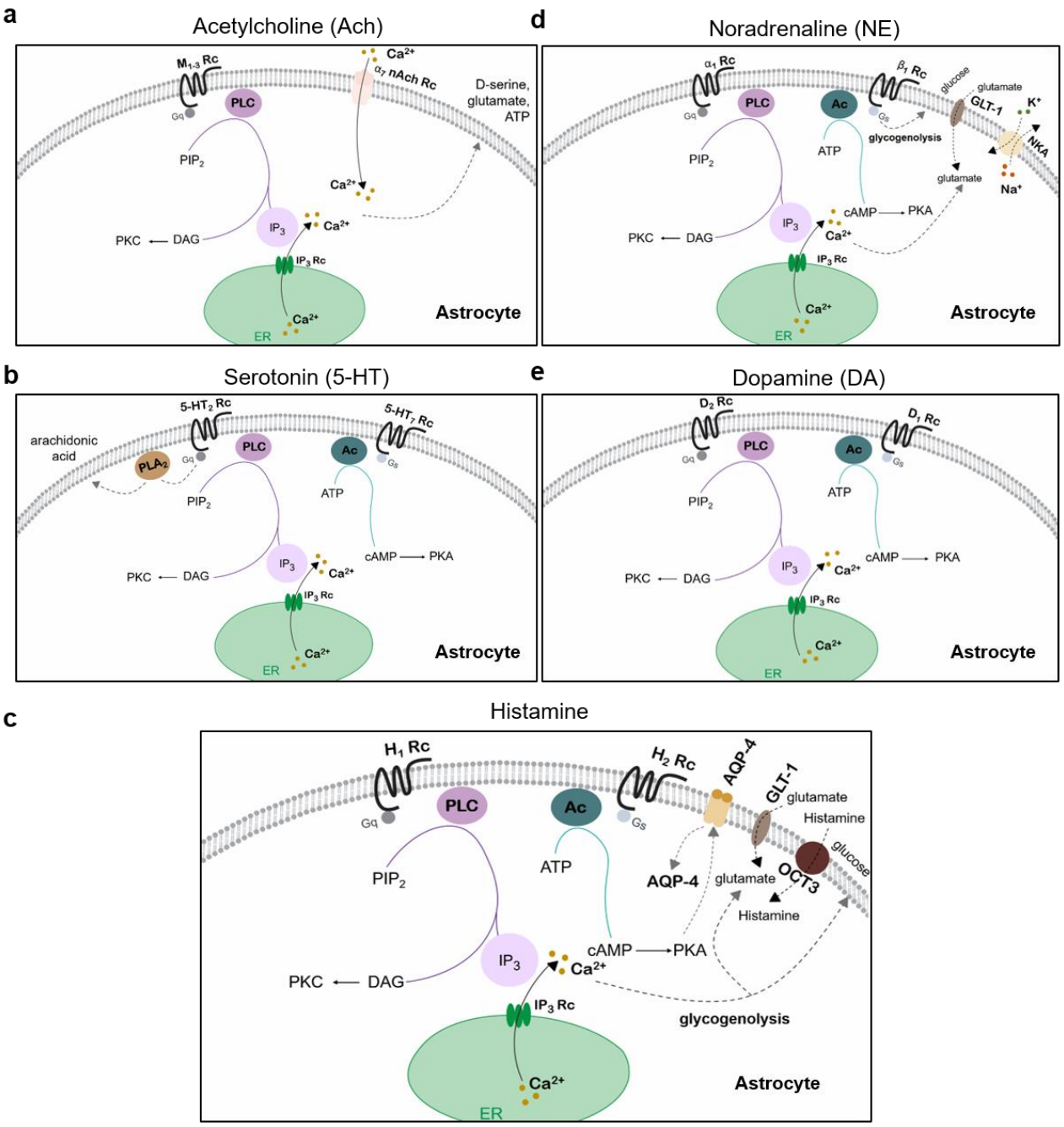

Figure 1.2 Neuromodulators evoke $[Ca^{2+}]_i$ increases in astrocytes. a-e) Schematic diagrams describing the main type of astrocytic receptors and signalling cascades activated by Acetylcholine (ACh, a), Serotonin (5-HT, b), Histamine (c), Noradrenaline (NE, d) and Dopamine (DA, e). Activation of muscarinic ACh receptors ($M_{1\text{-}3}$, a), 5-HT_2 receptors (b), H_1 receptors (c), α_1-adrenergic receptors (d) and D_2 receptors (e) results in Ca^{2+} release from internal stores (endoplasmic reticulum, ER). *PLC: phospholipase C, PIP_2: Phosphatidylinositol 4,5-bisphosphate, DAG: D-1,2-Diacilglicerol, PKC: protein kinase C, IP_3: inositol 1,4,5-triphosphate, Ac: adenylyl cyclase, cAMP: 3',5'-cyclic adenosine monophosphate, PKA: protein kinase A, PLA_2: phospholipase A_2, GLT-1: glutamate transporter 1, NKA: Na^+-K^+ ATPase pump, AQP-4: aquaporin 4, OCT3: organic cation transporter 3*

More recently, Mariotti and colleagues (2016, 2018)[383,384] demonstrated that astrocytic modulation and signalling are circuit-specific, as cortical astrocytes not only respond to excitatory inputs, but also react to inhibitory interneurons (i.e. parvalbumin *vs* somatostatin) both *in situ* and *in vivo*, by eliciting weak or strong $[Ca^{2+}]_i$ elevations following activation of $GABA_B$ receptors linked to $G_{i/o}$-coupled receptors and IP_3 signalling. In addition, two-photon imaging experiments revealed that cortical astrocytes are fast enough to respond to sensory stimulation by evoking fast Ca^{2+} events that were independent of both neuromodulation and IP_3-mediated signalling[385]. Together, these results suggest that astrocytes are able to process different patterns of network activation with a variety of Ca^{2+} signals in order to decode and integrate local synaptic activity, as well as other physiological processes (e.g. neurovascular coupling).

Hence, by responding to different neuronal populations with activity-driven Ca^{2+} elevations, astrocytes take part in many physiological processes, including blood vessel vasodilation and constriction through nitric oxide[308,386], K^+ signalling[387], release of trophic factors (e.g. fibroblast growth factor, neurotrophin-3)[388], metabolic agents (e.g. L-lactate)[310] or inflammatory mediators (e.g. tumour necrosis factor-α)[389] involved in network disorders, together with synaptic transmission[390] and plasticity[391,392]. In fact, gliotransmitters released through several pathways (e.g. exocytosis from storage organelles or via anion channels and pumps in the plasma membrane from the cytosol) can activate neuronal receptors[393,394], thereby establishing reciprocal interactions between neurons and astrocytes that result in the overall modulation of the network excitability and behaviour[395,396] (Figure 1.3). Consistently, astrocytic $[Ca^{2+}]_i$ rises lead to glutamate release, which targets extrasynaptic NR1/NR2B-containing NMDA receptors in neurons, resulting in changes in individual cellular excitability, as well as in activation of synchronous activities within groups of neurons[397].

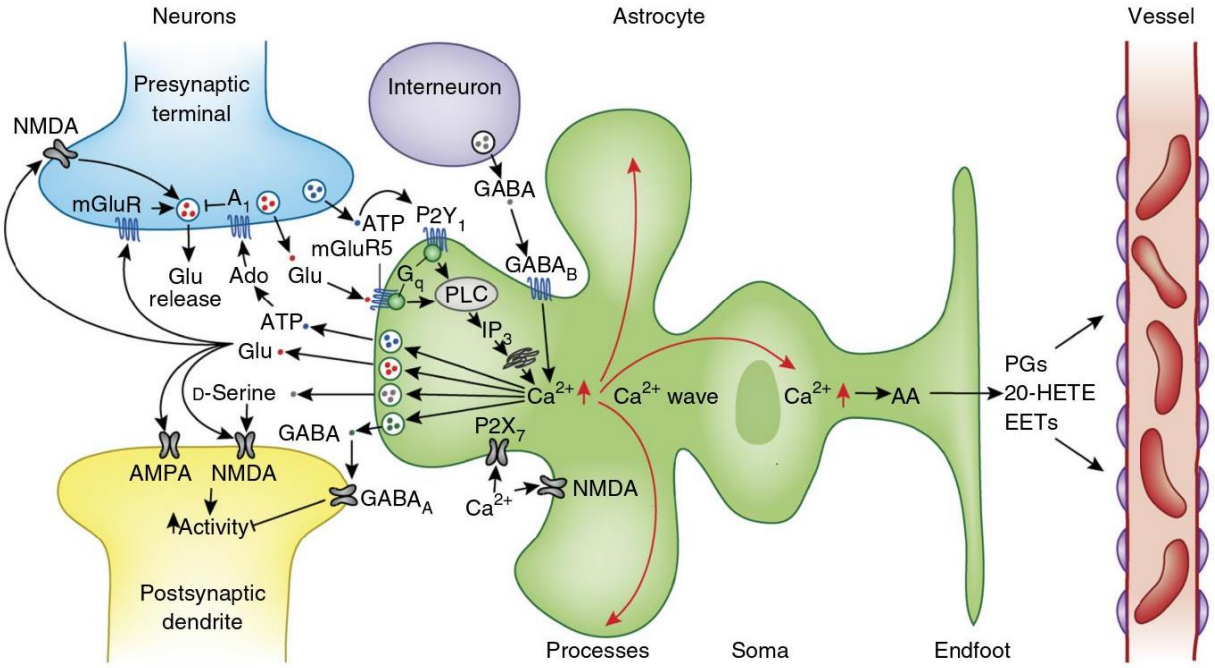

Figure 1.3 Gliotransmission pathways for synaptic regulation. Synaptically released neurotransmitters activate astrocytic receptors leading to $[Ca^{2+}]_i$ increases and gliotransmitter release from astrocytes, which can affect synaptic transmission both presynaptically, via glutamate, ATP or adenosine, and postsynaptically, via glutamate, D-serine or GABA. *AA: arachidonic acid, PGs: prostaglandins, 20-HETE: 20-hydroxyeicosatetraenoic acid, EETs: epoxyeicosatrienoic acids, PLC: phospholipase C, IP_3: inositol 1,4,5-triphosphate, Ado: adenosine, A_1: adenosine's A_1 receptor, $P2Y_1$: ATP's $P2Y_1$ receptor, $P2X_7$: ATP's $P2X_7$ receptor, Glu: glutamate, mGluR5: metabotropic glutamate receptor 5.* Adapted from Bazargani and Attwell (2016)[398]

Astrocytes achieve long distance communication not only via Ca^{2+} waves but also through ATP release[399,400], which is followed by its degradation to adenosine by extracellular nucleotidases, leading to synaptic inhibition of neurotransmission[401]. Consistently, ATP release from neocortical astrocytes has been found to activate purinergic currents in pyramidal neurons, followed by attenuation of synaptic and tonic inhibition[402]. These results suggest that cortical astrocytes, via exocytosis of ATP, could also play a role in the modulation of neuronal GABA release and thus phasic and tonic inhibition, which eventually could contribute to the generation of hypersynchronous oscillations (e.g. status epilepticus) at the network level.

Moreover, the fact that astrocytes can regulate the activity of individual neurons prompted Covelo and Araque (2016)[403] to propose a new concept of network modulation termed "lateral astrocyte synaptic regulation". Accordingly, astrocytic regulation of synaptic transmission is heterosynaptic, involving the active synapse together with distant tripartite synapses communicating via a form of paracrine signalling that depends on the morphological and functional properties of astrocytes, thereby acting as nodes that can influence neuronal properties over wide brain regions[404]. However, gliotransmitter release has been reliably demonstrated only *in vitro* and brain slice experiments are often accompanied by manipulations (e.g. high frequency stimulation) that can affect astrocytic channels or receptors leading to impaired signalling cascades. This experimental design imposes questions about the physiological role of gliotransmission in the brain. Although previous studies found no correlation between astrocytic Ca^{2+} signalling and gliotransmitter release[405,406,407], there is increasing evidence supporting the importance of both the topology and function of astrocytic networks for neuronal-astrocytic communication and control of neuronal network activity. Consequently, astrocytic alterations likely lead to aberrant modulation of both synaptic transmission and network synchronization, which is also accompanied by impaired behavioural performance. However, little is known about how neurons and astrocytes interact to mediate transitions between different oscillatory regimes in the cortex.

1.3 Astrocytic modulation of neuronal excitability through K^+ spatial buffering

The following review article published in Neuroscience and Biobehavioural Reviews in March 2017 provides a comprehensive introduction to the functional role astrocytes play in network modulation through their K^+ clearance capabilities[305], a theory that was first raised 50 years ago[408].

Neuroscience and Biobehavioral Reviews 77 (2017) 87–97

Contents lists available at ScienceDirect

Neuroscience and Biobehavioral Reviews

journal homepage: www.elsevier.com/locate/neubiorev

Review article

Astrocytic modulation of neuronal excitability through K^+ spatial buffering

Alba Bellot-Saez, Orsolya Kékesi, John W. Morley, Yossi Buskila*

Biomedical Engineering and Neuroscience group, The MARCS Institute, School of Medicine, Western Sydney University, Penrith, NSW, Australia

ARTICLE INFO

Article history:
Received 15 November 2016
Received in revised form 5 March 2017
Accepted 5 March 2017
Available online 6 March 2017

Keywords:
Astrocytic domain
K^+ spatial buffering
Gap junction
Network oscillations

ABSTRACT

The human brain contains two major cell populations, neurons and glia. While neurons are electrically excitable and capable of discharging short voltage pulses known as action potentials, glial cells are not. However, astrocytes, the prevailing subtype of glia in the cortex, are highly connected and can modulate the excitability of neurons by changing the concentration of potassium ions in the extracellular environment, a process called K^+ clearance.

During the past decade, astrocytes have been the focus of much research, mainly due to their close association with synapses and their modulatory impact on neuronal activity. It has been shown that astrocytes play an essential role in normal brain function including: nitrosative regulation of synaptic release in the neocortex, synaptogenesis, synaptic transmission and plasticity. Here, we discuss the role of astrocytes in network modulation through their K^+ clearance capabilities, a theory that was first raised 50 years ago by Orkand and Kuffler. We will discuss the functional alterations in astrocytic activity that leads to aberrant modulation of network oscillations and synchronous activity.

Contents

* Corresponding author at: The MARCS Institute, Western Sydney University, Penrith, NSW, Australia.
E-mail address: Y.buskila@Westernsydney.edu.au (Y. Buskila).

http://dx.doi.org/10.1016/j.neubiorev.2017.03.002

1. Astrocytes are critical regulators of brain circuits

The term *Neuroglia* (nerve-glue) was first introduced in 1856 by Rudolf Virchow, the father of modern pathology. It was further developed in his book *Cellular Pathology* (1858) claiming that it was a "cement that binds the nervous elements together", rather than individual neuroglial cells, reviewed by (Kettenmann and Ransom, 2004), which was in line with the reticular theory claiming that the nervous system is made of a continuous network of nerve processes. It was only a few years later, with the emergence of two pioneering studies, and the neuron doctrine by Ramon y Cajal, that the immense pleomorphism and morphological diversity of glial cells, particularly of astrocytes, was discovered (Cajal, 1897; Navarrete and Araque, 2014).

For many years glial cells were considered to merely provide trophic and structural support, with no relevant contribution to synaptic activity or cognitive functions (Verkhratsky and Butt, 2013). However, numerous studies over the past decade have demonstrated that glial cells are active players in signal processing. Among glial cells, astrocytes have been established to be key participants in the modulation of neuronal network activity, mainly through their uptake of GABA and glutamate, as well as their syncytium like behaviour mediated by the activity of gap junctions (GJs) (Araque et al., 1999; Ma et al., 2016).

In this review we will focus on protoplasmic cortical astrocytes as they form the third part of what has been termed the tripartite synapse, in which a synapse consists of the presynaptic terminal, postsynaptic terminal and an astrocytic process that enwraps both pre- and postsynaptic terminals (Araque et al., 1999), and therefore plays a role in modulating synaptic transmission and network synchrony through their syncytium activity (Newman and Zahs, 1998; Poskanzer and Yuste, 2011). Furthermore, as this is the 50th anniversary of the K^+ spatial buffering hypothesis that emerged from the seminal work of Stephen Kuffler's group (Kuffler et al., 1966; Kuffler and Potter, 1964; Orkand et al., 1966), we will highlight recent advances and ask whether K^+ buffering is a process that is mainly used by the astrocytic network for ion homeostasis, or it is also being used as a mean of promoting hyperexcitability and thus engaging specific network activity.

1.1. Active role of astrocytes in brain function: spatial and functional domains

Ramon y Cajal's original drawings first elucidated the existence of "independent stellate cells" in the cortex, referring to protoplasmic astrocytes with processess showing little overlap (Cajal, 1897). Advances in imaging techniques allowed the visualization of the astrocytic organization into spatial tessellating domains with little overlapping of processes from other astrocytes across different brain areas, including the hippocampus (Bushong et al., 2002; Ogata and Kosaka, 2002) and the cortex (Halassa et al., 2007; Oberheim et al., 2008, 2006).

Although the functional consequences of astrocytic overlapping territories still remain unclear, it has been suggested that astrocytic ***spatial domains*** endow each astrocyte with its own territory to establish autonomous interactions with cohorts of surrounding synapses (Mitterauer, 2010) (Fig. 1). Haydon's group estimated that a single cortical astrocyte enwraps between 4 and 8 neuronal somas and contacts 300–600 neuronal dendrites (Halassa et al., 2007). Following these observations, they proposed the concept of "functional islands of synapses", in which clusters of synpases confined within the astrocytic domain are modulated by the gliotransmitter environment controlled by that particular astrocyte. Loss of astrocytic spatial domain organization has been associated with gliosis and recurrent excitation in epileptic murine models (Oberheim et al., 2008), and increase in overlapping astrocytic territories correlated with aging (Grosche et al., 2013).

Further to their anatomical organization into spatial domains, the membrane of single protoplasmic astrocytes has ***functional domains*** (Bushong et al., 2002). The first functional domain consists of a large portion of the astrocytic membrane that sends multiple processes to enwrap the neuronal presynaptic and postsynaptic terminals, as part of the tripartite synapse (Araque et al., 1999). Another functional domain forms a neurovascular unit through specialized processes called endfeet, which ensheath blood capillaries and some reach to the pial surface, where they form subpial endfeet (Nagelhus et al., 1999; Simard et al., 2003), as noted in some of the earliest descriptions by Cajal and Golgi (Navarrete and Araque, 2014). Astrocytic-mediated neurovascular coupling is crucial for the formation and maintenance of the blood-brain barrier that supplies neurons with essential nutrients and releases the excess of neurotransmitters and toxic molecules into the bloodstream (Abbott et al., 2010). Recently it has been shown that astrocytes also play a role in waste removal from the CNS as part of the glymphatic system, in which the cerebrospinal fluid (CSF) enters the brain parenchyma to remove interstitial fluid and extracellular solutes (Jessen et al., 2015). This macroscopic waste clearance system is facilitated by astrocytic aquaporin-4 (AQP-4) water channels, suggesting the flow via influx and efflux routes are supported by astrocytic water transport (Iliff et al., 2012). The role of AQP-4 in K^+ clearance has been suggested by the Ottersen group (Nielsen et al., 1997) and we refer the reader to a recent review about the role of AQP-4 in K^+ homeostasis (Nagelhus and Ottersen, 2013).

The strategic location and organization of astrocytes in the cortex into specific domains allows them to take part in all aspects of brain physiology, including blood flow regulation (Paulson and Newman, 1987), synaptic transmission (Buskila and Amitai, 2010), metabolic regulation (Tsacopoulos and Magistretti, 1996), maintenance of ion homeostasis (Wallraff et al., 2006) and waste removal (Iliff et al., 2012). Furthermore, neuronal-astrocytic interactions permit local regulation of neuronal excitability, which is crucial to synchronize local synaptic activity during normal brain development and function (Nedergaard et al., 2003). Therefore, disturbances in astrocytic morphology or domain organization likely impact synaptic transmission, which can lead to abberant functionality at the network level (Oberheim et al., 2008).

1.2. Astroglial communication: GJ-mediated networks

Much of our current knowledge about glial physiology is due to the pioneering work of Stephen Kuffler, David Potter, John Nicholls and Richard Orkand, who extensively studied the glial properties in the leech and mudpuppy optic nerve. In 1964, Kuffler and Potter were first to report on "low resistance connections" that form "bridges that connect the glial cells to one another" (Kuffler et al., 1966; Kuffler and Potter, 1964), which was a milestone in recognising that astrocytes function as a syncytium.

Ultrastructural observations with electron microscopy, and later electrophysiological and dye coupling studies, showed that mature protoplasmic astrocytes are electrically coupled through GJs formed by two directly opposing hemichannels that connect the cytoplasm of adjacent cells, forming the bridges formerly reported by Kuffler's group (Axelsen et al., 2013).

Mammalian GJs are composed of the connexin, innexin and pannexin families of transmembrane proteins. The membrane proteins connexin 30 and 43 (Cx30 and Cx43) are highly expressed in mature protoplasmic astrocytes, and typically assembled in packed hexameric rings or connexons to form the complete channels (Hofer and Dermietzel, 1998). Previous work on astrocytic coupling failed to differentiate between astrocytic and neuronal GJs, mainly due to

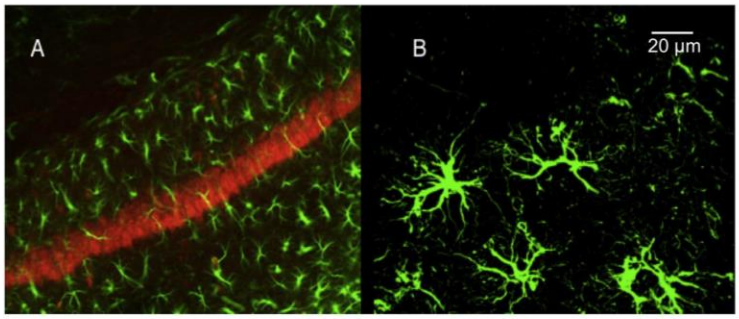

Fig. 1. Protoplasmic astrocytes are organized into spatial domains. Confocal images of glial fibrillary acidic protein (GFAP) staining in the hippocampus (A) and cortex (B) show non-overlapping astrocytic spatial domains (green). Neuronal somata stained with NeuN in the hippocampus is shown in red. (For interpretation of the references to colour in this figure legend, the reader is referred to the web version of this article.)

lack of selective astrocytic GJ blockers (Wallraff et al., 2006). However, the advent of more specific mimetic peptides derived from the intracellular (*e.g.* GAP-19) or extracellular loops (*e.g.* GAP-26, GAP-27) of Cx43 in astrocytes, together with the development of genetically modified mice and imaging techniques, have allowed researchers to specifically address the role of astrocytic GJs in brain circuits, including the hippocampus (Samoilova et al., 2008; Theis et al., 2003; Wallraff et al., 2006) and the cortex (Abudara et al., 2014; Dermietzel et al., 2000).

Combination of dye-coupling experiments and immunostaining with sulforhodamine B to stain astrocytes, showed that the expression of Cx43 and Cx30 proteins is enriched in the barrel cortex and that GJ communication is restricted from one barrel to its neighbour, suggesting preferential orientation of coupling between astrocytes that contributes to shaping panglial astrocytic networks (Houades et al., 2008). Furthermore, using mice with genetically uncoupled astrocytes in the hippocampus, Wallraff and colleagues showed that astrocytic GJs accelerate K^+ clearance from the extracellular space and limit K^+ accumulation during synchronized neuronal firing (Wallraff et al., 2006). Similarly, it has been reported that double knockout (KO) mice for Cx43 and Cx30 had a complete lack of astrocytic GJ coupling (Theis et al., 2003), altered energy metabolite trafficking (Rouach et al., 2008) and parenchymal vacuolation (Lutz et al., 2009).

Astrocytic GJs also play a crucial role in extracellular ion (*e.g.* Na^+, K^+, Ca^{2+}) homeostasis (Rose and Ransom, 1997), and strong GJ coupling has been recently shown to provide isopotentiality to the astrocytic network by minimizing the membrane potential depolarization that follows increased levels of K^+, thus maintaining the K^+ inward driving force which is critical for efficient astrocytic control of brain homeostasis (Ma et al., 2016).

1.3. Astrocytes as network modulators: oscillations and synchrony

The building units of neuronal oscillations are network-driven fluctuations in the neuronal membrane potential known as 'up' or rising states, and 'down' or falling states (Sanchez-Vives and McCormick, 2000). During 'up states' individual neurons are depolarized for up to hundreds of milliseconds, which may lead to propagating waves of activity spreading throughout the cortex (Cossart et al., 2003), and likely play a role in the synchronization of distant cortical territories to produce coherent network activity (Fries, 2005). However, little is known about how these mechanisms interact to mediate transitions between different oscillatory regimes within the cortex.

Several factors have been suggested to affect the neuronal bursting activity underlying the generation of network oscillations, including activation of intrinsic conductances by neuromodulation, influence of dendritic structure, and changes in extracellular ions (Buzsaki, 2006; Buzsáki and Draguhn, 2004), but it is only in the last decade that astrocytes have been reported to play a role in synchronisation of neuronal activity and network oscillations (Carmignoto and Fellin, 2006; Fellin et al., 2004; Poskanzer and Yuste, 2016).

Several studies suggested that the glial synchronisation of neural networks can be mediated through gliotransmission. Using calcium imaging with electrophysiological recordings from CA1 pyramidal neurons, two independent groups found that neuronal synchrony in the hippocampus is partially mediated through Ca^{2+}-dependent release of glutamate (Angulo et al., 2004; Fellin et al., 2004), which activate extrasynaptic NMDA receptors. Carmignoto and Fellin have further suggested that astrocytes in the hippocampus may work as "excitatory interneurons" that promote the synchronous activity of a distinct set of neurons (Carmignoto and Fellin, 2006). However, the fast time scale of neural synchronization (100 ms) casts doubt on the involvement of calcium waves spreading through the glial network (Angulo et al., 2004).

Glutamate release from astrocytes is mediated through six different processes (Malarkey and Parpura, 2008), including a non-vesicular mechanism that involves the reverse activation of glutamate transporters and calcium dependent vesicular release through voltage gated calcium channels (VGCC). As glutamate uptake through glutamate transporters is affected by extracellular K^+ concentration as well as astrocytic depolarization (Szatkowski et al., 1990), it is plausible that local alterations of K^+ buffering by astrocytes results in exceptionally high concentrations of $[K^+]_o$ and local astrocytic depolarization, leading to inverse glutamate uptake and vesicular glutamate release which then leads to synchronous activity of the nearby neurons (Szatkowski et al., 1990; Yaguchi and Nishizaki, 2010). In line with this suggestion, *in vivo* experiments using transgenic mice, in which astrocytic Ca^{2+}-dependent vesicular release of glutamate was blocked by tetanus neurotoxin (TeNT), showed a marked reduction in cortical gamma oscillations, while neuronal synaptic activity remained intact (Lee et al., 2014).

Recently, Sasaki and colleagues showed that neural depolarization is driven by the astrocytic syncytium, rather than activation of sporadic astrocytes (Sasaki et al., 2011), as only cluster activity of astrocytes in both hippocampus and cortex led to depolarization of the dendrites in their vicinity. Consistent with this idea, Nathalie Rouach's group showed that a syncytium of gap junction-coupled astrocytic networks can modulate synaptic strength and plasticity through facilitation of glutamate and K^+ removal during synaptic activity (Pannasch et al., 2011). Furthermore, the astrocytic syncytium promotes bursts of neuronal networks by increasing neuronal release probability and favouring the recruitment of neuronal assemblies (Chever et al., 2016). Moreover, McCarthy's group

demonstrated that K^+ redistribution through astrocytes enhances GJ conductance, suggesting that K^+ buffering increases the number of coupled astrocytes within the astrocytic syncytium (Enkvist and McCarthy, 1994). Consistently, electrophysiological and Ca^{2+} imaging experiments in neocortical slices showed that electrical stimulation of a single astrocyte activates other astrocytes of the surrounding local network, and also triggers 'up-state' synchronizations of neighbouring neurons (Poskanzer and Yuste, 2011). These reports imply that K^+ redistribution through astrocytes impact the extent of astrocytic syncytium which mediate, in part, neural synchronisation.

Altogether, these studies support that alterations in astrocytic regulatory mechanisms, including K^+ spatial buffering, could lead to aberrant modulation of both synaptic transmission and network synchronisation, which is also accompanied by impaired behavioral performance (Lee et al., 2014).

2. Astrocytic K^+ modulation of neuronal excitability

Extracellular K^+ is critical in defining the resting membrane potential of neurons and astrocytes, and is normally maintained at ~3 mM (Somjen, 1979). Neuronal activity within the physiological range leads to local increases of less than 1 mM in the extracellular concentration of K^+ ($[K^+]_o$) and up to 10–12 mM during excessive activity (seizures) in the cortex, known as the ceiling or plateau level, which influences synaptic transmission and plasticity (Heinemann and Dieter Lux, 1977). Once the plateau state of $[K^+]_o$ accumulation has been reached, no further rise in $[K^+]_o$ will occur despite continued electrical stimulation, indicating that during normal brain function, K^+ is rapidly removed by active transport from the synaptic cleft through K^+ clearance mechanisms, as originally hypothesized by Leif Hertz (Hertz, 1965), and further developed by Orkand, Nicholls and Kuffler (Orkand et al., 1966). Effective removal of K^+ from the extracellular space is vital for maintaining brain homeostasis and likely limits network hyperexcitability during normal brain function, as disruptions in K^+ clearance have been linked to pathological conditions, including epilepsy ($[K^+]_o > 15$ mM) (David et al., 2009), spreading depression ($[K^+]_o = 30–80$ mM) (Somjen, 2002), and cell death after prolonged ischemia (Leis et al., 2005).

2.1. Astrocytic K^+ clearance mechanisms

In his pioneering work, Hertz suggested that reuptake of $[K^+]_o$ is mediated through the Na^+-K^+-ATPase (NKA), as addition of K^+ doubled the respiration levels in brain slices (Hertz, 1965). Hertz speculated that neuroglial cells possess a great capacity for ion transport, which is stimulated by an increased concentration of K^+. A year later, Orkand, Kuffler and colleagues published their work assessing the membrane properties of glial cells in the optic nerve of the mudpuppy. Consistent with Hertz's hypothesis, their experiments demonstrated that glial cells show high permeability for K^+ ions and impulses in nerve fibers led to changes in the $[K^+]_o$ and caused a slow depolarization of the membrane potential in the surrounding glial cells (Kuffler et al., 1966; Orkand et al., 1966). Two decades later, astrocytes were found to be the key mediators of extracellular K^+ clearance in the olfactory cortex (Ballanyi et al., 1987) and K^+ siphoning in the retina (Newman et al., 1984).

Two mechanisms for K^+ clearance have been established: net K^+ uptake and K^+ spatial buffering, and their role in modulating neuronal excitability has been the focus of extensive research over the past decades (Kofuji and Newman, 2004).

2.1.1. Net K^+ uptake: role of NKA pump and NKCC cotransporter

In the cerebral cortex, net K^+ uptake is primarily mediated by the astrocytic NKA, as shown by early experiments in both cultured astrocytes (Hajek et al., 1996) and in brain slices (Schousboe and Hertz, 1971). The NKA is a transmembrane enzyme acting as an electrogenic pump that drives out three Na^+ ions in exchange for two K^+ ions into the cell, against their concentration gradient, which is essential for maintaining Na^+ and K^+ gradients across the neuronal and astrocytic membranes (Crambert and Geering, 2003). Due to different combinations of α and β subunits isoforms of NKA in neurons and astrocytes, their kinetic characteristics and binding affinity are different, allowing astrocytes to respond faster to the immediate release of K^+, reviewed by (Larsen et al., 2016). Hence, during normal brain activity, the astrocytic NKA temporarily sequesters the residual K^+ ions (≤10 mM), leading to decreased $[K^+]_o$ and neuronal hyperpolarization (Orkand, 1986; Orkand et al., 1966).

When higher extracellular increases in $[K^+]_o$ take place (10–12 mM), the astrocytic NKA is assisted by the Na^+-K^+-$2Cl^-$ cotransporter (NKCC), which utilizes the Na^+ electrochemical gradient to transfer Cl^-, K^+ and Na^+ ions along with water influx through the membrane, thereby resulting in overall astrocytic swelling (Walz and Hertz, 1984). Hence, cellular swelling has been used as a marker of astrocytic net K^+ uptake.

Recently, Xu and colleagues (Xu et al., 2013) showed that astrocytic net K^+ uptake through NKA is abolished after glycogenolysis inhibition, indicating that astrocytic K^+ uptake pathways may require glycogenolytically provided energy for correct functioning. The authors speculated that such a mechanism would allow astrocytes to start accumulating excess of $[K^+]_o$, as long as glycogen is supplied, and once absent, other processes (*e.g.* K^+ spatial buffering) restore the $[K^+]_o$.

2.1.2. K^+ spatial buffering: role of GJ-coupled networks and K_{ir} channels

The fact that astrocytes are electrically coupled through extensive GJ-mediated networks, together with their high permeability for K^+ ions, allowed Kuffler and colleagues to postulate a second mechanism for astrocytic K^+ clearance, which involved transferring K^+ ions from areas where K^+ is high to regions with lower $[K^+]_o$ without additional energy requirements (Orkand et al., 1966). They coined the term "Spatial buffering", which has been the focus for many studies since then. According to the spatial buffering hypothesis, during basal conditions ($[K^+]_o = 3$ mM; $[K^+]_i = 130$ mM), the astrocytic resting membrane potential is typically less negative than the equilibrium potential for K^+ ($V_k \sim -95$ mV), ranging from −60 mV to −85 mV, which facilitates an outwardly directed driving force for K^+ (Buskila et al., 2007, 2005; Ma et al., 2014; McKhann et al., 1997; Tong et al., 2014). Elevated $[K^+]_o$ at the synaptic cleft drives V_K towards more positive potentials, leading to depolarization of the astrocytic membrane potential (Fig. 2A). However, K^+ influx requires the astrocytic membrane potential to be more negative than the V_K. To face this challenge during K^+ spatial buffering, astrocytes use the collective astrocytic membrane of the GJ-coupled network to provide isopotentiality to the astrocytic network, as recently reported by (Ma et al., 2016). Hence, by minimizing the local membrane potential depolarization that follows increased levels of K^+, astrocytes maintain the local K^+ inward driving force in areas with high K^+, and increase K^+ release in distant regions (Ma et al., 2016), which is critical for efficient astrocytic control of K^+ homeostasis as illustrated in Fig. 2B.

The conditions for passive K^+ influx and efflux were analysed by Gardner-Medwin, who described the spatial buffering as a space-dependent process (Gardner-Medwin, 1983a). Using the constant field equation to measure V_m, and the Nernst potential for K^+ (V_k) at different areas along the buffering axis, and assuming that extracellular diffusion is augmented by the spatial buffer mechanism, they have built a simple model for transcellular K^+ flux, which was in agreement with both the time course and the distribution of the

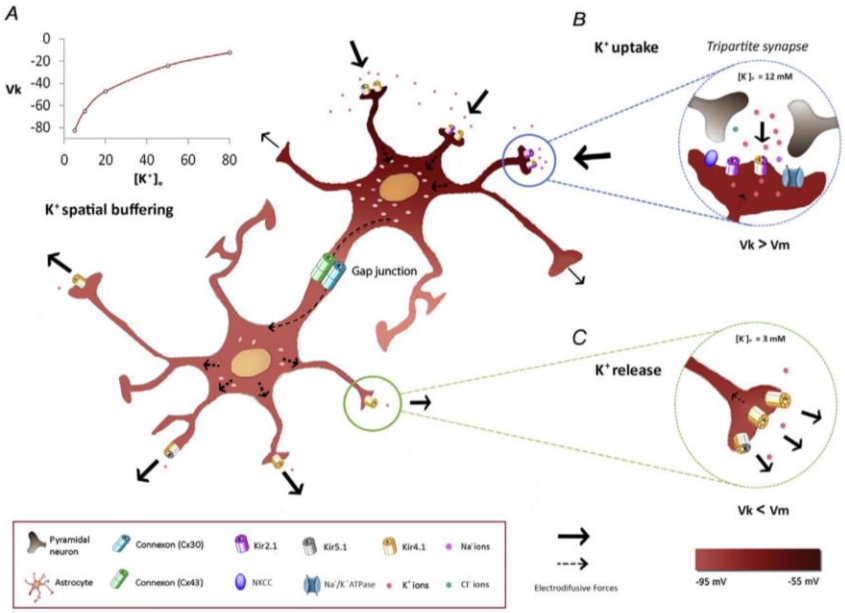

Fig. 2. Astrocytic modulation of neuronal networks. A) Plot showing changes in the V_k (mV) following increases in the $[K^+]_o$ (mM), as calculated from the Nernst equation (T = 20 °C; $[K^+]_i$ = 130 mM). B) Schematic diagram describing the three mechanisms taking place during K^+ buffering immediately after $[K^+]_o$ stress. Top-right inset – Neuronal firing leads to local increase of the $[K^+]_o$ (~12 mM), which transiently renders the V_k in the astrocytic process surrounding the synaptic cleft to −60 mV. Although under these conditions the GHK equation predicts a 25.4 mV depolarization to −56 mV (PCl = 0; PNa/Pk = 0.015; $[K^+]_o$ = 3 mM; $[K^+]_i$ = 130 mM; $[Na^+]_o$ = 145 mM; $[Na^+]_i$ = 15 mM; $[Cl^-]_o$ = 135 mM; $[Cl^-]_i$ = 5 mM;), due to strong GJ-coupling which forms isopotentiality, the proximal astrocytic membrane potential depolarisation is attenuated to ~5 mV and therefore becomes more negative than the V_K, which leads to inward current of K^+ as reported by (Ma et al., 2016). Eventually, this K^+ increase flows intracellulary through GJ-connected astrocytes and promotes a distal outward current to the extracellular space, where K^+ is low (~3 mM) as shown in the lower inset. Arrows indicate the direction of K^+ driving force.

observed $[K^+]$ (Gardner-Medwin, 1983a; Orkand, 1986). Using this model they have shown that following local $[K^+]_o$ elevations, the proximal astrocytic membrane potential depolarize towards the V_k, however because it is electrically connected to regions of membrane where $[K^+]_o$ is not raised, it does not reach the new V_k values, and thus mediates passive K^+ influx into the astrocyte. Consistent with their results, Ma and colleagues demonstrated that astrocytic membrane potential *in situ* does not follow the estimated membrane potential calculated by the constant field equation, mainly due to syncytial isopotentiality that reduces astrocytic depolarization following local increase of $[K^+]_o$ (Ma et al., 2016).

Based on reanalysis of Gardner-Medwin's mathematical model, Chen and Nicholson built a two compartment model to describe the transient profiles of ionic concentrations (Chen and Nicholson, 2000). Using this simplified linear model, they have shown that the maximal current at the endfoot depends on the distribution and asymmetrical activity of K_{ir} channels along the astrocytic membrane, which occurs when the glial geometric length is equal to the corresponding electrotonic space constant.

In a recent electrodifussive model, which constantly updated the intracellular and extracellular K^+ concentrations, Halnes and colleagues showed that despite the existence of a small outwardly directed K_{ir} current, the minimization of the membrane potential depolarization that follows increased levels of K^+, together with the K^+ current driven by the astrocytic NKA pump, allow astrocytes to maintain a net local K^+ inward current and transport it intracellularly until it was released back to the extracellular space in distal areas (Halnes et al., 2013).

The spatial buffering hypothesis has been supported by many experiments, however, its relative contribution to the overall K^+ clearance process is still debatable, as reviewed by Macaulay and Zeuthen, 2012.

2.1.3. Role of GJ-coupled networks

Early support for K^+ spatial buffering in the rat cortex was provided by Gardner-Medwin (Gardner-Medwin, 1983a, 1983b, 1983c) who showed that $[K^+]_o$ varies with depth and time in a manner consistent with transcellular transfer of K^+ ions. Further dye-coupling experiments in cultured cortical astrocytes demonstrated that membrane depolarization as a result of increased $[K^+]_o$ enhanced GJ conductance, suggesting that K^+ could facilitate its own buffering by increasing the degree of coupled astrocytes in the network (Enkvist and McCarthy, 1994). On the other hand, a genetic deletion of astrocytic GJs showed that in the stratum radiatum, GJ-mediated currents represented only 30% of the overall astrocytic conductance and K^+ clearance was only slightly reduced (Wallraff et al., 2006), suggesting only a partial role for GJ-coupled networks during astrocytic K^+ spatial buffering. They further showed that K^+ distribution was significantly smaller in the stratum lacunosum moleculare of the transgenic mice, suggesting unequal contribution of GJs to radial transport of $[K^+]_o$ within hippocampal layers.

2.1.4. Role of K_{ir} channels

Pharmacological studies suggest an important role for K^+ inwardly rectifying (K_{ir}) channels in K^+ spatial buffering. K_{ir} channels consist of 16 channels divided into seven subfamilies ($K_{ir1.x}$-$K_{ir7.x}$), which share similar membrane topology, and are characterised by an asymmetric conductance that reduces with membrane depolarization, while increases with hyperpolarization (Kubo et al., 1993).

At potentials above V_k, a voltage-dependent block by polyamines (*e.g.* spermine) or intracellular Mg^{2+} plug the channel pore, resulting in decreased outward currents or inward rectification (Lopatin et al., 1995). As a result, K_{ir} channels show high open probability and large inward K^+ conductance that contributes to

hyperpolarized membrane potentials (negative to V_k) required for K^+ spatial buffering.

A special case of spatial buffering has been demonstrated in individual retinal Mülller cells, a process termed K^+ siphoning (Newman et al., 1984). In a series of studies performed by Eric Newman's group, it was shown that efflux of K^+ from the endfeet of dissociated salamander Müller cells occurred almost concurrently with K^+ influx from the distal end of the Müller cell surface and was driven by an electromotive rather than a diffusional force (Newman et al., 1984). Furthermore, light-evoked changes in $[K^+]_o$ lead to K^+ accumulation in the vitrous humour and did not affect K^+ increases in the inner plexiform layer (Karwoski et al., 1989), supporting the hypothesis of K^+ "siphoning" by Müller cells to the vitreous humor (Newman et al., 1984; Newman, 1987).

The impact of K_{ir} channels on spatial buffering was also seen in acute slices from the olfactory cortex, where Ballanyi and colleagues showed that the selective K_{ir} channel blocker Barium (Ba^{2+}) inhibits K^+ influx in astrocytes (Ballanyi et al., 1987). Furthermore, Kivi and colleagues reported that in human hippocampal slices taken from patients with temporal lobe epilepsy, Ba^{2+} augmented the rises in $[K^+]_o$ and prolonged the recovery, suggesting a significant contribution of K_{ir} channels to K^+ spatial buffering (Kivi et al., 2000).

These early observations prompted other groups to validate the specific role of astrocytic K_{ir} channels, specifically $K_{ir4.1}$, which has been postulated to be largely responsible for mediating the astrocytic K^+ spatial buffering, both *in situ* and *in vivo*, reviewed by (Larsen and Macaulay, 2014). Ba^{2+} blockade (100 μM) or RNAi-mediated knock-down of $K_{ir4.1}$ channels resulted in inhibition of glutamate uptake and impaired transmembrane K^+ flow in cultured cortical astrocytes (Kucheryavykh et al., 2007). Further experiments using glial-conditional $K_{ir4.1}$ KO mice have reported astrocytic membrane depolarization and impaired K^+ clearance following synaptic activity (Djukic et al., 2007) as well as epileptical activity (Haj-Yasein et al., 2011). Recently, a tri-compartment computational model assessing K^+ dynamics between neurons, astrocytes and the extracellular space showed that astrocytic $K_{ir4.1}$ channels are responsible and sufficient to mediate astrocytic membrane depolarization and K^+ clearance within 6–9 s following neuronal activity (Sibille et al., 2015).

Although numerous studies support $K_{ir4.1}$ channels as fundamental in maintaining K^+ homeostasis (Haj-Yasein et al., 2011), their contribution to K^+ clearance has been questioned, as some reports have failed to observe a significant contribution of $K_{ir4.1}$ channels to the astrocytic K^+ clearance in different brain areas, such as the optic nerve (Ransom et al., 2000) and the dentate gyrus (Xiong and Stringer, 2000). More recent studies have shown that $K_{ir4.1}$ channels account for approximately 45% of the K^+ buffering capacity of mature hippocampal astrocytes (Kiyoshi et al., 2015). These results suggest that the relative importance of K^+ homeostatic mechanisms differs depending on the brain region and on the $K_{ir4.1}$ channel expression levels.

Aside from the $K_{ir4.1}$ channel, astrocytes express other members of the K_{ir} family, namely $K_{ir5.1}$ and $K_{ir2.1}$ channels. Although the contribution of the different K_{ir} channels to spatial buffering is not conclusive, their distinct biophysical properties enable them to take part in a diverse range of functions. Electrophysiological recordings showed that $K_{ir2.1}$ (Kubo et al., 1993) and $K_{ir2.3}$ (Lagrutta et al., 1996) are more likely to drive K^+ influx, as they show steep inward current once $V_m < V_k$ and minimal outward current when $V_m > V_k$. Conversely, $K_{ir4.1}$ channels are weekly rectifying and thus more likely to mediate K^+ efflux (Lagrutta et al., 1996). However, K_{ir} channels are often expressed as heteromeric channels with different biophysical properties than the homomeric channels, which adds further complexity (Isomoto et al., 1997).

Using an immunohistochemical approach, Kofuji and colleagues (Kofuji et al., 2002) showed that in the mouse retina, $K_{ir2.1}$ channels were located predominantly in the membrane domains facing synapses, while $K_{ir4.1}$ channels were found to be expressed at high densities in the endfoot membrane. The authors speculated that $K_{ir2.1}$ channels mediate K^+ influx, while $K_{ir4.1}$ channels are mainly responsible for K^+ efflux in Müller cells. Consistent with Kofuji's model, Butt and Kalsi proposed that $K_{ir4.1/Kir5.1}$ channels, together with $K_{ir4.1/Kir2.1}$ channels and homomeric $K_{ir2.1}$ channels mediate K^+ uptake close to neuronal synapses, which then travels via GJ-coupled networks to distal areas where K^+ is low, where it is sinked via homomeric $K_{ir4.1}$ channels (Butt and Kalsi, 2006).

In cortical astrocytes, heteromeric $K_{ir4.1/5.1}$ channels and homomeric $K_{ir4.1}$ channels are expressed in a region-specific fashion. While heteromeric $K_{ir4.1/5.1}$ channels have been identified in both neocortex and olfactory bulb, homomeric $K_{ir4.1}$ channels were confined to the hippocampus and thalamus, suggesting region-specific differential contributions to K^+ spatial buffering during physiological activity (Hibino et al., 2004).

2.2. Impact of astrocytic K^+ spatial buffering on neuronal oscillations

The strategic location of cortical astrocytes as part of the tripartite synapse allows bidirectional interaction between neurons and astrocytes to efficiently control $[K^+]_o$. This may be viewed as a protective mechanism to prevent toxic accumulation of K^+ at the synaptic cleft, but also as a means to rapidly modulate neuronal synchronization and network activity, as suggested by (Wang et al., 2012b). Furthermore, Sylantyev and colleagues showed that local electrical fields generated by synaptic currents flowing through AMPA receptors are voltage dependent, and can tune the excitatory synaptic response by altering the dwell time of charged neurotransmitters such as glutamate (Sylantyev et al., 2008). Thus, changes of $[K^+]_o$ due to alterations in astrocytic K^+ clearance mechanisms are likely to influence local electrical fields and thus shape synaptic current waveforms, ultimately impacting on the integration and synchronization of the whole network (Amiri and Hosseinmardi, 2013). Moreover, a recent computational model showed that regulation of local $[K^+]_o$ clearance during basal and repetitive firing modulates slow neural oscillations (Sibille et al., 2015).

We would like to extend this view and suggest that excessive K^+ accumulation at the synaptic cleft modifies the neuronal membrane potential and therefore alters the neuronal resonance frequency, which has been reported to be dependent on the interplay between K^+ and Na^+ currents (Gutfreund et al., 1995), thereby affecting the transition between dominant subthreshold frequencies and network oscillations. In support of this idea, Segev's group reported that K^+ current kinetics are sufficient to produce resonance frequency behaviour in neurons (Gutfreund et al., 1995). Moreover, Amzica and colleagues performed *in vivo* simultaneous recordings from neurons and glia, together with extracellular K^+ and Ca^{2+} measurements in the cortex to assess the role of K^+ spatial buffering in modulating neuronal oscillations. Their results demonstrated that astrocytes mediated local K^+ clearance during the depolarization phase of slow sleep oscillations, whereas K^+ redistribution was faster and reached further cortical areas during spike-wave seizures, indicating that K^+ spatial buffering likely mediates synchronization and spreading of paroxysomal oscillations (Amzica et al., 2002). Furthermore, Ding and colleagues found that $[K^+]_o$ is increased during arousal state and reduced during sleep state, while the extracellular volume as well as the Ca^{2+}, Mg^{2+} and H^+ concentrations showed the opposite behaviour during sleep-wake cycle *in vivo* (Ding et al., 2016). Pannasch and colleagues (Pannasch et al., 2011) demonstrated that GJ-coupled astrocytic networks control synaptic strength and plasticity, as alterations in Cx30 and Cx43

led to increased synaptic activity due to the inability of uncoupled astrocytes to redistribute glutamate and K^+ during synaptic activity. Consistently, astrocytic GJ's have been proposed to promote coordinated bursts of neuronal networks by favouring the recruitment of neuronal assemblies, which developed into epileptiform events *in vivo* (Chever et al., 2016).

Further support comes from computational and mathematical models, which have been developed to assess the impact of astrocytic K^+ regulation on neuronal excitability in the cortex. Using a model of a neocortical circuit with extracellular K^+ dynamics, Fröhlich and colleagues showed that alterations in $[K^+]_o$ are capable of modulating neuronal activity and mediate slow transitions between tonic and phasic neuronal oscillations (Fröhlich et al., 2006). They further suggested that the wide dynamic oscillation repertoire of cortical networks is based on multistabilities, which are intrinsic to the network and depend on the effectiveness of K^+ regulation. These results further indicate that the positive feedback mechanism of the extracellular K^+ dynamics can stabilize cortical network oscillations (Fröhlich et al., 2010). Other network models predicted that the transition between stable to perturbed oscillation states within the network is mediated by glial activity, as seizure-like activity was observed when glial cells were unable to maintain extracellular ionic homeostasis (Ullah et al., 2009).

The regulation of neural oscillations by astrocytes is also supported by a recent computational simulation of cortical networks developed by Kuriu and colleagues (Kuriu et al., 2015), which showed that astrocytes induced depolarization in neighbouring neurons that lasted for hundreds of milliseconds and led to synchonized 'up states'. This phenomenon was previously reported in neocortical slices (Poskanzer and Yuste, 2011), in which electrical stimulation of a single astrocyte activated other astrocytes in their vicinity and triggered Ca^{2+}-dependent 'up state' synchronizations of neighboring neurons. Using *in vivo* Ca^{2+} imaging, Poskanzer and Yuste recently showed that astrocytic Ca^{2+} activity precedes circuit shifts that dominate the slow-oscillation state (Poskanzer and Yuste, 2016), suggesting a link between astrocytic Ca^{2+} oscillations and transient glutamate release. Although the authors did not check K^+ concentrations, a previous *in vivo* study reported that Ca^{2+} oscillations are correlated to K^+ spatial buffering activity in astrocytes (Amzica et al., 2002), thereby implying a role for K^+ spatial buffering in generating cortical 'up states' in neuronal networks. The exact molecular mechanism that connects Ca^{2+} activity with K^+ spatial buffering remains to be elucidated.

3. Astrocytic alterations in network disorders

Alterations in normal astrocytic physiology have been associated with several neuropsychiatric, neurodevelopmental, and neurodegenerative diseases (Verkhratsky et al., 2016). In the present review, we have focused on brain disorders associated with defective astrocytic K^+ clearance mechanisms (Table 1), as they likely contribute to modifications of the overall network synchronous activity, and therefore should be considered as future therapeutic targets for restoring compromised neuronal network excitability.

3.1. K^+ clearance perturbations in epilepsy

Epileptic seizures occur when a group of neurons fire in a synchronous and excessive manner (neural hyperexcitability), resulting in burst like activity that spreads across the cortex. As K^+ currents play an essential role in modulating neuronal activity, it has been suggested that under conditions of enhanced neuronal activity, K^+ accumulation in the extracellular space results in local neuronal depolarization, which if not removed could trigger the onset of epileptic seizures (David et al., 2009). Indeed, early experiments by Penfield and colleagues (Penfield, 1927), found that glial scars are the source of ictal activity that develops after anoxic or traumatic brain injury. Later studies showed alterations in K^+ buffering in astrocytes from glial scars (Bordey and Sontheimer, 1998; Kivi et al., 2000), indicating a plausible mechanism involving abnormal K^+ buffering activity. Consistently, studies have reported altered expression, localization and function of astrocytic $K_{ir4.1}$ channels in brain tissue from epileptic patients (Bockenhauer et al., 2009; Buono et al., 2004; Heuser et al., 2012; Schroder et al., 2000)

Another plausible mechanism for alteration of K^+ homeostasis is a modification of astrocytic coupling through GJs, which allows redistribution of K^+ to distant cortical areas. Hence, excessive accumulation of $[K^+]_o$ could lead to synchronized neuronal depolarizations mediated by astrocytic GJ-coupled networks in the cortex, which under atypical conditions may contribute to circuit hyperexcitability and epileptic seizures. However, the impact of astrocytic coupling on epileptical activity is still controversial. On one hand, selective blockade of GJ-mediated astrocytic communication using Cx43 mimetic peptides leads to a dose-dependent neuroprotective effect against epileptiform activity, indicating that specific astrocytic GJ blockers could serve as a potential therapeutic treatment for epilepsy (Samoilova et al., 2008; Yoon et al., 2010). Furthermore, experiments performed in slices from epileptic patients using the selective Cx43 activator GAP-134, which facilitates the opening of astrocytic GJs, demonstrated that increased astrocytic coupling enhanced the frequency of epileptic activity (Gigout et al., 2016). On the other hand, astrocytic uncoupling likely leads to impairments of K^+ buffering, and has been proposed to cause seizures and neuronal death in patients with mesial temporal lobe epilepsy with sclerosis, as well as in animal models of epilepsy (Bedner et al., 2015). This controversy might be due to different phases of the hyperexcitable network. While astrocytic coupling is important to prevent prolonged local depolarization and initiation of ictal activity by buffering the $[K^+]_o$, once epileptic activity has started, astrocytic coupling might serve as a tool to ease the propagation of this synchronous activity.

3.2. K^+ clearance perturbations in other neurological diseases

Loss-of-function mutations in the methyl CpG binding protein 2 (MECP2) gene cause Rett syndrome, which is an autistic spectrum disorder (ASD) characterized by seizures, ataxia and breathing instability, together with learning and motor impairments (Turovsky et al., 2015). Recent data suggests that MeCP2 protein positively modulates $K_{ir4.1}$ gene transcription (Olsen et al., 2015), and mutations in the KCNJ10 gene, encoding for $K_{ir4.1}$ channels, have been found in both epileptic and ASD patients (Sicca et al., 2011), implying that dysfunction of astrocytic K^+ buffering could be a common mechanism contributing to seizures and abnormal synaptic function, as recently suggested by (Guglielmi et al., 2015).

Other network disorders associated with alterations in K^+ spatial buffering also involve reactive astrocytes, in which there is a loss of astrocyte polarization, as well as decreased functional expression of astrocytic $K_{ir4.1}$ channels. Defective extracellular K^+ clearance mechanisms have also been observed in experimental models of Amyotrophic Lateral Sclerosis (Kaiser et al., 2006), Alzheimer's disease (Olabarria et al., 2010; Yang et al., 2011), Huntington's Disease (Tong et al., 2014), Familial hemiplegic migraine type 2 (Capuani et al., 2016), and Hyperammonemia (Thrane et al., 2013), as summarized in Table 1.

4. Conclusions

This year marks the 50th anniversary of the first proclamation of the K^+ spatial buffering hypothesis by Kuffler and colleagues.

Table 1
Neuronal network disorders associated with alterations in astrocytic K+ regulatory mechanisms.

Disorder	K^+ Disturbances	Models	Phenotype	References
Epilepsy	Loss of $K_{ir4.1}$ protein Decreased K_{ir} currents	$K_{ir4.1}$ KO mice $K_{ir4.1}$ cKO mice	Severe seizures Hyperexcitability	Coulter and Steinhauser (2015)
Rett syndrome	Increased $K_{ir4.1}$ protein expression	*Mecp2* KO mice	Breathing anomalies	Turovsky et al. (2015)
Amyotrophic lateral sclerosis	Loss of EAAT2 SOD1 mutations Loss of $K_{ir4.1}$ channels	SOD1 (G93A) mice	Impaired perineural K^+ homeostasis Motor neuron loss	Kaiser et al. (2006)
Alzheimer's disease	Impaired K^+ homeostasis Loss of astrocyte polarization	3xTg-AD mice	Reduced GFAP levels Astrocyte hypertrophy Amyloid deposits	Olabarria et al. (2010)
Huntington's disease	Reduced $K_{ir4.1}$ protein expression Disturbed K^+ buffering	R6/2 mice	Motor impairments Depolarized membrane potentials Lower conductances	Tong et al. (2014)
Familial hemiplegic migraine type 2	Reduced expression of astrocytic α2 NKA Decreased astrocytic glutamate and K^+ clearance	Acute cortical slices (W887R FHM2 mutation) FHM2 KI mice	Facilitation of cortical spreading depression	Capuani et al. (2016)
Hyperammonemia	Overactivation of neuronal NKCC1 Impaired astrocytic K^+ buffering	$Otc^{spf\text{-}ash}$ mice	Excess of $[K^+]_o$ Clonic seizures Decreased movement Neurological dysfunction	Thrane et al. (2013)

Although this ingenious hypothesis has been well supported by experimental evidence, including K^+ accumulation in cortical astrocytes following repetitive neural activity (Ballanyi et al., 1987) and K^+ siphoning in the retina (Newman et al., 1984), there are several aspects of this model that remain unclear, mainly regarding the molecular identity of this process (Larsen and Macaulay, 2014). Direct demonstration of K^+ spatial buffering in GJ-coupled astrocytes *in situ* or *in vivo* is still technically challenging. Recent advances in K^+ imaging have the potential to provide a detailed description of the spatiotemporal K^+ distribution (Depauw et al., 2016; Rimmele and Chatton, 2014), and thus a better understanding of this process. However, the current dyes need to be improved in terms of K^+ selectivity, affinity constants and kinetics to allow fast and accurate K^+ imaging over a wide range of concentrations.

Although the molecular identity of this process requires further clarification, the role of astrocytes in the K^+ clearance process has been shown experimentally many times. The present manuscript provides an overview on the modulatory effects of local cortical astrocytes over individual and networks of neurons, aiming to extend the view that K^+ buffering not only is required for ion homeostasis, but also can be used by the network as a means to promote hyperexcitability and engage specific network activity (Wang et al., 2012a,b). It is therefore suggested that astrocytes, in addition to their modulation of neuronal excitability at the synaptic level, are strategically located to act as "synaptic managers" that oversee the overall synaptic activity within their spatial domain, and are capable of regulating $[K^+]_o$ levels locally to modulate network oscillations. As such, K^+ buffering should be viewed as a physiological tool to first impact neuronal excitability within their spatial domain and later mediate the transitions between neuronal oscillations at different frequencies that may spread to other brain areas, leading to synchronization among different neuronal networks.

Since malfunction of astrocytic K^+ clearance likely contributes to excitation-to-inhibition imbalance and aberrant circuitry connections, a better understanding of the bidirectional communication between neurons and astrocytes, particulary finding molecular agents that impact on the astrocytic K^+ clearance process, is essential for understanding the way the brain processes and transmits information.

Acknowlegdments

This study was supported by IPRA to ABS and seed funding grant (WSU) to Y.B.

References

Abbott, N.J., Patabendige, A.A.K., Dolman, D.E.M., Yusof, S.R., Begley, D.J., 2010. Structure and function of the blood-brain barrier. Neurobiol. Dis. 37, 13–25, http://dx.doi.org/10.1016/j.nbd.2009.07.030.

Abudara, V., Bechberger, J., Freitas-Andrade, M., De Bock, M., Wang, N., Bultynck, G., Naus, C.C., Leybaert, L., Giaume, C., 2014. The connexin43 mimetic peptide Gap19 inhibits hemichannels without altering gap junctional communication in astrocytes. Front. Cell. Neurosci. 8, 306, http://dx.doi.org/10.3389/fncel.2014.00306.

Amiri, M., Hosseinmardi, N., 2013. Astrocyte- neuron interaction as a mechanism responsible for generation of neural synchrony: a study based on modeling and experiments. J. Comput. Neurosci. 34, 489–504, http://dx.doi.org/10.1007/s10827-012-0432-6.

Amzica, F., Massimini, M., Manfridi, A., 2002. Spatial buffering during slow and paroxysmal sleep oscillations in cortical networks of glial cells in vivo. J. Neurosci. 22, 1042–1053.

Angulo, C., Kozlov, S., Charpak, S., Audinat, E., Ancı, M., Universitaria, C., 2004. Glutamate released from glial cells synchronizes neuronal activity in the hippocampus. J. Neurosci. 24, 6920–6927, http://dx.doi.org/10.1523/JNEUROSCI.0473-04.2004.

Araque, A., Parpura, V., Sanzgiri, R.P., Haydon, P.G., 1999. Tripartite synapses: glia, the unacknowledged partner. Trends Neurosci. 22, 208–215, http://dx.doi.org/10.1016/S0166-2236(98)01349-6.

Axelsen, L.N., Calloe, K., Holstein-Rathlou, N.-H., Nielsen, M.S., 2013. Managing the complexity of communication: regulation of gap junctions by post-translational modification. Front. Pharmacol. 4, 130, http://dx.doi.org/10.3389/fphar.2013.00130.

Ballanyi, K., Grafe, P., ten Bruggencate, G., 1987. Ion activities and potassium uptake mechanisms of glial cells in guinea-pig olfactory cortex slices. J. Physiol. 382, 159–174, http://dx.doi.org/10.1113/jphysiol.1987.sp016361.

Bedner, P., Dupper, A., Huttmann, K., Muller, J., Herde, M.K., Dublin, P., Deshpande, T., Schramm, J., Haussler, U., Haas, C.a., Henneberger, C., Theis, M., Steinhauser, C., 2015. Astrocyte uncoupling as a cause of human temporal lobe epilepsy. Brain 1–15, 5, http://dx.doi.org/10.1093/brain/awv067.

Bockenhauer, D., Feather, S., Stanescu, H.C., Bandulik, S., Zdebik, A.A., Reichold, M., Tobin, J., Lieberer, E., Sterner, C., Landoure, G., Arora, R., Sirimanna, T., Thompson, D., Helen Cross, J., Hoff van't, W., Masri Al, O., Tullus, K., Yeung, S., Anikster, Y, Klootwijk, E., Hubank, M., Dillon, M.J., Heitzmann, D., Arcos-Burgos, M., Knepper, M.A., Dobbie, A., Gahl, W.A., Warth, R., Sheridan, E., Kleta, R., 2009. Epilepsy, ataxia, sensorineural deafness, tubulopathy, and KCNJ10 mutations. N. Engl. J. Med. 360, 1960–1970, http://dx.doi.org/10.1056/NEJMoa0810276. Epilepsy.

Bordey, A., Sontheimer, H., 1998. Properties of human glial cells associated with epileptic seizure foci. Epilepsy Res. 32, 286–303.

Buono, R.J., Lohoff, F.W., Sander, T., Sperling, M.R., Connor, M.J.O., Dlugos, D.J., Ryan, S.G., Golden, G.T., Zhao, H., Scattergood, T.M., Berrettini, W.H., Ferraro, T.N., 2004. Association between variation in the human KCNJ10 potassium ion channel gene and seizure susceptibility. Epilepsy Res. 58, 175–183, http://dx.doi.org/10.1016/j.eplepsyres.2004.02.003.

Bushong, E., a Martone, M.E., Jones, Y.Z., Ellisman, M.H., 2002. Protoplasmic astrocytes in CA1 stratum radiatum occupy separate anatomical domains. J. Neurosci. 22, 183–192, 22/1/183 [pii].

Buskila, Y., Amitai, Y., 2010. Astrocytic iNOS-dependent enhancement of synaptic release in mouse neocortex. J. Neurophysiol. 103, 1322–1328.

Buskila, Y., Farkash, S., Hershfinkel, M., Amitai, Y., 2005. Rapid and reactive nitric oxide production by astrocytes in mouse neocortical slices. Glia 52, 169–176.

Buskila, Y., Abu-Ghanem, Y., Levi, Y., Moran, A., Grauer, E., Amitai, Y., 2007. Enhanced astrocytic nitric oxide production and neuronal modifications in the neocortex of a NOS2 mutant mouse. PLoS One 2, 9, http://dx.doi.org/10.1371/journal.pone.0000843.

Butt, A.M., Kalsi, A., 2006. Inwardly rectifying potassium channels (Kir) in central nervous system glia: a special role for Kir4.1 in glial functions. J. Cell. Mol. Med. 10, 33–44, http://dx.doi.org/10.1111/j.1582-4934.2006. tb00289.x.
Buzsáki, G., Draguhn, A., 2004. Neuronal oscillations in cortical networks. Science 80 (304), 1926–1929, http://dx.doi.org/10.1126/science.1099745.
Buzsaki, G., 2006. Rhythms of the brain. Cycle, http://dx.doi.org/10.1093/acprof.
Cajal, S.R.y., 1897. Algo sobre la significación fisiológica de la neuroglia. Rev. Trimest. Microgr. 1, 3–47.
Capuani, C., Melone, M., Tottene, A., Bragina, L., Crivellaro, G., Santello, M., Casari, G., Conti, F., Pietrobon, D., 2016. Defective glutamate and K + clearance by cortical astrocytes in familial hemiplegic migraine type 2. EMBO Mol. Med. 8, 967–986, http://dx.doi.org/10.15252/emmm.201505944.
Carmignoto, G., Fellin, T., 2006. Glutamate release from astrocytes as a non-synaptic mechanism for neuronal synchronization in the hippocampus. J. Physiol. Paris 99, 98–102, http://dx.doi.org/10.1016/j.jphysparis.2005.12.008.
Chen, K.C., Nicholson, C., 2000. Spatial buffering of potassium ions in brain extracellular space. Biophys. J. 78, 2776–2797, http://dx.doi.org/10.1016/S0006-3495(00)76822-6.
Chever, O., Dossi, E., Pannasch, U., Derangeon, M., Rouach, N., 2016. Astroglial networks promote neuronal coordination. Sci. Signal. 9, 1–9, http://dx.doi.org/10.1126/scisignal.aad3066.
Cossart, R., Aronov, D., Yuste, R., 2003. Attractor dynamics of network UP states in the neocortex. Nature 423, 283–288, http://dx.doi.org/10.1038/nature01614.
Coulter, D.A., Steinhauser, C., 2015. Role of astrocytes in epilepsy. Cold Spring Harb. Perspect. Med. 5, http://dx.doi.org/10.1101/cshperspect.a022434.
Crambert, G., Geering, K., 2003. FXYD proteins: new tissue-specific regulators of the ubiquitous Na,K-ATPase. Sci. STKE 2003, http://dx.doi.org/10.1126/stke.2003.166.re1, RE1.
David, Y., Cacheaux, L.P., Ivens, S., Lapilover, E., Heinemann, U., Kaufer, D., Friedman, A., 2009. Astrocytic dysfunction in epileptogenesis: consequence of altered potassium and glutamate homeostasis? J. Neurosci. 29, 10588–10599, http://dx.doi.org/10.1523/JNEUROSCI.2323-09.2009.
Depauw, A., Dossi, E., Kumar, N., Fiorini-debuisschert, C.Ø., Huberfeld, G., Ha-thi, M., Rouach, N., Leray, I., 2016. A highly selective potassium sensor for the detection of potassium in living tissues. Chem. A Eur. J. 22, 14902–14911, http://dx.doi.org/10.1002/chem.201602209.
Dermietzel, R., Gao, Y., Scemes, E., Vieira, D., Urban, M., Kremer, M., Bennett, M.V.L., Spray, D.C., 2000. Connexin43 null mice reveal that astrocytes express multiple connexins. Brain Res. Rev. 32, 45–56, http://dx.doi.org/10.1016/S0165-0173(99)00067-3.
Ding, F., O'Donnell, J., Xu, Q., Kang, N., Goldman, N., Nedergaard1, M., 2016. Changes in the composition of brain interstitial ions control the sleep-wake cycle. Science 80 (352), 550–555, http://dx.doi.org/10.1126/science.aad4821.
Djukic, B., Casper, K.B., Philpot, B.D., Chin, L.-S., McCarthy, K.D., 2007. Conditional knock-out of Kir4.1 leads to glial membrane depolarization, inhibition of potassium and glutamate uptake, and enhanced short-term synaptic potentiation. J. Neurosci. 27, 11354–11365, http://dx.doi.org/10.1523/JNEUROSCI.0723-07.2007.
Enkvist, M.O.K., McCarthy, K.D., 1994. Astroglial gap junction communication is increased by treatment with either glutamate or high K+ concentration. J. Neurochem. 62, 489–495, http://dx.doi.org/10.1046/j.1471-4159.1994.62020489.x.
Fellin, T., Pascual, O., Gobbo, S., Pozzan, T., Haydon, P.G., Carmignoto, G., 2004. Neuronal synchrony mediated by astrocytic glutamate through activation of extrasynaptic NMDA receptors. Neuron 43, 729–743, http://dx.doi.org/10.1016/j.neuron.2004.08.011.
Fröhlich, F., Bazhenov, M., Timofeev, I., Steriade, M., Sejnowski, T.J., 2006. Slow state transitions of sustained neural oscillations by activity-dependent modulation of intrinsic excitability. J. Neurosci. 26, 6153–6162, http://dx.doi.org/10.1523/JNEUROSCI.5509-05.2006.
Fröhlich, F., Sejnowski, T.J., Bazhenov, M., 2010. Network bistability mediates spontaneous transitions between normal and pathological brain states. J. Neurosci. 30, 10734–10743, http://dx.doi.org/10.1523/JNEUROSCI.1239-10.2010.
Fries, P., 2005. A mechanism for cognitive dynamics: neuronal communication through neuronal coherence. Trends Cogn. Sci. 9, 474–480, http://dx.doi.org/10.1016/j.tics.2005.08.011.
Gardner-Medwin, A., 1983a. Changes of extracellular potassium activity induced by electric current through brain tissue in the rat. J. Physiol., 375–392.
Gardner-Medwin, A., 1983b. Analysis of potassium dynamics in mammalian brain tissue. J. Physiol. 335, 393–426.
Gardner-Medwin, A., 1983c. A study of the mechanisms by which potassium moves through brain tissue in the rat. J. Physiol. 335, 353–374.
Gigout, S., Deisz, R.A., Dehnicke, C., Turak, B., Devaux, B., Pumain, R., Louvel, J., 2016. Role of gap junctions on synchronization in human neocortical networks. Brain Res. 1637, 14–21, http://dx.doi.org/10.1016/j.brainres.2016.02.005.
Grosche, A., Grosche, J., Tackenberg, M., Scheller, D., Gerstner, G., Gumprecht, A., Pannicke, T., Hirrlinger, P.G., Wilhelmsson, U., Hüttmann, K., Härtig, W., Steinhäuser, C., Pekny, M., Reichenbach, A., 2013. Versatile and simple approach to determine astrocyte territories in mouse neocortex and hippocampus. PLoS One 8, http://dx.doi.org/10.1371/journal.pone.0069143.
Guglielmi, L., Servettini, I., Caramia, M., Catacuzzeno, L., Franciolini, F., D'Adamo, M.C., Pessia, M., 2015. Update on the implication of potassium channels in autism: k+ channelautism spectrum disorder. Front. Cell. Neurosci. 9, 1–14, http://dx.doi.org/10.3389/fncel.2015.00034.
Gutfreund, Y., Yarom, Y., Segev, I., 1995. Subthreshold oscillations and resonant frequency in guinea-pig cortical neurons: physiology and modelling. J. Physiol. 483, 621–640.
Haj-Yasein, N.N., Jensen, V., Vindedal, G.F., Gundersen, G.A., Klungland, A., Ottersen, O.P., Hvalby, O., Nagelhus, E.A., 2011. Evidence that compromised K+ spatial buffering contributes to the epileptogenic effect of mutations in the human Kir4.1 gene (KCNJ10). Glia 59, 1635–1642, http://dx.doi.org/10.1002/glia.21205.
Hajek, I., Subbarao, K.V., Hertz, L., 1996. Acute and chronic effects of potassium and noradrenaline on Na+, K+-ATPase activity in cultured mouse neurons and astrocytes. Neurochem. Int. 28, 335–342, 019701869500081X [pii].
Halassa, M.M., Fellin, T., Takano, H., Dong, J.-H., Haydon, P.G., 2007. Synaptic islands defined by the territory of a single astrocyte. J. Neurosci. 27, 6473–6477, http://dx.doi.org/10.1523/JNEUROSCI.1419-07.2007.
Halnes, G., Østby, I., Pettersen, K.H., Omholt, S.W., Einevoll, G.T., 2013. Electrodiffusive model for astrocytic and neuronal ion concentration dynamics. PLoS Comput. Biol. 9, http://dx.doi.org/10.1371/journal.pcbi.1003386.
Heinemann, U., Dieter Lux, H., 1977. Ceiling of stimulus induced rises in extracellular potassium concentration in the cerebral cortex of cat. Brain Res. 120, 231–249, http://dx.doi.org/10.1016/0006-8993(77)90903-9.
Hertz, L., 1965. Possible role of neuroglia: a potassium-mediated neuronal-neuroglial-neuronal impulse transmission system. Nature 206, 1091–1094.
Heuser, K., Eid, T., Lauritzen, F., Thoren, A.E., Vindedal, G.F., Taubøll, E., Gjerstad, L., Spencer, D.D., Ottersen, O.P., Nagelhus, E.A., de Lanerolle, N.C., 2012. Loss of perivascular kir4.1 potassium channels in the sclerotic hippocampus of patients with mesial temporal lobe epilepsy. J. Neuropathol. Exp. Neurol. 71, 814–825, http://dx.doi.org/10.1038/jid.2014.371.
Hibino, H., Fujita, A., Iwai, K., Yamada, M., Kurachi, Y., 2004. Differential assembly of inwardly rectifying K channel subunits, kir4.1 and kir5.1, in brain astrocytes. J. Biol. Chem. 279, 44065–44073, http://dx.doi.org/10.1074/jbc.M405985200.
Hofer, A., Dermietzel, R., 1998. Visualization and functional blocking of gap junction hemichannels (connexons) with antibodies against external loop domains in astrocytes. Glia 24, 141–154, http://dx.doi.org/10.1002/(SICI)1098-1136(199809)24:1<141:AID-GLIA13>3.0.CO;2-R.
Houades, V., Koulakoff, A., Ezan, P., Seif, I., Giaume, C., 2008. Gap junction-mediated astrocytic networks in the mouse barrel cortex. J. Neurosci. 28, 5207–5217, http://dx.doi.org/10.1523/JNEUROSCI.5100-07.2008.
Iliff, J.J., Wang, M., Liao, Y., Plogg, B.A., Peng, W., Goldman, S.A., Nagelhus, E.A., Nedergaard, M., 2012. A paravascular pathway facilitates CSF flow through the brain parenchyma and the clearance of interstitial solutes, including amyloid β. Sci. Transl. Med., 4, http://dx.doi.org/10.1126/scitranslmed.3003748.
Isomoto, S., Kondo, C., Kurachi, Y., 1997. Inwardly rectifying potassium channels: their molecular heterogeneity and function. Jpn. J. Physiol., http://dx.doi.org/10.2170/jjphysiol.47.11.
Jessen, N.A., Munk, A.S.F., Lundgaard, I., Nedergaard, Maiken, 2015. The glymphatic system –a beginner's guide. Neurochem. Res. 40, 2583–2599, http://dx.doi.org/10.1177/0963721412473755.Surging.
Kaiser, M., Maletzki, I., Hülsmann, S., Holtmann, B., Schulz-Schaeffer, W., Kirchhoff, F., Bähr, M., Neusch, C., 2006. Progressive loss of a glial potassium channel (KCNJ10) in the spinal cord of the SOD1 (G93A) transgenic mouse model of amyotrophic lateral sclerosis. J. Neurochem. 99, 900–912, http://dx.doi.org/10.1111/j.1471-4159.2006.04131.x.
Karwoski, C.J., Lu, H.-K., Newman, E.A., 1989. Spatial buffering of light-evoked potassium increases by retinal Müller (Glial) cells. Science 80 (244), 578–580.
Kettenmann, H., Ransom, B.R., 2004. The Concept of Neuroglia: A Historical Perspective, Neuroglia. Oxford University Press.
Kivi, A., Lehmann, T.N., Kovács, R., Eilers, A., Jauch, R., Meencke, H.J., Von Deimling, A., Heinemann, U., Gabriel, S., 2000. Effects of barium on stimulus-induced rises of $[K^+]_o$ in human epileptic non-sclerotic and sclerotic hippocampal area CA1. Eur. J. Neurosci. 12, 2039–2048, http://dx.doi.org/10.1046/j.1460-9568.2000.00103.x.
Kiyoshi, et al., 2015. The Relative Contribution of Kir4.1, Two-Pore Domain K+ Channels and KCNN2 to the Passive Conductance of Mature Hippocampal Astrocytes. SFN, Abstr. p. 121.18.
Kofuji, P., Newman, E.a., 2004. Potassium Buffering in the central nervous system. Neuroscience 129, 1045–1056.
Kofuji, P., Biedermann, B., Siddharthan, V., Raap, M., Iandiev, I., Milenkovic, I., Thomzig, A., Veh, R.W., Bringmann, A., Reichenbach, A., 2002. Kir potassium channel subunit expression in retinal glial cells: implications for spatial potassium buffering. Glia 39, 292–303, http://dx.doi.org/10.1002/glia.10112.
Kubo, Y., Baldwin, T.J., Jan, Y.N., Jan, L.Y., 1993. Primary structure and functional expression of a mouse inward rectifier potassium channel. Nature 362, 127–133.
Kucheryavykh, Y., Kucheryavykh, V., Nichols, L.Y., Maldonado, C.G., Baksi, H.M.K., 2007. Downregulation of kir4. 1 inward rectifying potassium channel subunits by RNAi impairs potassium transfer and glutamate uptake by cultured cortical astrocytes. Glia 281, 274–281, http://dx.doi.org/10.1002/glia.
Kuffler, S.W., Potter, D.D., 1964. Glia in the leech central nervous system: physiological properties and neuron-glia relationship. J. Neurophysiol. 27, 290–320.
Kuffler, S.W., Nicholls, J.G., Orkand, R.K., 1966. Physiological properties of glial cells in the central nervous system of amphibia. J. Neurophysiol. 29, 768–787, MO1.
Kuriu, T., Kakimoto, Y., Araki, O., 2015. Computational simulation: astrocyte-induced depolarization of neighboring neurons mediates

synchronous UP states in a neural network. J. Biol. Phys. 41, 377–390, http://dx.doi.org/10.1007/s10867-015-9385-0.
Lagrutta, A.A., Bond, C.T., Pessia, M., Xia, X.M., Tucker, S., Adelman, J.P., 1996. Inward rectifier potassium channels cloning, expression and structure-function studies. Jpn. Hear. J. 37, 651–660.
Larsen, B.R., Macaulay, N., 2014. Kir4.1-mediated spatial buffering of KC: experimental challenges in determination of its temporal and quantitative contribution to KC clearance in the brain. Channels 8, 1–7.
Larsen, B.R., Stoica, A., Macaulay, N., 2016. Managing brain extracellular k + during neuronal activity: the physiological role of the Na + /K+-ATPase subunit isoforms. Front. Physiol. 7, 1–10, http://dx.doi.org/10.3389/fphys.2016.00141.
Lee, H.S., Ghetti, A., Pinto-Duarte, A., Wang, X., Dziewczapolski, G., Galimi, F., Huitron-Resendiz, S., Pina-Crespo, J.C., Roberts, A.J., Verma, I.M., Sejnowski, T.J., Heinemann, S.F., 2014. Astrocytes contribute to gamma oscillations and recognition memory. PNAS 111, E3343–52, http://dx.doi.org/10.1073/pnas.1410893111.
Leis, J.a., Bekar, L.K., Walz, W., 2005. Potassium homeostasis in the ischemic brain. Glia 50, 407–416, http://dx.doi.org/10.1002/glia.20145.
Lopatin, A.N., Makhina, E.N., Nichols, C.G., 1995. The mechanism of inward rectification of potassium channels: long-pore plugging by cytoplasmic polyamines. J. Gen. Physiol., 106.
Lutz, S.E., Zhao, Y., Gulinello, M., Lee, S.C., Raine, C.S., Brosnan, C.F., 2009. Deletion of astrocyte connexin 43 43 and 30 leads to a dysmyelinating phenotype and hyppocampal CA1 vacuolation. J. Neurosci. 29, 7743–7752.
Ma, B., Xu, G., Wang, W., Enyeart, J.J., Zhou, M., 2014. Dual patch voltage clamp study of low membrane resistance astrocytes in situ. Mol. Brain 7, 1–12.
Ma, B., Buckalew, R., Du, Y., Kiyoshi, C.M., Alford, C.C., Wang, W., Mctigue, D.M., Enyeart, J.J., Terman, D., Zhou, M., 2016. Gap junction coupling confers isopotentiality on astrocyte syncytium. Glia 64, 214–226, http://dx.doi.org/10.1002/glia.22924.
Macaulay, N., Zeuthen, T., 2012. Glial K+ clearance and cell swelling: key roles for cotransporters and pumps. Neurochem. Res. 37, 2299–2309, http://dx.doi.org/10.1007/s11064-012-0731-3.
Malarkey, E.B., Parpura, V., 2008. Mechanisms of glutamate release from astrocytes. Neurochem. Int. 52, 142–154.
McKhann, G.M., D'Ambrosio, R., Janigro, D., 1997. Heterogeneity of astrocyte resting membrane potentials and intercellular coupling revealed by whole-cell and gramicidin-perforated patch recordings from cultured neocortical and hippocampal slice astrocytes. J. Neurosci. 17, 6850–6863, MO1.
Mitterauer, B.J., 2010. Significance of the astrocyte domain organization for qualitative information structuring in the brain. Adv. Biosci. Biotechnol. 1, 391–397, http://dx.doi.org/10.4236/abb.2010.15052.
Nagelhus, E.a., Ottersen, O.P., 2013. Physiological roles of aquaporin-4 in brain. Physiol. Rev. 93, 1543–1562, http://dx.doi.org/10.1152/physrev.00011.2013.
Nagelhus, E.A., Horio, Y., Inanobe, A., Fujita, A., Haug, F.M., Nielsen, S., Kuhachi, Y., Ottersen, O.P., 1999. Immunogold evidence suggests that coupling of K+ siphoning and water transport in rat retinal Muller cells is mediated by a coenrichment of Kir4.1 and AQP4 in specific membrane domains. Glia 26, 47–54, http://dx.doi.org/10.1002/(SICI)1098-1136(199903)26:1<47:AID-GLIA5>3.0.CO;2-5.
Navarrete, M., Araque, A., 2014. The Cajal school and the physiological role of astrocytes: a way of thinking. Front. Neuroanat. 8, 33, http://dx.doi.org/10.3389/fnana.2014.00033.
Nedergaard, M., Ransom, B., Goldman, S.a., 2003. New roles for astrocytes: redefining the functional architecture of the brain. Trends Neurosci. 26, 523–530, http://dx.doi.org/10.1016/j.tins.2003.08.008.
Newman, E., a Zahs, K.R., 1998. Modulation of neuronal activity by glial cells in the retina. J. Neurosci. 18, 4022–4028.
Newman, E., Frambach, D., Oddette, L., 1984. Control of extracellular potassium levels by retinal glial cell K+ siphoning. Science 80 (225), 1174–1175, http://dx.doi.org/10.1126/scisignal.2001449.Engineering.
Newman, E.A., 1987. Regulation of potassium levels by Müller cells in the vertebrate retina. Can. J. Physiol. Pharmacol. 65, 1028–1032.
Nielsen, S., Nagelhus, E.A., Amiry-Moghaddam, M., Bourque, C., Agre, P., Ottersen, O.P., 1997. Specialized membrane domains for water transport in glial cells: high-resolution immunogold cytochemistry of aquaporin-4 in rat brain. J. Neurosci. 17, 171–180.
Oberheim, N.A., Wang, X., Goldman, S., Nedergaard, M., 2006. Astrocytic complexity distinguishes the human brain. Trends Neurosci. 29, 547–553, http://dx.doi.org/10.1016/j.tins.2006.08.004.
Oberheim, N.A., Tian, G.-F., Han, X., Peng, W., Takano, T., Ransom, B., Nedergaard, M., 2008. Loss of astrocytic domain organization in the epileptic brain. J. Neurosci. 28, 3264–3276, http://dx.doi.org/10.1523/JNEUROSCI.4980-07.2008.
Ogata, K., Kosaka, T., 2002. Structural and quantitative analysis of astrocytes in the mouse hippocampus. Neuroscience 113, 221–233, http://dx.doi.org/10.1016/S0306-4522(02)00041-6.
Olabarria, M., Noristani, H.N., Verkhratsky, A., Rodríguez, J.J., 2010. Concomitant astroglial atrophy and astrogliosis in a triple transgenic animal model of Alzheimer's disease. Glia 58, 831–838, http://dx.doi.org/10.1002/glia.20967.
Olsen, M.L., Khakh, B.S., Skatchkov, S.N., Zhou, M., Lee, C.J., Rouach, N., 2015. New insights on astrocyte ion channels: critical for homeostasis and neuron-glia signaling. J. Neurosci. 35, 13827–13835, http://dx.doi.org/10.1523/JNEUROSCI.2603-15.2015.
Orkand, R.K., Nicholls, J.G., Kuffler, S.W., 1966. Effect of nerve impulses on the membrane potential of glial cells in the central nervous system of amphibia. J. Neurophysiol. 29, 788–806.
Orkand, R.K., 1986. Glial-interstitial fluid exchange. Ann. N. Y. Acad. Sci. 481, 269–272, http://dx.doi.org/10.1111/j.1749-6632.1986. tb27157.x.
Pannasch, U., Vargová, L., Reingruber, J., Ezan, P., Holcman, D., Giaume, C., 2011. Astroglial networks scale synaptic activity and plasticity. Proc. Natl. Acad. Sci. U. S. A. 108, 8467–8472, http://dx.doi.org/10.1073/pnas.1016650108.
Paulson, O.B., Newman, E.A., 1987. Does the release of potassium from astrocyte endfeet regulate cerebral blood flow? Science 237, 896–898, http://dx.doi.org/10.1016/j.bbi.2008.05.010.
Penfield, W., 1927. The mechanism of cicatricial contraction in the brain. Brain 50, 499–517, http://dx.doi.org/10.1093/brain/50.3-4.499.
Poskanzer, K.E., Yuste, R., 2011. Astrocytic regulation of cortical UP states. PNAS 108, 18453–18458, http://dx.doi.org/10.1073/pnas.1112378108.
Poskanzer, K.E., Yuste, R., 2016. Astrocytes regulate cortical state switching in vivo. PNAS 2675–2684, http://dx.doi.org/10.1073/pnas.1520759113.
Ransom, C.B., Ransom, B.R., Sontheimer, H., 2000. Activity-dependent extracellular K+ accumulation in rat optic nerve: the role of glial and axonal Na+ pumps. J. Physiol. 522.
Rimmele, T.S., Chatton, J.-Y., 2014. A novel optical intracellular imaging approach for potassium dynamics in astrocytes. PLoS One 9, e109243, http://dx.doi.org/10.1371/journal.pone.0109243.
Rose, C.R., Ransom, B.R., 1997. Gap junctions equalize intracellular Na+ concentration in astrocytes. Glia 20, 299–307, http://dx.doi.org/10.1002/(SICI)1098-1136(199708)20:4<299:AID-GLIA3>3.0.CO;2-1.
Rouach, N., Koulakoff, A., Abudara, V., Willecke, K., Giaume, C., 2008. Astroglial metabolic networks sustain hippocampal synaptic transmission. Science 322, 1551–1555, http://dx.doi.org/10.1126/science.1164022.
Samoilova, M., Wentlandt, K., Adamchik, Y., Velumian, A.A., Carlen, P.L., 2008. Connexin 43 mimetic peptides inhibit spontaneous epileptiform activity in organotypic hippocampal slice cultures. Exp. Neurol. 210, 762–775, http://dx.doi.org/10.1016/j.expneurol.2008.01.005.
Sanchez-Vives, M.V., McCormick, D.a., 2000. Cellular and network mechanisms of rhythmic recurrent activity in neocortex. Nat. Neurosci. 3, 1027–1034, http://dx.doi.org/10.1038/79848.
Sasaki, T., Kuga, N., Namiki, S., Matsuki, N., Ikegaya, Y., 2011. Locally synchronized astrocytes. Cereb. Cortex 21, 1889–1900, http://dx.doi.org/10.1093/cercor/bhq256.
Schousboe, A., Hertz, L., 1971. Effects of potassium on concentrations of ions and proteins and on pH in brain-cortex slices from new-born and adult rats. Int. J. Neurosci. 1, 235–242, http://dx.doi.org/10.3109/00207457109146976.
Schroder, W., Hinterkeuser, S., Seifert, G., Schramm, J., Jabs, R., Wilkin, G.P., Steinhauser, C., 2000. Functional and molecular properties of human astrocytes in acute hippocampal slices obtained from patients with temporal lobe epilepsy. Epilepsia 41, 181–184.
Sibille, J., Duc, K.D., Holcman, D., Rouach, N., 2015. The neuroglial potassium cycle during neurotransmission: role of Kir4. 1 channels. PLoS Comput. Biol. 11, 1–22, http://dx.doi.org/10.1371/journal.pcbi.1004137.
Sicca, F., Imbrici, P., Cristina, M., Adamo, D., Moro, F., Bonatti, F., Brovedani, P., Grottesi, A., Guerrini, R., Masi, G., Maria, F., Pessia, M., 2011. Autism with seizures and intellectual disability: possible causative role of gain-of-function of the inwardly-rectifying K+ channel kir4.1. Neurobiol. Dis. 43, 239–247, http://dx.doi.org/10.1016/j.nbd.2011.03.016.
Simard, M., Arcuino, G., Takano, T., Liu, Q.S., Nedergaard, M., 2003. Signaling at the gliovascular interface. J. Neurosci. 23, 9254–9262, 14534260.
Somjen, G.G., 1979. Extracellular potassium in the mammalian central nervous system. Annu. Rev. Physiol. 41, 159–177, http://dx.doi.org/10.1146/annurev.ph.41.030179.001111.
Somjen, G.G., 2002. Ion regulation in the brain: implications for pathophysiology. Neurosci 8, 254–267, http://dx.doi.org/10.1177/10758402008003011.
Sylantyev, S., Savtchenko, L.P., Niu, Y., Ivanov, A.I., Jensen, P., Kullmann, D.M., Xiao, M., Rusakov, D.A., 2008. Electric fields due to synaptic currents sharpen excitatory transmission. Science 80 (319), 1845–1849, http://dx.doi.org/10.1126/science.1154330.Electric.
Szatkowski, M., Barbour, B., Attwell, D., 1990. Non-vesicular release of glutamate from glial cells by reversed electrogenic glutamate uptake. Nature 348, 443–446.
Theis, M., Jauch, R., Zhuo, L., Speidel, D., Wallraff, A., Do, B., Frisch, C., So, G., Teubner, B., Euwens, C., Huston, J., Steinha, C., Messing, A., Heinemann, U., Willecke, K., 2003. Accelerated hippocampal spreading depression and enhanced locomotory activity in mice with astrocyte-directed inactivation of connexin43. J. Neurosci. 23, 766–776.
Rangroo Thrane, V., Thrane, A.S., Wang, F., Cotrina, M.L., Smith, N.a., Chen, M., Xu, Q., Kang, N., Fujita, T., Nagelhus, E., Nedergaard, M.a., 2013. Ammonia triggers neuronal disinhibition and seizures by impairing astrocyte potassium buffering. Nat. Med. 19, 1643–1648, http://dx.doi.org/10.1038/nm.3400.
Tong, X., Ao, Y., Faas, G.C., Nwaobi, S.E., Xu, J., Haustein, M.D., Anderson, M.a., Mody, I., Olsen, M.L., Sofroniew, M.V., Khakh, B.S., 2014. Astrocyte Kir4.1 ion channel deficits contribute to neuronal dysfunction in Huntington's disease model mice. Nat. Neurosci. 17, 694–703, http://dx.doi.org/10.1038/nn.3691.
Tsacopoulos, M., Magistretti, P.J., 1996. Metabolic coupling between glia and neurons. J. Neurosci. 16, 877–885.
Turovsky, E., Karagiannis, A., Abdala, A.P., Gourine, A.V., 2015. Impaired CO2 sensitivity of astrocytes in a mouse model of Rett syndrome. J. Physiol. 593, 3159–3168, http://dx.doi.org/10.1113/JP270369.
Ullah, G., Cressman, J.R., Barreto, E., Schiff, S.J., 2009. The influence of sodium and potassium dynamics on excitability, seizures, and the stability of persistent

states: II. Network and glial dynamics. J. Comput. Neurosci. 26, 171–183, http://dx.doi.org/10.1007/s10827-008-0130-6.
Verkhratsky, A., Butt, A.M., 2013. Glial physiology and pathophysiology. In: Neuroglia: Definition, Classification, Evolution, Numbers, Development, p. Chapter 3.
Verkhratsky, A., Zorec, R., Rodriguez, J.J., Parpura, V., 2016. Astroglia dynamics in ageing and Alzheimer's disease. Curr. Opin. Pharmacol. 26, 74–79, http://dx.doi.org/10.1016/j.coph.2015.09.011.
Wallraff, A., Köhling, R., Heinemann, U., Theis, M., Willecke, K., Steinhäuser, C., 2006. The impact of astrocytic gap junctional coupling on potassium buffering in the hippocampus. J. Neurosci. 26, 5438–5447, http://dx.doi.org/10.1523/JNEUROSCI.0037-06.2006.
Walz, W., Hertz, L., 1984. Intense furosemide-sensitive potassium accumulation in astrocytes in the presence of pathologically high extracellular potassium levels. J. Cereb. Blood Flow Metab. 4, 301–304, http://dx.doi.org/10.1038/jcbfm.1984.42.
Wang, F., Xu, Q., Wang, W., Takano, T., Nedergaard, M., 2012a. Bergmann glia modulate cerebellar Purkinje cell bistability via Ca2+-dependent K+ uptake. Proc. Natl. Acad. Sci. 109, 7911–7916, http://dx.doi.org/10.1073/pnas.1120380109.
Wang, Fushun, Smith, Nathan a, Xu, Q., Fujita, T., Baba, A., Matsuda, T., Takano, T., Bekar, L., Nedergaard, M., 2012b. Astrocytes modulate neural network activity by Ca^2+ dependent uptake of extracellular K+. Sci. Signal. 5, 1–15, http://dx.doi.org/10.1126/scisignal.2002334.
Xiong, Z.Q., Stringer, J.L., 2000. Sodium pump activity, not glial spatial buffering, clears potassium after epileptiform activity induced in the dentate gyrus. J. Neurophysiol. 83, 1443–1451.
Xu, J., Song, D., Xue, Z., Gu, L., Hertz, L., Peng, L., 2013. Requirement of glycogenolysis for uptake of increased extracellular K + in astrocytes: potential implications for K+ homeostasis and glycogen usage in brain. Neurochem. Res. 38, 472–485, http://dx.doi.org/10.1007/s11064-012-0938-3.
Yaguchi, T., Nishizaki, T., 2010. Extracellular high K^+ stimulates vesicular glutamate release from astrocytes by activating voltage-dependent calcium channels. J. Cell. Physiol. 225, 512–518, http://dx.doi.org/10.1002/jcp.22231.
Yang, J., Lunde, L.K., Nuntagij, P., Oguchi, T., Camassa, L.M.A., Nilsson, L.N.G., Lannfelt, L., Xu, Y., Amiry-Moghaddam, M., Ottersen, O.P., Torp, R., 2011. Loss of astrocyte polarization in the Tg-ArcSwe mouse model of Alzheimer's disease. J. Alzheimer's Dis. 27, 711–722, http://dx.doi.org/10.3233/JAD-2011-110725.
Yoon, J.J., Nicholson, L.F.B., Feng, S.X., Vis, J.C., Green, C.R., 2010. A novel method of organotypic brain slice culture using connexin-specific antisense oligodeoxynucleotides to improve neuronal survival. Brain Res. 1353, 194–203, http://dx.doi.org/10.1016/j.brainres.2010.07.005.

1.4 Hypothesis and aims

We hypothesize that the strategic location of cortical astrocytes as part of the tripartite synapse allows them to respond to network demands and to fine-tune individual neuronal membrane properties, by specifically manipulating $[K^+]_o$ through K^+ clearance mechanisms, thereby leading to the recruitment and synchronization of neuronal assemblies, which influences the **transitions** between brain waves oscillating at different frequencies, and thus behaviour.

The aims of this thesis are:

1. To investigate the impact of astrocytic K^+ clearance mechanisms on neuronal network oscillations and on individual neuronal membrane properties within different subcellular compartments.

2. To describe specific contributions of astrocytic K^+ clearance mechanisms, including net K^+ uptake and K^+ spatial buffering, as well as passive diffusion to the spatiotemporal dynamics and rate of K^+ clearance.

3. To identify potential neuronal mechanisms affecting the astrocytic K^+ clearance processes.

CHAPTER 2:

ASTROCYTIC MODULATION OF NEURONAL NETWORK OSCILLATIONS

"Discovering a dynamic brain phenomenon is one thing. Understanding its meaning and its role in behaviour and cognition is quite another."

—*György Buzsáki*

2.1 Introduction

Switching between different behavioural states in response to environmental changes requires alteration of different network oscillatory regimes and being able to mediate the transition among the different frequencies at which these oscillations fluctuate. The brain achieves this goal by fine-tuning neuronal oscillations that are associated with different brain functions and behaviours (Table 1.1, Chapter 1), thus allowing adaptation and survival.

At least ten distinct mechanisms have been suggested to affect the generation of neuronal network oscillations in the cortex, including changes in cellular excitability or in the concentration of extracellular ions (i.e. $[K^+]_o$; Chapter 1)[2,11]. However, the mechanism that gears the transition between different oscillatory frequencies, thereby leading to switching between behavioural states to allow adaptation and our own survival, remains unclear.

The following paper published in Scientific Reports (Nature Publishing Group) in August 2018 investigates the potential role of astrocytic K^+ clearance mechanisms in modulating **cortical oscillatory dynamics** at different frequencies both at the network and cellular levels[409].

Sections 2.2 and 2.3 provide further methods and results not included in the original paper relating to (1) extracellular recordings of the network activity following facilitation of K^+ clearance mechanisms after photolysis of caged guanosine-5'-triphosphate (GTP) compounds, and (2) intracellular recordings from different subcellular compartments of layer V pyramidal neurons, including proximal and distal apical dendrites, which provide additional support to the project hypothesis, as discussed in section 2.4.

SCIENTIFIC REPORTS

OPEN

Astrocytic modulation of cortical oscillations

Alba Bellot-Saez[1,2], Greg Cohen[1], André van Schaik[1], Lezanne Ooi[3], John W Morley[1,2] & Yossi Buskila[1,2]

Received: 26 March 2018
Accepted: 20 July 2018
Published online: 01 August 2018

Brain waves are rhythmic voltage oscillations emerging from the synchronization of individual neurons into a neuronal network. These oscillations range from slow to fast fluctuations, and are classified by power and frequency band, with different frequency bands being associated with specific behaviours. It has been postulated that at least ten distinct mechanisms are required to cover the frequency range of neural oscillations, however the mechanisms that gear the transition between distinct oscillatory frequencies are unknown. In this study, we have used electrophysiological recordings to explore the involvement of astrocytic K^+ clearance processes in modulating neural oscillations at both network and cellular levels. Our results indicate that impairment of astrocytic K^+ clearance capabilities, either through blockade of K^+ uptake or astrocytic connectivity, enhance network excitability and form high power network oscillations over a wide range of frequencies. At the cellular level, local increases in extracellular K^+ results in modulation of the oscillatory behaviour of individual neurons, which underlies the network behaviour. Since astrocytes are central for maintaining K^+ homeostasis, our study suggests that modulation of their inherent capabilities to clear K^+ from the extracellular milieu is a potential mechanism to optimise neural resonance behaviour and thus tune neural oscillations.

Neural oscillations are rhythmic voltage fluctuations emerging from the synchronization of individual neurons that form a neuronal network. They emerge in all brain regions, and their patterns of synchrony and coherence underlie the neural code for sensory representation and short term memory[1]. The oscillations range from very slow (0.02 Hz) to fast (600 Hz) fluctuations, and are classified on the basis of power and frequency band, with different frequency bands being associated with specific behaviours[2].

Cortical neural networks are functionally organized to enable appropriate balance of excitation and inhibition, which impacts on their synchronized activity that is fundamental for their operation. These networks are constantly alternating between different dynamic states to accommodate the large rhythmic patterns underlying the diverse cognitive functions administrated by the cortex. However, the full extent of the functional structure of these networks, especially the interactions with astrocytic networks is poorly understood.

On the local network level, neural oscillations are formed by cortical circuits that span through six layers of the cerebral cortex. The building units of these synchronous oscillations are the fluctuations in membrane potential of individual neurons known as 'up' (rising) and 'down' (falling) states. These oscillations occur both *in vitro* and *in vivo*[3], and are routinely recorded as local field potentials[4]. Biophysical studies have revealed that single neurons are endowed with complex dynamics, including their intrinsic ability to resonate over a specific range of frequencies[5–7]. This allows them to act as resonators that respond preferentially to inputs at certain frequencies. It has been reported that many oscillatory neurons have a peak resonance frequency that is correlated with the network oscillatory activity[8,9], and different subcellular compartments have distinct resonance properties which are also voltage dependent[10,11].

More than a decade ago, Penttonen and Buzsáki postulated that at least ten distinct mechanisms are required to cover the large frequency range of cortical network oscillations[12,13], and it has been reported that some frequency oscillations are driven by multiple mechanisms[14]. Several factors have been suggested to affect individual neuronal activity that underlie the generation of network oscillations, including the activation of intrinsic conductances by neuromodulators[6,13], the influence of the dendritic structure[15], activation of extrasynaptic receptors[16], activation of astrocytic calcium activity[17–19], cellular excitability[6,14] and the hyperpolarization-activated

[1]Biomedical Engineering and Neuroscience group, The MARCS Institute, Western Sydney University, Penrith, NSW, Australia. [2]School of Medicine, Western Sydney University, Campbelltown, NSW, Australia. [3]Illawarra Health and Medical Research Institute, School of Biological Sciences, University of Wollongong, Wollongong, NSW, Australia. Correspondence and requests for materials should be addressed to Y.B. (email: Y.buskila@Westernsydney.edu.au)

inward current I_h, which can modulate membrane resonance in neurons[9] and is capable of regulating the strength and frequency of network oscillations[20].

A recent report showed that altering the degree of excitation between different laminae of the auditory cortex can effectively switch the dominant network oscillation from granular to supragranular layers[14]. Another study showed that acetylcholine increases pyramidal cell excitability, enhances the gamma oscillations in evoked potentials and can induce theta rhythm oscillatory dynamics[6]. Thus, we hypothesise that factors that modulate ***cellular excitability*** are likely to impact network oscillatory activity.

Intrinsic cellular excitability partially depends on the reversal potential for potassium-mediated currents, as extracellular potassium concentration $[K^+]_o$ is critical in defining the resting membrane potential (RMP) of neurons and astrocytes, and is normally maintained at ~3 mM[21,22]. Sustained neuronal activity leads to local increases of $[K^+]_o$, which impact synaptic transmission and plasticity[23,24]. Hence, effective removal of K^+ from the extracellular space is vital for maintaining physiological neuronal activity, as excessive K^+ accumulation in the extracellular space impacts neuronal excitability and has been linked to pathological conditions[21,25,26]. For these reasons, the Sejnowski group studied the impact of $[K^+]_o$ modulation on the excitability of neurons and neuronal networks using computational models[27,28]. They found that $[K^+]_o$ dynamics can potentially modulate intrinsic conductances in neurons and thus mediate transitions between tonic spiking and bursting activity. Using their computational model, they predicted that modifications of $[K^+]_o$ can lead to alterations between fast and slow oscillatory firing modes. More recently, an *in vivo* study from Nedergaard's group reported that neuromodulators can impact the concentration of $[K^+]_o$, regardless of synaptic activity[29]. They suggested that neuromodulators work in parallel on both neuronal spiking activity and state dependent ion homeostasis, to shift between sleep and awake states, however the exact mechanisms that govern $[K^+]_o$ were not revealed.

In the central nervous system, K^+ homeostasis is mainly regulated by astrocytic activity, through a process termed K^+ clearance, reviewed by[30]. Since its first proposal in 1966 by Kuffler and colleagues[31], two major mechanisms of astrocytic K^+ clearance have been established: *net K^+ uptake*, in which the excess of $[K^+]_o$ during physiological activity is taken up by the astrocytic processes at several synapses lying within their spatial domain, and *K^+ spatial buffering*, in which K^+ ions propagate through gap-junction mediated astrocytic networks to more distal regions of the astrocytic networks[21,32].

Physiological processes that impact neuronal depolarization can impact membrane oscillation frequency and amplitude[33]. Several studies have reported on the impact of increased $[K^+]_o$ on neuronal depolarization, however the majority of these reports were in regards to pathological conditions, such as ALS[34], epilepsy, Rett syndrome and Huntington's disease, reviewed by[30]. Here, we have used electrophysiological and pharmacological tools to investigate the impact of astrocytic K^+ clearance in modulating neural oscillations at both cellular and network levels.

Results

High extracellular K^+ impacts cortical oscillatory dynamics. To investigate the impact of alterations in extracellular K^+ concentrations ($[K^+]_o$) on local network excitability and rhythmic activity, we have monitored cortical network oscillations using extracellular recordings. Two electrodes were positioned in layers II/III of the somatosensory cortex with a distance of approximately 200 µm (Fig. 1) to monitor oscillation propagation. To increase $[K^+]_o$ locally, a third electrode was used to apply high K^+ solution (30 mM KCl) in the vicinity of the first recording electrode (Fig. 1).

Extracellular field recordings were divided into three sequential periods termed '***Baseline***' - referring to non-stimulated network activity, "***High K^+***" - the episode immediately following brief (1 sec) local application of KCl for defining the immediate effect of high $[K^+]_o$ (10 sec, based on multi-unit activity (MUA), see Supplementary Fig. S1), and "***Recovery***" - the recovery period during which $[K^+]_o$ was decreased by both diffusion and the K^+ clearance process (Fig. 1). Analysis of the field recordings at each period revealed a substantial increase of both network oscillations and multi-unit (MU) activity immediately following the application of 30 mM KCl (Fig. 1b,c). While during the 'Baseline' period the average MU frequency was 0.13 ± 0.04 Hz ($n = 15$), during the 'High K^+' period, MU frequency increased significantly to 2.45 ± 0.39 Hz ($p < 0.01$; student t-test), and returned to baseline levels during the 'Recovery' period (0.08 ± 0.02; Fig. 1c). Power spectrum analysis of the **network oscillations** showed that the dominant subthreshold network oscillation frequency in the 'Baseline' period was < 1 Hz (Supplementary Fig. S2), which is consistent with previous *in vitro* studies[3]. However, following local application of 30 mM KCl in the vicinity of the recording electrode, the oscillation power increased across a wide range of frequencies, as shown in Fig. 1d.

To evaluate the impact of increased $[K^+]_o$ on ***high frequency network oscillations***, which are usually absent in slice preparations due to limited circuitry[3], we repeated the above experiments in the presence of the cholinergic agonist Carbachol (100µM) that has been shown to elicit network oscillations in the gamma frequency range *in vitro*[35–37]. Our results show that bath application of Carbachol augmented the amplitude of subthreshold network oscillations at all periods (Fig. 1e). Moreover, a transient increase of $[K^+]_o$ in the presence of Carbachol led to an increase of oscillation amplitude across a wide range of frequencies, with maximum peaks at 25 & 35 Hz. These results support the concept that $[K^+]_o$ concentration can impact the network activity during both low and high frequency oscillations.

We then studied the impact of a rise in $[K^+]_o$ on the passive and active properties of layer V cortical neurons, employing intracellular recordings (Fig. 2a). Consistent with the Goldman-Hodgkin-Katz equation for the resting membrane potential (RMP)[38], transient bath application of KCl at different concentrations (5–30 mM) led to depolarization of the RMP of nearby neurons, in a concentration-dependent manner (Fig. 2b). The changes in membrane potential were accompanied with alterations in membrane conductance, as the membrane input resistance (R_n) and time constant (τ) were inversely correlated to the increase in membrane potential (Fig. 2b,c; Supplementary Table S1). These alterations in membrane potential, input resistance and time constant were

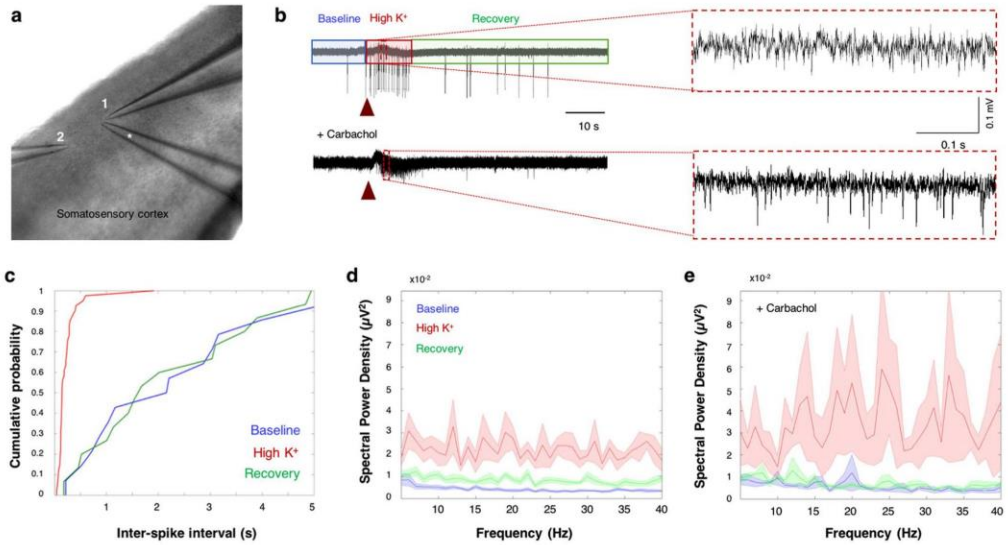

Figure 1. High extracellular K^+ leads to network excitability. (**a**) Experimental setup showing the position of two recording electrodes in layer II/III of the somatosensory cortex for dual extracellular recordings. High KCl (30 mM) is locally applied to the vicinity of recording electrode 1 using a third 'puff electrode' (*). (**b**) Local field potentials (LFP) traces showing the network activity before and after stimulus (red arrow), both in normal aCSF (top) and in the presence of 100 μM Carbachol (bottom). Note the low-frequency (top) and high-frequency (bottom) oscillations following application of 30 mM KCl (insets). (**c**) Quantitative analysis of the inter-spike intervals during the 60-second recordings reveals a significant increase in the network spiking frequency after stimulation with 30 mM KCl (red, 'High K^{+}') compared to 'Baseline' (blue) or 'Recovery' (green) periods under normal aCSF conditions ($n = 15$; KS-test $p < 0.01$). (**d**) Power spectrum analysis displaying the averaged (line) and standard error values (shade) of the dominating subthreshold oscillations during 'Baseline' (blue), 'High K^{+}' (red) and 'Recovery' (green) periods, under normal aCSF (**d**) and 100 μM Carbachol (**e**). Note the power increase in multiple frequencies at both low (normal aCSF) and high (Carbachol) frequency network oscillations following stimulus.

transient and returned to baseline values once $[K^+]_o$ was restored to 3 mM (Fig. 2c). These results are consistent with previous data showing that increased levels of $[K^+]_o$, above its physiological concentration (~3 mM), lead to significant membrane depolarization and altered synaptic function[28,39,40].

Alterations in $[K^+]_o$ also affected membrane resonance features. Neuronal membrane resonance is determined by the interplay between active and passive membrane properties and describes the ability of neurons to respond selectively to inputs at preferred frequencies (hence resonance frequency[5]). A recent study showed that the membrane resonance frequency is strongly correlated with the network oscillation frequencies[9]. In cortical neurons, the resonance frequency has been reported to be dependent on the interplay between two currents, a slowly activating K^+ current and a fast-persistent Na^+ current[33]. Thus, it is not surprising that excessive K^+ accumulation at the synaptic cleft affected the membrane resonance frequency of nearby neurons in a concentration-dependent manner. While the average peak resonance frequency at the soma was 1.5 ± 0.2 Hz at 3 mM $[K^+]_o$ ($n = 14$), it significantly increased to 2.5 ± 0.2 Hz at 30 mM $[K^+]_o$ ($n = 12$, $p > 0.01$; student t-test), whereas lower $[K^+]_o$ deviated the peak resonance frequency to a lesser extent (Supplementary Table S1, Supplementary Fig. S3). Moreover, following an increase in $[K^+]_o$, the full width at half amplitude (FWHA) of the impedance profile shifted significantly towards higher frequencies (3.8 ± 1.1 Hz at 30 mM $[K^+]_o$ vs 2.2 ± 0.3 Hz at 3 mM $[K^+]_o$; Fig. 2d), and restored to baseline values during the 'Recovery' period (2.1 ± 0.5 Hz; Fig. 2d).

Alterations of $[K^+]_o$ also affected active membrane properties, including spike rheobase and spike width at half amplitude (SWHA) in a concentration-dependent manner (Fig. 2e,f). During low $[K^+]_o$, the average spike rheobase was 47.8 ± 4.1 pA ($n = 68$) and decreased to 25.6 ± 4.6 pA, 21.1 ± 4.6 pA, 17.9 ± 2.8 pA, and 12.3 ± 1.0 pA following application of 5, 10, 15 and 30 mM $[K^+]_o$, respectively ($p < 0.01$, student t-test, Fig. 2e, Supplementary Table S1). The average SWHA at physiological K^+ concentrations (3 mM) was 2.3 ± 0.1 ms ($n = 70$) and significantly increased to 3.7 ± 0.3 ms at $[K^+]_o$ higher than 15 mM ($n = 31$; $p < 0.01$, student t-test; Fig. 2f). Once $[K^+]_o$ returned to baseline values (following washout with 3 mM K^+ aCSF), both spike rheobase and SWHA were restored to baseline values (Fig. 2e,f).

Neuronal spiking activity underlies the execution of neuronal output and is strongly dependent on neuronal membrane resonance frequency[9]. The spike threshold is determined by a complex interaction of

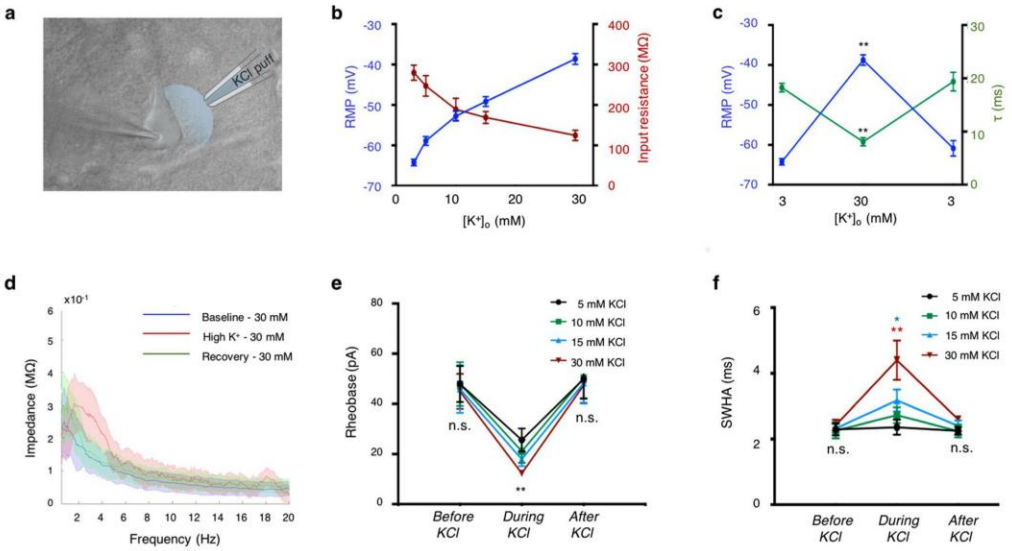

Figure 2. High extracellular K^+ affects individual neuronal excitability. (**a**) DIC image showing the experimental setup. Whole-cell patch-clamp recording of layer V cortical neuron during local application of various concentrations of KCl through a puff electrode to increase the extracellular K^+. (**b**) Elevation of $[K^+]_o$ lead to depolarization of the resting membrane potential (RMP) and decrease of the input resistance in a concentration-dependent manner. (**c**) The impact of high K^+ on RMP and membrane time constant (τ) is transient. Note the inverse correlation of τ and RMP following increase of extracellular K^+. (**d**) Impedance amplitude profile following ZAP protocol depicting the mean (line) and standard deviation values (shade) before, during and after local application of KCl (30 mM, color-coded) under normal aCSF conditions. Note the shift towards higher frequencies during application of elevated KCl. (**e,f**) Plots depicting the transient impact of high K^+ on spike threshold (**e**) and spike width at half amplitude (SWHA) (**f**), in a concentration-dependent manner (30 mM n = 18; 15 mM n = 17; 10 mM n = 15; 5 mM n = 15). *$P < 0.05$; **$P < 0.01$; *student t-test*.

voltage-dependent inward and outward currents, and reflects the membrane excitability. As the membrane potential of cortical neurons is constantly oscillating, as a result of the influence of local network activity, their excitability should be investigated under similar conditions. In order to evaluate the relationship between membrane oscillation frequencies and spike threshold, we injected sinusoidal currents at different intensities (30–250 pA chirp current) in increasing frequencies (0.1–100 Hz; Fig. 3a). This protocol detects neuronal excitability at instantaneous sinusoidal frequencies[41], and allows an evaluation of the relationship between neuronal excitability and oscillatory behaviour (Fig. 3a), depicted by the Frequency-Spiking plot (Fig. 3b).

Our results indicate that a transient increase of $[K^+]_o$ led to a shift of the frequency excitability range towards higher frequencies, in a concentration-dependent manner across different stimulus intensities (Fig. 3b). Under baseline conditions (3 mM of $[K^+]_o$), the maximal frequency in which layer V cortical neurons were excitable was 18.9 ± 1.1 Hz (250 pA, n = 43), and increased to 36.8 ± 1.8 Hz once local $[K^+]_o$ increased to 30 mM. The frequency excitability range returned to previous values, once $[K^+]_o$ returned to baseline (18.7 ± 1.7 Hz; Fig. 3b). These results emphasize the impact of a rise in $[K^+]_o$ on neuronal excitability at both cellular and network levels, supporting an active role for K^+ homeostasis in modulating network activity.

Modulation of astrocytic K^+ clearance impacts neuronal excitability and network rhythmicity. Astrocytic K^+ clearance following neuronal activity is mediated via several transporting mechanisms, commencing with K^+ uptake via Kir4.1 channels and Na^+/K^+-ATPase, through distribution of K^+ across astrocytic gap junctions (Cx30/Cx43) to astrocytes with lower K^+ concentration, and terminated by redistribution of K^+ to distant cortical areas[30]. To study the dynamic role of *astrocytic K^+ clearance* mechanisms in modulating network oscillations, we have measured the local network activity while modifying either K^+ uptake through Kir4.1 channels that are selectively expressed in astrocytes and are responsible for ~45% of the K^+ uptake[32,42,43], or K^+ distribution through the astrocytic syncytium via selective blockade of Cx43 gap junctions.

Modulation of K^+ uptake by astrocytes. Barium is a non-specific K^+ channel inhibitor, but concentrations up to 100 µM predominantly inhibit the Kir subfamily[44], whereas higher concentrations affect the Na^+/K^+-ATPase (reviewed by[32]). Bath application of $BaCl_2$ at low concentration (100 µM) did not affect the network activity during the baseline period (Fig. 4a), as cortical slices usually have low spiking activity in the absence of stimulation[3]. However, following local application of KCl (30 mM), inhibition of astrocytic Kir channels led to

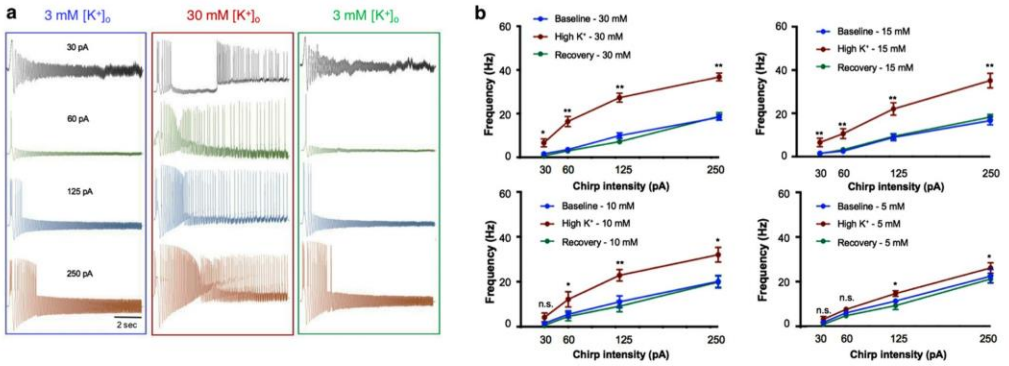

Figure 3. The impact of extracellular K^+ on frequency-excitability range. (**a**) Sample traces following sinusoidal chirp stimulation (0.1–100 Hz) at different intensities (from top to bottom: 30 pA, 60 pA, 125 pA, 250 pA), recorded from the neuronal soma before (left), during (middle) and after (right) application of 30 mM KCl under normal aCSF conditions. (**b**) Frequency – excitability plot depicting the relationship between the oscillation intensity and the maximal frequency at which the cell is still excitable. Note the upward shift in the maximal frequency following application of KCl at various concentrations (30 mM KCl n = 18; 15 mM KCl n = 17; 10 mM KCl n = 15; 5 mM KCl n = 15). *$P < 0.05$; **$P < 0.01$; *student t-test.*

a substantial increase in network excitability, expressed as a significant rise of the MU frequency (27.1 ± 3.6 vs 2.45 ± 0.4, n = 16; $p < 0.01$; student t-test; Fig. 4b) and reduction of the inter-spike intervals ($BaCl_2$ vs ACSF; $p < 0.01$, KS-test, Fig. 4c). Similarly, analysis of the 'Recovery' period, during which K^+ is cleared from the extracellular milieu, showed that compared to normal aCSF, blockade of K^+ uptake by astrocytes led to a significant increase of the MU frequency (1.8 ± 0.4 Hz vs 0.08 ± 0.02 Hz, $p < 0.01$, student t-test; Fig. 4b) and reduction in the inter-spike intervals ($p < 0.01$, KS-Test; Fig. 4c), indicating network hyperexcitability. Moreover, Barium significantly increased the duration of the 'Recovery' period compared to normal aCSF (Supplementary Fig. S1, aCSF vs $BaCl_2$, $p < 0.01$), indicating that modulation of astrocytic Kir4.1 channel activity, which affects the removal of excessive $[K^+]_o$, can extend the hyper-synchronous firing activity at the network level.

Analysis of the field potential during Barium application showed that the power of cortical oscillations increases significantly across multiple frequencies at both ***'High K^{+}'*** and '***Recovery***' periods (Fig. 4d). To compare between the spectrum densities of network oscillations, we divided the power spectrum into five frequency bands: delta (1–4 Hz), theta (4–8 Hz), alpha (8–12 Hz), beta (12–30 Hz) and gamma (> 30 Hz). Our results indicate that blockade of Kir4.1 channels led to an increase of the oscillation amplitude across different frequencies, peaking in the beta and gamma range during the 'High K^+' period (Fig. 4d; Fig. 5d,e), and theta and beta range during the 'Recovery' period (Figs 4d, and 5). These results indicate that high frequency network oscillations are supported by enhanced network excitability, mediated by a significant rise of $[K^+]_o$.

Modulation of K^+ distribution via the astrocytic syncytium. We next assessed the impact of K^+ clearance via the astrocytic syncytium on the network activity. To selectively disrupt the astrocytic syncytium activity, we incubated the slices with a mixture of connexin 43 mimetic peptides (GAP-26, 200μM and GAP-27, 300μM), that selectively decrease astrocytic connectivity via electrical gap junctions (Fig. 6a,b), as previously reported by[45,46]. This led to a decrease in astrocytic coupling, as indicated by a significant decline of directly connected astrocytes from 19.8 ± 1.8 to 1.9 ± 0.3 (n = 12, $p < 0.01$; Fig. 5b; see also Supplementary Fig. S4).

Following modulation of astrocytic connectivity, we observed a significant increase of neuronal excitability during the 'High K^+' and 'Recovery' periods, expressed as an increase in MU frequency (13.36 ± 2.73 Hz vs 2.45 ± 0.39 Hz at 'High K^+', and 1.12 ± 0.13 vs 0.08 ± 0.02 at 'Recovery' period; n = 13; $p < 0.01$, student t-test; Fig. 6c) and reduction in the inter-spike intervals ($p < 0.01$, KS-test; Fig. 6d). Moreover, the oscillation power increased across a wide range of frequencies, especially at the beta and gamma range during 'High K^+' (Figs 6e and 5), and most frequencies during the 'Recovery' period, indicating that modulation of the processes that affect the removal of excessive $[K^+]_o$ result in hyperexcitable activity at the network level.

Alterations of astrocytic K^+ clearance modulate the oscillatory properties of neurons. Evaluation of the impact of local alterations in astrocytic K^+ uptake and buffering on nearby layer V cortical neurons revealed a substantial influence on both passive and active membrane properties. While in the 'Baseline' period, all membrane properties were comparable, either following bath application of $BaCl_2$ (n = 63) or GAP-26/27 mixture ((n = 60; Fig. 7a–c), during the 'High K^+' period, the membrane resonance peaked at higher frequencies ($BaCl_2$ = 4.4 ± 0.2 Hz, n = 12; GAP 26/27 = 4.1 ± 0.3 Hz, n = 13; $p < 0.01$ student t-test; Fig. 7d), and the impedance profile indicated a widening of the FWHA from 3.8 ± 1.1 Hz to 6.7 ± 0.8 Hz with $BaCl_2$, and to 8.0 ± 1.3 Hz with Gap26/27, suggesting that the membrane can resonate over a wider range of frequencies once astrocytic clearance is impaired. These alterations in the impedance profile were more noticeable in the 'Recovery' period,

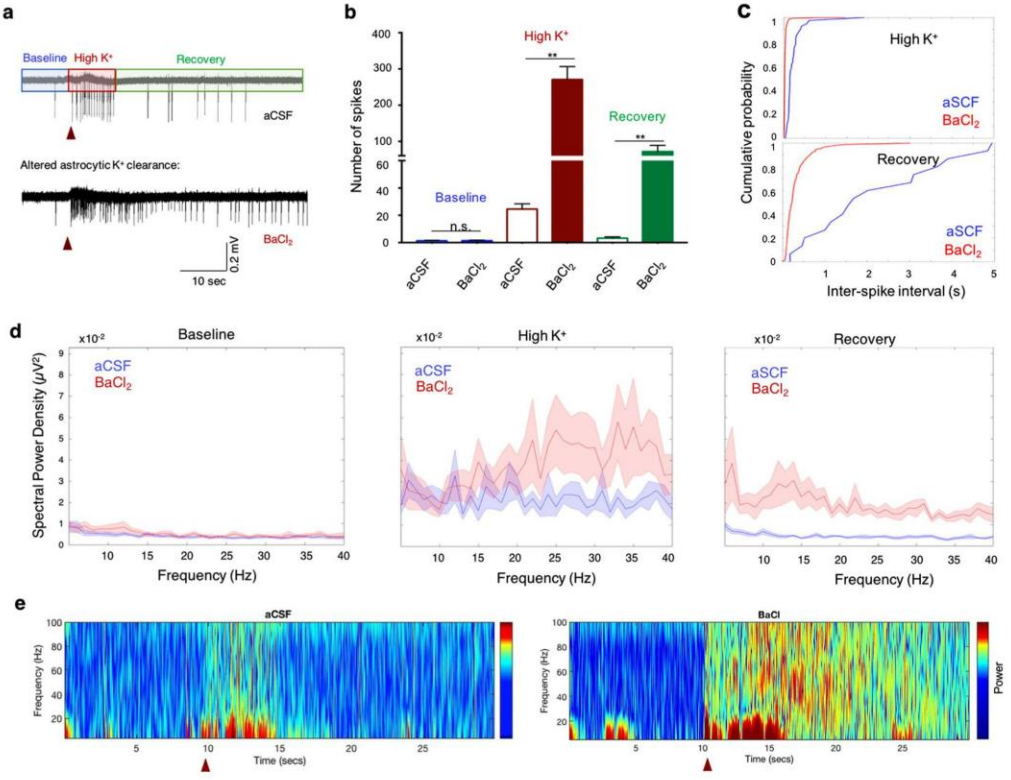

Figure 4. Modulation of astrocytic K^+ uptake affects network excitability. (**a**) Extracellular recordings showing the network activity before and after stimulus with 30 mM KCl (red arrow), in normal aCSF (top) and after bath application of 100 μM $BaCl_2$ (bottom). The network spiking activity has been divided into three periods for subsequent analysis: 'Baseline', 'High K^+' and 'Recovery' periods. (**b**) Quantitative analysis of the network excitability during the different episodes (color-coded) revealed an increase in the number of spikes following stimulus (High K^+), which decrease during the "Recovery" period in normal aCSF (n = 15). Blocking K^+ uptake via bath application of $BaCl_2$ results in a significant increase in the number of spikes (**b**) and decrease in inter-spike intervals (**c**) during both 'High K^+' and 'Recovery' periods (n = 16; $p < 0.01$; KS-test $p < 0.01$). (**d**) Power spectrum analysis depicting the averaged (line) and standard error values (shade) of the dominant oscillation frequencies governing Baseline, High K^+ and Recovery periods under normal aCSF and reduced astrocytic K^+ clearance ($BaCl_2$, top) conditions. Note the increase in the oscillation power at frequencies in the beta and gamma range under 100 μM $BaCl_2$. (**e**) Colour coded spectrogram of the network oscillations in normal aCSF (left) and following bath application of 100 μM $BaCl_2$ (right). Red triangles at the bottom indicate the time of local application of 30 mM KCl. *$P < 0.05$; **$P < 0.01$; *student t-test.*

in which the FWHA increased from 2.1 ± 0.5 Hz to 4.8 ± 0.6 with $BaCl_2$, and 5.2 ± 1.1 Hz following incubation with Gap26/27 (Fig. 7d; Supplementary Table S1).

These deviations in membrane resonance were accompanied with a decrease of the input resistance during both 'High K^+' and 'Recovery' periods (Fig. 7f,i) and depolarization of the resting membrane potential during the 'Recovery' period (Fig. 7h), consistent with the results of high $[K^+]_o$ (Fig. 2b). Moreover, modulation of astrocytic K^+ clearance led to firing of action potentials at higher frequencies as indicated by an upward shift of the frequency spiking range at both 'High K^+' (Fig. 7g) and 'Recovery' periods (Fig. 7j).

Discussion

Network rhythmic oscillations are a product of complex neural activity in networks of multiple neurons that are activated synchronously. This synchronous activity of oscillating networks is viewed as the critical link between single-neuron activity and behaviour, or 'brain state', and as such, it is a diagnostic tool used both clinically and in brain research, reviewed by[2]. In a recent paper, Lee & Dan suggested that there are two fundamental questions concerning brain states: i) what mechanisms control brain states and ii) what is the function of each state[47]. We

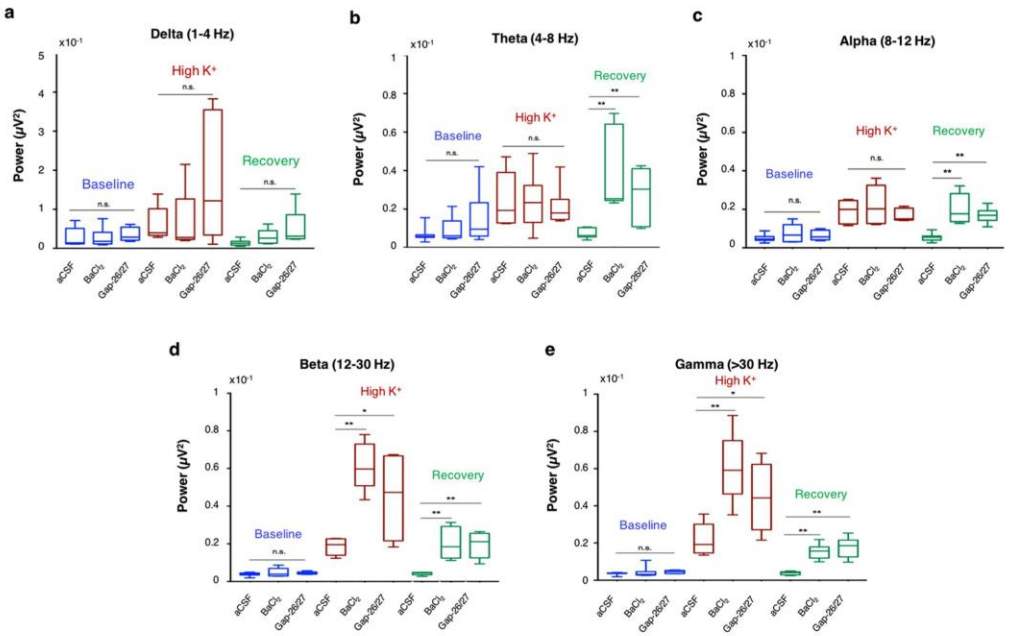

Figure 5. Modulation of astrocytic K^+ clearance increase the power of cortical oscillations at multiple frequencies. (**a**) Power spectrum density of cortical oscillations were divided into five frequency bands: delta (1–4 Hz), theta (4–8 Hz), alpha (8–12 Hz), beta (12–30 Hz) and gamma (>30 Hz) (**a**–**e**). The average power for each trial was than plotted during 'Baseline', 'High K^+' and 'Recovery' periods. Comparison of the average power during the 'High K^+' period revealed that modulation of astrocytic K^+ clearance by $BaCl_2$ or Gap-26/27 lead to significant rise at the Beta and Gamma range (**d**,**e**). Comparison of the average power during the 'Recovery' period show a significant rise in the theta, alpha, beta and gamma frequencies, once astrocytic K^+ clearance is impaired. *$P < 0.05$; **$P < 0.01$; student t-test.

suggest that astrocytes play an essential role in the mechanisms that gear the transition between the different brain states.

The transition between distinctive network oscillation frequencies is due to recruitment of discrete neural networks, which are associated with different behavioural tasks, such as sleep, learning, and attention[2,48,49]. Animals constantly switch between behavioural states, and thus oscillation frequencies, as a reaction to the ever-changing environment. Regulation of the transition between these oscillations is essential for animal survival, and disruption of the normal regulatory mechanisms results in disorders such as epilepsy, Rett syndrome and sleep apnoea, reviewed by[30]. However much remains to be learned about the exact mechanisms that modulate this transition.

Our results indicate that alteration of $[K^+]_o$ modulates network excitability, affecting both low and high frequency oscillations (Figs 1, 5). At the cellular level, enhanced excitability of individual neurons is seen by the transient decrease in the rheobase, accompanied by alterations in membrane properties including decrease of input resistance, reduced time constant, depolarization of the resting membrane potential, and shift of the oscillatory properties towards higher frequencies (Fig. 2), that result in an upward shift of the frequency range in which neurons were still excitable (Fig. 3). These results are consistent with experimental *in vivo*, *in vitro*, and modelling studies of transitions between cortical active and silent states, showing that periods of high activity are accompanied by a decrease in input resistance mediated by a simultaneous increase in both excitation and inhibition[28,50,51], as well as increase in voltage-gated conductances as a consequence of membrane depolarization[52]. At the network level, enhanced excitability is depicted as increased MU frequency and increase in oscillation power over a wide spectrum of frequencies (Figs 1, 4).

Subthreshold membrane potential fluctuations of individual neurons are strongly correlated with their local network activity[53,54], which is also influenced by their resonance frequency[2]. The resonance frequency is an intrinsic property of the neuron, emerging from the effects of the membrane leak conductance and capacitance, however it can be modulated by voltage dependent currents[5,33]. Previous reports showed that network oscillations are dependent on K^+ dynamics[55], however the exact mechanism was not resolved. Here we show for the first time that modulation of astrocytic K^+ clearance can impact the resonance frequency of single neurons (Fig. 7d), promoting their oscillatory activity over a wider frequency spectrum (Figs 7g,j), that impacts the network oscillatory behaviour (Figs 4d and 6d).

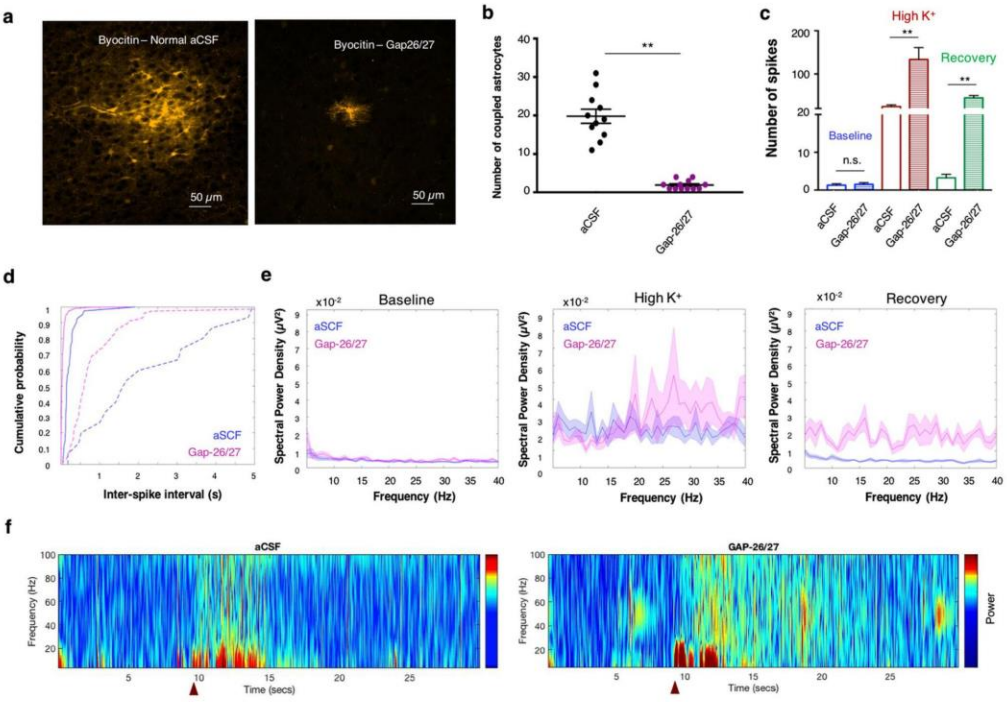

Figure 6. Reduced astrocytic connectivity impacts on network excitability and oscillation frequencies. (**a**) 40x confocal image of biocytin-stained astrocytes in layer II/III of the somatosensory cortex, depicting the astrocytic network under normal aCSF conditions (left) and following application of GAP-26/27 (right). (**b**) Selective blockade of connexin 43 by pretreatment of GAP26/27 mixture significantly decreases astrocytic connectivity compared to normal aCSF conditions ($n = 12$, $p < 0.01$). (**c**) Quantitative analysis of the network excitability at the different periods (color-coded) reveals that reduction in astrocytic connectivity leads to a significant increase in the number of spikes during both "High K^+" and "Recovery" periods compared to normal aCSF ($n = 13$, $p < 0.01$). (**d**) Cumulative probability distribution of inter-spike intervals during "High K^+" (continuous line) and "Recovery" (dashed line) periods is shifted towards the left in the presence of Gap-26/27 compared to normal aCSF ($n = 13$, KS-test $p < 0.01$). (**e**) Power spectrum analysis depicting the averaged (line) and standard error values (shade) of the dominant subthreshold oscillation frequencies governing Baseline, High K^+ and Recovery periods under normal aCSF and Gap-26/27 conditions. Note the increase in the oscillation power at frequencies in the beta and gamma range. (**f**) Colour coded spectrogram of the network oscillations in normal aCSF (left) and following bath application of GAP-26/27 (right). Red triangles at the bottom indicate the time of local application of 30 mM KCl. ***P < 0.01; student t-test.*

For proper function, astrocytes can function either individually within their spatial domain[56], or as a syncytium, reviewed by[30]. K^+ clearance from the extracellular milieu is a multi-step process that requires firstly K^+ taken up by individual astrocytic processes, and then recruiting of the astrocytic network to transfer the excess K^+ ions to regions with low K^+ concentration. We have divided the extracellular recordings into three periods that are correlated to the different stages of the astrocytic clearance process. During the 'Baseline' period, $[K^+]_o$ concentration is low (3 mM), obviating the need for clearing mechanisms. The 'High K^+' period is characterized by an immediate local increase in $[K^+]_o$ as occurs following repetitive spiking activity, or release of neuromodulators[29], which slowly decreases due to activation of K^+ uptake by astrocytes, as well as diffusion to distant regions. Although we refer to this time window as a single period, it is not homogenous, as the $[K^+]_o$ concentration and thus uptake mechanism reduces with time. The recovery period characterizes the processes taking place while high $[K^+]_o$ is washing out, and local $[K^+]_o$ is slowly decreasing to baseline values. During this period, $[K^+]_o$ is mainly decreased via astrocytic uptake and less through diffusion.

Blocking astrocytic K^+ uptake with a low concentration of Barium ($BaCl_2$, 100 μM) enhanced the resonance frequency range of individual neurons at both 'High K^+' and 'Recovery' periods (Fig. 7, Supplementary Fig. S3), which led to a significant increase of the maximal spiking frequency (Fig. 7) and MU frequency (Fig. 4, Supplementary Fig. S1). At the network oscillations level, blocking Kir channels results in augmentation of the

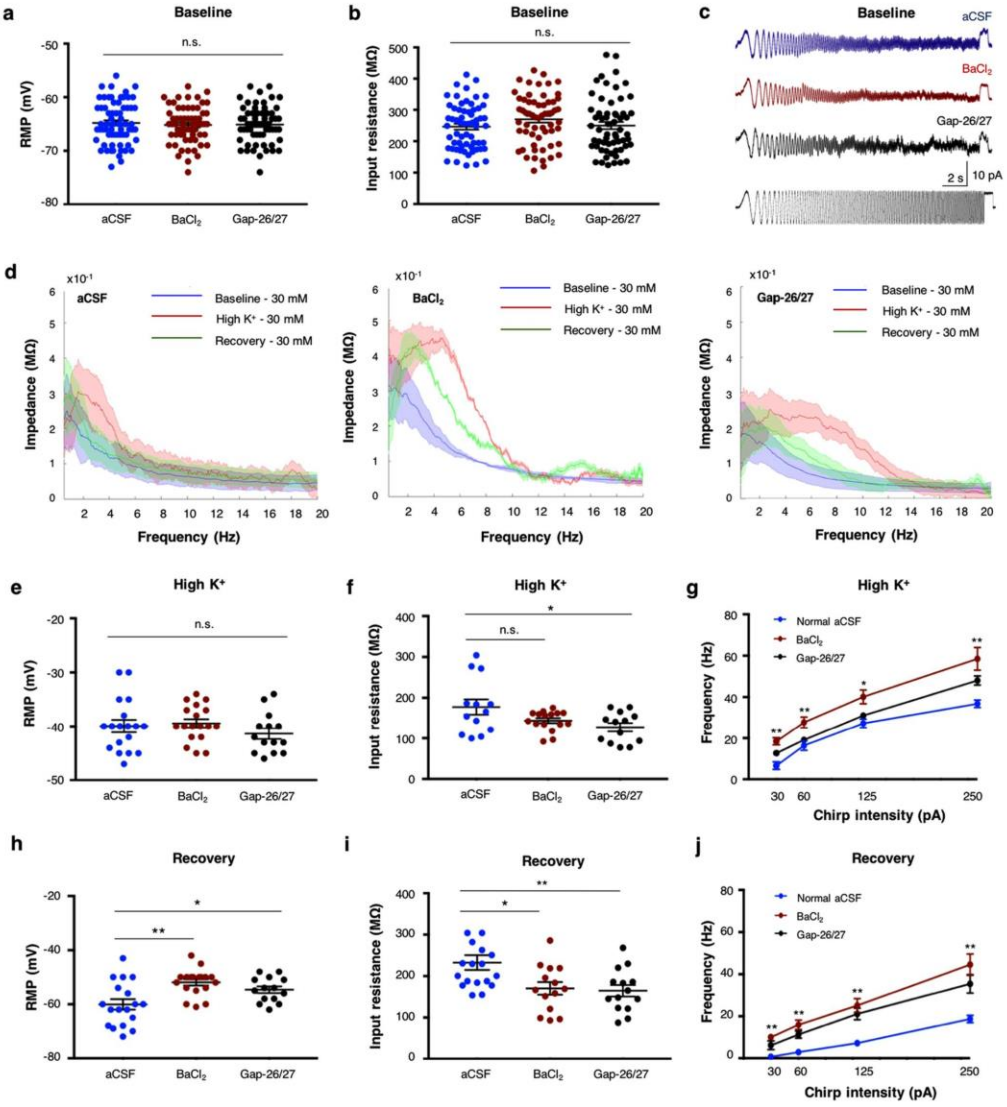

Figure 7. Modulation of astrocytic K^+ clearance impacts on membrane properties of nearby neurons. (**a**) Comparison of the membrane properties between normal aCSF (n = 66), $BaCl_2$ (n = 63) and Gap-26/27 (n = 60) conditions, depict no significant differences in RMP (**a**) or input resistance (**b**) during the 'Baseline' period. (**c**) Sample traces of membrane oscillations recorded during sinusoidal subthreshold ZAP stimulation (10 pA, bottom trace) under normal aCSF (top), $BaCl_2$ (middle) and Gap-26/27 (bottom) conditions at the 'Baseline' period. (**d**) Impedance frequency profiles depicting the averaged (line) and standard deviation (shade) values of the resonance frequency recorded at the soma before, during and after application of 30 mM KCl (color-coded), under normal aCSF (left), 100 μM $BaCl_2$ (middle) and GAP-26/27 (right) conditions. (**e**) Comparison of the membrane properties between normal aCSF (n = 18), $BaCl_2$ (n = 18) and Gap-26/27 (n = 14) conditions at the 'High K^+' period, depict no alterations in RMP (**e**) and decrease in input resistance following application of Gap-26/27 (**f**); $p < 0.05$). (**g**) Plot of the frequency-excitability range during the 'High K^+' period depicts a significant increase in the maximum frequency under $BaCl_2$ (n = 18) and GAP 26/27 (n = 14) compared to normal aCSF (n = 18). (**h**) Alterations in astrocytic K^+ clearance result in a significant depolarization of the RMP (**h**) and decrease of the input resistance (**i**), which led to an upward shift of the frequency-excitability range (**j**). *$P < 0.05$; **$P < 0.01$; student t-test.*

oscillation power at the beta and gamma frequency range during the 'High K^+' period, and most frequencies during the 'Recovery' period (Figs 4, 5).

Consistent with these results, incubation of cortical slices with a mixture of Cx-43 antagonists (GAP-26, GAP-27), that interrupt the astrocytic coupling and thus stopped them from working as a syncytium (Fig. 6), increased the duration of the 'Recovery' period (Supplementary Fig. S1). Moreover, blocking astrocytic coupling boosted the maximal spiking frequency at both 'High K^+' and 'Recovery' periods (Fig. 6), and enhanced the resonance frequency range (Fig. 7, Supplementary Fig. S3) that led to enhancement of the oscillation power in the beta and gamma range during the 'High K^+' period. Furthermore, disruption of the astrocytic coupling augmented power oscillations across most frequencies during the 'Recovery' period (Figs 5, 6), emphasizing the importance of astrocytic coupling in mediating K^+ homeostasis and facilitating the transition between network oscillations. However, blocking gap junctions can also effect other processes that require astrocytic coupling for their physiological activity, including calcium waves, which might affect the power of these cortical oscillations.

In his seminal work, Steriade showed that the network oscillation frequencies are inversely correlated to the oscillations power, and that fast oscillations correspond to desynchronized states, while slow frequency-high amplitude oscillations correspond to synchronised network activity[48]. The recruitment of neurons into specific networks that control each brain state has been attributed to the activity of neuromodulators such as acetylcholine (ACh), noradrenaline (NA), serotonin (5-HT), dopamine (DA), and histamine (HA), originating from distinct groups of neurons located in subcortical areas[47,57,58]. While agonists of these neuromodulators affects arousal and attention, leading to desynchronization of cortical activity[47,58,59], their antagonists promote sleep and synchronous network activity. Yet, despite their crucial role in brain function, it remains unclear how these neuromodulators coordinate state-dependent, global changes in neuronal activity.

Recently Ma and colleagues showed that neuromodulators can signal through astrocytes, by affecting their calcium oscillations, to alter neuronal network activity[60]. Consistent with their work, Nedergaard's group showed that neuromodulators can impact the concentration of extracellular K^+, regardless of synaptic activity[29], and suggested that neuromodulators work in parallel on both neurons and astrocytes, to maximise their impact on synchronous activity and recruitment of neurons into networks. Our results depicting the astrocytic impact on $[K^+]_o$ dynamics and network oscillatory behaviour are consistent with this view. We show that modulation of different phases in the clearance process, either at the uptake level or buffering through the astrocytic network, results in alterations of the oscillatory activity of individual neurons, as well as the network behaviour.

Materials and Methods

Animals. We used P21-P28 days-old mice expressing GFP under a GFAP promoter (strain 003257, Jax laboratories). All animals were healthy and handled with standard conditions of temperature, humidity, twelve hours light/dark cycle, free access to food and water, and without any intended stress stimuli. All experiments were approved and performed in accordance with Western Sydney University committee for animal use and care guidelines (Animal Research Authority #A10588).

Slice preparation. Animals were deeply anesthetized by inhalation of isoflurane (5%), decapitated, and their brains were quickly removed and placed into ice-cold physiological solution (artificial CSF, aCSF) containing (in mM): 125 NaCl, 2.5 KCl, 1 $MgCl_2$, 1.25 NaH_2PO_4, 2 $CaCl_2$, 25 $NaHCO_3$, 25 glucose and saturated with carbogen (95% O_2−5% CO_2 mixture; pH 7.4). Parasagittal brain slices (300 μm thick) were cut with a vibrating microtome (Leica VT1200S) and transferred to the Braincubator™ (PaYo Scientific, Sydney), as reported previously[61]. The Braincubator is an incubation system that closely monitors and controls pH, carbogen flow and temperature, as well as irradiating bacteria through a separate UV chamber[62,63]. Slices were initially incubated for 12 min at 35 °C, after which they were allowed to cool to 15–16 °C and kept in the Braincubator™ for at least 30 min before any measurement[64].

Electrophysiological recording and stimulation. The recording chamber was mounted on an Olympus BX-51 microscope equipped with IR/DIC optics and Polygon 400 patterned illuminator (Mightex). Following the incubation period in the Braincubator, slices were mounted in the recording chamber for a minimum of 15 min, to allow them to warm up to room temperature (~22 °C), and were constantly perfused at a rate of 2–3 ml/min with carbogenated aCSF, as reported previously[65].

Extracellular recordings of network oscillations were performed by placing two recording electrodes, tip diameter of 1 μm (2–3 MΩ), in layer II/III of the somatosensory cortex, with an inter-electrode distance of one barrel (appx 200 μm). Network oscillations were induced by reducing the concentration of Ca^{2+} (1.2 mM) and Mg^{2+} (1 mM) in the bath solution, as previously reported[3]. Transient increase of extracellular K^+ was achieved by applying a 1-second positive pressure (~0.2 ml) of potassium chloride (KCl) at different concentration through a puffing electrode (tip diameter of 2 μm, ~1 MΩ) placed in the vicinity of the 1st recording electrode (Fig. 1).

Whole-cell intracellular recordings from layer V pyramidal neurons in the somatosensory cortex were obtained with patch pipettes (5–7 MΩ) containing (in mM): 130 K-Methansulfate, 10 HEPES, 0.05 EGTA, 7 KCl, 0.5 Na_2GTP, 2 Na_2ATP, 2 MgATP, 7 phosphocreatine, and titrated with KOH to pH 7.2 (~285 mOsm). Voltages were recorded in current clamp mode using a multiclamp 700B dual patch-clamp amplifier (Molecular Devices), digitally sampled at 30–50 kHz, filtered at 10 kHz, and analysed off-line using pClamp 10 software[41]. Cells were considered stable and suitable for analysis if the input resistance did not change more than 20% during the baseline recordings, before any treatment.

Membrane properties were obtained before, during and after local application of KCl at different concentrations (30, 15, 10, 5 mM), applied through a puffing electrode placed in the vicinity of the recording electrode. Following application of KCl, the puffing electrode was removed to allow potassium wash-out for 2 minutes before resuming intracellular recordings.

Suprathreshold sinusoidal stimulus protocol. In order to evaluate the alterations in suprathreshold oscillation frequencies under different conditions, 10-second stimulating protocols of sinusoidal current (chirp stimulation), in which there was a linear increase in the frequency from 0.1 to 100 Hz, were designed at 30, 60, 125 and 250 pA, using the pClamp 10 software suit (Molecular devices, Sunnyvale, CA) and injected to the neuronal soma through the recording electrode.

Measuring astrocytic coupling. To evaluate the degree of astrocytic coupling, individual astrocytes were loaded with intracellular solution containing biocytin (0.3%; Sigma) for 12 min in whole cell mode (supplementary Fig. S4). After a 12-min labelling period, the slices were immersed in fixative (4% paraformaldehyde in phosphate-buffered saline (PBS), pH 7.4) at 4°C for at least 24 h and then stored in PBS. To visualize the biocytin-filled cells, the slices were treated with 1:200 Alexa-Fluo conjugated Streptavidin in PBS with 1% Triton X-100 for 48 h, followed by washing in PBS, as previously described by[66].

To inhibit gap junction coupling in astrocytes, slices were pre-treated with a mixture of GAP-26 (200 μM, AnaSpec) and GAP-27 (300 μM, AnaSpec) for 15 min before patch clamp recordings. Stained astrocytes were counted using the "pointpicker" plugin of ImageJ. The average intensity of the Biocytin signals was used as cut-off to distinguish the recorded cells from other cells that were coupled to it. For each slice, z-stacks were typically acquired to include the entire biocytin-stained syncytia.

Power spectral density. To assess the dominant frequencies of the network oscillations under different conditions we used power spectrum density (PSD) analysis. The principal frequencies were disclosed by applying Fast Fourier Transform (FFT) directly to the raw data, as previously described by[67]. Each recording was divided into three distinct sections: 'Baseline', '$High\ K^+$', and 'Recovery', based on inter-spike interval observations under normal conditions, as described in supplementary Fig. S1. As there are multiple trials of each experiment, the PSD was calculated for each period using an appropriately sized Hamming window and the DC component was discarded. The power spectrum was binned into 1 Hz frequency bands, from which the mean and the standard error of the power were extracted and averaged for all trials. Only the first 40 Hz of the power spectrum is examined, and the results shown using the same y-axis limits to allow for comparison.

Spectrum analysis. To measure the resonance frequency of individual neurons, a 20-second subthreshold sinusoidal current at 10 pA, with a linear increase in frequency from 0.1 to 20 Hz (chirp stimulation) was applied through the recording electrode, as previously described[41]. The resonance frequency was determined as the peak in the impedance amplitude profile (ZAP) generated by dividing the Fourier transforms of the voltage signal by that of the current signal, as previously described by[33]. The voltage recordings were recorded in millivolts and the current signal recorded in picoamps and adjusted accordingly such that the resulting complex impedance can be measured in Ohms. The DC component of each FFT was discarded by removing the first element of each FFT signal, and only the real component of the resulting impedance was considered.

To better assess the effect of the interventions, the Full Width at Half Maximum (FWHM) was calculated for the impedance of each recording in each condition. The baseline impedance was removed from the signal by subtracting the mean impedance in the 18 Hz to 20 Hz frequency band prior to calculating the FWHM. The first five impedance samples of each recording were also discarded due to variations in the DC offsets in the signals used to calculate the impedance. The FWHM was calculated by normalizing the signal to a range of [-0.5, 0.5] and finding the distance in the x-axis between the first two zero crossings.

To visualize the changes in oscillation strength over time, we have plotted the data via spectrogram. The spectrogram is the decomposition of the extracellular signal into its spectral components (power by frequency) across time[68]. The target period for this analysis was 10 sec before KCl application and 20 sec after KCl application.

Drugs. All drugs were stored in frozen stock solutions and were added to aCSF just before recordings. Some experiments were performed in the presence of Carbachol (100 μM, Sigma Aldrich) to elicit high frequency oscillations, or $BaCl_2$ (100 μM, Sigma Aldrich) to block astrocytic Kir4.1 channels, in the bath solution. To assess the role of Cx43-composed gap junctions, brain slices were incubated with GAP-26 (200 μM, AnaSpec) and GAP-27 (300 μM, AnaSpec) mixture for 15 minutes and then transferred to the recording chamber for electrophysiological recordings.

Statistical analysis. Unless stated, data is reported as mean ± S.E.M. Statistical comparisons were done with Prism (GraphPad Software; San Diego, CA) using two-tailed unpaired student t-test and one-way ANOVA, according to the experimental design. Power spectrum and resonance frequency analyses were performed using Matlab (Mathworks). Probability values < 0.05 were considered statistically significant.

Data availability statement. All data generated or analysed during this study are included in this published article (and its Supplementary Information files).

References

1. Kaiser, J. & Lutzenberger, W. Human gamma-band activity: A window to cognitive processing. *Neuroreport* **16**, 207–211 (2005).
2. Buzsáki, G. & Draguhn, A. Neuronal oscillations in cortical networks. *Science (80-.).* **304**, 1926–9 (2004).
3. Sanchez-Vives, M. V. & McCormick, D. a. *Cellular and network mechanisms of rhythmic recurrent activity in neocortex. Nat. Neurosci.* **3**, 1027–34 (2000).
4. Fröhlich, F. & McCormick, Da Endogenous electric fields may guide neocortical network activity. *Neuron* **67**, 129–43 (2010).
5. Hutcheon, B. & Yarom, Y. Resonance, oscillation and the intrinsic frequency preferences of neurons. *Trends Neurosci.* **23**, 216–222 (2000).
6. Liljenström, H. & Hasselmo, M. In *Computation and Neural Systems* 523–530 (1993).

7. Llinas, R. The intrinsic electrophysiological properties of mammalian neurons: insights into central nervous system function. *Science (80-).* **242**, 1654–1664 (1988).
8. Lampl, I. & Yarom, Y. Subthrethold Oscillations and Resonant Behavior: Two Manifestations of the same. *Neuroscience* **78**, 325–341 (1997).
9. Tohidi, V. & Nadim, F. Membrane resonance in bursting pacemaker neurons of an oscillatory network is correlated with network frequency. *J. Neurosci.* **29**, 6427–35 (2009).
10. Narayanan, R. & Johnston, D. Long-term potentiation in rat hippocampal neurons is accompanied by spatially widespread changes in intrinsic oscillatory dynamics and excitability. *Neuron* **56**, 1061–75 (2007).
11. Yoshida, M., Giocomo, L. M., Boardman, I., Michael, E. & Hasselmo Frequency of subthreshold oscillations at different membrane potential voltages in neurons at different anatomical positions on the dorso-ventral axis in the rat medial entorhinal cortex. *J. Neurosci.* **31**, 12683–12694 (2011).
12. Penttonen, M. & Buzsáki, G. Natural logarithmic relationship between brain oscillators. *Thalamus and Related Systems* **2**, 145–152 (2003).
13. Buzsaki, G. *Rhythms of the Brain. Oxford University Press, 2011*, https://doi.org/10.1093/acprof (2006).
14. Ainsworth, M. *et al.* Dual Gamma Rhythm Generators Control Interlaminar Synchrony in Auditory Cortex. *J. Neurosci.* **31**, 17040–17051 (2011).
15. LaBerge, D. & Kasevich, R. S. Neuroelectric Tuning of Cortical Oscillations by Apical Dendrites in Loop Circuits. *Front. Syst. Neurosci.* **11**, 37 (2017).
16. Fellin, T. *et al.* Neuronal synchrony mediated by astrocytic glutamate through activation of extrasynaptic NMDA receptors. *Neuron* **43**, 729–743 (2004).
17. Poskanzer, K. E. & Yuste, R. Astrocytic regulation of cortical UP states. *PNAS* **108**, 18453–8 (2011).
18. Poskanzer, K. E. & Yuste, R. Astrocytes regulate cortical state switching *in vivo*. *PNAS* 2675–2684, https://doi.org/10.1073/pnas.1520759113 (2016).
19. Kantevari, S., Buskila, Y. & Ellis-Davies, G. C. R. Synthesis and characterization of cell-permeant 6-nitrodibenzofuranyl-caged IP3. *Photochem. Photobiol. Sci.* **11**, 508–13 (2012).
20. Yue, B. W. & Huguenard, J. R. The role of H-current in regulating strength and frequency of thalamic network oscillations. *Thalamus Relat Syst.* **1**, 95–103 (2001).
21. Kofuji, P. & Newman, Ea Potassium Buffering in the central nervous system. *Neuroscience* **129**, 1045–1056 (2004).
22. Sofroniew, M. V & Vinters, H. V. Astrocytes: biology and pathology. *Acta Neuorpathol* 7–35, https://doi.org/10.1007/s00401-009-0619-8 (2010).
23. Spray, E. S. & D., C. Extracellular K+ and Astrocyte Signaling via Connexin and Pannexin Channels. *Neurochem Res.* **37**, 2310–2316 (2012).
24. Buskila, Y., Crowe, S. E. & Ellis-Davies, G. C. R. Synaptic deficits in layer 5 neurons precede overt structural decay in 5xFAD mice. *Neuroscience* **254**, 152–159 (2013).
25. David, Y. *et al.* Astrocytic dysfunction in epileptogenesis: consequence of altered potassium and glutamate homeostasis? *J. Neurosci.* **29**, 10588–99 (2009).
26. Leis, Ja, Bekar, L. K. & Walz, W. Potassium homeostasis in the ischemic brain. *Glia* **50**, 407–16 (2005).
27. Bazhenov, M., Timofeev, I., Steriade, M. & Sejnowski, T. J. Potassium Model for Slow (2–3 Hz) *In Vivo* Neocortical Paroxysmal Oscillations. 1116–1132 (2004).
28. Fröhlich, F., Bazhenov, M., Timofeev, I., Steriade, M. & Sejnowski, T. J. Slow state transitions of sustained neural oscillations by activity-dependent modulation of intrinsic excitability. *J. Neurosci.* **26**, 6153–62 (2006).
29. Ding, F. *et al.* Changes in the composition of brain interstitial ions control the sleep-wake cycle. *Science (80-)* **352**, 550–555 (2016).
30. Bellot-Saez, A., Kékesi, O., Morley, J. W. & Buskila, Y. Astrocytic modulation of neuronal excitability through K+ spatial buffering. *Neurosci. Biobehav. Rev.* **77**, 87–97 (2017).
31. Kuffler, S. W., Nicholls, J. G. & Orkand, R. K. Physiological properties of glial cells in the central nervous system of amphibia. *J. Neurophysiol.* **29**, 768–787 (1966).
32. Larsen, B. R. & Macaulay, N. Kir4.1-mediated spatial buffering of KC: Experimental challenges in determination of its temporal and quantitative contribution to KC clearance in the brain. *Channels* **8**, 1–7 (2014).
33. Gutfreund, Y., Yarom, Y. & Segev, I. Subthreshold oscillations and resonant frequency in guinea-pig cortical neurons: physiology and modelling. *J. Physiol.* **483**, 621–40 (1995).
34. Do-Ha, D., Buskila, Y. & Ooi, L. Impairments in Motor Neurons, Interneurons and Astrocytes Contribute to Hyperexcitability in ALS: Underlying Mechanisms and Paths to Therapy. *Mol. Neurobiol.* 1–9, https://doi.org/10.1007/s12035-017-0392-y (2017).
35. Hájos, N. & Mody, I. Establishing a physiological environment for visualized *in vitro* brain slice recordings by increasing oxygen supply and modifying aCSF content. *J. Neurosci. Methods* **183**, 107–113 (2009).
36. Traub, R. D. *et al.* A model of gamma-frequency network oscillations induced in the rat CA3 region by carbachol *in vitro*. *Eur. J. Neurosci.* **12**, 4093–4106 (2000).
37. Lévesque, M., Salami, P., Shiri, Z. & Avoli, M. Interictal oscillations and focal epileptic disorders. *Eur. J. Neurosci.* 1–13, https://doi.org/10.1111/ejn.13628 (2017).
38. Goldman, D. E. Potential, Impedance, and Rectification in membranes. *J. Gen. Physiol.* 37–60, https://doi.org/10.1085/jgp.27.1.37 (1943).
39. Núñez-Abades, Pa, Pattillo, J. M., Hodgson, T. M. & Cameron, W. E. Role of synaptic inputs in determining input resistance of developing brain stem motoneurons. *J. Neurophysiol.* **84**, 2317–2329 (2000).
40. Somjen, G. G. Extracellular potassium in the mammalian central nervous system. *Annu Rev Physiol* **41**, 159–177 (1979).
41. Buskila, Y., Morley, J. W., Tapson, J. & van Schaik, A. The adaptation of spike backpropagation delays in cortical neurons. *Front. Cell. Neurosci.* **7** (2013).
42. Du, Y. *et al.* Genetic Deletion of TREK-1 or TWIK-1/TREK-1 Potassium Channels does not Alter the Basic Electrophysiological Properties of Mature Hippocampal Astrocytes. *In Situ. Front. Cell. Neurosci.* **10**, 13 (2016).
43. Ma, B., Xu, G., Wang, W., Enyeart, J. J. & Zhou, M. Dual patch voltage clamp study of low membrane resistance astrocytes *in situ*. *Mol. Brain* **7**, 1–12 (2014).
44. Jansen, L. A., Uhlmann, E. J., Crino, P. B., Gutmann, D. H. & Wong, M. Epileptogenesis and Reduced Inward Rectifier Potassium Current in Tuberous Sclerosis Complex-1 – Deficient Astrocytes. *Epilepsia* **46**, 1871–1880 (2005).
45. Samoilova, M., Wentlandt, K., Adamchik, Y., Velumian, A. A. & Carlen, P. L. Connexin 43 mimetic peptides inhibit spontaneous epileptiform activity in organotypic hippocampal slice cultures. *Exp. Neurol.* **210**, 762–775 (2008).
46. Roux, L., Benchenane, K., Rothstein, J. D., Bonvento, G. & Giaume, C. Plasticity of astroglial networks in olfactory glomeruli. *Proc. Natl. Acad. Sci.* **108**, 18442–18446 (2011).
47. Lee, S. & Dan, Y. Review Neuromodulation of Brain States. *Neuron* **76**, 209–222 (2012).
48. Steriade, M., McCormick, D. A. & Sejnowski, T. J. Thalamocortical Oscillations in the Sleeping and Aroused Brain. *Science (80-.).* **262**, 679–685 (1993).
49. Steriade, M. & McCarley, R. W. *Brain Control of Wakefulness and Sleep*. (Springer, 2005).
50. Steriade, M. Impact of Network Activities on Neuronal Properties in Corticothalamic Systems. *J. Neurophysiol.* 1–39 (2001).

51. Compte, A., Sanchez-Vives, M. V., McCormick, D. A. & Wang, X.-J. Cellular and network mechanisms of slow oscillatory activity and wave propagations in a cortical network model. *J Neurophysiol* **89**, 2707–2725 (2003).
52. Dominguez, G. & Fozzard, H. A. Influence of extracellular K+ concentration on cable properties and excitability of sheep cardiac Purkinje fibers. *Circ. Res.* **26**, 565–574 (1970).
53. Poulet, J. F. A. & Petersen, C. C. H. Internal brain state regulates membrane potential synchrony in barrel cortex of behaving mice. *Nature* **454**, 881–887 (2008).
54. Okun, M., Naim, A. & Lampl, I. The Subthreshold Relation between Cortical Local Field Potential and Neuronal Firing Unveiled by Intracellular Recordings in Awake Rats. *J. Neurosci.* **30**, 4440–4448 (2010).
55. Amzica, F., Massimini, M. & Manfridi, A. Spatial buffering during slow and paroxysmal sleep oscillations in cortical networks of glial cells *in vivo*. *J Neurosci.* **22**, 1042–53 (2002).
56. Buskila, Y., Farkash, S., Hershfinkel, M. & Amitai, Y. Rapid and reactive nitric oxide production by astrocytes in mouse neocortical slices. *Glia* **52**, 169–176 (2005).
57. Yague, J. G., Tsunematsu, T. & Sakata, S. Distinct Temporal Coordination of Spontaneous Population Activity between Basal Forebrain and Auditory Cortex. *Front. Neural Circuits* **11**, 1–14 (2017).
58. Kalmbach, A., Hedrick, T. & Waters, J. Selective optogenetic stimulation of cholinergic axons in neocortex. *J Neurophysiol.* **2**, 2008–2019 (2012).
59. Jones, B. E. Arousal Systems. *Front. Biosci. a J. virtual Libr* **8**, s438–s451 (2003).
60. Ma, Z., Stork, T., Bergles, D. E. & Freeman, M. R. Neuromodulators signal through astrocytes to alter neural circuit activity and behavior. *Nature* **17**, 428–432 (2016).
61. Cameron, M. *et al*. Calcium imaging of AM dyes following prolonged incubation in acute neuronal tissue. *PLoS One* **11** (2016).
62. Breen, P. P. & Buskila, Y. Braincubator: An incubation system to extend brain slice lifespan for use in neurophysiology. in *Engineering in Medicine and Biology Society (EMBC), 2014 36th Annual International Conference of the IEEE* 4864–4867 (IEEE, 2014).
63. Buskila, Y. *et al*. Extending the viability of acute brain slices. *Sci. Rep.* **4**, 4–10 (2014).
64. Cameron, M. A. *et al*. Prolonged Incubation of Acute Neuronal Tissue for Electrophysiology and. *J. Vis. Exp.* **120**, 1–6 (2017).
65. Buskila, Y. & Amitai, Y. Astrocytic iNOS-dependent enhancement of synaptic release in mouse neocortex. *J. Neurophysiol.* **103**, 1322–1328 (2010).
66. Lin, X., Ling-Hui, Z. & Wong, M. impaired astrocytic gap junctions coupling and potassium Buffering in a Mouse Model of Tuberous Sclerosis Complex. *Neurobiol. Dis.* **34**, 291–299 (2009).
67. Lee, H. S. *et al*. Astrocytes contribute to gamma oscillations and recognition memory. *Proc. Natl. Acad. Sci.* https://doi.org/10.1073/pnas.1410893111 (2014).
68. Pavone, K. J. *et al*. Nitrous oxide-induced slow and delta oscillations. *Clin. Neurophysiol* **127**, 556–564 (2016).

Acknowledgements
We would like to thank Sindy Kueh and Patrick Kasi and Ram Kuber Singh for technical assistance and Morven Cameron for fruitful discussions. This work was supported by seed funding grant (UWS) to Y.B. and the innovation office at UWS.

Author Contributions
Y.B. conceived the project. Y.B., A.v.S., L.O. and J.W.M. designed the experiments. A.B.S. and G.C. performed and analysed the electrophysiological recordings. All authors wrote and approved the paper.

Additional Information
Supplementary information accompanies this paper at https://doi.org/10.1038/s41598-018-30003-w.

Competing Interests: The authors declare no competing interests.

Publisher's note: Springer Nature remains neutral with regard to jurisdictional claims in published maps and institutional affiliations.

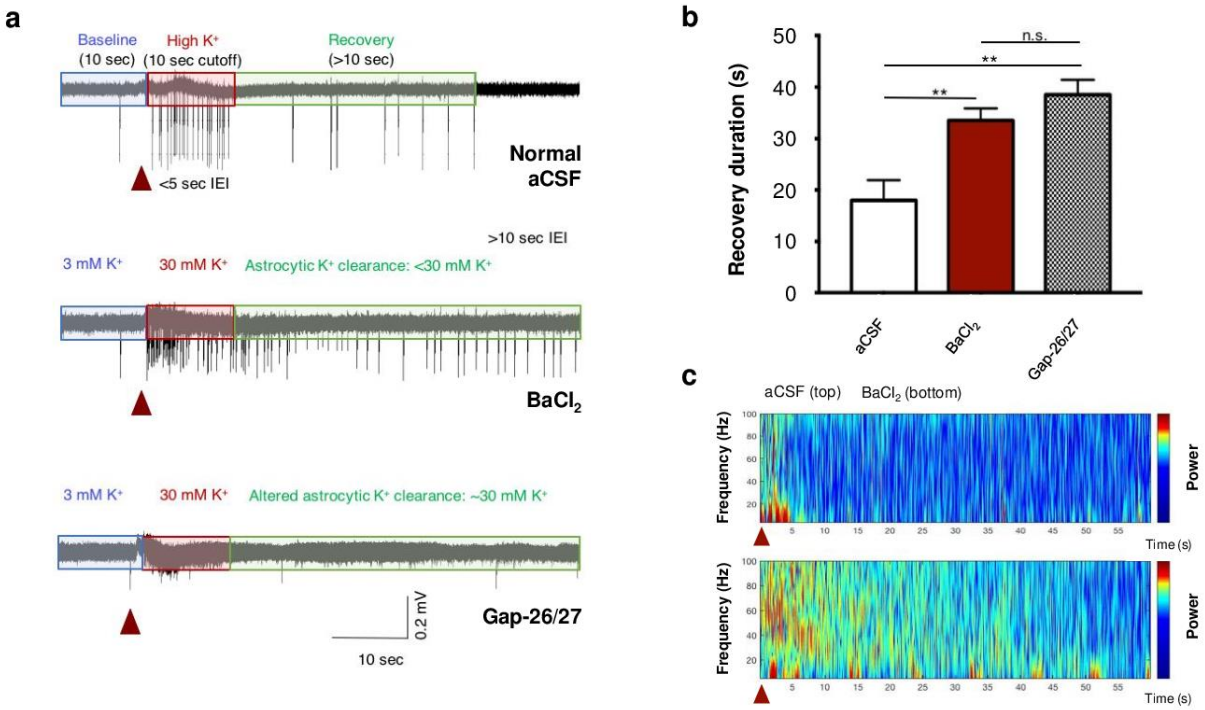

Supplementary Figure S1. Measuring network excitability. a) Traces of extracellular recordings showing the network activity before and after brief (1 second) application of 30 mM KCl (red arrow), in normal aCSF (3mM K^+, top) and after bath application of 100 µM $BaCl_2$ (middle) or Gap-26/27 (bottom). For subsequent analysis, the network activity was divided into three episodes: "Baseline", the period prior to stimulation; "High K^+", the immediate period following application of 30 mM KCl. The duration of the "High K^+" period was set to 10 seconds as this was the average time in which the inter-spike intervals was <5 seconds (3 mM K^+ aCSF, n=15). The third period was termed "Recovery", as this is the period where $[K^+]_o$ decreases to baseline levels due to diffusion and astrocytic K^+ clearance. The duration of the "Recovery" period was set as the period where the inter-spike intervals were <10 seconds. b) Bar graph depicting the impact of impairment of K^+ uptake ($BaCl_2$, n=16) and gap junction blockers (Gap-26/27, n=13) on the duration of the "Recovery" period. c) The power spectrogram of extracellular oscillations following KCl application (time 0, red triangles) depicting the increase in power at higher frequencies during the "High K^+" (first 10 seconds) and "Recovery" (from 10 seconds onwards) periods. ***p < 0.01; student t-test*

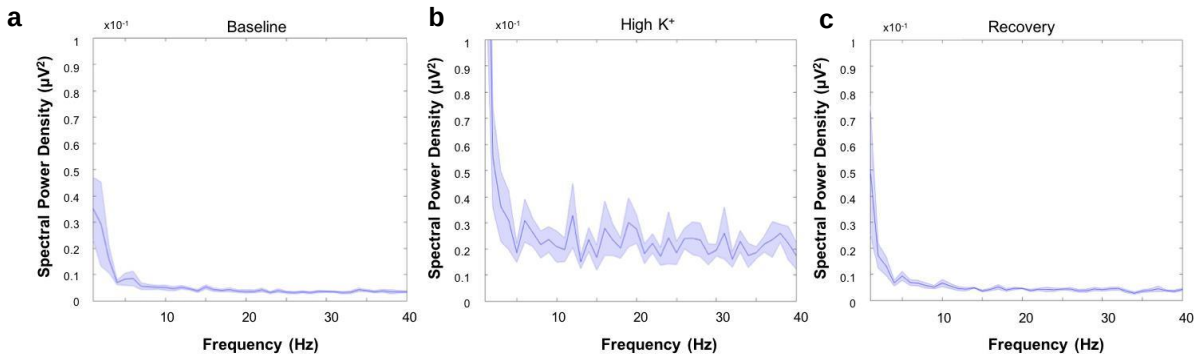

Supplementary Figure S2. Power spectrum analysis of low frequency network oscillations. Power spectrum analysis depicting the averaged (line) and standard error values (shade) of the dominant oscillation frequencies governing "Baseline" (a), "High K^+" (b) and "Recovery" (c) periods depicting maximal power at oscillation frequencies <1 Hz under normal aCSF conditions.

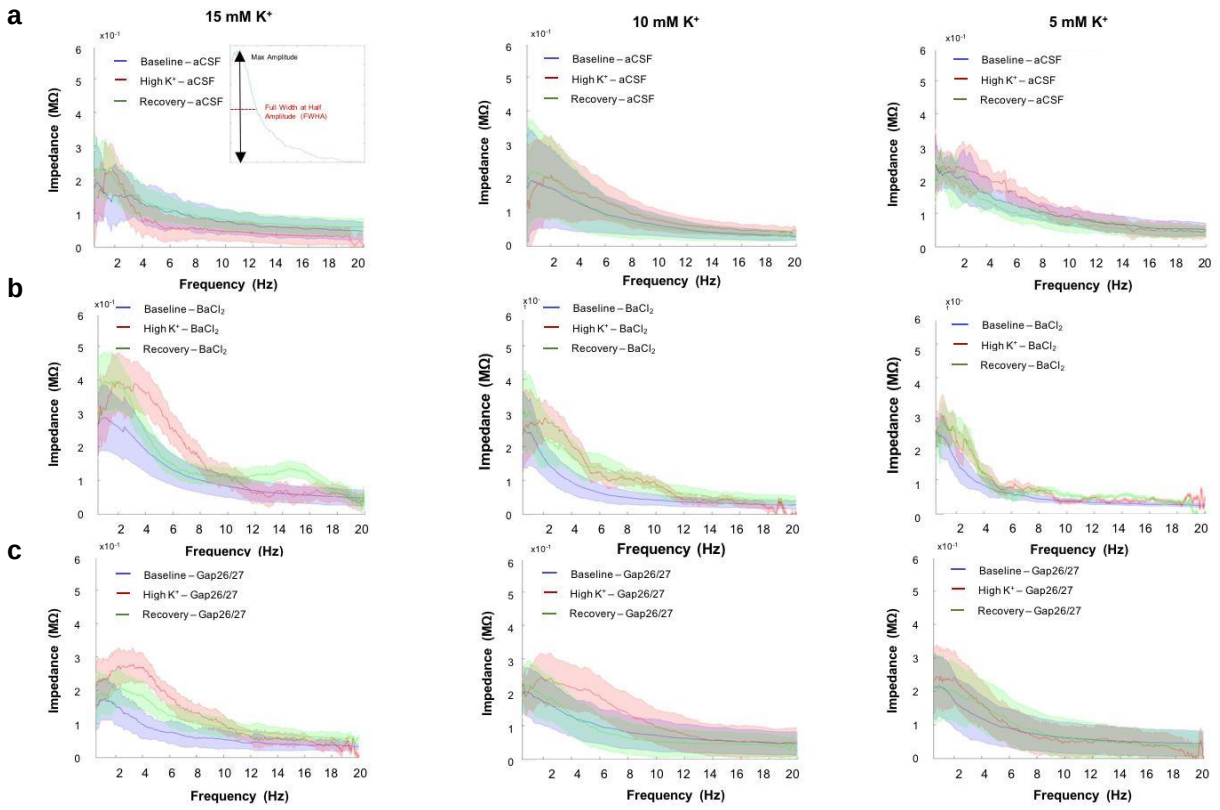

Supplementary Figure S3. The impact of $[K^+]_o$ on the resonance frequency. a) Impedance amplitude profile depicting the mean (line) and standard deviation values (shade) of the maximal voltage response to a subthreshold chirp stimulation (10 pA), before, during and after (colour-coded) stimulation at different concentrations of KCl (5 -15 mM) under normal aCSF conditions. Note the shift towards higher frequencies during the "High K^+" period. Inset - schematic representation of the Full Width at Half Amplitude (FWHA) calculated by MATLAB. The function first measures the maximal amplitude of the resonance frequency curve from baseline values at ~20 Hz to maximal peak, and then measures the full width of the maximum amplitude. b, c) ZAP profile under $BaCl_2$ (b) and Gap-26/27 (c) conditions. Note the shift towards higher frequencies during "High K^+" and "Recovery" periods compared to normal aCSF.

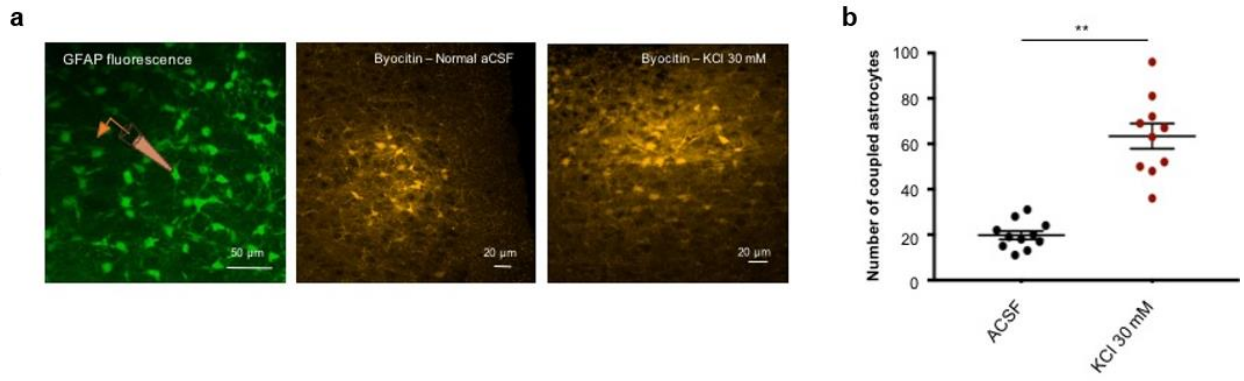

Supplementary Figure S4. High $[K^+]_o$ enhances astrocytic coupling in the cortex. a) Measuring astrocytic coupling through biocytin labelling. Left – image of an astrocyte from GFAP-GFP mouse filled with biocytin through the recording electrode (12 minutes) to determine its direct connections with surrounding astrocytes. Right – Confocal images (20x objective) showing the biocytin-stained astrocytic network in layer II/III of the somatosensory cortex from GFAP mouse under normal aCSF (middle) and following application of 30 mM KCl (right). b) Local application of 30 mM KCl significantly increases the degree of coupled astrocytes in layer II/III of the cortex. ***p < 0.01; student t-test*

$[K^+]_o$ (mM)		RMP (mV)	R_{in} (MΩ)	Rheobase (pA)	Spike width (ms)	f_R (Hz)	FWHA (Hz)
3	aCSF	-65.1±0.5 (n=66)	248.9±10.5 (n=65)	47.8±4.1 (n=68)	2.3±0.1 (n=70)	1.4±0.1 (n=51)	2.1±0.3 (n=51)
5	Before KCl puff	-65.8±1.2 (n=13)	264.7±22.5 (n=14)	46.2±6.8 (n=14)	2.3±0.2 (n=15)	1.4±0.2 (n=12)	2.2±0.6 (n=12)
	During KCl puff	-57.9±1.4 (n=13)	247.0±25.4 (n=14)	25.6±4.6 (n=13)	2.4±0.2 (n=14)	2.0±032 (n=12)	2.6±0.8 (n=12)
	After KCl puff	-65.3±1.8 (n=12)	257.0±30.1 (n=13)	47.5±7.2 (n=13)	2.3±0.1 (n=14)	1.3±0.2 (n=11)	2.3±0.7 (n=11)
10	Before KCl puff	-65.1±1.7 (n=13)	255.9±29.4 (n=12)	47.9±8.7 (n=14)	2.2±0.2 (n=15)	1.3±0.3 (n=12)	2.4±0.8 (n=12)
	During KCl puff	-52.8±1.2 (n=13)	189.2±27.2 (n=12)	21.1±4.6 (n=13)	2.7±0.2 (n=13)	2.0±0.2 (n=10)	2.7±0.4 (n=10)
	After KCl puff	-64.1±1.8 (n=12)	240.7±36.5 (n=12)	48.3±8.2 (n=13)	2.3±0.2 (n=13)	1.3±0.2 (n=12)	2.2±1.1 (n=12)
15	Before KCl puff	-64.4±0.9 (n=17)	232.8±18.8 (n=17)	47.3±10.1 (n=17)	2.3±0.1 (n=17)	1.5±0.2 (n=13)	1.8±0.9 (n=13)
	During KCl puff	-49.2±1.2 (n=17)	169.1±14.8 (n=16)	17.9±2.8 (n=16)	3.2±0.3 (n=16)	2.1±0.3 (n=13)	2.9±1.0 (n=13)
	After KCl puff	-64.2±1.8 (n=16)	223.9±25.0 (n=16)	50.4±8.1 (n=16)	2.4±0.2 (n=16)	1.2±0.1 (n=13)	1.9±0.4 (n=13)
30	Before KCl puff	-65.0±1.0 (n=18)	247.2±23.2 (n=17)	49.7±7.1 (n=18)	2.4±0.2 (n=18)	1.5±0.2 (n=14)	1.9±0.2 (n=14)
	During KCl puff	-38.6±1.3 (n=18)	125.5±14.4 (n=16)	12.3±1.0 (n=16)	4.4±0.6 (n=15)	2.5±0.2 (n=12)	3.8±1.1 (n=12)
	After KCl puff	-60.9±1.9 (n=18)	43.0±5.9 (n=16)	50.0±7.9 (n=16)	2.6±0.1 (n=15)	1.3±0.2 (n=11)	2.1±0.5 (n=11)

Supplementary Table S1. The impact of extracellular K^+ on the biophysiological properties of the soma of layer V cortical neurons. Data is reported as mean ± S.E.M (n = number of neurons recorded).

2.2 Extended material and methods

2.2.1 Animals and slice preparation

For extracellular recordings of the network activity we used P21-P28 days-old GFAP-GFP mice, in which astrocytes are selectively tagged with the green fluorescent protein (GFP) under a GFAP promoter (strain 003257, Jax laboratories). To simplify the technical challenges involved in dendritic recordings, Wistar rats (P21-P35) were used to perform proximal and distal recordings from apical dendrites in layer V pyramidal neurons. Animal handling and slice preparation were performed as previously described in section 2.1.

2.2.2 Electrophysiological recording and stimulation

The electrophysiological setup and steps following slice incubation in the Braincubator^{TM}, as well as stimulation protocol for both extracellular and intracellular recordings are described in detail in section 2.1. For apical dendritic recordings, I used high impedance patch pipettes (10-12 MΩ) containing in mM: 130 K-Methansulfate, 10 HEPES (4-(2- hydroxyethyl)-1-piperazineethanesulfonic acid), 0.05 EGTA (ethylene glycol-bis(β-aminoethyl ether)-N,N,N′,N′-tetraacetic acid), 7 KCl, 0.5 Na_2GTP, 2 Na_2ATP, 2 MgATP, 7 phosphocreatine, and titrated with KOH to pH 7.2 (~285 mOsm). Membrane potentials were recorded in current clamp mode, as previously described for somatic recordings (section 2.1). Dendritic recordings were grouped according to their distance from the soma (0 µm). Proximal recordings were defined as recordings from distances between 0-100 µm. Greater distances (>100 µm) were classified as distal recordings. In cases were dendrites were difficult to observe under differential interference contrast (DIC) optics, dual somato-dendritic recordings were performed with patch pipettes filled with the same internal solution and the fluorescent dye Alexa Fluor-488 (Molecular Probes; Figure 2.4 B).

Dendritic membrane properties were obtained before, during and after (10 sec) local application of high potassium chloride (KCl, 30 mM) through a puffing pipette placed in the vicinity of the recording electrode. Following brief application of KCl (~1 sec), the puffing pipette was removed to allow K^+ washout for 2 minutes before resuming intracellular recordings, as previously described (section 2.1).

2.2.3 Drugs

To measure the impact of global activation of G-proteins by GTP, brain slices were incubated with Na^+ salt compounds (NPE-caged GTP, 100 μM, Jenna Bioscience) for 1 hour to allow diffusion of the caged molecules. Local photolysis[410] with ultraviolet light (UV, ~340 nm) was applied in the vicinity of the recoding electrode for 5 seconds prior to stimulation with KCl (Figure 2.1 A). The application of pharmacological agents used to impair astrocytic K^+ clearance mechanisms, including $K_{ir}4.1$ channels with barium chloride ($BaCl_2$) or gap junctions (GJs) with a mixture of connexin 43 (Cx43) mimetic peptides (Gap-26-27), is described in section 2.1.

2.2.4 Statistical analysis

Similar to previous experiments detailed in section 2.1, analysis of extracellular and intracellular recordings is based on three episodes corresponding to different stages of the K^+ clearance process, including "**Baseline**", "**High K^+**" and "**Recovery**".

Unless stated, data is reported as mean ± S.E.M. Statistical comparisons were done with Prism 7 (GraphPad So ware; San Diego, CA) using two-tailed unpaired or paired student t-test, as well as one-way ANOVA followed by Tukey's post hoc test, according to the experimental design.

Power spectrum density (PSD) and impedance amplitude profile (ZAP) to reveal the resonance frequency (f_R) were analysed using custom-made codes written with MATLAB (MathWorks), as stated in the previous section 2.1. Probability values < 0.05 were considered statistically significant.

2.3 Extended results

The present section provides complimentary experiments that support a crucial role for astrocytic K^+ clearance mechanisms in modulating subcompartments of individual neurons underlying the generation of cortical oscillations at the network level.

2.3.1 Facilitation of net K^+ uptake modulates cortical oscillations

In a separate series of experiments, I studied the impact of facilitation of the astrocytic net K^+ uptake process by global activation of G-proteins via focal photolysis of NPE-caged GTP, as reported previously[411]. Focal release of GTP for 5 seconds prior to local application of high K^+ (~30 mM KCl) led to a significant decrease of the multi-unit frequency and increased the inter-spike intervals during the "High K^+" period (0.48±0.09 Hz, uncaged GTP n=18 *vs* 2.45±0.39 Hz, normal aCSF n=15; $p < 0.01$, unpaired student t-test; $p < 0.01$, KS-test, Figure 2.1 B-D).

However, GTP release did not affect the "Recovery" period, as neither the interspike-intervals ($p > 0.05$, KS-test, Figure 2.1 D) nor the average duration of this episode were significantly different from control conditions (artificial cerebrospinal fluid, aCSF), despite showing an increasing trend ($p = 0.07$, unpaired student t-test, Figure 2.1 C).

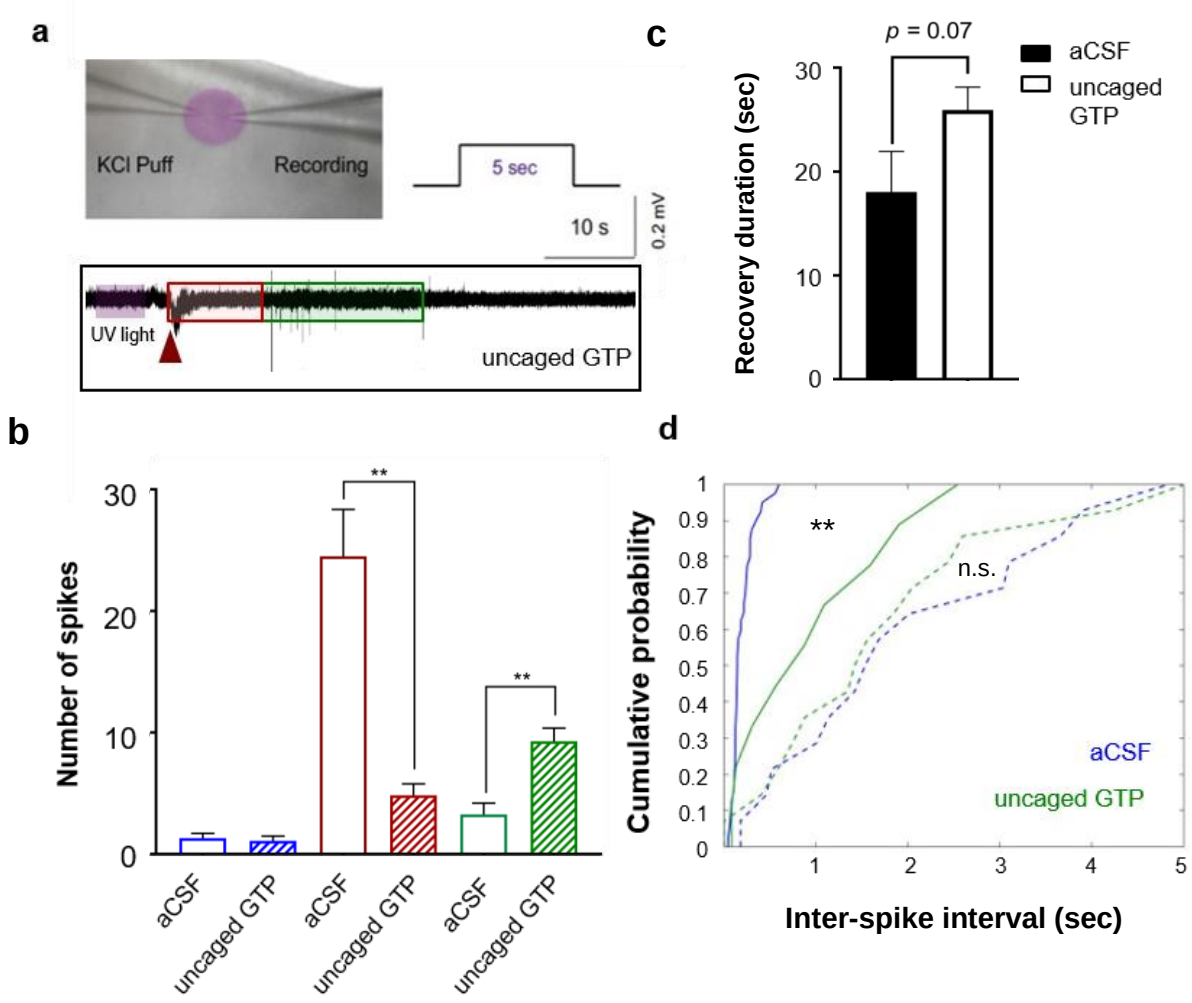

Figure 2.1 Modulation of net K^+ uptake via GTP release impacts on cortical network dynamics. a) Image of the experimental setup (top) depicting the area (purple) that was photo-activated with UV light (~340 nm) for 5 seconds prior to local application of 30 mM KCl and representative extracellular recording (bottom) of the network activity following local photostimulation of 100 µM NPE-caged-GTP (purple). b) Bar graph depicting the impact of photolysis of caged GTP compounds on the average duration of the "Recovery" period (18±3.9 seconds aCSF *vs* 26±2.2 seconds uncaged GTP; $p > 0.05$, unpaired student t-test). c) Analysis of the network excitability during the different episodes (colour-coded) indicating an increase of the number of spikes recorded following local application of KCl ("High K^+"), which decreases during the "Recovery" period in normal aCSF. Enhancement of net K^+ uptake via K_{ir} channel upregulation (through local uncaging of GTP prior to the KCl stimulus) leads to a reduction of the number of spikes during the "High K^+" period and increase during the "Recovery" episode, compared to control conditions ($p < 0.01$, unpaired student t-test). d) Cumulative probability distribution of inter-spike intervals during the "High K^+" (continuous lines) and the "Recovery" (dashed lines) periods showing a right shift following photolysis of caged GTP during the "High K^+" episode ($p < 0.01$, KS-test). Data is reported as mean ± SEM (uncaged GTP n=18; aCSF n=15). ***p < 0.01; unpaired student t-test*

This tendency, together with the observed increase of the multi-unit frequency compared to normal aCSF conditions during the "Recovery" period ($p < 0.01$, unpaired student t-test, Figure 2.1 B), may be due to the fact that GTP affects numerous intracellular processes, including inhibition of Cx43 activity and thus astrocytic GJ coupling[412].

Moreover, GTP uncaging resulted in a substantial decrease in the oscillation power during the "High K^+" episode (Figure 2.2 A), in particular at frequencies in the beta and gamma range compared to normal aCSF conditions (0.009 ± 0.002 μV^2 *vs* 0.019 ± 0.002 μV^2 at beta band, 0.007 ± 0.002 μV^2 *vs* 0.021 ± 0.003 μV^2 at gamma band; $p < 0.01$, unpaired student t-test, Figure 2.3 D-E).

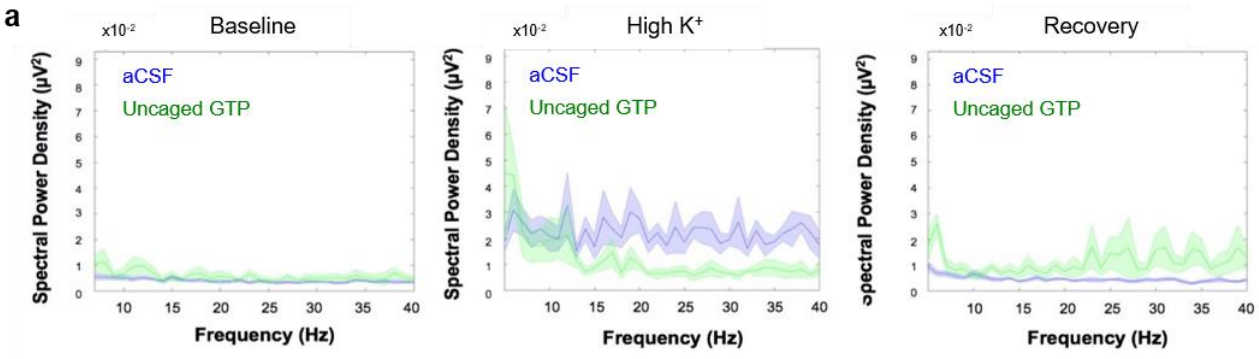

Figure 2.2 Facilitation of net K^+ uptake affects the power of cortical networks oscillations. a) Power spectrum analysis depicting the averaged (line) and standard error (shade) values of the dominant oscillation frequencies governing the "Baseline", "High K^+" and "Recovery" periods, under normal aCSF *vs* enhanced astrocytic net K^+ uptake conditions following photolysis of caged GTP compounds. Note the shift towards lower frequency oscillations following GTP uncaging compared to normal conditions.

In addition, the oscillation power during the "Recovery" period was significantly higher at the delta, theta and gamma bands ($p < 0.05$, unpaired student t-test; Figures 2.2 A, 2.3 A, B, E), indicating a decrease in K^+ spatial buffering through astrocytic networks and thus an increase in neuronal excitability at these frequencies.

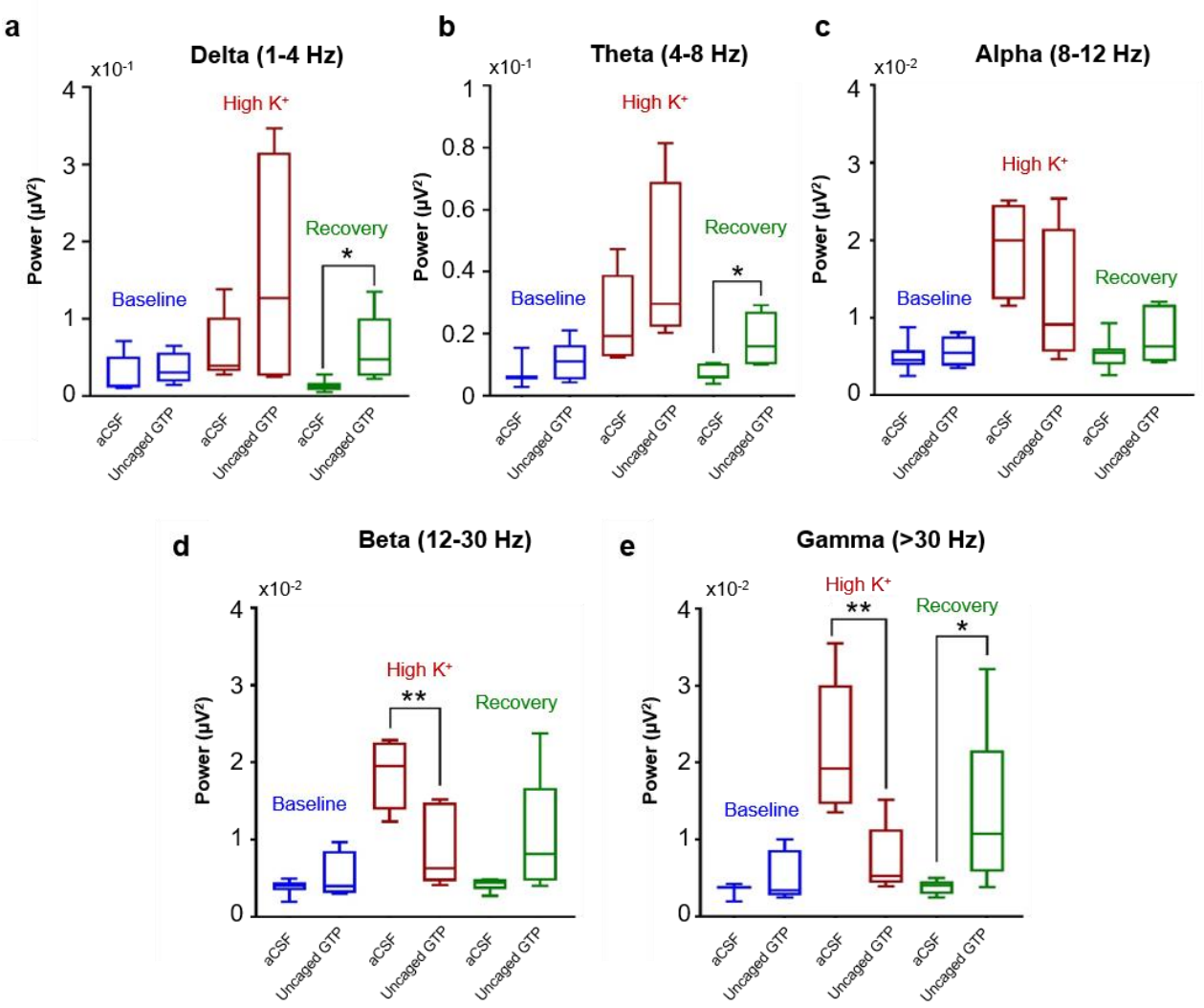

Figure 2.3 Enhancement of net K^+ uptake modulates the power of cortical oscillations at multiple frequencies. a-e) Power spectrum density of cortical oscillations was divided into five frequency bands: delta (1-4 Hz), theta (4-8 Hz), alpha (8-12 Hz), beta (12-30 Hz) and gamma (>30 Hz). The average power for each frequency band was plotted during the "Baseline", "High K^+" and "Recovery" periods. Comparison of the average power during the "High K^+" period reveals that facilitation of K^+ clearance via local release of GTP compounds leads to a significant decrease of the oscillation power at beta and gamma frequencies. Comparison of the average power during the "Recovery" period shows a significant rise in the power of delta, theta and gamma frequencies once astrocytic net K^+ uptake is facilitated. The box upper and lower limits are the 25^{th} and 75^{th} quartiles, respectively. The whiskers depict the lowest and highest data points, while the horizontal line through the box represents the median. Data is reported as mean ± SEM. *$p < 0.05$; **$p < 0.01$; *unpaired student t-test*

2.3.2 The impact of high $[K^+]_o$ on different subcellular compartments of layer V pyramidal neurons

Dendrites play a critical role in regulating and filtering inputs to integrate the overall network activity[413]. In addition, the fact that neuronal membrane resonance significantly differs between subcellular compartments[414] led us to further examine the impact of high levels of $[K^+]_o$, namely 30 mM, specifically on the excitability and resonant properties of both proximal and distal apical dendrites from layer V pyramidal neurons in the somatosensory cortex (Figure 2.4).

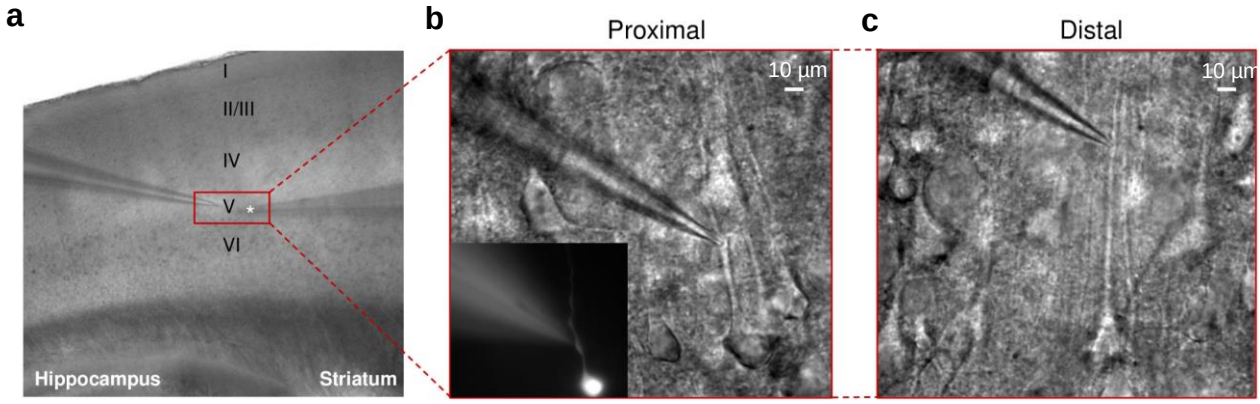

Figure 2.4 Experimental setup for dendritic recordings from layer V cortical neurons. a) DIC image showing the experimental setup for whole-cell patch-clamp recordings from layer V pyramidal neurons in the somatosensory cortex. KCl (~30 mM) was locally applied to the vicinity of the recording electrode using a puffing pipette (*). b-c) Representative DIC images showing the position of the recording electrode on proximal (b, < 100 µm) or distal (c, > 100 µm) apical dendrites of layer V cortical neurons. Note the filling of the soma and dendrite using Alexa Fluor-488 in the intracellular solution (b, lower left inset).

Under physiological conditions, local application of 30 mM KCl puffs had similar effects on membrane properties of both proximal (n=23) and distal dendrites (n=7) compared to the soma (n=18). These included depolarization of the RMP, which recovered back to baseline values after KCl washout ($p < 0.01$, unpaired student t-test, Table 2.1), and decrease in the input resistance (R_{in}), which was greater at distal dendrites during the "High K^+" period compared to the soma ($p < 0.01$, unpaired student t-test, Figure 2.5 A-B, Table 2.1).

Distance (µm)	30 mM KCl	RMP (mV)	R_{in} (MΩ)	Rheobase (pA)	Spike width (ms)	I_h (mV)	f_R (Hz)
Proximal < 100	Baseline	-67.5±0.9	214.1±14.1	51.2±6.8	2.4±0.1	5.2±0.5	1.6±0.2
	High K^+	-40.4±1.1	111.4±12.8	18.7±3.8	3.5±0.3	1.9±0.4	5.7±0.6
	Recovery	-65.8±1.0	190.4±15.5	57.8±6.4	2.5±0.1	5.5±0.8	1.7±0.2
Distal > 100	Baseline	-66.7±4.7	179.4±12.6	83.3±15.2	3.2±0.6	7.6±1.9	6.6±1.6
	High K^+	-41.6±3.7	85.70±25.3	29.2±10.0	6.6±0.7	2.0±1.2	3.9±0.3
	Recovery	-61.8±1.1	171.7±22.7	61.7±26.8	4.0±0.3	9.2±2.0	2.3±0.2

Table 2.1 The impact of high $[K^+]_o$ on the physiological properties of proximal and distal dendrites from layer V cortical neurons. Data is reported as mean ± S.E.M.

During the "Baseline" episode, the spike rheobase was higher at distal dendrites (83.3±15.2 pA) compared to proximal dendrites (51.2±6.8 pA; $p < 0.01$, unpaired student t-test, Figure 2.5 C, Table 2.1) and the soma (47.8±4.1 pA, Supplementary Table S1), indicating that neuronal excitability reduces with increasing distance from the soma. Application of high levels of $[K^+]_o$ led to a decrease of the rheobase (Figure 2.5 C) and increase of the spike width at half amplitude (SWHA) both at proximal and distal dendrites, the latter showing a more significant effect reaching average values of 6.6±0.7 milliseconds ($p < 0.01$, unpaired student t-test, Figure 2.5 D), while somatic spikes were narrower (4.4±0.6 milliseconds, Supplementary Table S1) under the same conditions ("High K^+" episode).

Narayanan and Johnston previously showed that hippocampal neurons display increased resonance frequencies with increasing distance from the soma[414]. Consistent with their results, during "Baseline" conditions the resonance frequency of layer V cortical neurons followed the same trajectory, reaching higher values in distal dendrites, in particular at ~300 µm (11.5±1.3 Hz *vs* 1.4±0.1 Hz at the soma; $p < 0.01$, unpaired student t-test, Figure 2.5 E).

Hyperpolarization-activated cyclic nucleotide-gated (HCN) channels are responsible for mediating I_h currents that are activated following hyperpolarization of the membrane potential[415] and are required for the regulation of both neuronal excitability and network synchronous activity[137].

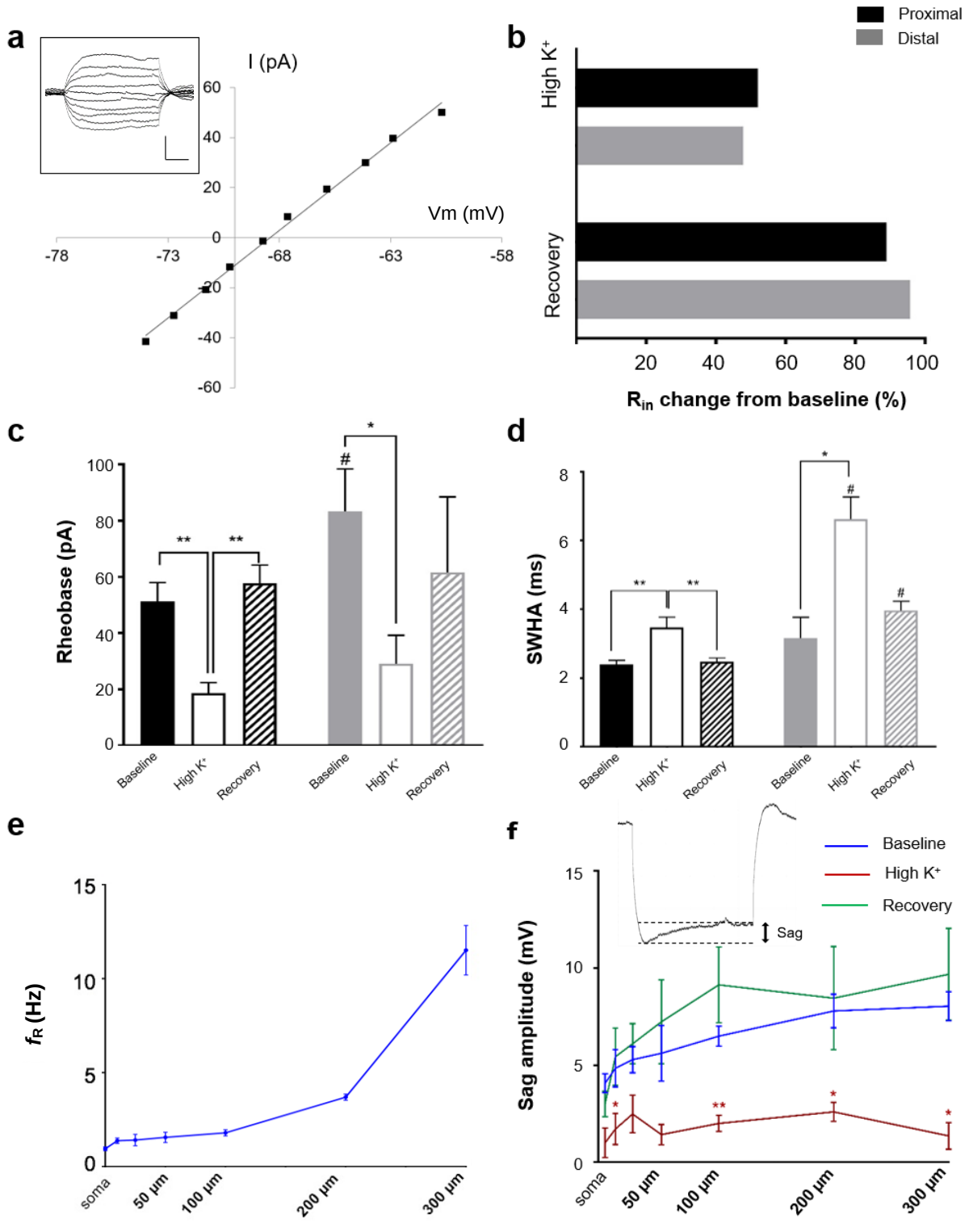

Figure 2.5 High $[K^+]_o$ alters dendritic neuronal excitability and resonance properties. a) A plot of the current pulse intensity (I) *vs* the voltage deflection (equilibrium membrane potential, V_m) was used to assess the input resistance (scale bar x = 100 ms, y = 4 mV).

b) Elevation of $[K^+]_o$ following local application of KCl (~30 mM) leads to a transient decrease of the input resistance (R_{in}) in both proximal (black) and distal (grey) dendrites during the "High K^+" episode. c-d) Plots depicting the transient impact of 30 mM KCl puffs on spike rheobase (c) and spike width at half amplitude (SWHA, d) in proximal (black) and distal (grey) dendrites. e) The resonance frequency (f_R) increases with increasing distance from the soma under normal aCSF. f) High $[K^+]_o$ (~30 mM) significantly reduces sag amplitudes in both proximal and distal dendrites. *Inset* - sample trace depicting the sag amplitude recorded from the neuronal soma following administration of hyperpolarizing current (soma n=18; proximal dendrites n=23; distal dendrites n=7). Data is reported as mean ± SEM. Asterisks represent significance levels between different episodes within the same group (proximal or distal dendrites). Pound signs represent significance levels between different groups (proximal *vs* distal dendrites) at the same episode. *#p < 0.05; unpaired student t-test; *p < 0.05; **p < 0.01; paired student t-test*

Analysis of the hyperpolarization-"sag" amplitude (Figure 2.5 F, inset), mainly mediated by the I_h currents, indicated a reduction following administration of 30 mM KCl puffs ("High K^+" period), especially at distal dendrites (>100 µm), which recovered back to normal values during the "Recovery" episode ($p < 0.05$, paired student t-test, Figure 2.5 F).

Interestingly, distal dendrites showed significantly higher average sag amplitudes (7.6±1.9 mV) compared to the soma (4.1±1.5 mV) and proximal dendrites (5.2±0.5 mV) at "Baseline" $[K^+]_o$ levels (~3 mM), which is consistent with a trend showing a decrease in R_{in} away from the soma ($p > 0.05$, unpaired student t-test, Table 2.1) and previous studies suggesting an increased density of HCN channels at distal locations[416,413].

2.3.3 Altered astrocytic K^+ clearance modulates neuronal dendritic excitability and resonance properties

To examine the impact of local alterations in astrocytic K^+ clearance mechanisms on proximal dendrites of nearby layer V cortical neurons, similar experiments were performed in the presence of 100 µM $BaCl_2$ or selective astrocytic GJ blockers (Gap-26/27) to impair net K^+ uptake via $K_{ir}4.1$ channels or K^+ spatial buffering through astrocytic networks, respectively (Figure 2.6).

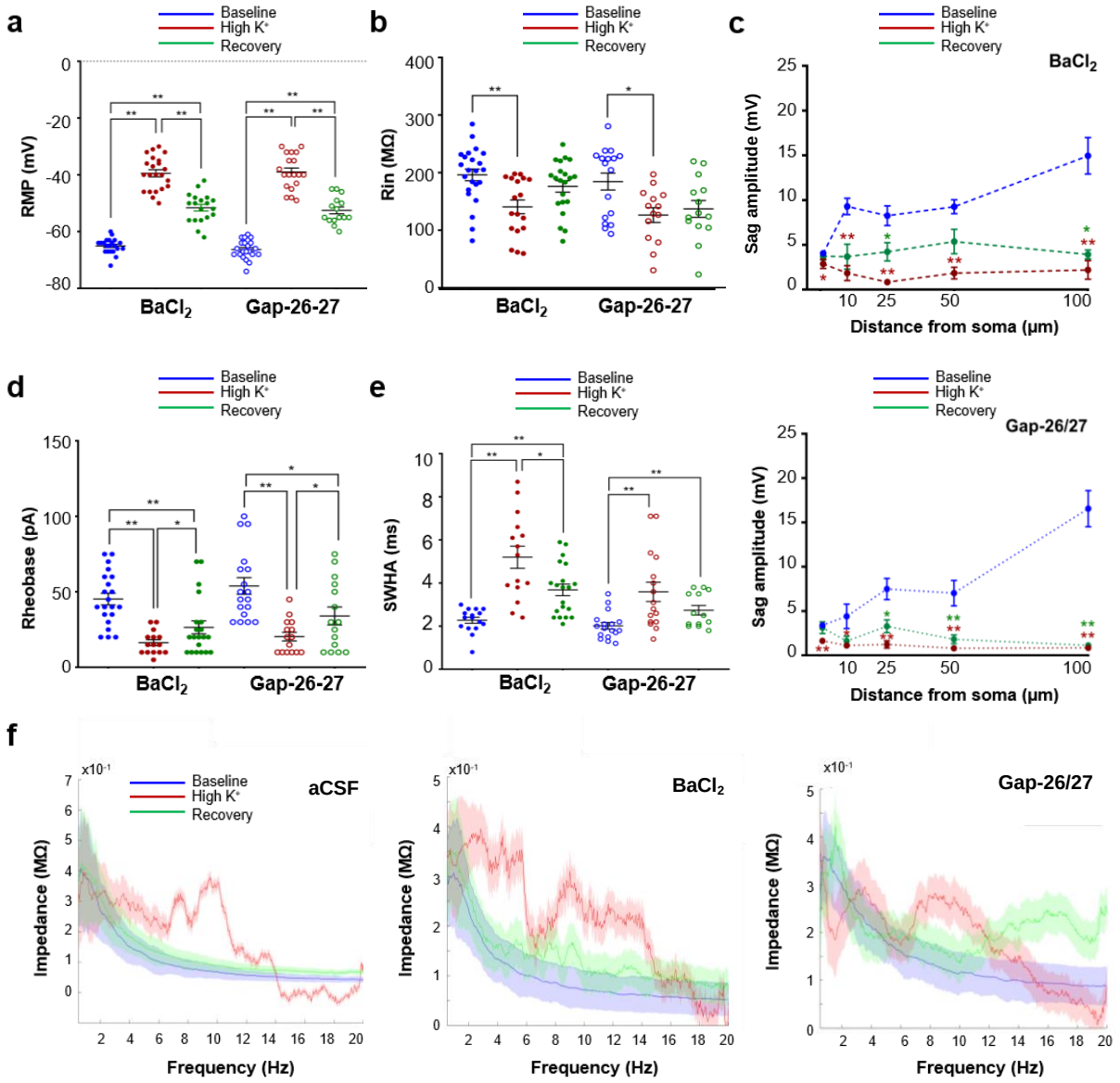

Figure 2.6 Modulation of astrocytic K^+ clearance affects dendritic excitability. a-e) Plots depicting the transient impact of high K^+ (~30 mM) on the resting membrane potential (RMP, a), input resistance (R_{in}, b), sag amplitudes (c), spike rheobase (d) and spike width at half amplitude (SWHA, e) under impaired K^+ clearance conditions (100 µM $BaCl_2$ and Gap-26-27) on proximal dendrites (up to 100 µm from the soma) during the "Baseline" (blue), "High K^+" (red) and "Recovery" (green) episodes. High $[K^+]_o$ (~30 mM) significantly reduces sag amplitudes on proximal dendrites under $K_{ir}4.1$ channel (top) and GJ blockade (bottom) conditions, which persist during the "Recovery" period. f) Impedance frequency (ZAP) profiles depicting the averaged (mean) and standard deviation (shade) values of the resonance frequency recorded from proximal dendrites under normal aCSF (left), 100 µM $BaCl_2$ (middle) and GAP-26/27 (right) conditions. Note the shift towards higher frequencies during the "High K^+" (red) and "Recovery" (green) periods under altered K^+ clearance conditions compared to normal aCSF conditions. (aCSF n=23; $BaCl_2$ n=22; Gap-26-27 n=22). Data is reported as mean ± SEM. *$p < 0.05$; **$p < 0.01$; paired student t-test*

During the "High K^+" episode, blockade of astrocytic K^+ clearance at different stages led to depolarization of the RMP, decreased R_{in} and spike rheobase, as well as increased SWHA in proximal dendrites ($BaCl_2$ n=22; Gap-26/27 n=22; $p < 0.0001$, one-way ANOVA with Tukey's post hoc test, Figure 2.6 A-B, D-E). Similarly, analysis of I_h conductances identified a reduction of the sag amplitude during the "High K^+" episode under altered K^+ clearance conditions compared to the "Baseline" period prior to stimulation ($p < 0.01$; paired student t-test; Figure 2.6 C). Furthermore, these alterations in membrane properties persisted during the "Recovery" period when K^+ clearance was impaired (Figure 2.6), compared to dendritic recordings under normal aCSF, which recovered back to baseline values after KCl washout (Figure 2.5).

Proximal dendritic recordings of the resonance frequency revealed that the range of frequencies affected during the "High K^+" episode was higher (6-10 Hz, Figure 2.6 F), compared to somatic recordings resonating at ~1-2 Hz (Figure 7, Supplementary Table S1; section 2.1). Moreover, whereas under normal aCSF conditions the resonance frequency in proximal dendrites at the "Recovery" period returned to baseline values, alterations in astrocytic K^+ clearance conditions led to a persistent resonation at higher frequencies, both during the "High K^+" and "Recovery" periods (Figure 2.6 F).

2.4 Extended discussion

Previous studies reported that network oscillations are dependent on K^+ dynamics[51,142,304,417,418], however the exact mechanism still remains to be resolved. In this chapter[409], I have shown that impairments in astrocytic K^+ clearance mechanisms enhance individual somatic excitability properties, depicted as a decrease of the R_{in}, reduction of the membrane time constant (τ) and RMP depolarization.

Together with alterations of the active membrane properties, these changes impose alterations in network excitability that affect both low and high frequency oscillations (section 2.1).

Additional extracellular recordings of the network activity further showed that facilitation of astrocytic net K^+ uptake by activation of G-proteins had a dual impact on the network oscillatory behaviour, expressed first as reduced excitability during the "High K^+" period, followed by enhanced excitability during the "Recovery" period. While reducing the multi-unit frequency (Figure 2.1) and oscillation power at the beta and gamma range during the "High K^+" period as expected (Figures 2.2-2.3), photolysis of caged GTP compounds led to a slight increase of the multi-unit frequency (Figure 2.1) and oscillation power at the delta, theta and gamma frequency bands during the "Recovery" period (Figures 2.2-2.3). This multifaceted impact is probably due to the complex activity of G-proteins on intracellular processes in both neurons and glial cells, which on one hand facilitates net K^+ uptake by activation of K_{ir} channels[411], and on the other hand reduces K^+ spatial buffering via the astrocytic syncytium by downregulating astrocytic coupling via Cx43[412].

Active dendrites are essential players in the computations of neuronal circuits due to their frequency-dependent processing capabilities of slow *vs* fast inputs, which allow them to integrate or filter inputs from other neurons, thus optimizing the preferred network oscillation activity[413,419]. Our previous experiments provided evidence that the resonance frequency at the soma fluctuates around 1 Hz (section 2.1). Furthermore, modulation of the K^+ clearance process at different stages using $BaCl_2$ or GJ blockers led to a shift of the peak resonance frequency at the soma up to ~5 Hz and ~7 Hz, respectively. However, these frequencies are still below beta (12-30 Hz) and gamma (>30 Hz) oscillatory frequencies, which are the main frequencies affected at the network level under altered K^+ clearance conditions (section 2.1).

Network oscillations are mainly affected by subthreshold oscillations occurring in the dendrites. Indeed, our complimentary dendritic recordings showed that the resonance frequency in layer V pyramidal neurons rises exponentially with increasing distance from the soma, reaching the highest values at around ~300 µm on apical dendrites (Figure 2.5), as previously reported for hippocampal neurons[414]. Modulation of astrocytic K^+ clearance mechanisms led to alterations in the resonance behaviour of dendrites at higher frequencies >10 Hz and fluctuations at wider frequency ranges compared to the soma (Figure 2.6). These results support our previous observations that modulation of the K^+ clearance machinery in cortical astrocytes has the potential to impact on high frequency oscillations, mainly in the beta and gamma frequency bands (section 2.1). Interestingly, previous observations revealed a role for HCN channel-mediated I_h currents in modulating the neuronal resonance frequency[136], as well as synaptic and dendritic integration[420]. Consistent with this view, the observed alterations in neuronal sag amplitudes under high $[K^+]_o$ (~30 mM) could be one of the underlying mechanisms explaining the shifts of the resonance frequency towards higher frequencies during the "High K^+" episode.

Altogether I show that modulation of different phases in the K^+ clearance process, either at the uptake level or buffering through the astrocytic network, results in alterations of the excitability profile of different subcellular compartments within individual neurons that critically influence and correlate with the observed alterations in the network oscillatory activity, thereby supporting an active role for the astrocytic-mediated K^+ homeostasis in modulating neuronal excitability and network oscillations.

CHAPTER 3:

QUANTITATIVE DETERMINATION AND DETECTION OF EXTRACELLULAR K^+ ALTERATIONS

"We shall not fail or falter; we shall not weaken or tire…
Give us the tools and we will finish the job."
—*Winston Churchill*

3.1 Introduction

K^+ homeostasis in the CNS is paramount for proper brain activity. The extracellular K^+ concentration ($[K^+]_o$) is normally maintained at low levels (~3 mM), which relies on effective removal of excessive K^+ accumulation from the synaptic cleft occurring following neuronal activity. Since increases above ceiling or plateau levels (>12 mM)[421] lead to membrane potential depolarization, and thus enhanced excitability[422,423], maintaining K^+ homeostasis is essential for normal physiology. In the brain, this crucial process is mainly mediated via passive diffusion through the extracellular space and active transport through astrocytes[424]. Hence, alterations of the astrocytic K^+ clearance rate can lead to pathological conditions, such as epileptic seizures or spreading depression, reviewed by[305] (Chapter 1).

To better understand the impact of cellular mediators on the spatiotemporal dynamics of the K^+ clearance process within the astrocytic domain, it is imperative to quantitatively determine how $[K^+]_o$ is dispersed under both physiological and pathological conditions.

However, despite the initial proposal of the astrocytic K^+ spatial buffering hypothesis more than 50 years ago[425], we are still lacking evidence and an accurate description of the temporal spreading and local distribution of K^+ ions across GJ-mediated astrocytic networks.

K^+-selective microelectrodes detect electrical potentials in response to changes in $[K^+]_o$[426], thus providing an accurate and reliable tool to measure the temporal dynamics of $[K^+]_o$. Indeed, this approach has been the method of choice over the past decades by many research groups in order to decipher the molecular identity of astrocytic K^+ spatial buffering and net K^+ uptake mechanisms, both under physiological[423,427,428] and pathological[353,429,430,431] conditions.

Early *in vivo* studies of K^+ spatial buffering used K^+-selective microelectrodes to show that cortical astrocytes are able to buffer $[K^+]_o$ towards local or more distal areas, depending on the behavioural state (sleep *vs* seizures)[51]. Following those observations, Amzica's group (2011)[423] further developed a micro-optrode, consisting of optical fibers coupled to a double-barrelled K^+-selective microelectrode, which allowed them to simultaneously follow the network activity while recording both intracellular and extracellular K^+ alterations in mice performing different behaviours. Their findings suggest that comatose states were associated with a decrease of ~1.3 mM in $[K^+]_o$ accompanied by an increase of the intracellular K^+ (~40 %), whereas paroxysmal discharges were associated with higher variability of $[K^+]_o$, likely reflecting the involvement of different cell types (e.g. glia *vs* neurons). To better comprehend the role of GJs during K^+ spatial buffering, Bazzigaluppi and colleagues (2017)[432] also took advantage of K^+-selective microelectrodes to demonstrate that *in vivo* blockade of astrocytic connectivity results in elevated $[K^+]_o$ (~10 mM), which depresses somatosensory evoked LFPs without inducing seizures in the neocortex, suggesting that the spatiotemporal nature of the increase in $[K^+]_o$ (global through all brain regions *vs* local) can determine the nature of cortical oscillations.

K^+-selective microelectrode experiments have also revealed alterations in $[K^+]_o$ associated with net K^+ uptake mechanisms. For instance, astrocytic depolarization and decrease of the NKA pump-mediated K^+ influx, as occurs during hyperammonemia, result in transient elevations of $[K^+]_o$[433]. Additionally, Ca^{2+}-mediated activation of the NKA pump in astrocytes decreases $[K^+]_o$, which leads to neuronal hyperpolarization and reduced network excitability[304]. Together these studies imply a role for astrocytes in modulating neuronal synchronization to engage specific network activity, as previously suggested[304,305].

While the temporal resolution of K^+-selective microelectrodes has improved over the past decades, with lower capacitance and resistance leading to faster response times in the millisecond range[434], they still show narrow spatial resolution, providing limited information from single-point measurements[435]. This configuration makes it difficult to follow the spread and distribution of K^+ ions across brain regions, even using several K^+-selective microelectrodes simultaneously. Moreover, since these electrodes are not commercially available, special skills are needed to build them and consequently direct demonstration of the astrocytic K^+ spatial buffering process *in vivo* still remains technically challenging[436].

To overcome this limitation and provide a detailed spatiotemporal mapping of the distribution of K^+ ions, scientists developed imaging approaches, such as K^+-sensitive fluorescent probes[435,437]. However, K^+ imaging is still an emerging field with very few available indicators, including Potassium-Binding Benzofuran Isophthalate (PBFI), which requires far-UV excitation and shows several limitations in terms of intracellular loading, weak fluorescence and low affinity for K^+[423]. In 2014, Rimmele and Chatton developed a novel K^+ indicator called Asante Potassium Green-1 (APG-1), characterized by easy loading into the cells, slow leakage and good photostability[438].

Since then, optimized probes of APG-1 have been released, including APG-2 and its intracellular version APG-2 AM. Whereas APG-2 AM is useful for monitoring changes in the intracellular K^+ concentration ($[K^+]_i$)[438], the extracellular version (APG-2 salt) can be used to monitor $[K^+]_o$ by means of wide-field fluorescence fluctuations[439]. Recently, APG probes, once commercialized by TEFLabs, have been renamed to Ion Potassium Green (IPG) fluorescent indicators and are available from the Ion Indicators website (https://ionindicators.com/).

In our previous experiments, I showed that i) high $[K^+]_o$ impacts the network excitability and oscillation amplitude across a wide range of frequencies, and that ii) impairments of different stages in the astrocytic K^+ clearance process affect both neuronal excitability and resonance frequency of individual neurons, which correlates with the observed changes in the network oscillation frequency[409] (Chapter 2). In order to study the **spatiotemporal dynamics and effectors** of the astrocytic K^+ clearance process I have used a combination of both K^+-selective microelectrodes and K^+ imaging techniques.

3.2 Materials and methods

3.2 1 Animals and slice preparation

For $[K^+]_o$ measurements with K^+-selective microelectrodes combined with K^+ imaging, I used 4-6-week-old B6SJL/J mice. Animal handling and slice preparation were performed as previously described in Chapter 2.

3.2.2 Double-barrelled K^+-selective microelectrodes

There are different types of K^+-selective microelectrodes, such as liquid-membrane, gas-membrane, all-solid state or concentric electrodes, which can be built from different glass capillaries, including single-barrelled, double-barrelled, multi-barrelled or theta glass[440]. Despite having many options when building them, most K^+-selective microelectrodes share its basic structure consisting of two separate channels in close proximity, one acting as the ion (i.e. K^+) sensor that contains a cocktail ionophore and the other one serving as the reference[441,442].

Three types of K^+-selective microelectrodes were tested for optimization procedures, including single-barrelled electrodes (SB), double-barrelled electrodes with big tips of ~3 µm (DB-3) and double-barrelled electrodes with small tips of ~1 µm (DB-1), which I found to be the most accurate and stable electrodes when measuring alterations in $[K^+]_o$ following KCl puffs at various concentrations, thereby becoming the electrode of choice for the K^+ clearance rate experiments detailed below (Appendix Figure 1, Appendix Table 1).

3.2.2.1 Preparation

In order to build K^+-selective microelectrodes, a hydrophobic K^+ ionophore is needed to fill the sensor barrel. However, under normal ambient conditions, the inner surface of the glass capillaries is usually covered with chemically bound hydroxyl groups and water molecules[443], thus making it hydrophilic. If this ionophore is introduced into an untreated hydrophilic glass capillary, it will be immediately displaced once the tip of the K^+-selective microelectrode touches the aCSF solution**.** Hence, the first step in building K^+-selective microelectrodes consists of rendering the inner surface of the sensor channel hydrophobic through a process called "silanization"[434]. Silanes are silicon compounds that replace the hydrogen from the hydroxyl groups present on the inner surface of the glass capillaries by a silicon atom, making them hydrophobic, hence the term "silanization"[444,445].

Cleaning and pulling: A successful silanization process requires very careful cleaning of the glass capillaries. Different cleansing treatments have been widely used during the past decades, including acetone with absolute ethanol washes[434] or nitric acid, followed by distilled water rinses[444]. In our lab, double-barrelled borosilicate glass capillaries with filament (O.D.: 1.5 mm; I.D.: 0.86 mm; Sutter Instrument) were cleansed overnight with acetone 100 %, followed by 3 rinses with absolute ethanol, as previously described[441].

A vertical puller (P-30 micropipette puller, Sutter Instrument) with 3 heating protocols (Heat #1, 999 x1 times; Heat #2, 946 x2 times; Pull 220) was used to build double-barrelled glass electrodes with small tips (~1 µm) separated by a distance of ~20 µm.

Silanization: The pulled glass capillaries can be incubated with silanes, either via pressure/suction of the liquid compounds or incubation of the preheated chemical vapours. While many silane compounds are available, aminosilanes, such as trimethylchlorosilane (TMCS[444]), dimethyltrimethylsilylamine (TMSDMA[436]), dimethyldichlorosilane (DMDCS[423,432]) or hexamethyldisilazane (HMDS[434]), have proven to be more effective than chlorosilanes in rendering the surface of the glass hydrophobic[444]. The method I used consisted of preheating 20 ml of HMDS liquid at 40°C to allow the vapor to get inside the cleansed glass capillaries, which were vertically placed on a custom-made holder on top of the bottle containing the pre-warmed silane for 70 minutes (Figure 3.1 A).

Of relevance, silanization of the reference barrel must be avoided (e.g. by applying dental wax at the bottom end), as otherwise some interference between channels might appear. Another important consideration is the ambient humidity, as silanes can react with water molecules, thereby leading to polymerization and formation of silicones[444].

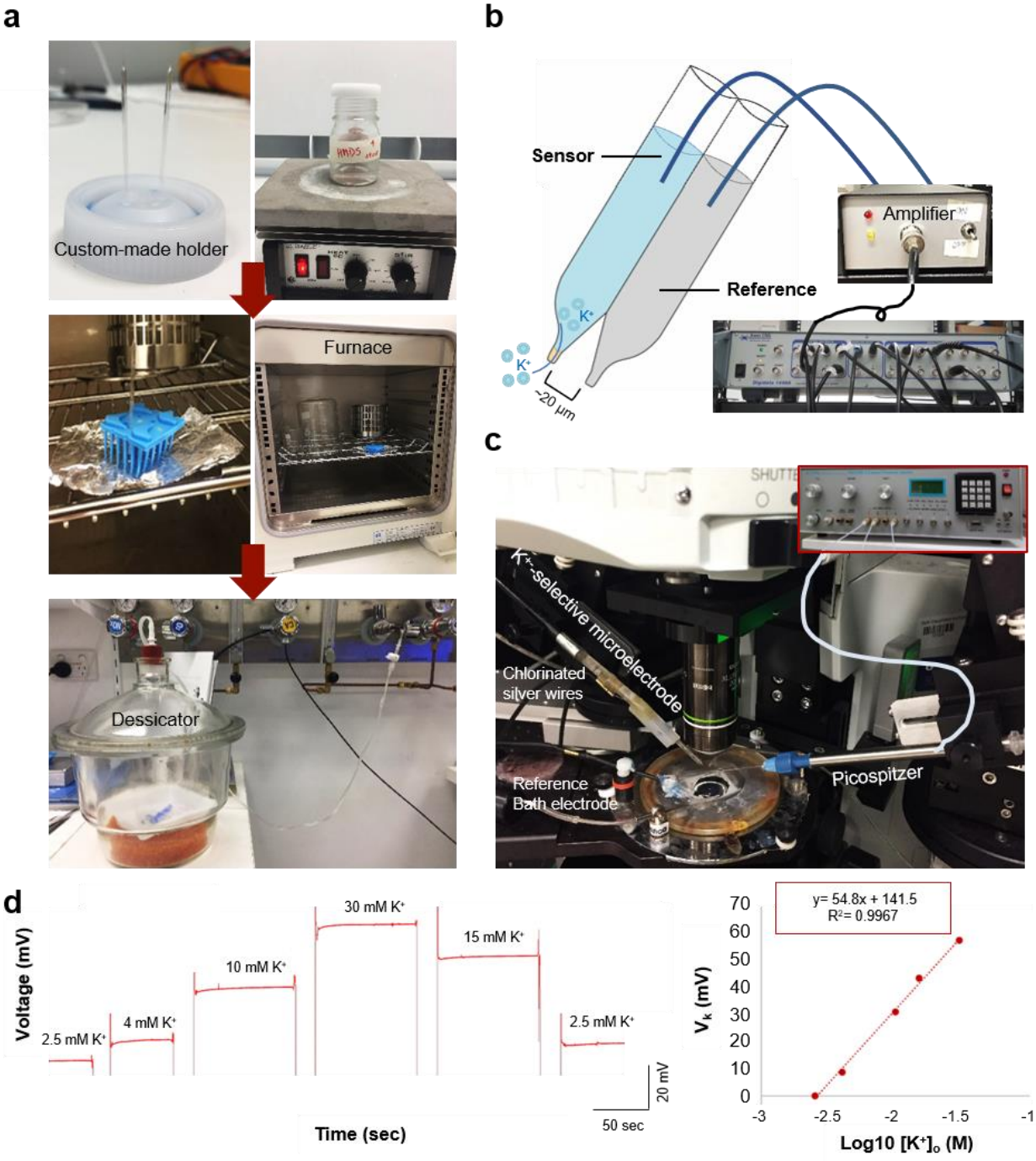

Figure 3.1 Building K^+-selective microelectrodes. a) Images depicting the main silanization steps for building K^+-selective microelectrodes (from top to bottom): a custom-made holder with pulled glass capillaries facing up is placed on top of a pre-warmed HMDS bottle (~20 ml) at 40°C for 70 minutes. After silanization, capillaries are transferred to a heat-proof plastic stand and placed into the furnace at 200°C for 2 hours. Capillaries are then kept dry in the desiccator until experimental use. b) Schematic illustration showing the architecture of a double-barrelled K^+-selective microelectrode with a tip diameter of ~1 µm and an interchannel distance of ~20 µm. The sensor barrel is first filled with a K^+ ionophore cocktail (yellow) and backfilled with 100 mM KCl (blue).

The reference channel is filled with HEPES-buffered saline solution (grey). Chlorinated silver wires are inserted into both channels and connected to the corresponding head stages of a custom-built differential amplifier attached to a digitizer (Digidata 1440). c) Picture of the experimental workspace under the microscope depicting the K^+-selective microelectrode (left), the 20x oil-immersion objective lens (middle) and the puffing KCl electrode connected to a PM2000 programmable cell microinjector (Picospitzer, top right inset). d) Calibration of K^+-selective microelectrodes. Left - traces depicting the change in voltage following insertion of the K^+-selective microelectrode into saline with different $[K^+]_o$. Right - Half-logarithmic plot of $[K^+]_o$ *vs* V_k (equilibrium potential for K^+) from individual calibration recordings used to determine the slope for future $[K^+]_o$ measurements.

For this reason, after silanization, capillaries were transferred to a heat-proof plastic stand, placed in the furnace to dry out for 2 hours at 200°C and stored in a desiccator for several weeks until use[434] (Figure 3.1 A).

Salines: On the day of the experiment, the silanized sensor channel was filled using a Hamilton syringe with a small amount (~0.5 µl) of K^+ ionophore cocktail B (Sigma) with the carrier molecule valinomycin, a dodecadepsi-peptide that binds K^+ in a fully enclosed internal polar cavity.

The lipophilic sensor was then overlaid with an aqueous solution consisting of 100 mM KCl, with caution not to insert additional air bubbles (Figure 3.1 B). The reference barrel was filled with a HEPES-buffered saline solution (containing in mM: 125 NaCl, 2.5 KCl, 2 $CaCl_2$, 2 $MgSO_4$, 1.25 NaH_2PO_4 and 25 HEPES, buffered with NaOH to pH of 7.4), similar in composition to the extracellular aCSF[434]. If silanization is successful, the ionophore should be seen as a clearly concaved surface against the backfilled solution (Figure 3.1 B).

Once both barrels of the K^+-selective microelectrode were filled, chlorinated silver wires were inserted into the sensor and reference channels, without touching each other, until they reached the backfill (avoiding the sensor) and the HEPES-buffered solutions, respectively, and were electronically connected to their corresponding head stages of a custom-built differential amplifier (Figure 3.1 B) attached to a digitizer (Digidata 1440).

Notably, K^+-selective microelectrodes were always placed in the same position on the holder, with the sensor channel towards the microscope and the reference channel closer to the researcher (Figure 3.1 C).

3.2.2.2 Calibration

The voltage response of the silanized K^+-selective microelectrodes was calibrated before and after experiments within the experimental chamber by placing the electrode in aCSF containing different KCl concentrations (2.5 mM or "normal" aCSF, 4 mM, 10 mM, 15 mM and 30 mM).

Calibration solutions were prepared from a "K^+-free" stock solution containing (in mM): 0 KCl, 125 NaCl and 25 HEPES, buffered with NaOH to pH of 7.4, as previously described[441]. Once the electrode potential reached a steady state, a dose-response curve was calculated using a half-logarithmic (Log_{10}) plot. A linear plot of the data reveals the slope (*s*), which has been established to be around -58 mV for K^+-selective microelectrodes with some deviation accepted[434], as shown in Figure 3.1 D. The slope value can then be fit into **equation 1** to determine the change in $[K^+]_o$ ($\Delta[K^+]_o$) at that particular area, according to the Nernst Equation[434], where *s* is the calibration slope and $[K^+]_B$ is the baseline $[K^+]_o$ (~2.5 mM), while the difference in the Nernst potential for potassium (ΔV_k) reflects the changes in the potential of the K^+ sensor during the experiment.

Equation 1: $$\Delta[K^+]_o = [K^+]_B \times \left(10^{\frac{\Delta V_{K^+}}{s}} - 1\right)$$

K^+-selective microelectrodes were considered good if the recorded voltage baseline was stable and the voltage response was essentially the same before and after its experimental usage (~10 % deviation).

3.2.2.3 Optimization

One way to optimize the electrode response times is by achieving shorter distances between the sensor and the reference channels, for instance using theta glass capillaries. Although they are easy to build, the septum that separates both barrels becomes thin and porous after pulling, which often leads to poor silanization, due to salt bridge formation and interference between channels[441]. More recently, higher resolution times have been achieved using concentric electrodes, although their construction is time-consuming and requires specific technical skills[434,446]. Alternatively, it is possible to reduce the amount of ionophore inside the sensor barrel.

The concentration gradient between the liquid outside and the backfill solution inside of the electrode drives the diffusion of K^+ ions through the sensor layer and generates an electric potential[441]. For this reason, the less ionophore thickness (less distance between aqueous phases outside and inside the electrode), the faster responses to K^+ changes in the medium. In order to get such low quantities of ionophore of about ≤1 µl, I used Hamilton syringes of 0.5 µl to load the ionophore into the glass capillary. This optimization step greatly reduced both the rise and decay times of $[K^+]_o$ transients measured with DB-1 electrodes compared to other suboptimal electrodes (i.e. SB or DB-3 electrodes; Appendix Figure 1, Appendix Table 1).

Finally, to apply accurate quantities of K^+, I took advantage of the semi-automatic PM2000 Programmable Cell Microinjector ("Picospitzer", MicroData Instrument, Inc.), which allowed injecting pressure controlled KCl puffs with high temporal resolution (Figure 3.1 C).

3.2.3 Electrophysiological recording and stimulation

The recording chamber was mounted on an Olympus BX-51 microscope equipped with IR/DIC optics and Polygon 400 patterned illuminator (Mightex).

Following the recovery period in the Braincubator™, slices of somatosensory cortex were mounted in the recording chamber, for a minimum of 15 minutes, to allow them to warm up to room temperature (~22°C) and were constantly perfused at a rate of 2-3 ml/min with carbogenated aCSF. Recordings with optimized K^+-selective microelectrodes and K^+ imaging were made from layer II/III of the somatosensory cortex under normal aCSF or altered K^+ clearance conditions. K^+-selective microelectrodes were placed nearby a selected "astrocyte Alpha" stained with Sulforhodamine 101 (SR101).

Different KCl concentrations, corresponding to **low** (~5 mM), **high** (~15 mM) and **excessive** (~30 mM), were locally applied at a constant distance (~10 µm) from the K^+-selective microelectrode through a puffing pipette with tip diameter of 1 µm (~2-3 MΩ; O.D.: 1.0 mm; I.D.: 0.58 mm; 10 cm length; SDR clinical technology) for 0.1-seconds (input pressure ~77.6 psi) using a Picospitzer, as detailed above.

3.2.4 K^+ imaging

To ensure specific staining of astrocytes, dye loading with fluorescent K^+ probes was performed in combination with SR101, a water-soluble red fluorescent dye useful for rapid and high-contrast identification of astrocytes through local dye uptake, followed by GJ-mediated spread[447]. SR101 loading was achieved by incubating slices in 2 ml of aCSF with 1 µM SR101 at 37°C for 20 minutes.

3.2.4.1 Intracellular fluorescent K^+ indicator APG-2 AM

The **intracellular** fluorescent K^+ indicator APG-2 AM (TEFlabs, K_d = 18 mM, 50µg) was first diluted in 50 µl of DMSO and 2.5 µl of 20 % Pluronic acid.

After 15 minutes of sonication, the stock solution was dissolved in 2 ml of aCSF (containing in mM: 125 NaCl, 2.5 KCl, 1 $MgCl_2$, 1.25 NaH_2PO_4, 2 $CaCl_2$, 25 $NaHCO_3$, 25 glucose; saturated with carbogen, 95 % O_2 – 5 % CO_2 mixture, pH 7.4) to a final concentration of 12 µM. Brain slices were incubated at 37°C for 50 minutes in order to allow the dye to diffuse into the cells where non-specific esterases hydrolyse the AM to release the dye. Stock solutions were stored at -20°C.

3.2.4.2 Extracellular fluorescent K^+ indicator APG-2 salt

The **extracellular** fluorescent K^+ indicator APG-2 salt (TEFlabs, K_d = 18 mM, 25µg) was dissolved in 225 µl of aCSF (containing in mM: 125 NaCl, 2.5 KCl, 1 $MgCl_2$, 1.25 NaH_2PO_4, 2 $CaCl_2$, 25 $NaHCO_3$, 25 glucose; saturated with carbogen, 95 % O_2 – 5 % CO_2 mixture, pH 7.4) to a stock solution at final concentration of 100 µM. The stock solution was either diluted with the aCSF from the recording chamber (~ 2 ml aCSF) or mixed with the 30 mM, 15 mM or 5 mM KCl solution in the puffing pipette to reach a final concentration of 1 µM. Stock solutions were stored at -20°C.

3.2.4.3 Image acquisition

Following incubation with APG-2 AM and SR101, slices were transferred back to the Braincubator™ for 20-30 minutes prior to any experimental recordings. Fluorescence images were acquired using a high numerical aperture (NA, 1.0) 20x oil-immersion objective lens (XLUMPlanFLN, Olympus). For APG-2 imaging, the excitation light was filtered through a 470–495 nm band pass filter and the emission light passed through a 510–550 nm band pass filter. SR101 was excited at 510-550 nm and emitted at 640 nm. Consecutive images (500 frames with 200 ms intervals) were acquired in combination with K^+-selective microelectrode recordings using a 12-bit cooled CCD camera, controlled by the software Micromanager (ImageJ).

3.2.4.4 Image analysis

Image J/Fiji (http://fiji.sc/Fiji)[448] and GraphPad Prism software were used to analyse the APG-2 AM and salt fluorescence images under the different conditions. Fluorescence signals were quantified by measuring the mean pixel value of a manually selected somatic area of an astrocyte (region of interest, ROI) for each frame of the image stack. Delta (Δ) F/F0 values were measured by calculating the ratio between the change in fluorescence signal intensity (ΔF) and baseline fluorescence (F0), corresponding to the averaged minimum intensity value of the first 5 frames. To reduce the bleaching effect and highlight changes in fluorescence intensity between frames, raw image sequences were processed using the TopoJ tool.

To measure the spatial distribution of K^+ ions, sholl analysis was applied using a scale of 50 µm between concentric circles. Data from ROIs corresponding to identified astrocytes (double-stained for SR101 and APG-2 AM) within the field of view were exported to GraphPad Prism and the fluorescence ΔF/F0 change was analysed. K^+ elevations were defined as transient increases above baseline values (ΔF/F0 = 0). Area under the curve (XY analysis) was applied to extract the starting and ending frames for each K^+ transient, as well as the amplitude using the function "Peak Y – Baseline", defined as the average of the first 5 frames. Finally, GraphPad Prism data was loaded into excel to reveal the rise and decay times for K^+ elevations and corresponding averages were calculated across conditions.

3.2.5 Drugs

All drugs were stored as frozen stock solutions and were added to aCSF just before recordings. Some experiments were performed in the presence of $BaCl_2$ (100 µM, Sigma Aldrich) in the bath solution to block astrocytic $K_{ir}4.1$ channels.

To assess the role of Cx43-composed GJs, brain slices were incubated with a mixture of GAP-26 (200 μM, AnaSpec) and GAP-27 (300 μM, AnaSpec) for 15 minutes and then transferred to the recording chamber for electrophysiological recordings.

3.2.6 Statistical analysis

Unless stated, data is reported as mean ± S.E.M. Statistical comparisons were done with Prism 7 (GraphPad Software; San Diego, CA) using one-way or two-way ANOVA followed by Tukey's post hoc test, according to the experimental design. Probability values < 0.05 were considered statistically significant.

3.3 Results

3.3.1 The impact of astrocytic K^+ clearance mechanisms on $[K^+]_o$ temporal dynamics

To quantitatively measure the astrocytic K^+ clearance time course, I have optimized a method in our lab for building double-barrelled K^+-selective microelectrodes, as described in the methods section 3.2 (Appendix Figure 1, Appendix Table 1). Optimized electrodes were used to monitor $[K^+]_o$ changes following local application of different KCl concentrations, namely **low** (~5 mM), **high** (~15 mM) and **excessive** (~30 mM). K^+-selective microelectrodes were calibrated before and after experiments, as previously stated. For analysis purposes, a MATLAB code was developed to calculate the amplitude (from baseline to peak), the rise time (10-90 %), the decay time (90-10 %) and the peak area (top 10 %) of the K^+ transients (Figure 3.2 A).

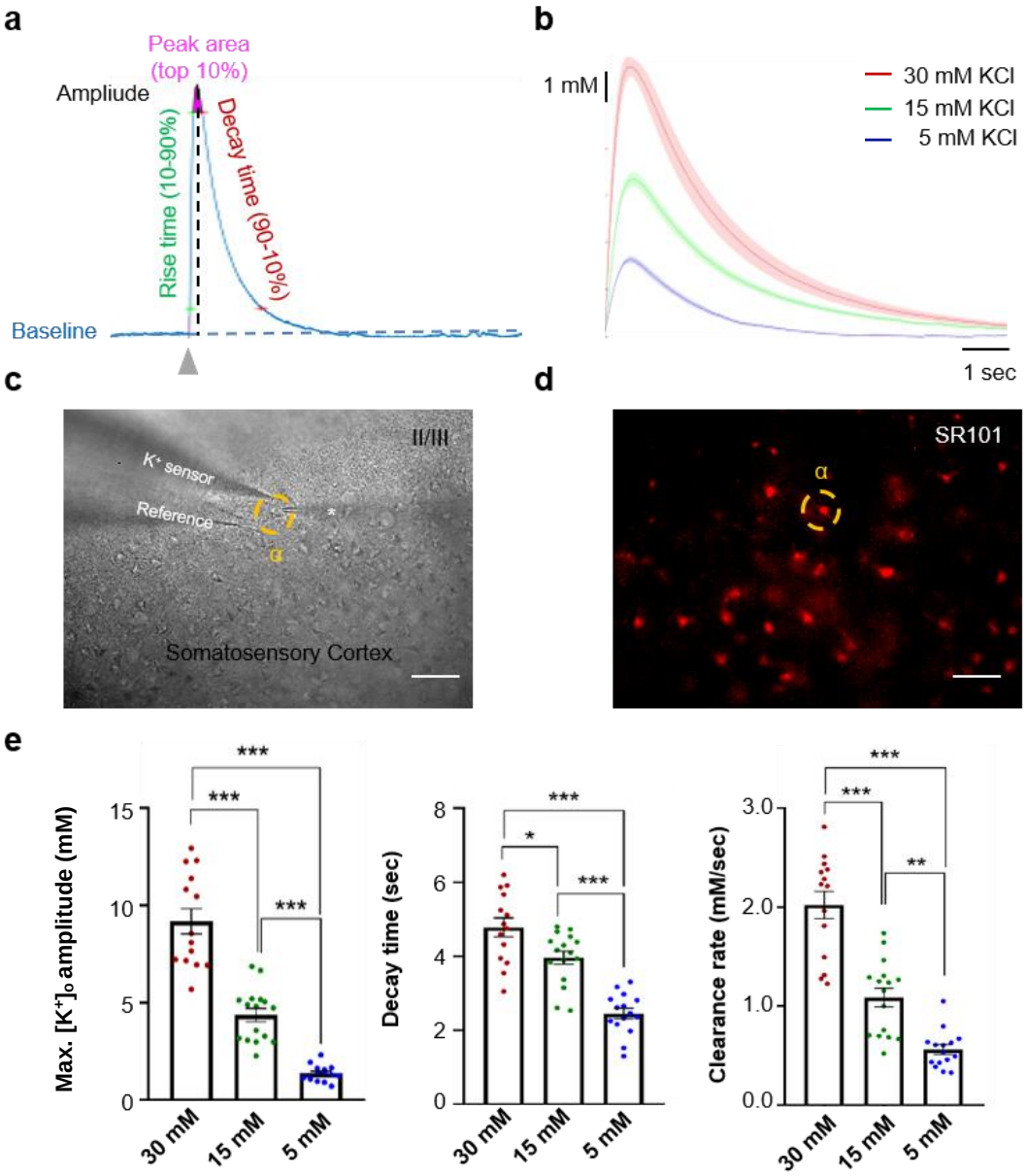

Figure 3.2 Measurements of $[K^+]_o$ in acute brain slices. a) Sample trace of a $[K^+]_o$ recording depicting the peak parameters (amplitude, rise time, decay time, peak area) calculated with MATLAB (MathWorks) following local application of KCl (arrow). b) Average traces of $[K^+]_o$ recordings depicting the mean (line) and standard error (shade) values of the average K^+ clearance time course following local application of 30 mM (red), 15 mM (green) and 5 mM (blue) KCl puffs under normal aCSF conditions. c-d) DIC image (c) showing the experimental setup. K^+-selective microelectrodes are placed in layer II/III of the somatosensory cortex nearby an astrocyte ("astrocyte Alpha", yellow circle) stained with SR101 (d). A puffing pipette (*) is used to locally increase $[K^+]_o$ at a constant distance from the recording electrode (~10 µm). e) Quantitative analysis of the impact of 30 mM, 15 mM and 5 mM KCl puffs on the K^+ clearance rate (in mM/sec, right) obtained by dividing the $[K^+]_o$ amplitude (in mM, left) by the 90-10 % decay time (in sec, middle) of the K^+ transients (30 mM n=14 recordings, 15 mM n=16 recordings, 5 mM n=15 recordings). Scale bar 20 µm. Data is reported as mean ± SEM. *$p < 0.05$; **$p < 0.01$; ***$p < 0.0001$; *one-way ANOVA*

Experiments were performed by placing a K^+-selective microelectrode in layer II/III of the somatosensory cortex, close to a selected "astrocyte Alpha" (stained with SR101). A puffing pipette was located at a constant distance of 10 µm from the recording electrode in order to apply short (100 milliseconds) and local increases of KCl at various concentrations (30 mM, 15 mM and 5 mM KCl), as depicted in Figure 3.2 B-D.

Under normal physiological conditions, local application of KCl led to $[K^+]_o$ increases (in mM) of 9.19±0.65 for 30 mM KCl (n=14), 4.38±0.34 for 15 mM KCl (n=16) and 1.38±0.11 for 5 mM KCl (n=15, $p < 0.0001$, one-way ANOVA with Tukey's post hoc test, Figure 3.2 E). The differences between the applied concentrations (puff) and the measured concentrations at the K^+-selective microelectrode were due to the dilution of the applied KCl solution.

The average $[K^+]_o$ recovery time-course (decay slope) following local application of 30 mM KCl (n=14) was 4.78±0.26 seconds, which decreased to 3.96±0.18 seconds and 2.45±0.15 seconds, following application of 15 mM KCl (n=16) and 5 mM KCl (n=15), respectively ($p < 0.0001$, one-way ANOVA with Tukey's post hoc test, Figure 3.2 E). The K^+ clearance rate was calculated by converting the voltage to concentration using **equation 1** from section 3.2 and dividing the $[K^+]_o$ amplitude by the average decay times. Under normal aCSF, the K^+ clearance rate was concentration-dependent, ranging from 2.02±0.14 mM/sec at excessive $[K^+]_o$ (30 mM; n=14), to 1.09±0.09 mM/sec at high $[K^+]_o$ (15 mM; n=16) and 0.56±0.05 mM/sec at low $[K^+]_o$ (5 mM; n=15; $p < 0.0001$, one-way ANOVA with Tukey's post hoc test, Figure 3.2 E, Appendix Table 2). These results suggest that our custom-built K^+-selective microelectrodes are very sensitive and capable of deciphering small changes in $[K^+]_o$, which usually occur during physiological neuronal activity.

I next performed similar experiments to assess the specific contributions of astrocytic K^+ clearance mechanisms on the removal of $[K^+]_o$ from the extracellular milieu. To assess the impact of net K^+ uptake on the K^+ clearance rate, slices were bath applied with $BaCl_2$ (100 µM) that selectively blocks $K_{ir}4.1$ channels, as previously reported[449]. Bath application of $BaCl_2$ significantly ($F_{(1, 83)}$ = 103.6, $p < 0.0001$, two-way ANOVA) reduced the K^+ clearance rate for all $[K^+]_o$ tested (30 mM, 0.66±0.07 mM/sec, n=18; 15 mM, 0.71±0.04 mM/sec, n=14; 5 mM, 0.28±0.01 mM/sec, n=12; $p < 0.0001$, two-way ANOVA with Tukey's post hoc test, Figure 3.3, Appendix Table 2), indicating a slower rate of $[K^+]_o$ removal from the extracellular space when net K^+ uptake is impaired.

To selectively block K^+ distribution through the astrocytic network, I incubated the slices with a mixture of Cx43 mimetic peptides (GAP-26, 200µM and GAP-27, 300µM) that selectively decrease astrocytic connectivity via electrical GJ, as previously reported[409]. GJ blockade significantly reduced the K^+ clearance rate, depicted as a significant decrease ($F_{(1, 82)}$ = 58.54, $p < 0.0001$, two-way ANOVA, Figure 3.3, Appendix Table 2). However, disruption of the astrocytic connectivity had a differential impact on the K^+ clearance rate compared to $K_{ir}4.1$ channel blockade, as it affected K^+ transients only at high (15 mM, 0.81±0.08 mM/sec, n=15) and excessive (30 mM, 0.71±0.08 mM/sec, n=17) $[K^+]_o$ levels ($p < 0.0001$, two-way ANOVA with Tukey's post hoc test, Figure 3.3).

Low $[K^+]_o$ did not lead to significant alterations in the K^+ clearance rate compared to control conditions (5 mM, 0.49±0.05 mM/sec, n=11; $p > 0.05$, two-way ANOVA, Figure 3.3, Appendix Table 2), confirming the hypothesis that net K^+ uptake is the dominant process used to clear low levels of $[K^+]_o$ and astrocytic K^+ spatial buffering via GJ takes place at higher levels of network activity[450].

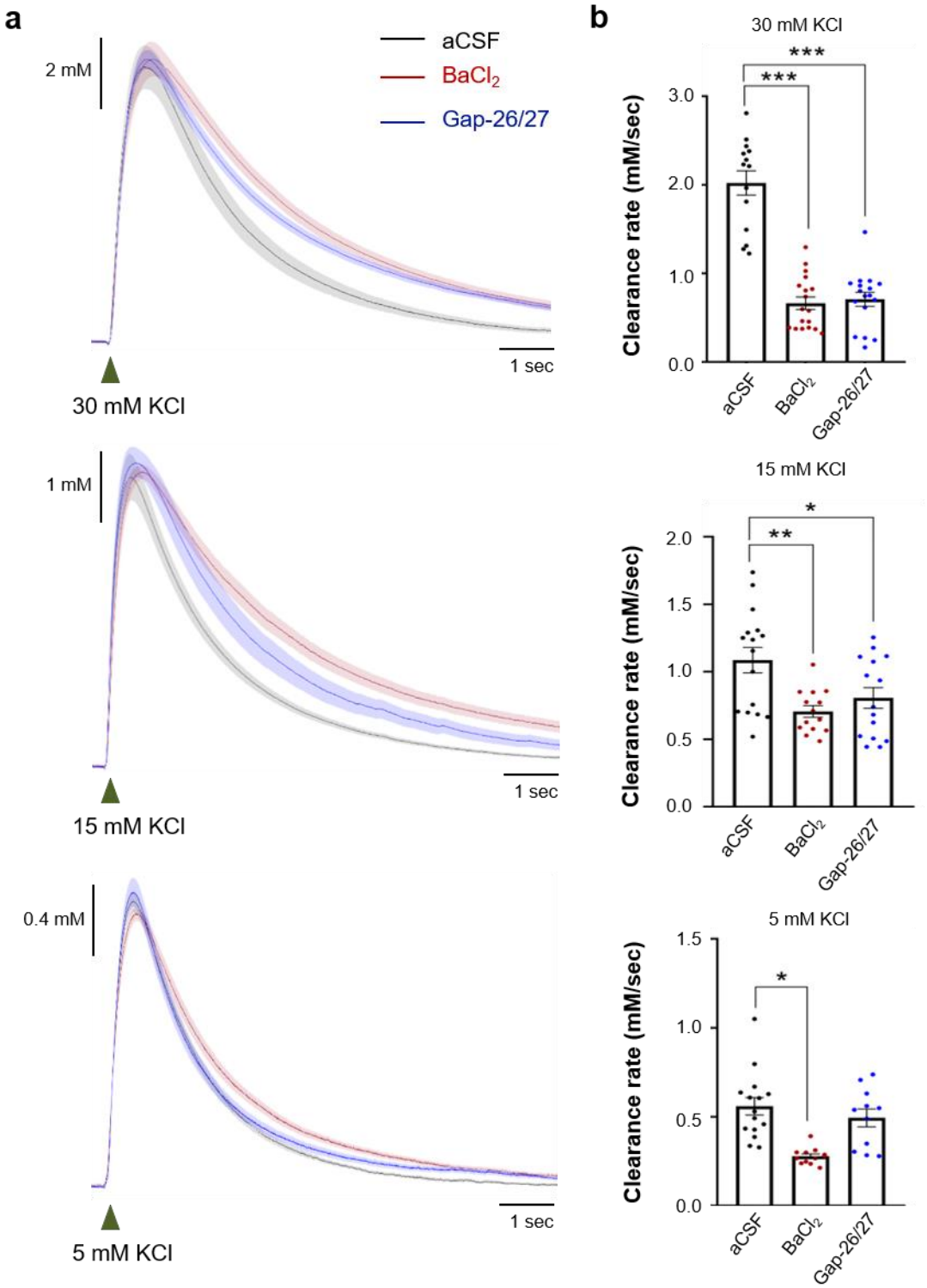

Figure 3.3 Impaired astrocytic K^+ clearance reduces the K^+ clearance rate. a) Average traces of $[K^+]_o$ recordings depicting the mean (line) and standard error (shade) values of the average K^+ clearance time course following local application of 30 mM (top), 15 mM (middle) or 5 mM (bottom) KCl puffs, under normal aCSF (black) and altered K^+ clearance conditions (100 µM $BaCl_2$ in red, Gap-26/27 in blue).

b) Quantitative analysis of the impact of local application of KCl at various concentrations (from top to bottom: 30 mM, 15 mM and 5 mM) on the K^+ clearance rate under normal aCSF (black; 30 mM n=14 recordings, 15 mM n=16 recordings, 5 mM n=15 recordings), 100 µM $BaCl_2$ (red; 30 mM n=18 recordings, 15 mM n=14 recordings, 5 mM n=12 recordings) or Gap-26/27 (blue; 30 mM n=17 recordings, 15 mM n=15 recordings, 5 mM n=11 recordings) conditions. Data is reported as mean ± SEM. **p < 0.05; **p < 0.01; ***p < 0.0001; two-way ANOVA*

3.3.2 High $[K^+]_o$ activates bigger astrocytic networks

To determine the spatiotemporal distribution of K^+ ions through the astrocytic network, I have measured the intracellular APG-2 fluorescence levels (ΔF/F0) within astrocytes located at layers II/III of the somatosensory cortex following application of various KCl concentrations (30 mM, 15 mM and 5 mM), as shown in Figure 3.4 A-B. Astrocytes were considered as "responding" when their $[K^+]_i$ increased within 2 seconds of the KCl puff.

While local application of 30 mM KCl led to $[K^+]_i$ elevations in ~74.0±5.1 % of the astrocytes within the field of view (n=8), 15 mM puffs resulted in a lower percentage of responding astrocytes (~63.3±4.2 %, n=8; Figure 3.4 C). However, local application of 5 mM KCl did not result in $[K^+]_i$ elevations in neighbouring astrocytes (n=10; Figure 3.4 C), suggesting that APG-2 AM is not an optimal dye for detecting small changes in K^+ levels.

Indeed, previous studies showed that APG-2 is insensitive to K^+ changes at amounts that can be physiologically exchanged with Na^{+}[451], whereas higher $[K^+]_o$ levels completely saturate the NKA pump (Appendix Table 3), thus allowing for a more discriminative detection of ionic alterations between intracellular and extracellular compartments. An alternative explanation could be the fact that the low KCl concentration (~5 mM) was within the physiological range after dilution in the aCSF bath, and therefore did not activate the astrocytic network.

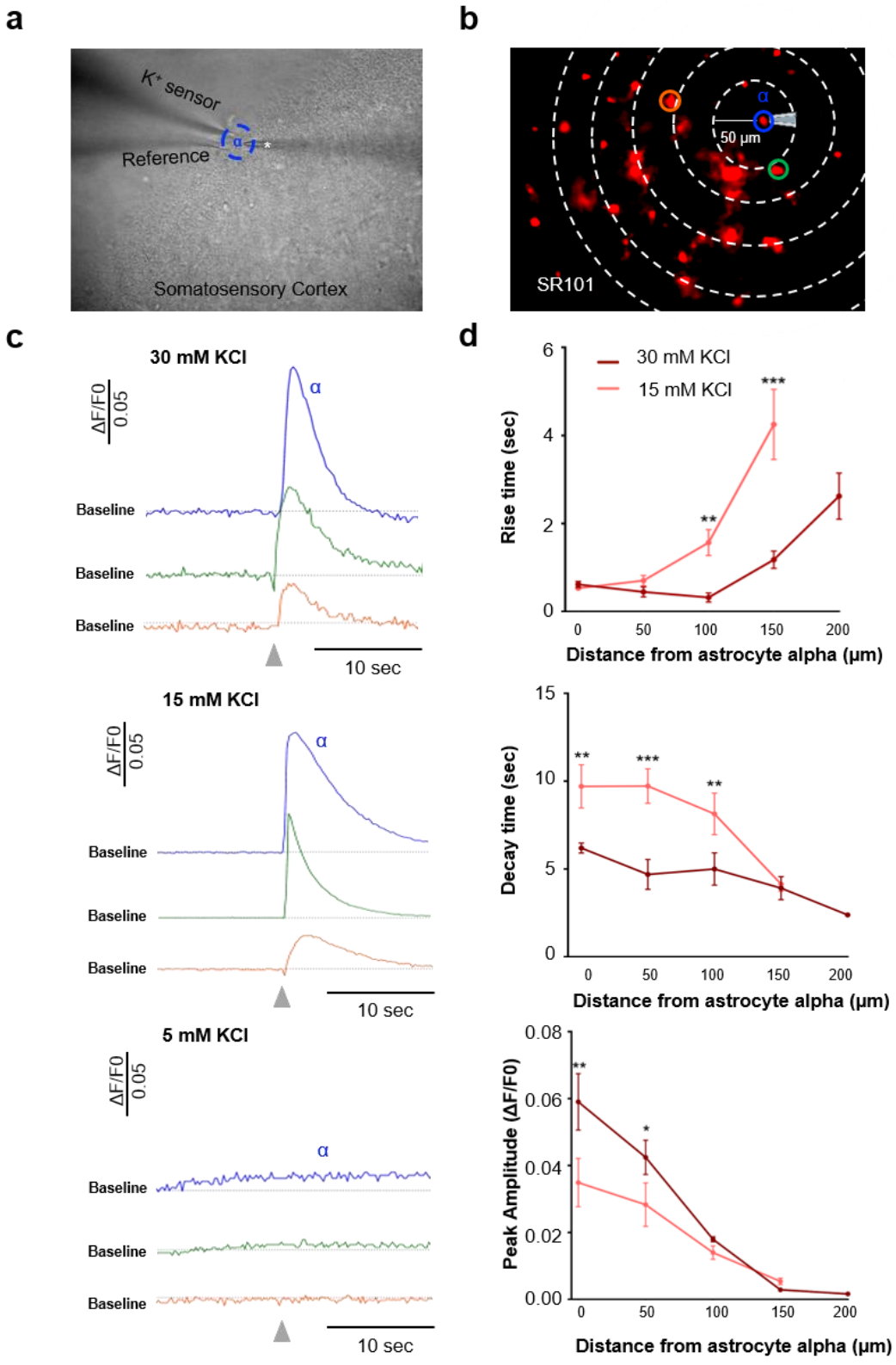

Figure 3.4 Spatial distribution of $[K^+]_o$ within astrocytic networks. a) DIC image showing the experimental setup.

K^+-selective microelectrodes are placed in layer II/III of the somatosensory cortex nearby an astrocyte ("astrocyte Alpha", blue circle). b) Sholl analysis describing the distance at which astrocytes are located in reference to "astrocyte Alpha", defined as distance 0 µm. c) Sample $[K^+]_i$ traces of APG-2 AM loaded astrocytes (colour-coded in b) located at 0 µm ("astrocyte Alpha", blue), 50 µm (green) and 100 µm (orange), showing changes from baseline ΔF/F0 fluorescence levels following local application (arrow) of 30 mM (top), 15 mM (middle) or 5 mM (bottom) KCl puffs under normal aCSF. d) Quantitative analysis of the impact of $[K^+]_o$ on the APG-2AM fluorescence signal rise time (top), decay time (middle) and peak amplitude (bottom) under normal aCSF (30 mM, n=8 recordings; 15 mM KCl, n=8 recordings; 5 mM, n=10 recordings). Data is reported as mean ± SEM. **p < 0.05; **p < 0.01; ***p < 0.0001; two-way ANOVA*

Sholl analysis further indicates that there is a correlation between the increase in $[K^+]_o$ and the maximal distance of active astrocytes, as local application of excessive $[K^+]_o$ (30 mM) recruited larger astrocytic networks, with responding astrocytes located more distally from "astrocyte Alpha" (~200 µm) compared to 15 mM KCl, at which the responding astrocytes were located up to 150 µm from "astrocyte Alpha" ($p < 0.0001$, two-way ANOVA with Tukey's post hoc test, Figure 3.4 D). These results are consistent with the view that $[K^+]_o$ above physiological levels likely activates the K^+ spatial buffering process to restore brain homeostasis by redistributing K^+ ions through GJs to distal areas, indicating an activity-dependent role for K^+ clearance mechanisms.

In addition, to correlate the observed $[K^+]_o$ dynamics with the spreading of K^+ ions throughout the astrocytic network under altered K^+ clearance conditions, I used the intracellular fluorescent probe APG-2 AM, together with $BaCl_2$ or Gap-26/27. In the presence of $BaCl_2$, local application of 30 mM KCl puffs nearby "astrocyte Alpha" did not elicit $[K^+]_i$ elevations in any of the astrocytes within the field of view (n=10; Figure 3.5 A), as $K_{ir}4.1$ channels are pharmacologically blocked and the NKA pump is saturated above physiological $[K^+]_o$ levels[452] (Appendix Table 3). However, local application of excessive $[K^+]_o$ (30 mM) while astrocytic GJ-connectivity was impaired led to $[K^+]_i$ transients in proximal astrocytes (n=10, Figure 3.5 A).

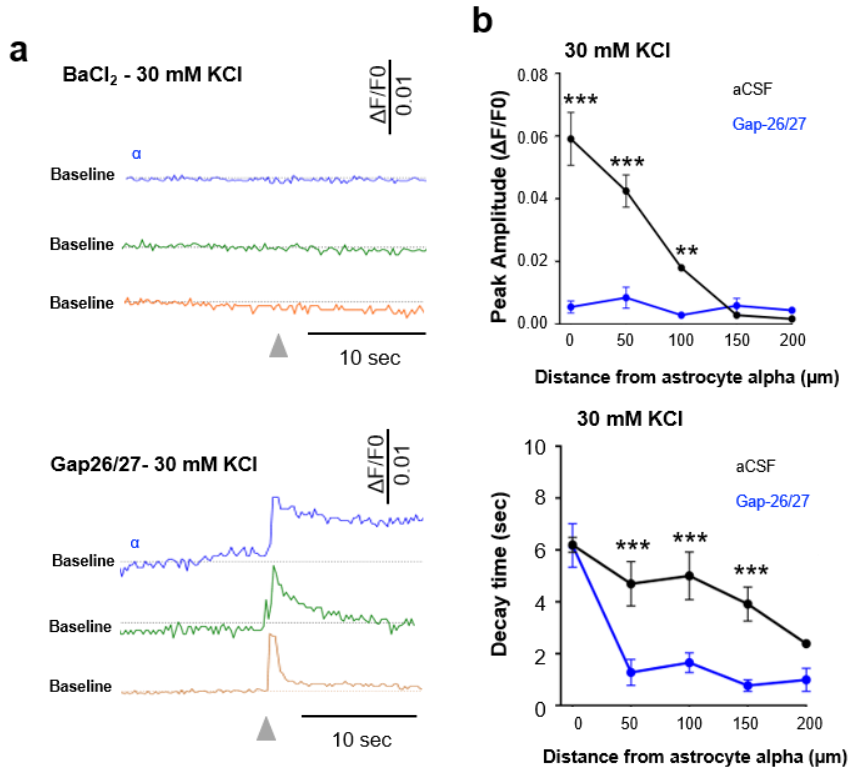

Figure 3.5 Alterations in astrocytic K^+ clearance impact on $[K^+]_i$ dynamics. a) Sample $[K^+]_i$ traces of APG-2 AM loaded astrocytes located at 0 µm ("astrocyte Alpha", blue), 50 µm (green) and 100 µm (orange), showing changes from baseline ΔF/F0 fluorescence levels following local application (arrow) of 30 mM KCl puffs under 100 µM $BaCl_2$ (top) or Gap-26/27 (bottom). b) Plots depicting the impact of 30 mM KCl puffs on the K^+ transients' peak amplitude (top) and decay time (bottom) under normal aCSF and following disruption of the astrocytic connectivity with Gap-26/27 (aCSF, n=8 recordings; Gap-26/27, n=10 recordings). Data is reported as mean ± SEM. **p < 0.01; **p < 0.0001; two-way ANOVA*

These $[K^+]_i$ transients were typically characterized by significantly reduced amplitudes compared to normal aCSF (n=8; $F_{(2, 115)} = 106.6$, $p < 0.0001$, for the factor "treatment", $F_{(4, 115)} = 30.11$, $p < 0.0001$, for the factor "distance" and $F_{(8, 115)} = 26.38$, $p < 0.0001$, for the factor "interaction") at proximal distances up to 100 µm, as well as by decreased decay times, especially within 50-150 µm ($F_{(2, 115)} = 95.14$, $p < 0.0001$, for the factor "treatment", $F_{(4, 115)} = 16.43$, $p < 0.0001$, for the factor "distance" and $F_{(8, 115)} = 6.65$, $p < 0.0001$, for the factor "interaction", two-way ANOVA with Tukey's post hoc test, Figure 3.5 B).

Intriguingly, in the presence of astrocytic GJ blockers, the peak amplitudes remained similar at all distances ($p > 0.05$, one-way ANOVA, Figure 3.5 B), suggesting that the net K^+ uptake process within these astrocytes is functioning, albeit the $[K^+]_i$ transients are due to the passive diffusion of $[K^+]_o$ via the extracellular milieu and net K^+ uptake mechanisms rather than K^+ spatial buffering via the astrocytic syncytium.

3.4 Discussion

The rate of K^+ clearance from the extracellular milieu is determined by a combination of passive diffusion through the extracellular space and active clearance by astrocytic processes[424,453]. According to Fick's first law of diffusion, when the temperature, distance and concentration gradients are constant, the diffusion coefficient D_i, and thus the ion flux remains the same[454,455]. In these experiments, I have (1) a constant flow of aCSF in the experimental recording chamber, (2) a constant temperature, and (3) a constant distance between the K^+-selective microelectrode and the puffing pipette. Therefore, I assume that the $[K^+]_o$ diffusion rate within the same brain slice is constant. Consequently, the specific measurement of the decaying slope of $[K^+]_o$ transients after local application of KCl allows the direct assessment of the active K^+ clearance rate.

Here, I assessed the impact of alterations in astrocytic K^+ clearance mechanisms on the clearance rate and spatiotemporal distribution of K^+ ions in *in vitro* brain slice preparations, which allow the fine control of the extracellular environment while providing mechanical stability[456]. Results show that local application of different KCl concentrations corresponding to **low** (~5 mM), **high** (~15 mM) and **excessive** (~30 mM), led to different K^+ clearance rates under normal aCSF conditions (Figure 3.2, Appendix Table 2). These results are consistent with previous reports indicating that the K^+ clearance process is multifaceted and concentration-dependent[365,425,452,457,458].

Moreover, application of $BaCl_2$ or GJ blockers, affecting astrocytic activity, led to alterations in the K^+ clearance rate, which also was $[K^+]_o$ concentration-dependent. (Figure 3.3, Appendix Table 2). While blockade of $K_{ir}4.1$ channels led to a decrease of the K^+ clearance rate at all concentrations tested (Figure 3.3), blocking GJ-mediated astrocytic connectivity decreased the K^+ clearance rate only at excessive (30 Mm) and high (15 mM) $[K^+]_o$. Unlike $BaCl_2$, selective astrocytic GJ blockers did not affect the K^+ clearance rate at low $[K^+]_o$ (~5 mM KCl, Figure 3.3), consistent with previous reports showing that the net K^+ uptake mechanism via K_{ir} channels is the dominant clearance process at physiological $[K^+]_o$, whereas K^+ spatial buffering via GJ takes place once $[K^+]_o$ increases beyond the ceiling level (~12 mM; Appendix Table 3)[421,450,452]. Intriguingly, under $K_{ir}4.1$ channel blockade conditions I observed no significant differences between the effect of 15 mM or 30 mM KCl on the K^+ clearance rate (Figure 3.3), suggesting that once this threshold or ceiling level is surpassed (>12 mM), the impact on the K^+ clearance time course might be concentration-independent.

Recent advances in K^+ imaging have the potential to provide a detailed description of the spatiotemporal distribution of K^+ ions[437,438], and thus a better understanding of $[K^+]_o$ dynamics that compliments and validates the information gathered with K^+-selective microelectrodes. The spatiotemporal dynamics of the K^+ clearance process at various $[K^+]_o$ were assessed via fluorescence measurements of both $[K^+]_i$ and $[K^+]_o$ levels in nearby astrocytes using APG-2 AM and APG-2 salt, respectively. Brain slices incubated with the cell permeant indicator APG-2 AM displayed astrocytic $[K^+]_i$ elevations following high (15 mM) or excessive (30 mM) KCl concentrations, characterized by longer rise times and smaller peak amplitudes with increasing distance from "astrocyte Alpha" (Figure 3.4). However, under normal conditions, APG-2 AM fluorescence revealed minimal changes in $[K^+]_i$ following application of low $[K^+]_o$ (~5 mM; Figure

3.4 C). This was an unexpected result, as under physiological conditions net K^+ uptake actively takes up small $[K^+]_o$ elevations mainly through the NKA pump and $K_{ir}4.1$ channels, leading to increased $[K^+]_i$, reviewed by[305]. I suspect that these results are due to poor sensitivity of APG-2 AM in detecting low K^+ changes, as previously reported by[451]. Whereas impairments of the net K^+ uptake mechanism with $BaCl_2$ abolished all astrocytic $[K^+]_i$ elevations following 30 mM KCl puffs, blocking K^+ spatial buffering via GJ with Gap-26-27 led to increased $[K^+]_i$ at these excessive KCl concentrations (30 mM; Figure 3.5 A), likely mediated via functional uptake through $K_{ir}4.1$ channels. Furthermore, following 30 mM KCl puffs alterations in astrocytic connectivity affecting the K^+ spatial buffering process resulted in $[K^+]_i$ increases with similar peak amplitudes between proximal and distal astrocytes (Figure 3.5 B). These results suggest that when astrocytic connectivity is impaired, $[K^+]_o$ diffuses to more distal areas, where indirectly connected astrocytes capture $[K^+]_o$ via net K^+ uptake mechanisms.

To assess the spatiotemporal dynamics of $[K^+]_o$ distribution, I combined K^+ imaging with the extracellular fluorescent probe APG-2 salt and K^+-selective microelectrode recordings. Although $[K^+]_o$ imaging with APG-2 salt revealed similar properties of K^+ transients compared to $[K^+]_o$ measurements using K^+-selective microelectrodes (e.g. decay time), I found some incongruences regarding other K^+ transient parameters analysed (e.g. slower rise times; see Appendix Figure 2), likely due to similar affinities for other monovalent ions, such as Na^+, especially in *in vitro* preparations (1.2:1, K^+ over Na^+)[437,451], which needs to be taken into account due to the high concentration of Na^+ in the extracellular space. Indeed, due to the differential ionic concentrations across the plasma membrane some dyes that are effective intracellularly may not be useful for extracellular ionic measurements (i.e. PBFI). Furthermore, $[K^+]_o$ imaging in acute brain slices is hampered by the constant superfusion of aCSF causing a rapid dye washout compared to *in vivo*

experiments[435]. Other limiting factors regarding K^+ imaging include the emitted fluorescence (~540 nm), which can be partly masked by the tissue autofluorescence as a result of the oxidation of flavoproteins, making it possible that the recorded signal does not completely relate to $[K^+]_o$ changes[437]. Hence, despite being successfully used for wide-field imaging of $[K^+]_o$ dynamics in the cortex *ex vivo*[459] and *in vivo*[439], the APG-2 probe still needs improvements regarding noise, Na^+/K^+ selectivity, affinity constants and kinetics, to allow fast and accurate K^+ imaging over a wide range of concentrations. Accordingly, the obtained results suggest that APG-2 salt is not a reliable tool for accurately imaging $[K^+]_o$ dynamics at least in brain slice preparations.

In order to improve APG-2 sensitivity and selectivity for K^+, Chatton's group (2017)[435] developed the APG-4 probe using dendrimer nanotechnology, thanks to which the dye is more hydrophobic than previous versions (i.e. APG-2) and therefore can be retained for longer periods of time in the extracellular space of acute brain slices. Other K^+ sensors have been tested both *in situ* and *in vivo*, including the Calix-COU-Alkyne and the Calix-COU-Am[437], as well as the long-wavelength K^+ sensor TAC-Red[460], which shows high selectivity for small variations in $[K^+]_o$, within the mM range, even in the presence of abundant Na^+. More recently, promising K^+-sensitive genetically encoded probes, based on Förster resonance energy transfer-(FRET), have enabled real-time imaging of K^+ influx and efflux from living cells using two-photon microscopy both *in vivo*[461] and *in vitro*[462].

In conclusion, the above-mentioned experiments shed light on the average K^+ clearance time course within acute brain slices, as well as on the relative impact of the astrocytic net K^+ uptake mechanism, via $K_{ir}4.1$ channels, and the K^+ spatial buffering process, through GJ-mediated astrocytic networks, on the spatiotemporal distribution of $[K^+]_o$.

CHAPTER 4:

NEUROMODULATION OF ASTROCYTIC K^+ CLEARANCE

"We are shaped by our thoughts; we become what we think.
When the mind is pure, joy follows like a shadow that never leaves."
—*Buddha*

4.1 Introduction

Animal survival is highly dependent on the ability to adapt to the everchanging environment. To do so, animals are constantly switching between behavioural states, which are correlated with different network oscillations. Historically, network oscillations have been considered to be highly affected by neuromodulators[463] (discussed in Chapter 1). In fact, previous studies reported on a crucial role for neuromodulators in mediating the shift between certain behavioural states (e.g. sleep, arousal)[463,464,465]. Consistently, selective blockade of the receptors activated by neuromodulators has been associated with impairments of various behaviours and their activation leads to increased neuronal excitability[466], yet the exact molecular mechanisms activated by each neuromodulator during different behaviours are still debatable.

In previous chapters, I have shown that alterations in $[K^+]_o$ can also affect the neuronal network oscillatory activity and that specific changes in astrocytic K^+ clearance mechanisms impact on the resonance and oscillatory behaviour of neurons both at single-cell and network levels, implying that astrocytes have the potential to modulate network activity (Chapter 2).

However, the cellular and molecular mechanisms that may influence the K^+ clearance process by astrocytes are still unknown.

Cortical astrocytes express a wide variety of receptors for several neuromodulators, such as Acetylcholine (ACh, nicotinic α/β and metabotropic M_{1-4})[338,339], Histamine (H_{1-3})[467], Serotonin (5-$HT_{1,2,5,6,7}$)[340], Noradrenaline (NE, $\alpha_{1,2}$-adrenoreceptors and $\beta_{1,2}$-adrenoreceptors)[468,469] and Dopamine (DA, D_{1-5})[470,471]. Importantly, activation of these receptors by different neuromodulators has been previously reported to evoke $[Ca^{2+}]_i$ increases in neighbouring astrocytes that affect astrocytic function, mainly via Ca^{2+}-dependent signalling pathways[472,473]. For instance, previous studies have shown that Histamine leads to astrocytic $[Ca^{2+}]_i$ increases *in vitro*[376] and mediates the upregulation of the glutamate transporter 1 (GLT-1) through astrocytic H_1 receptors, leading to reduced extracellular glutamate levels[474] and thus playing a neuroprotective role against excitotoxicity. Similar to Histamine, NE[375,475,476], DA[377,477,478], 5-HT[378,479,480] and ACh[338,481,482] also exert a modulatory role on astrocytes by eliciting $[Ca^{2+}]_i$ elevations independent of neuronal activity (Figure 1.2).

Astrocytic Ca^{2+} signalling and glutamate clearance play crucial roles in the regulation of the network activity and K^+ homeostasis, which ultimately affects neuronal excitability underlying network oscillations[142,304]. Indeed, Ma *et al.* (2016)[483] showed that neuromodulators can signal through astrocytes, by affecting their Ca^{2+} oscillations to alter neuronal network activity and consequently behavioural output. In line with these observations, Nedergaard's group (2016)[142] further demonstrated that bath application of cortical brain slices with a **cocktail of neuromodulators**, containing ACh, Histamine, NE, DA and Orexin, resulted in increased $[K^+]_o$ regardless of synaptic activity, suggesting that this could serve as a mechanism to maximize the impact of neuromodulators on synchronous activity and recruitment of neurons into networks.

In the present chapter, I aimed at answering three fundamental questions: (1) which neuromodulators from that cocktail[142] are responsible for the observed increase in $[K^+]_o$?; (2) which neuromodulators can affect astrocytic K^+ clearance mechanisms (including net K^+ uptake through $K_{ir}4.1$ channels and K^+ spatial buffering via GJs) to adjust $[K^+]_o$ levels to the network oscillatory state?; and (3) is there a correlation between astrocytic K^+ clearance mechanisms and Ca^{2+} activity?

To this end, I will correlate the observed alterations in the K^+ clearance time course induced by neuromodulators with Ca^{2+} oscillations within the soma of nearby astrocytes by performing $[K^+]_o$ measurements with K^+-selective microelectrodes and Ca^{2+} imaging experiments using the fluorescent dye Fluo-4 AM, thereby providing valuable details on the bidirectional communication between neurons and astrocytes within cortical networks.

4.2 Materials and methods

4.2.1 Animals and slice preparation

For $[K^+]_o$ measurements with K^+-selective microelectrodes and Ca^{2+} imaging experiments with Fluo-4 AM, I used 4-8-week-old B6SJL/J mice. Animal handling and slice preparation were performed as previously described in Chapter 2.

4.2.2 Electrophysiological recording and stimulation

The recording chamber was mounted on an Olympus BX-51 microscope equipped with IR/DIC optics and Polygon 400 patterned illuminator (Mightex). Following the recovery period in the Braincubator™ after staining (Fluo-4 AM, SR101), slices of somatosensory cortex were mounted in the recording chamber, for a minimum of 15 minutes, to allow them to warm up to room

temperature (~22°C) and were constantly perfused at a rate of 2-3 ml/min with carbogenated aCSF. $[K^+]_o$ measurements were performed from layer II/III of the somatosensory cortex, by placing the K^+-selective microelectrode nearby a selected "astrocyte Alpha" stained with SR101. Various KCl concentrations, corresponding to **low** (~5 mM), **high** (~15 mM) and **excessive** (~30 mM), were locally applied at a constant distance (~10 µm) from the K^+-selective microelectrode through a puffing pipette (tip diameter of 1 µm), as previously described. Preparation and calibration of the K^+-selective microelectrodes were performed as detailed in Chapter 3.

To assess the impact of neuromodulators on the K^+ clearance rate, $[K^+]_o$ measurements were performed within the same brain slices before and after 5-minute bath application of different neuromodulators, including the cholinergic agonist Carbachol (100 µM), Histamine dihydrochloride (50 µM), Noradrenaline bitartrate (40 µM), NPEC-caged-Serotonin (30 µM) and NPEC-caged-Dopamine (10 µM). To exclude the involvement of neuronal activity, similar experiments were conducted after perfusing slices for 5 additional minutes with neuromodulators and tetrodoxin (TTX, 1 µM). Polygon400 illuminator (Mightex) was used to uncage NPEC-caged-Serotonin and NPEC-caged-Dopamine compounds by applying focal photolysis with UV light (~360 nm) in a selected area (~50 µm), including the surroundings of the K^+-selective microelectrode, the KCl puffing pipette and the selected astrocytic domain with its processes, for 1 second prior to local application of KCl (Figure 4.1 A).

4.2.3 Ca^{2+} imaging

To ensure specific staining of astrocytes, dye loading with Ca^{2+} dyes was performed in combination with the selective astrocytic marker SR101.

4.2.3.1 Fluo-4 AM

Stock solution of Fluo-4 AM (50 µg, Life Technologies) was prepared by dissolving the dye in 8 µl DMSO and 10 µl Pluronic acid-127 10 % (Molecular Probes), followed by sonication for 5 minutes. The solution was then diluted in 82 µl of aCSF (containing in mM: 125 NaCl, 2.5 KCl, 1 $MgCl_2$, 1.25 NaH_2PO_4, 2 $CaCl_2$, 25 $NaHCO_3$, 25 glucose; saturated with carbogen, 95 % O_2 – 5 % CO_2 mixture, pH 7.4) to reach a concentration of 500 µM. Two mice brain slices were placed in a loading chamber containing 2 ml of aCSF. 20 µl of stock solution (500 µM) were added to the chamber to reach a final concentration of 5 µM. Slices were loaded for 30 minutes at 37°C together with SR101 (1 µM). To ensure adequate oxygenation of the submerged slice during dye incubation, the loading chamber was kept in a closed container that was oxygenated continuously with 95 % O_2 – 5 % CO_2.

4.2.3.2 Image acquisition

Following incubation with Fluo-4 AM and SR101, slices were washed with aCSF and transferred back to the Braincubator™ for 20-30 minutes prior to any experimental recordings. Fluorescence images were acquired using a high NA (1.0) 20x oil-immersion objective lens (XLUMPlanFLN, Olympus). For Fluo-4 AM imaging, the excitation light was filtered through a 470–495 nm band pass filter and the emission light passed through a BA520 nm band pass filter. SR101 was excited at 510-550 nm and emitted at 640 nm. Consecutive images were captured using a 12-bit cooled CCD camera, controlled by the software Micromanager (ImageJ). To assess spontaneous and evoked astrocytic Ca^{2+} responses, images were acquired at 2 Hz for 300 seconds. Following 2 minutes of imaging spontaneous Ca^{2+} activity, KCl puffs at different concentrations (5 mM, 15 mM and 30 mM) were applied through a puffing pipette (tip diameter of 1 µm) using a Picospitzer located close to a selected astrocyte double-stained for Fluo-4 AM and SR101.

The impact of neuromodulators on astrocytic Ca^{2+} signalling was assessed via bath application of different neuromodulators, as described above.

4.2.3.3 Image analysis

Image J/Fiji (http://fiji.sc/Fiji)[448] and GraphPad Prism software were used to analyse the Fluo-4 AM fluorescence images under different conditions. Fluorescence signals were quantified by measuring the mean pixel value of a manually selected somatic area of an astrocyte (ROI) for each frame of the image stack. ΔF/F0 values were measured by calculating the ratio between the change in fluorescence signal intensity (ΔF) and baseline fluorescence (F0), corresponding to the averaged minimum intensity value of the first 5 frames. To reduce the bleaching effect and highlight changes in fluorescence intensity between frames, raw image sequences were processed using the TopoJ tool. To measure the spatiotemporal dynamics of Ca^{2+} signals within astrocytes, sholl analysis was applied using a scale of 50 µm between concentric circles. Data from ROIs corresponding to identified astrocytes (double-stained for SR101 and Fluo-4 AM) within the field of view were exported to GraphPad Prism and the fluorescence ΔF/F0 change was analysed. Astrocytic Ca^{2+} elevations were defined as transient increases above baseline values (ΔF/F0 = 0) and were classified as "spontaneous" or "evoked" when occurring before (within the first 2 minutes) or after (within 10 seconds) local application of KCl, respectively.

4.2.4 Drugs

All drugs were stored as frozen stock solutions and were added to aCSF just before recordings. Neuromodulators, including NE, Histamine, 5-HT and DA were purchased from Tocris Bioscience (In Vitro Technologies Pty Ltd). Noradrenaline bitartrate and Histamine dihydrochloride were dissolved in water to a stock solution at final concentration of 100 mM.

Carbachol (Sigma Aldrich) and caged neuromodulators, including NPEC-caged-Serotonin and NPEC-caged-Dopamine, were dissolved in DMSO to a stock solution at final concentrations of 1 M or 100 mM, respectively. All stock solutions were stored at -20°C and protected from light when required.

4.2.5 Statistical analysis

Unless stated, data is reported as mean ± S.E.M. Statistical comparisons were done with Prism 7 (GraphPad Software; San Diego, CA) using two-tailed paired student t-test and one-way or two-way ANOVA followed by Tukey's post hoc test, according to the experimental design. Analysis of K^+ transient properties was performed using a custom-made MATLAB code (MathWorks). The K^+ clearance rate was calculated by converting the voltage to concentration using **equation 1** from section 3.2 and dividing it by the decay time, as previously described in Chapter 3. Probability values < 0.05 were considered statistically significant.

4.3 Results

4.3.1 The impact of 5-HT on astrocytic K^+ clearance and Ca^{2+} signalling

Previous studies have demonstrated that astrocytes express different subtypes of serotonergic receptors across brain areas, including the cortex, corpus callosum, brain stem, spinal cord and hippocampus[340,480,484,485,486,487,488]. Cortical astrocytes have been found to express $5HT_{2b}$ receptors coupled to phospholipase A_2 (PLA_2) and PLC/G_q signalling cascades, whose activation leads to Ca^{2+} release from internal stores (i.e. ER)[489] and stimulation of glycogenolysis[490] (Figure 1.2).

To test the impact of 5-HT on the K^+ clearance rate, I applied focal photolysis (50 µm diameter; UV light[491]) of NPEC-caged-Serotonin (30 µM) to layer II/III of the somatosensory cortex, including the astrocytic domain, the K^+-selective microelectrode and the puffing pipette (Figure 4.1 A).

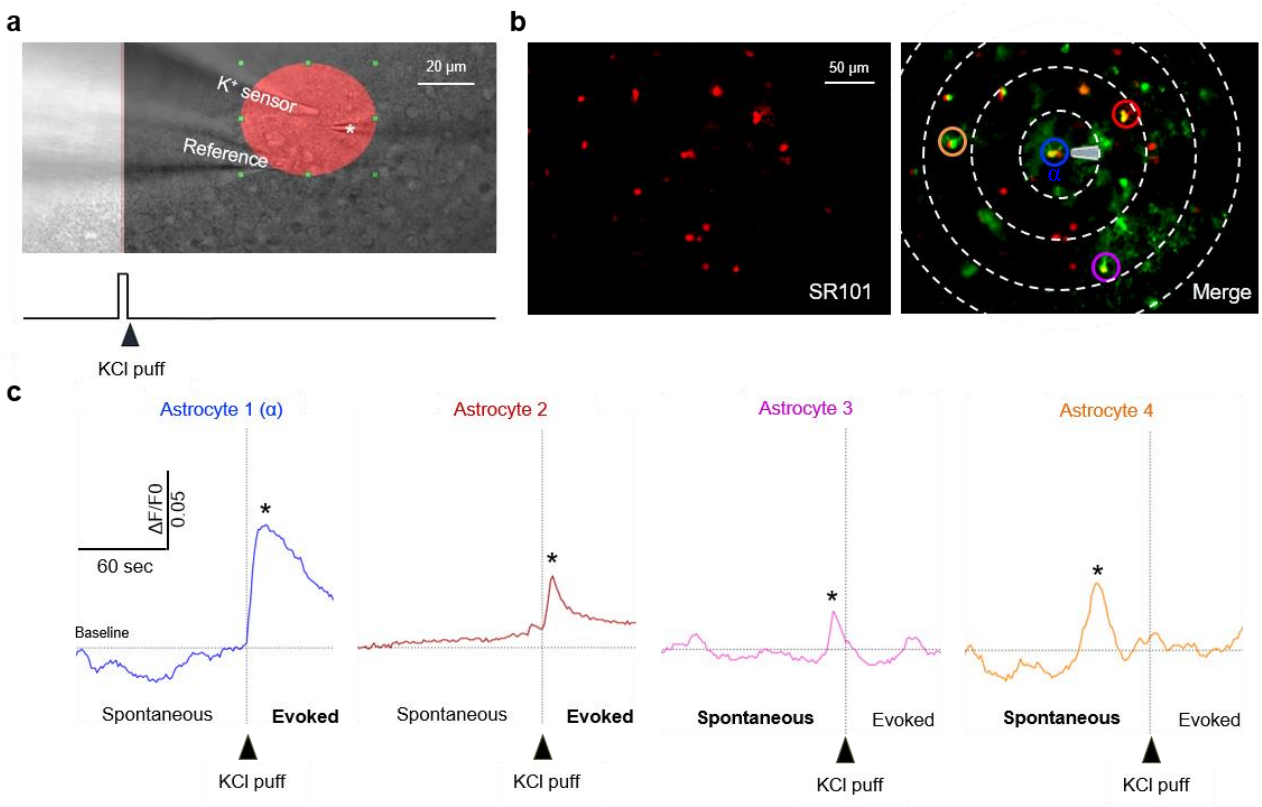

Figure 4.1 Measuring the impact of neuromodulators on astrocytic function. a) DIC image depicting the experimental setup (top) and uncaging protocol (bottom) used for application of the neuromodulators Serotonin and Dopamine (red circle, the area that was photo-activated with UV light, ~360 nm, Mightex) for 1 second prior to local application of KCl by the puffing pipette (*, arrow) in layer II/III of the somatosensory cortex. b) Fluorescence images (20x objective) of neocortical slices showing the SR101 staining (left, red: ~510-550/640 nm) and the "merge" staining in astrocytes depicting the colocalization (yellow) of SR101 and Fluo-4 AM (right, green: ~470-495/520 nm) fluorescent dyes. Sholl analysis was used to describe the distance at which double-stained astrocytes were located from "astrocyte Alpha" (blue circle), defined as distance 0 µm. c) Sample $[Ca^{2+}]_i$ traces imaged from astrocytes (colour-coded in b) showing changes from baseline ΔF/F0 fluorescence levels before (spontaneous, within 2 minutes) and after (evoked, within 10 seconds) local application of KCl puffs (arrow) under normal aCSF.

Results show that 5-HT uncaging decreased the K^+ clearance rate following transient application of excessive $[K^+]_o$ (~30 Mm, n=11), from 2.04±0.20 mM/sec to 1.33±0.14 mM/sec ($p < 0.01$, paired student t-test). However, application of lower KCl concentrations (15 mM and 5 mM) did not affect the K^+ clearance rate significantly (0.82±0.05 mM/sec, n=11 and 0.34±0.04 mM/sec, n=10 respectively; $p > 0.05$, paired student t-test, Figure 4.2 A-B, Table 4.1).

$[K^+]_o$	Condition	Clearance rate (mM/sec)	Amplitude (mM)	#Rise time (sec)	#Peak area (mMxsec)
30 mM	aCSF	2.04±0.20	6.40±0.53	0.32±0.02	1.25±0.08
15 mM	aCSF	0.84±0.06	2.76±0.16	0.34±0.01	0.66±0.04
5 mM	aCSF	0.37±0.03	1.07±0.21	0.28±0.03	0.25±0.02
30 mM	5-HT	1.33±0.14**	6.64 ±0.74	0.34±0.02	1.43±0.08*
15 mM	5-HT	0.82±0.05	2.73±0.22	0.34±0.02	0.63±0.05
5 mM	5-HT	0.34±0.04	0.98±0.03	0.27±0.03	0.26±0.04
30 mM	5-HT/TTX	1.29±0.11**	6.63±0.61	0.33±0.02	1.40±0.06*
15 mM	5-HT/TTX	0.79±0.05	2.69±0.19	0.33±0.02	0.67±0.04
5 mM	5-HT/TTX	0.39±0.04	0.99±0.05	0.27±0.04	0.25±0.03

Table 4.1 The impact of 5-HT on the K^+ clearance rate. Data is reported as mean ± S.E.M. #10-90 % rise time, top 10 % peak area. **p < 0.05; **p < 0.01; paired student t-test compared to the relevant aCSF group. 5-HT-serotonin; TTX-tetrodoxin*

Importantly, blockade of neuronal spiking activity with TTX (1 µM) did not result in any significant differences compared to the effect of 5-HT alone ($p > 0.05$, paired student t-test, Figure 4.2 A-B, Table 4.1), suggesting that the observed alterations in the K^+ clearance rate at excessive $[K^+]_o$ (~30 mM) are independent of neuronal activity and likely due to the direct effect of 5-HT on astrocytic mechanisms (i.e. K^+ spatial buffering).

To validate the impact of the different neuromodulators on the K^+ clearance rate, I additionally measured their effect on astrocytic Ca^{2+} oscillations. Ca^{2+} signals within the soma of individual astrocytes (double-stained for SR101 and Fluo-4 AM) were classified as **spontaneous** (spontaneous astrocytes), when recorded during the first 2 minutes prior to local application of KCl, or **evoked** (evoked astrocytes), if recorded within 10 seconds following the application of KCl (Figure 4.1 B-C).

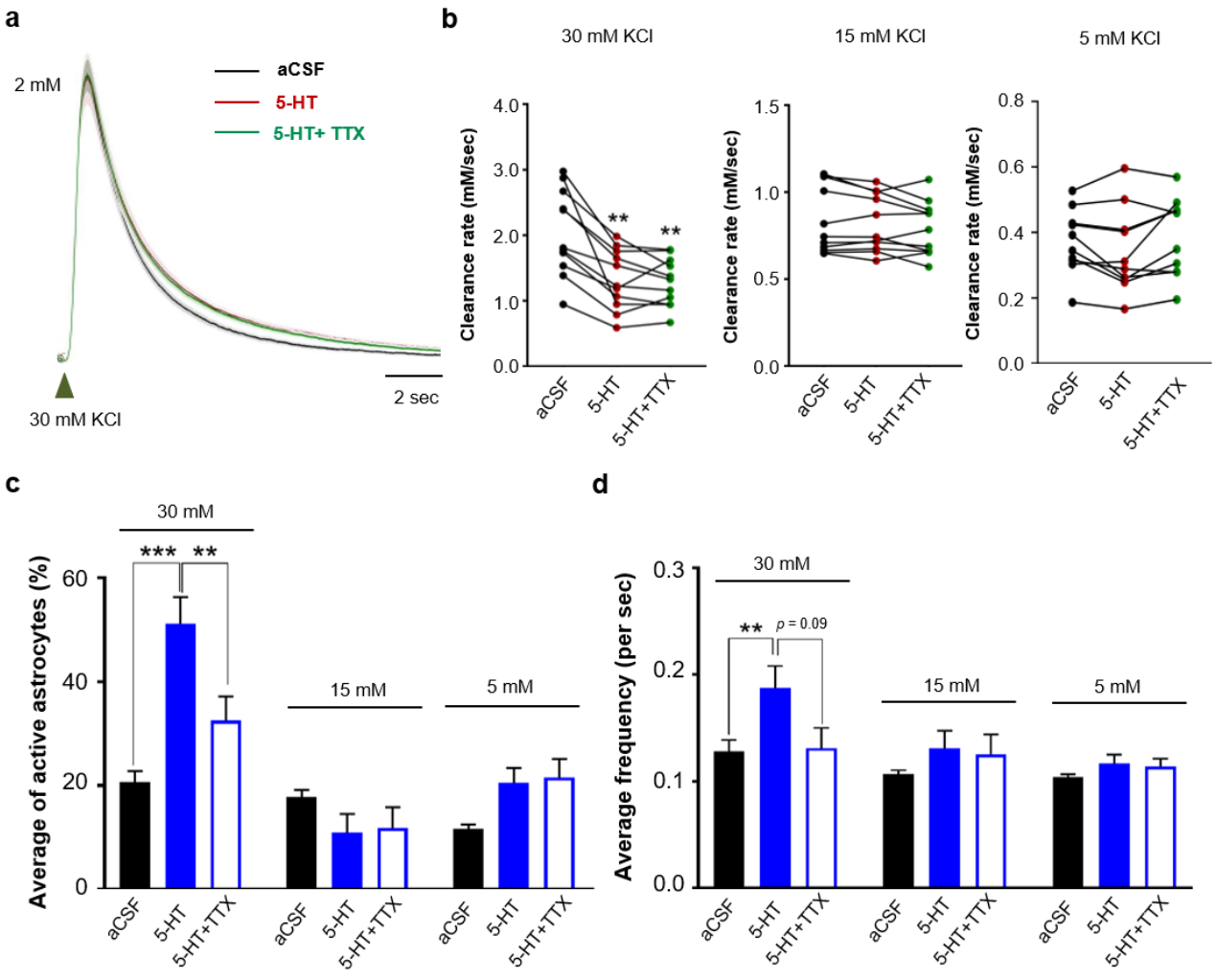

Figure 4.2 The impact of 5-HT on the K^+ clearance rate and astrocytic Ca^{2+} signalling. a) Average traces of $[K^+]_o$ recordings depicting the mean (line) and standard error (shade) values of the average K^+ clearance time course following local application of 30 mM KCl puffs (arrow), before (aCSF, black) and after focal photolysis of 30 µM caged Serotonin (5-HT, red) or 30 µM caged 5-HT with 1 µM TTX (green). b) Paired plots depicting the K^+ clearance rate following local application of KCl at different concentrations (from left to right: 30 mM, 15 mM and 5 mM), before (aCSF, black) and after 5-HT uncaging without (red) or with TTX (green; 30 mM n=11 recordings, 15 mM n=11 recordings, 5 mM n=10 recordings). c) Bar graph depicting the average percentage of active astrocytes within the field of view responding to KCl puffs (5-30 mM) with $[Ca^{2+}]_i$ elevations, before (aCSF, black) and after 5-HT uncaging without or with TTX (blue). d) Bar graph depicting the average frequency (per second) of evoked Ca^{2+} signals in cortical astrocytes following KCl puffs (5-30 mM), before (aCSF, black) and after 5-HT uncaging without or with TTX (blue; 30 mM, n=8 recordings; 15 mM, n=8 recordings; 5 mM, n=9 recordings). Data is reported as mean ± S.E.M. ***p < 0.01; ***p < 0.0001*

Under baseline conditions (aCSF), the average percentage of evoked astrocytes following local application of KCl was 20.7±2.1 % (30 mM, n=25), 17.8±1.3 % (15 mM, n=25) and 11.7±0.8 % (5 mM, n=24; $p < 0.01$ one-way ANOVA with Tukey's post hoc test) and their average Ca^{2+} signals frequency was 0.13±0.01, 0.11±0.01 and 0.10±0.01 events per second respectively ($p < 0.05$ one-way ANOVA with Tukey's post hoc test; Figure 4.2 C-D), suggesting a link between the levels of $[K^+]_o$ and astrocytic Ca^{2+} activity.

At excessive $[K^+]_o$, local photolysis of NPEC-caged-Serotonin compounds significantly ($F_{(2, 115)} = 13.31$, $p < 0.0001$, two-way ANOVA) increased the average percentage of evoked astrocytes, from 20.7±2.1 % up to 51.2±5.1 % (30 mM, n=8, $p < 0.0001$, two-way ANOVA with Tukey's post hoc test, Figure 4.2 C), as well as the average frequency of evoked Ca^{2+} responses (30 mM, 0.19±0.02 events per second, n=8; $p < 0.01$, two-way ANOVA with Tukey's post hoc test, Figure 4.2 D). However, these alterations in evoked Ca^{2+} signals decreased following TTX application (30 mM, 32.5±4.6 % evoked astrocytes and 0.13±0.02 events per second, n=8; $p > 0.05$, two-way ANOVA, Figure 4.2 C-D), suggesting that these serotonergic-mediated Ca^{2+} signals are, at least partially, due to the impact of 5-HT on neuronal activity and cannot be specifically attributed to its impact on astrocytes.

Application of 5-HT did not affect the average percentage of evoked astrocytes or the frequency of evoked Ca^{2+} oscillations following local application of lower $[K^+]_o$, including 15 mM (n=8) and 5 mM KCl puffs (n=9; $p > 0.05$, two-way ANOVA, Figure 4.2 C-D), which is consistent with the observed serotonergic impact on the K^+ clearance rate at these concentrations (Figure 4.2 A-B), and further suggests that 5-HT likely acts in parallel on both neurons and astrocytes to specifically modulate the K^+ spatial buffering process at excessive $[K^+]_o$.

4.3.2 The impact of DA on astrocytic K^+ clearance and Ca^{2+} signalling

DA receptors are classically grouped into D_1-like (D_1 and D_5) and D_2-like (D_2, D_3 and D_4) receptors that activate opposite signalling cascades[471]. On the one hand, DA binding to D_1-like receptors promotes an increase in 3',5'-cyclic adenosine monophosphate (cAMP) levels and the activation of protein kinase A (PKA) via adenylyl cyclase (AC)[492]. On the other hand, D_2-like receptors are coupled to PLC/IP_3 pathway, whose activation triggers Ca^{2+} release from internal stores and decreases cAMP levels[470] (Figure 1.2).

In order to assess the overall impact of DA on the K^+ clearance rate I performed local uncaging of NPEC-caged-Dopamine compounds (10 µM)[493], as described above for 5-HT (Figure 4.1 A). Focal photolysis of caged DA significantly reduced the K^+ clearance rate independent of neuronal activity at all $[K^+]_o$ tested, including 30 mM (1.68±0.25 mM/sec, n=13), 15 mM (1.21±0.15 mM/sec, n=12) and 5 mM (0.56±0.08 mM/sec, n=14; $p < 0.05$, paired student t-test, Figure 4.3 A-B, Table 4.2).

$[K^+]_o$	Condition	Clearance rate (mM/sec)	Amplitude (mM)	#Rise time (sec)	#Peak area (mMxsec)
30 mM	aCSF	2.46±0.28	7.51±1.05	0.27±0.03	1.96±0.15
15 mM	aCSF	1.60±0.25	4.24±0.43	0.27±0.02	0.99±0.08
5 mM	aCSF	0.80±0.11	1.46±0.16	0.26±0.02	0.35±0.02
30 mM	DA	1.61±0.26**	7.32±0.83	0.28±0.03	2.41±0.17**
15 mM	DA	1.35±0.17*	4.13±0.40	0.29±0.02	1.21±0.11*
5 mM	DA	0.60±0.09**	1.49±0.19	0.27±0.02	0.46±0.04**
30 mM	DA/TTX	1.68±0.25**	7.25±0.82	0.28±0.02	2.36±0.22**
15 mM	DA/TTX	1.21±0.15*	4.26±0.41	0.28±0.01	1.10±0.09*
5 mM	DA/TTX	0.56±0.08**	1.49±0.16	0.27±0.01	0.42±0.04*

Table 4.2 The impact of DA on the K^+ clearance rate. Data is reported as mean ± S.E.M. #10-90 % rise time, top 10 % peak area. **p < 0.05; **p < 0.01; paired student t-test compared to the relevant aCSF group. DA-dopamine; TTX-tetrodoxin*

Together, these results suggest that DA affects astrocytic K^+ clearance mechanisms at all $[K^+]_o$, regardless of its impact on neuronal activity.

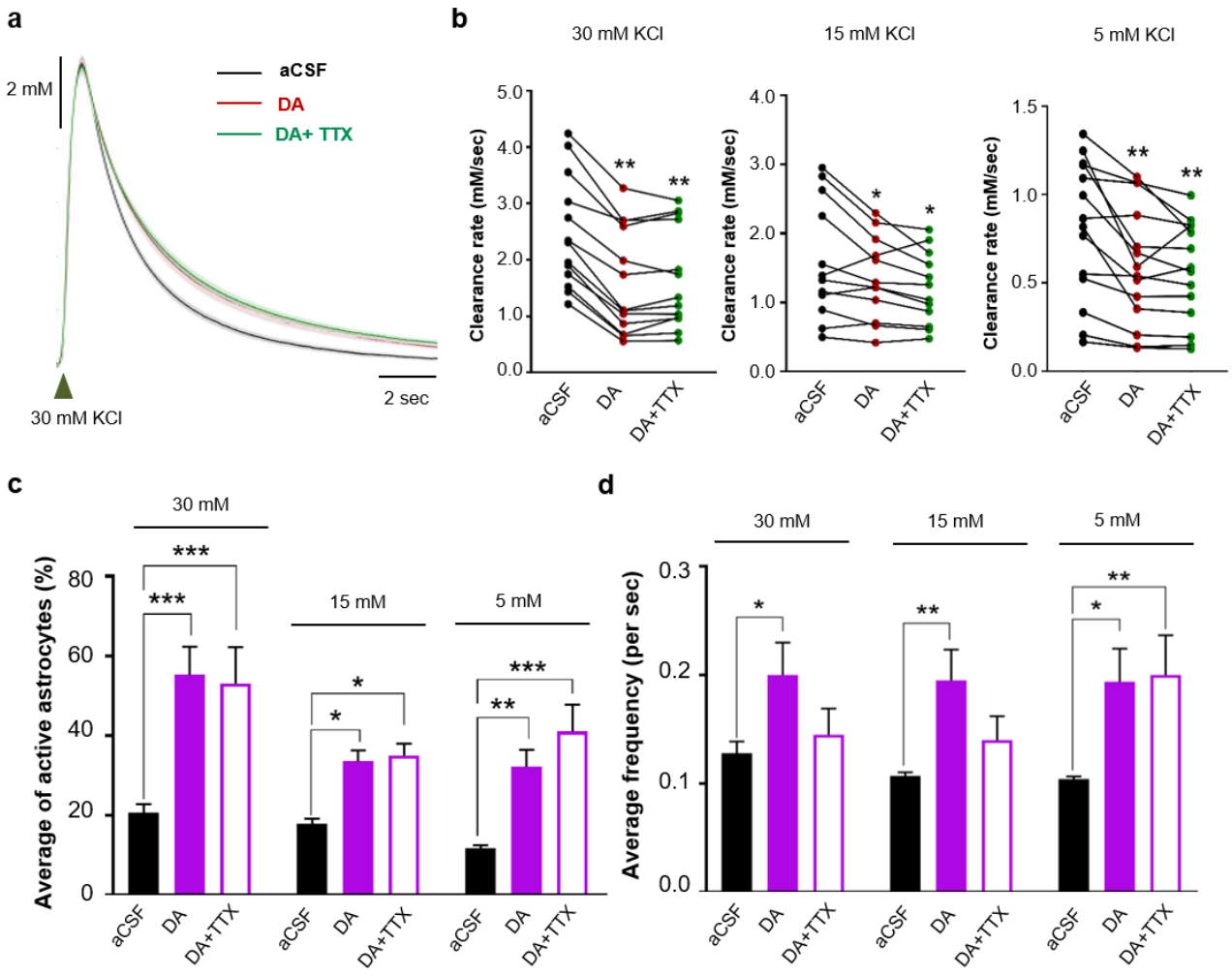

Figure 4.3 The impact of DA on the K^+ clearance rate and astrocytic Ca^{2+} signalling. a) Average traces of $[K^+]_o$ recordings depicting the mean (line) and standard error (shade) values of the average K^+ clearance time course following local application of 30 mM KCl puffs (arrow), before (aCSF, black) and after focal photolysis of 10 µM caged Dopamine (DA, red) or 10 µM caged DA with 1 µM TTX (green). b) Paired plots depicting the K^+ clearance rate following local application of KCl at different concentrations (from left to right: 30 mM, 15 mM and 5 mM), before (aCSF, black) and after DA uncaging without (red) or with TTX (green; 30 mM n=13 recordings, 15 mM n=12 recordings, 5 mM n=14 recordings). c) Bar graph depicting the average percentage of active astrocytes within the field of view responding to KCl puffs (5-30 mM) with $[Ca^{2+}]_i$ elevations, before (aCSF, black) and after DA uncaging without or with TTX (purple). d) Bar graph depicting the average frequency (per second) of evoked Ca^{2+} signals in cortical astrocytes following KCl puffs (5-30 mM), before (aCSF, black) and after DA uncaging without or with TTX (purple; 30 mM, n=10 recordings; 15 mM, n=10 recordings; 5 mM, n=8 recordings). Data is reported as mean ± S.E.M. **p <0.05; **p < 0.01; ***p < 0.0001*

Moreover, DA led to altered astrocytic Ca^{2+} signalling, by significantly ($F_{(2, 121)}$ = 56.60, p < 0.0001, two-way ANOVA) increasing the average percentage of evoked astrocytes (30 mM, 55.3±7.0 %; 15 mM, 33.5±2.8 %; 5 mM, 32.2±4.2 %; p < 0.05, two-way ANOVA with Tukey's post hoc test, Figure 4.3 C), as well as the frequencies of evoked Ca^{2+} oscillations for all $[K^+]_o$ tested (30 mM, 0.20±0.03 events per second, n=10; 15 mM, 0.20±0.03 events per second, n=10; 5 mM, 0.19±0.03 events per second, n=8; p ≤ 0.05, two-way ANOVA with Tukey's post hoc test, Figure 4.3 D).

Intriguingly, the observed impact on the frequency of evoked Ca^{2+} oscillations was independent of neuronal activity only following low concentrations of KCl (5 mM), as it persisted following application of TTX (0.20±0.04 events per second, n=8; p < 0.01, two-way ANOVA with Tukey's post hoc test, Figure 4.3 D). In comparison, the increased frequency of astrocytic Ca^{2+} elevations following application of excessive or high KCl returned to baseline levels when TTX was added to the aCSF solution (30 mM, 0.15±0.02 events per second, n=10; 15 mM, 0.14±0.02 events per second, n=10; p > 0.05, two-way ANOVA, Figure 4.3 D), suggesting a differential involvement of neurons in mediating the dopaminergic effects on astrocytic Ca^{2+} signals evoked by transient increases of $[K^+]_o$.

4.3.3 The impact of NE on astrocytic K^+ clearance and Ca^{2+} signalling

Astrocytes express receptors for NE, including α_1 and β_1-adrenergic receptors. Activation of α_1-adrenergic receptors elicits the PLC/IP_3 signalling cascade, which results in Ca^{2+} release from internal stores[375,494], triggering of both protein kinase C (PKC) and cAMP response element-binding (CREB)-dependent transcription[495], and exacerbation of glutamate re-uptake into astrocytes through GLT-1/GLAST glutamate transporters[496].

However, stimulation of astrocytic β_1-adrenergic receptors results in $[Ca^{2+}]_i$ increases[476], cAMP accumulation, PKA activation and glycogenolysis[497] (Figure 1.2).

Bath application of Noradrenaline bitartrate (40 µM) led to a decrease of the K^+ clearance rate following local application of high (15 mM, 0.70±0.06 mM/sec, n=16) and excessive $[K^+]_o$ (30 mM, 0.80±0.06 mM/sec, n=15) regardless of neuronal activity ($p < 0.01$, paired student t-test, Figure 4.4 A-B). However, NE did not affect the K^+ clearance rate at low $[K^+]_o$ (5 mM, 0.42±0.04 mM/sec, n=15; $p > 0.05$, paired student t-test, Figure 4.4 A-B, Table 4.3), suggesting it mainly affects the K^+ spatial buffering process.

$[K^+]_o$	Condition	Clearance rate (mM/sec)	Amplitude (mM)	#Rise time (sec)	#Peak area (mMxsec)
30 mM	aCSF	1.42±0.14	5.99±0.26	0.40±0.02	1.20±0.08
15 mM	aCSF	0.87±0.05	2.56±0.15	0.35±0.02	0.54±0.06
5 mM	aCSF	0.44±0.04	0.92±0.06	0.30±0.02	0.25±0.04
30 mM	NE	0.80±0.06**	5.94±0.45	0.39±0.03	1.45±0.07*
15 mM	NE	0.70±0.06**	2.52±0.11	0.36±0.02	0.78±0.08*
5 mM	NE	0.42±0.04	0.92±0.05	0.29±0.02	0.30±0.04
30 mM	NE/TTX	0.90±0.07**	5.76±0.41	0.38±0.03	1.54±0.10*
15 mM	NE/TTX	0.65±0.05**	2.49±0.09	0.35±0.02	0.77±0.08*
5 mM	NE/TTX	0.42±0.04	0.91±0.04	0.30±0.03	0.28±0.05

Table 4.3 The impact of NE on the K^+ clearance rate. Data is reported as mean ± S.E.M. #10-90 % rise time, top 10 % peak area. **p < 0.05; **p < 0.01; paired student t-test compared to the relevant aCSF group. NE-noradrenaline; TTX-tetrodoxin*

NE also affected Ca^{2+} activity in cortical astrocytes. Under normal aCSF (n=25), the average percentage of spontaneous astrocytes (during the first 2 minutes prior to the KCl puff) within the field of view was 14.8±1.5 % and their average Ca^{2+} oscillations frequency was 0.84±0.06 events per minute (Figure 4.4 C-D, left). Although the percentage of spontaneous astrocytes in the presence of NE was comparable to control conditions (13.3±1.7 %; $p > 0.05$, one-way ANOVA, Figure 4.4 C, left), NE led to a significant decrease in the average frequency of spontaneous Ca^{2+} oscillations (0.56±0.06 events per minute, n=9; $p < 0.05$, one-way ANOVA with Tukey's post hoc test).

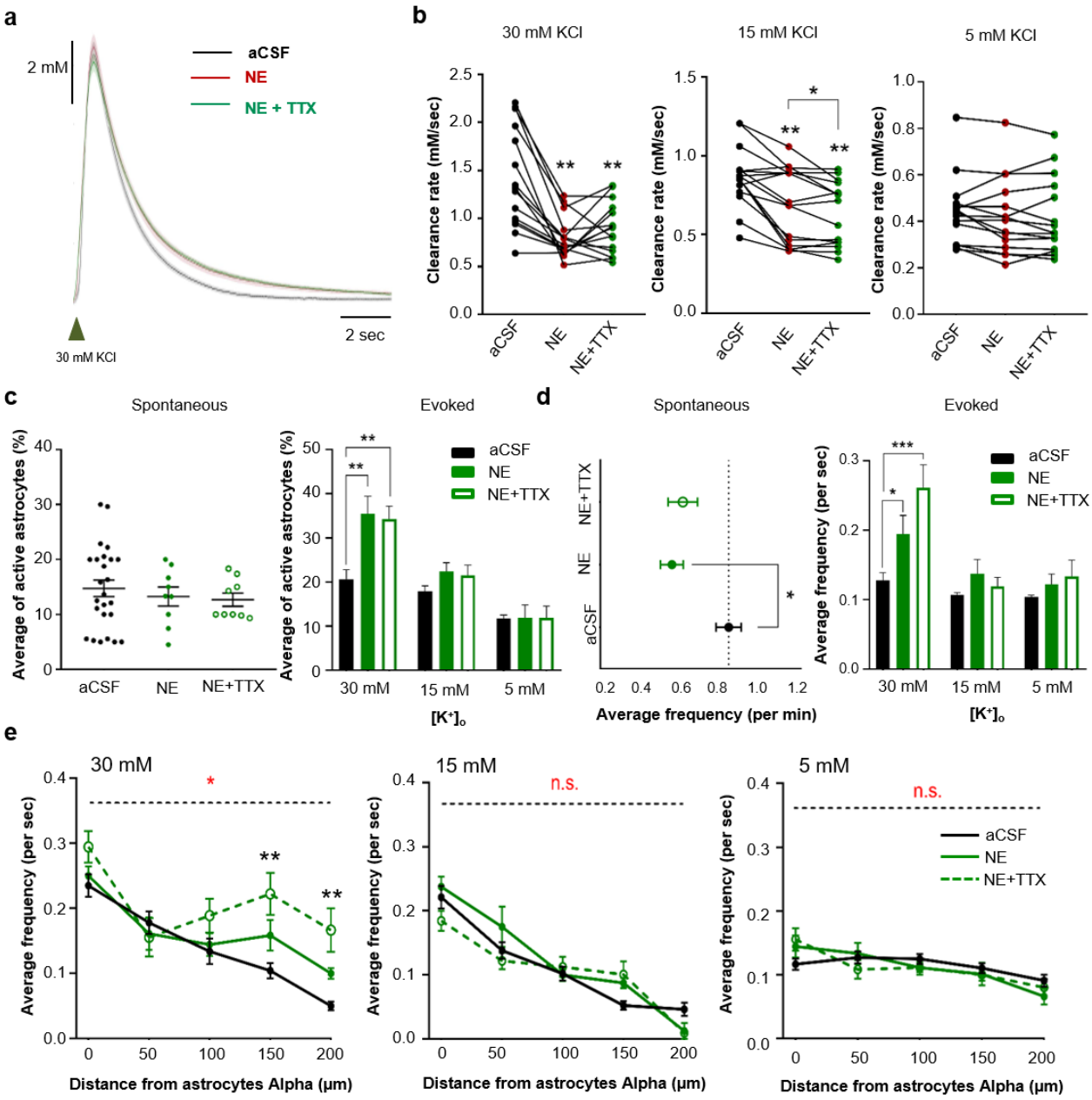

Figure 4.4 The impact of NE on the K^+ clearance rate and astrocytic Ca^{2+} signalling. a) Average traces of $[K^+]_o$ recordings depicting the mean (line) and standard error (shade) values of the average K^+ clearance time course following local application of 30 mM KCl puffs (arrow) before (aCSF, black) and after bath application of 40 µM Noradrenaline (NE, red) or 40 µM NE with 1 µM TTX (green). b) Paired plots depicting the K^+ clearance rate following local application of KCl at different concentrations (from left to right: 30 mM, 15 mM and 5 mM), before (aCSF, black) and after bath application of NE without (red) or with TTX (green; 30 mM n=15 recordings, 15 mM n=16 recordings, 5 mM n=15 recordings). c) Plots depicting the average percentage of active astrocytes within the field of view, responding before (spontaneous, left) and after (evoked, right) local application of KCl puffs (5-30 mM) with $[Ca^{2+}]_i$ elevations in normal aCSF (black), and following bath application of NE without or with TTX (green).

d) Plots depicting the average frequency of Ca^{2+} signals in cortical astrocytes, before (spontaneous, per minute, left) and after (evoked, per second, right) local application of KCl puffs (5-30 mM) in normal aCSF (black), and following bath application of NE without or with TTX (green). e) Plots depicting the relationship between the spatial distribution of astrocytes and the average frequency of evoked Ca^{2+} oscillations (per second) following different KCl concentrations (from left to right: 30 mM, 15 mM and 5 mM), before (aCSF, black, continuous line) and after bath application of NE (green, continuous line) and NE+TTX (green, dashed line; 30 mM, n=9 recordings; 15 mM, n=8 recordings; 5 mM, n=9 recordings). Data is reported as mean ± S.E.M. Asterisks below the dashed line in (e) represent the significance levels between groups following Tukey's post hoc test (black). Asterisks above the dashed line in (e) represent the level of interaction (red). *$*p <0.05; **p < 0.01; ***p < 0.0001$*

These results suggest that NE can affect the intrinsic Ca^{2+} activity in cortical astrocytes regardless of $[K^+]_o$.

In addition, NE significantly ($F_{(2, 117)} = 9.17$, $p < 0.01$, two-way ANOVA) increased both the percentage of evoked astrocytes (35.5±4.0 %; $p < 0.01$, two-way ANOVA with Tukey's post hoc test, Figure 4.4 C, right) and the frequency of evoked Ca^{2+} signals following application of 30 mM KCl (0.19±0.03 events per second, n=9; $p < 0.05$, two-way ANOVA with Tukey's post hoc test, Figure 4.4 D, right). Notably, the noradrenergic effect on the frequency of evoked Ca^{2+} oscillations following application of excessive $[K^+]_o$ was enhanced when neuronal spiking activity was blocked (30 mM, 0.26±0.03 events per second, n=9; $p < 0.0001$, two-way ANOVA with Tukey's post hoc test, Figure 4.4 D, right), suggesting that NE directly modulates Ca^{2+} signalling in astrocytes by facilitating evoked Ca^{2+} activity and recruitment of more astrocytes into the active network in the presence of excessive $[K^+]_o$ (30 mM; Figure 4.4 C, right). However, NE had no impact on the average percentage of evoked astrocytes or the average frequency of evoked Ca^{2+} oscillations following application of lower $[K^+]_o$ (15 mM, n=8; 5 mM, n=9; $p > 0.05$ two-way ANOVA, Figure 4.4 C-D).

Overall, these results suggest a complex activation of noradrenergic receptors and their corresponding signalling cascades to maintain K^+ homeostasis.

In order to evaluate the spatiotemporal impact of the different neuromodulators on the average frequency of evoked Ca^{2+} oscillations in cortical astrocytes, I used sholl analysis as described in methods section 4.2 and Figure 4.1 B-C. The spatiotemporal pattern of evoked Ca^{2+} activity was calculated within the first 100 seconds after local application of 30 mM (n=25) or 15 mM (n=25) KCl and was characterized by high frequencies of Ca^{2+} oscillations in proximal astrocytes, which decreased with distance from astrocyte α (aCSF; $p < 0.0001$, one-way ANOVA with Tukey's post hoc test, Figure 4.4 E).

However, this spatiotemporal pattern was absent following application of low KCl (5 mM, n=24; $p > 0.05$, one-way ANOVA; Figure 4.4 E), as under these conditions $[K^+]_o$ is rapidly buffered by net K^+ uptake mechanisms[452,498]. These observations support a link between $[K^+]_o$ levels and astrocytic Ca^{2+} activity, and further suggest that astrocytes increase their Ca^{2+} activity locally when there is $[K^+]_o$ accumulation (above ceiling level, >12 mM)[421], which likely contributes to the opening of GJs and redistribution of K^+ ions to distal areas[450]. Intriguingly, distal astrocytes displayed increased average frequencies of evoked Ca^{2+} oscillations at low $[K^+]_o$ (5 mM) compared to higher $[K^+]_o$ levels (30 mM and 15 mM; $p < 0.01$, one-way ANOVA with Tukey's post hoc test, Figure 4.4 E). Moreover, a comparison of the spatiotemporal activity between the different $[K^+]_o$ suggests that it was both the distance from astrocyte α ($F_{(4, 355)} = 48.6$, $p < 0.0001$, two-way ANOVA) and the $[K^+]_o$ levels ($F_{(2, 355)} = 8.10$, $p < 0.01$, two-way ANOVA, Figure 4.4 E), which affected the astrocytic spatiotemporal Ca^{2+} activity.

Application of NE itself had no effect on the spatiotemporal pattern of astrocytic Ca^{2+} signalling compared to normal aCSF conditions at any of the $[K^+]_o$ tested ($p > 0.05$, two-way ANOVA, Figure 4.4 E).

In this regard, NE also elicited increased frequencies of evoked Ca^{2+} oscillations in proximal astrocytes that were comparable to normal aCSF, as they declined at distal areas following application of excessive (30 mM, n=9) and high (15 mM, n=8) $[K^+]_o$ ($p < 0.0001$, one-way ANOVA with Tukey's post hoc test). In comparison, the average frequencies of Ca^{2+} oscillations remained similar at all distances following application of low $[K^+]_o$ (5 mM, n=9; $p > 0.05$, one-way ANOVA). Intriguingly, co-application of NE + TTX revealed a significant change following application of 30 mM KCl ($F_{(1, 160)} = 22.45$, $p < 0.0001$, two-way ANOVA) in the spatiotemporal dynamics of astrocytic Ca^{2+} activity, mainly in distal astrocytes which displayed increased frequencies of evoked Ca^{2+} oscillations at ≥150 µm (n=9; $p < 0.01$, two-way ANOVA with Tukey's post hoc test), suggesting that NE acts indirectly on distal astrocytes to affect their Ca^{2+} activity when there is excessive $[K^+]_o$ accumulation.

Together, these results suggest that NE has complex interactions with astrocytes, in which it directly leads to a decrease of the spontaneous Ca^{2+} activity, however following an increase of low $[K^+]_o$ it does not affect either the evoked Ca^{2+} activity nor the K^+ clearance process. Under high and excessive $[K^+]_o$, NE directly reduces the K^+ clearance rate and increases the evoked Ca^{2+} activity, without affecting the astrocytic Ca^{2+} spatiotemporal dynamics.

4.3.4 The impact of Histamine on astrocytic K^+ clearance and Ca^{2+} signalling

Astrocytes express different types of histaminergic receptors, including H_1, H_2 and H_3, which mediate multiple processes, such as glutamate clearance[474] and glucose homeostasis[499]. H_1 receptors are $G_{q/11}$-coupled and therefore associated with PKC and PLC signalling pathways, which lead to Ca^{2+} release from the ER[500].

H_2 receptors are G_s-coupled and have been found to participate in glycogen breakdown and energy supply via activation of PKA and stimulation of AC[501]. H_3 receptors are $G\alpha_{i/o}$-coupled and less abundant in cortical astrocytes compared to astrocytes from other brain regions (e.g. striatum, hippocampus)[502]. These receptors have been involved in mediating the inhibition of AC, while triggering PLA_2, MAP kinase and PI3K/AKT signalling pathways[503,504] (Figure 1.2).

Bath application of Histamine dihydrochloride (50 µM) significantly decreased the K^+ clearance rate following local application of excessive, high and low KCl (30 mM, 1.15±0.14 mM/sec, n=10; 15 mM, 0.84±0.08 mM/sec, n=10; 5 mM, 0.30±0.02 mM/sec, n=11; $p < 0.01$, paired student t-test, Figure 4.5 A-B, Table 4.4).

$[K^+]_o$	Condition	Clearance rate (mM/sec)	Amplitude (mM)	#Rise time (sec)	#Peak area (mMxsec)
30 mM	aCSF	2.02±0.38	6.52±0.77	0.31±0.01	0.74±0.03
15 mM	aCSF	1.12±0.09	3.50±0.32	0.28±0.01	0.51±0.04
5 mM	aCSF	0.51±0.05	0.93±0.09	0.26±0.01	0.15±0.01
30 mM	Histamine	1.15±0.14**	6.63±0.57	0.32±0.01	1.04±0.06*
15 mM	Histamine	0.84±0.08**	3.49±0.56	0.27±0.01	0.72±0.04**
5 mM	Histamine	0.30±0.02**	0.93±0.14	0.25±0.02	0.19±0.01*
30 mM	Histamine/TTX	1.19±0.16**	6.49±0.61	0.32±0.01	1.09±0.04**
15 mM	Histamine/TTX	1.09±0.12	3.41±0.54	0.27±0.02	0.63±0.05
5 mM	Histamine/TTX	0.46±0.03	0.91±0.07	0.26±0.01	0.17±0.01

Table 4.4 The impact of Histamine on the K^+ clearance rate. Data is reported as mean ± S.E.M. #10-90 % rise time, top 10 % peak area. **p < 0.05; **p < 0.01; paired student t-test compared to the relevant aCSF group. TTX-tetrodoxin*

However, while the histaminergic impact on the K^+ clearance rate at excessive $[K^+]_o$ was not affected by neuronal activity (30 mM, 1.19±0.16 mM/sec; $p > 0.05$, paired student t-test, Figure 4.5 A-B, Table 4.4), blockade of neuronal firing with TTX increased the K^+ clearance rate at high (15 mM) and low (5 mM) $[K^+]_o$ ($p < 0.05$, paired student t-test), indicating the involvement of neuronal activity in mediating the histaminergic effects at these concentrations.

Intriguingly, Histamine did not affect the average percentage of spontaneously active astrocytes within the field of view (15.6±1.7 %, n=10) or the frequency of spontaneous Ca^{2+} oscillations (0.70±0.08 events per minute) compared to normal aCSF conditions (14.8±1.5 % and 0.84±0.06 events per minute respectively, n=25; $p > 0.05$, one-way ANOVA, Figure 4.5 C-D, left). In contrast, Histamine increased the number of evoked astrocytes, as well as the frequency of evoked Ca^{2+} signals for all $[K^+]_o$ tested (30 mM, 33.4±1.6 % and 0.24±0.05 events per second, n=10; 15 mM, 31.8±2.2 % and 0.25±0.05 events per second, n=10; 5 mM, 26.3±1.5 % and 0.20±0.03 events per second, n=12; $p < 0.0001$, two-way ANOVA with Tukey's post hoc test, Figure 4.5 C-D, right). However, the rise in both the percentage of evoked astrocytes and the frequency of evoked Ca^{2+} oscillations following excessive increase in $[K^+]_o$ was highly dependent on neuronal activity, as application of TTX abolished the histaminergic effect (30 Mm, 18.9±1.4 % and 0.15±0.02 events per second respectively, n=10; $p > 0.05$, two-way ANOVA, Figure 4.5 C-D, right). These results suggest that the histaminergic regulation of astrocytic K^+ clearance mechanisms and Ca^{2+} signalling is $[K^+]_o$-dependent and involves direct and indirect activation via the neural network.

Furthermore, the impact of Histamine on the spatiotemporal activation of astrocytic Ca^{2+} signalling (within the first 100 seconds) was also $[K^+]_o$-dependent. Sholl analysis revealed that Histamine affected the spatiotemporal pattern of astrocytic Ca^{2+} oscillations following application of KCl at all concentrations tested (30 mM, $F_{(2, 210)} = 17.16$, $p < 0.0001$, for the factor "treatment", $F_{(4, 210)} = 32.06$, $p < 0.0001$, for the factor "distance" and $F_{(8, 210)} = 3.20$, $p < 0.01$, for the factor "interaction"; 15 mM, $F_{(2, 210)} = 22.92$, $p < 0.0001$, for the factor "treatment", $F_{(4, 210)} = 60.41$, $p < 0.0001$, for the factor "distance" and $F_{(8, 210)} = 3.54$, $p < 0.01$, for the factor "interaction"; 5 mM, $F_{(2, 225)} = 0.17$, $p > 0.05$, for the factor "treatment", $F_{(4, 225)} = 51.48$, $p < 0.0001$, for the factor "distance" and $F_{(8, 225)} = 8.76$, $p < 0.0001$, for the factor "interaction"; two-way ANOVA, Figure 4.5 E).

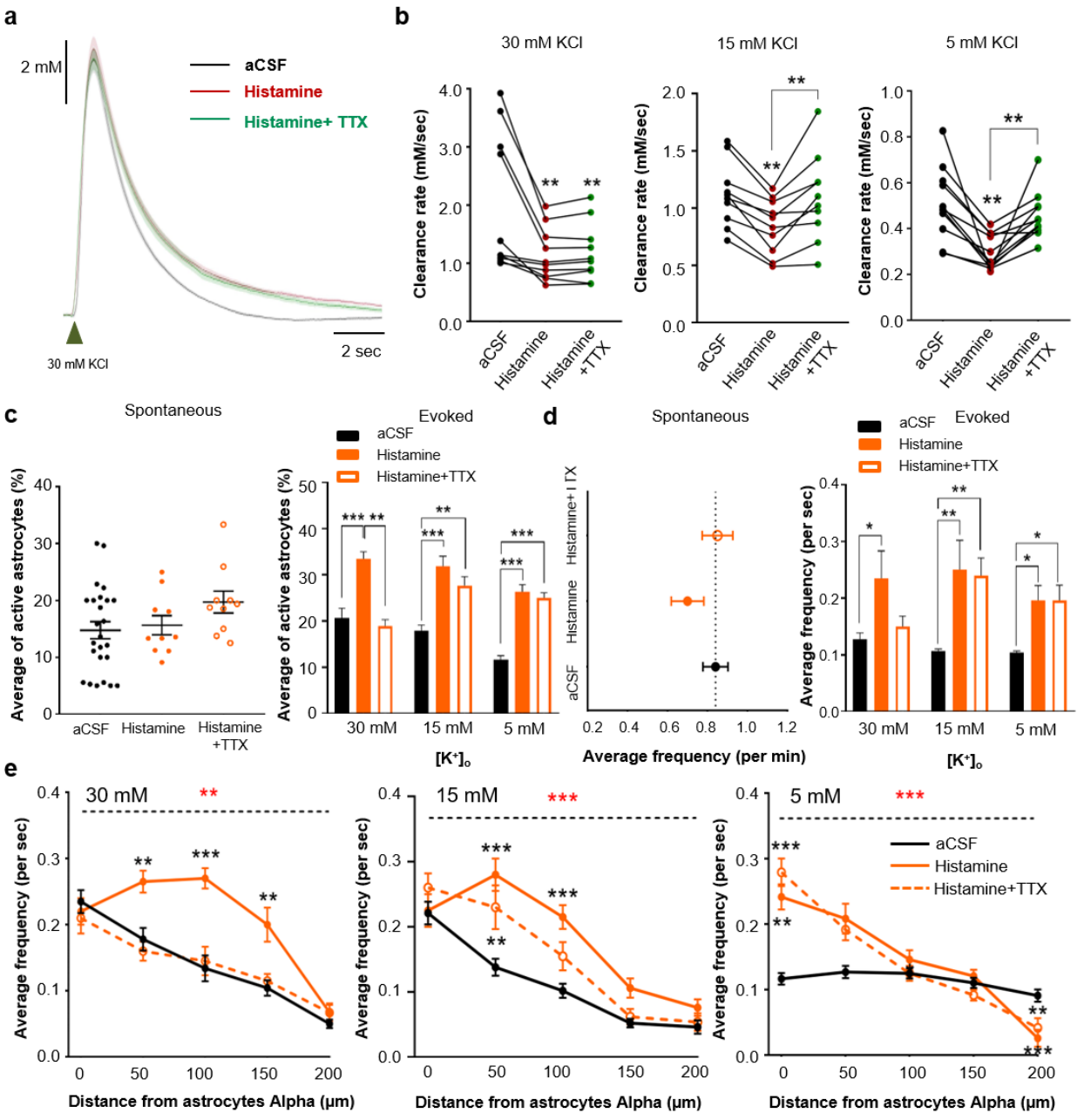

Figure 4.5 The impact of Histamine on the K^+ clearance rate and astrocytic Ca^{2+} signalling. a) Average traces of $[K^+]_o$ recordings depicting the mean (line) and standard error (shade) values of the average K^+ clearance time course following local application of 30 mM KCl puffs (arrow), before (aCSF, black) and after bath application of 50 µM Histamine (red) or 50 µM Histamine with 1 µM TTX (green). b) Paired plots depicting the K^+ clearance rate following local application of KCl at different concentrations (from left to right: 30 mM, 15 mM and 5 mM), before (aCSF, black) and after bath application of Histamine without (red) or with TTX (green; 30 mM n=10 recordings, 15 mM n=10 recordings, 5 mM n=11 recordings). c) Plots depicting the average percentage of active astrocytes within the field of view, responding before (spontaneous, left) and after (evoked, right) local application of KCl puffs (5-30 mM) with $[Ca^{2+}]_i$ elevations in normal aCSF (black), and following bath application of Histamine without or with TTX (orange).

d) Plots depicting the average frequency of Ca^{2+} signals in cortical astrocytes, before (spontaneous, per minute, left) and after (evoked, per second, right) local application of KCl puffs (5-30 mM) in normal aCSF (black), and following bath application of Histamine without or with TTX (orange). e) Plots depicting the relationship between the spatial distribution of astrocytes and the average frequency of evoked Ca^{2+} oscillations (per second) following different KCl concentrations (from left to right: 30 mM, 15 mM and 5 mM), before (aCSF, black, continuous line) and after bath application of Histamine (orange, continuous line) and Histamine+TTX (orange, dashed line; 30 mM, n=10 recordings; 15 mM, n=10 recordings; 5 mM, n=12 recordings). Data is reported as mean ± S.E.M. Asterisks below the dashed line in (e) represent the significance levels between groups following Tukey's post hoc test (black). Asterisks above the dashed line in (e) represent the level of interaction (red). **p <0.05; **p < 0.01; ***p < 0.0001*

Post-hoc analysis showed that, in the presence of Histamine, application of excessive (30 mM, n=10) and high (15 mM, n=10) $[K^+]_o$ led to increased frequencies of evoked Ca^{2+} oscillations, particularly in astrocytes located within 50-150 µm from astrocyte ∝ ($p < 0.01$, two-way ANOVA with Tukey's post hoc test, Figure 4.5 E). Intriguingly, these changes in the spatiotemporal pattern were mediated by neural activity only at excessive $[K^+]_o$, as application of TTX returned the trajectory of Ca^{2+} signals back to baseline conditions ($p > 0.05$, two-way ANOVA, Figure 4.5 E).

In contrast, following application of Histamine and low $[K^+]_o$ (5 mM) the average frequency of evoked Ca^{2+} responses in proximal astrocytes significantly increased to 0.24±0.02 events per second at 0 µm (n=12, $p < 0.01$, two-way ANOVA with Tukey's post hoc test). Importantly, this effect was independent of neuronal activity (0.28±0.02 events per second at 0 µm, n=12, $p < 0.0001$, two-way ANOVA with Tukey's post hoc test) and significantly decreased with distance from astrocyte α compared to normal conditions (200 µm, $p < 0.01$, two-way ANOVA with Tukey's post hoc test, Figure 4.5 E).

Overall, these data suggest that Histamine affects both neurons and astrocytes to modulate the K^+ clearance rate and this modulation is $[K^+]_o$-dependent. At excessive $[K^+]_o$, Histamine impacts on K^+ homeostasis directly through the modulation of the astrocytic network, however, at lower $[K^+]_o$, it exerts its modulation indirectly, via neuronal activity.

Moreover, there was no clear correlation between the astrocytic Ca^{2+} signalling and the K^+ clearance mechanisms that were affected by Histamine, as *i)* the increase in Ca^{2+} signalling following application of excessive $[K^+]_o$ was dependent on neural activity, unlike the changes in the K^+ clearance rate, and *ii)* the increase in astrocytic Ca^{2+} signalling at high and low $[K^+]_o$ was independent of neural activity, while at these $[K^+]_o$ the impact of Histamine on the K^+ clearance rate highly depended on neural activity.

4.3.5 The impact of ACh on astrocytic K^+ clearance and Ca^{2+} signalling

Astrocytes express both ionotropic receptors (α, β)[338] and muscarinic G protein-coupled receptors (GPCRs) for ACh (M_{1-3})[339,505]. While activation of the Ca^{2+}-permeable α7nACh receptor leads to $[Ca^{2+}]_i$ elevations due to Ca^{2+} entry from the extracellular mileu[506], activation of M_{1-3} receptors in astrocytes increases $[Ca^{2+}]_i$ via activation of PLC, which elevates IP_3 levels and promotes Ca^{2+} release from internal stores[481,507]. Subsequently, astrocytic $[Ca^{2+}]_i$ elevations induce gliotransmitter release of glutamate, ATP or D-serine, thereby leading to modulation of synaptic strength and transmission in both the hippocampus[508] and the cortex[509] (Figure 1.2).

To test the impact of ACh on the K^+ clearance rate, I bath applied slices with Carbachol (100 μM), a non-specific ACh agonist that binds and activates both nicotinic and muscarinic ACh receptors[510]. However, the K^+ clearance rate was comparable between normal aCSF and Carbachol conditions for all $[K^+]_o$ tested, as shown in Figure 4.6 A-B (30 mM KCl, 1.36±0.13 mM/sec; 15 mM KCl, 0.97±0.09 mM/sec; 5 mM KCl, 0.51±0.07 mM/sec; $p > 0.05$, paired student t-test, Table 4.5).

$[K^+]_o$	Condition	Clearance rate (mM/sec)	Amplitude (mM)	#Rise time (sec)	#Peak area (mMxsec)
30 mM	aCSF	1.30±0.12	6.63±0.39	0.31±0.02	1.29±0.07
15 mM	aCSF	1.02±0.10	3.26±0.40	0.27±0.02	0.83±0.09
5 mM	aCSF	0.52±0.06	1.34±0.24	0.22±0.01	0.26±0.03
30 mM	Carbachol	1.36±0.13	6.58±0.46	0.31±0.02	1.28±0.07
15 mM	Carbachol	0.97±0.09	3.28±0.42	0.27±0.01	0.77±0.07
5 mM	Carbachol	0.51±0.07	1.36±0.15	0.23±0.01	0.26±0.02
30 mM	Carbachol/TTX	1.37±0.11	6.79±0.56	0.30±0.02	1.22±0.08
15 mM	Carbachol/TTX	1.06±0.10	3.27±0.34	0.26±0.01	0.81±0.04
5 mM	Carbachol/TTX	0.54±0.07	1.39±0.18	0.23±0.01	0.25±0.01

Table 4.5 The impact of Carbachol on the K^+ clearance rate. Data is reported as mean ± S.E.M. #10-90 % rise time, top 10 % peak area. *TTX-tetrodoxin*

Since blockade of neuronal firing with TTX resulted in no significant alterations compared to control or Carbachol conditions (30 mM KCl, 1.37±0.11 mM/sec, n=15; 15 mM KCl, 1.06±0.10 mM/sec, n=10; 5 mM KCl, 0.54±0.07 mM/sec, n=10; $p > 0.05$, paired student t-test, Figure 4.6 A-B, Table 4.5), these results suggest that ACh has no direct impact on K^+ clearance mechanisms.

Consistent with these results, application of Carbachol had no significant effect on the astrocytic spontaneous nor evoked Ca^{2+} activity at any of the $[K^+]_o$ tested ($p > 0.05$, one-way ANOVA, Figure 4.6 C-D). However, co-application of Carbachol and TTX significantly increased the average percentage of spontaneously active astrocytes and the average frequency of spontaneous Ca^{2+} oscillations (22.4±2.0 % and 1.13±0.10 events per minute respectively, n=15; $p < 0.05$, one-way ANOVA with Tukey's post hoc test, Figure 4.6 C-D, left). Moreover, it decreased the number of evoked astrocytes at excessive $[K^+]_o$ (30 mM, 10.3±1.7 % n=14, $p < 0.01$, two-way ANOVA with Tukey's post hoc test), suggesting this effect is mediated by neuronal activity.

However, Carbachol had no effect on the evoked Ca^{2+} activity at lower $[K^+]_o$ (15 mM, n=15 and 5 mM, n=13; $p > 0.05$, two-way ANOVA, Figure 4.6 C-D, right), suggesting that the impact on astrocytic Ca^{2+} signalling is likely attributed to the effect of TTX itself on the neuronal network and not specifically to Carbachol.

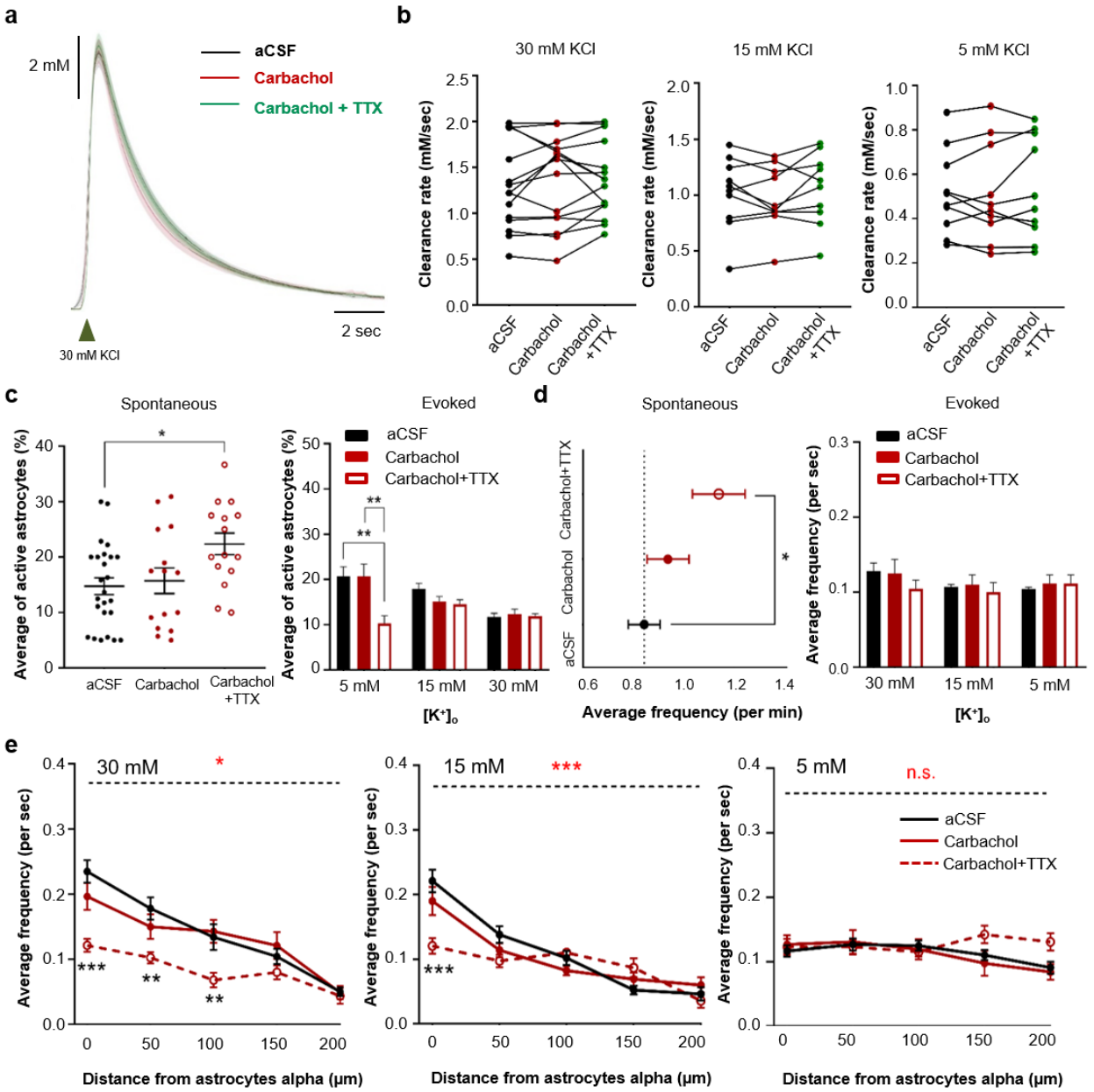

Figure 4.6 The impact of Carbachol on the K^+ clearance rate and astrocytic Ca^{2+} signalling. a) Average traces of $[K^+]_o$ recordings depicting the mean (line) and standard error (shade) values of the average K^+ clearance time course following local application of 30 mM KCl puffs (arrow), before (aCSF, black) and after bath application of 100 µM Carbachol (red) or 100 µM Carbachol with 1 µM TTX (green). b) Paired plots depicting the K^+ clearance rate following local application of KCl at different concentrations (from left to right: 30 mM, 15 mM and 5 mM), before (aCSF, black) and after bath application of Carbachol without (red) or with TTX (green; 30 mM n=15 recordings, 15 mM n=10 recordings, 5 mM n=10 recordings). c) Plots depicting the average percentage of active astrocytes within the field of view, responding before (spontaneous, left) and after (evoked, right) local application of KCl puffs (5-30 mM) with $[Ca^{2+}]_i$ elevations in normal aCSF (black), and following bath application of Carbachol without or with TTX (red).

d) Plots depicting the average frequency of Ca^{2+} signals in cortical astrocytes, before (spontaneous, per minute, left) and after (evoked, per second, right) local application of KCl puffs (5-30 mM) in normal aCSF (black), and following bath application of Carbachol without or with TTX (red). e) Plots depicting the relationship between the spatial distribution of astrocytes and the average frequency of evoked Ca^{2+} oscillations (per second) following different KCl concentrations (from left to right: 30 mM, 15 mM and 5 mM), before (aCSF, black, continuous line) and after bath application of Carbachol (red, continuous line) and Carbachol+TTX (red, dashed line; 30 mM, n=14 recordings; 15 mM, n=15 recordings; 5 mM, n=13 recordings). Data is reported as mean ± S.E.M. Asterisks below the dashed line in (e) represent the significance levels between groups following Tukey's post hoc test (black). Asterisks above the dashed line in (e) represent the level of interaction (red). **p <0.05; **p < 0.01; ***p < 0.0001*

Furthermore, whereas bath application of Carbachol did not affect the spatiotemporal pattern of evoked astrocytic Ca^{2+} oscillations (within the first 100 seconds) at any of the $[K^+]_o$ tested ($p > 0.05$, two-way ANOVA, Figure 4.6 E), the addition of TTX to the bath solution significantly altered the trajectories of Ca^{2+} signals following application of excessive and high $[K^+]_o$ (30 mM, $F_{(2, 250)} = 17.59$, $p < 0.0001$, for the factor "treatment", $F_{(4, 250)} = 28.86$, $p < 0.0001$, for the factor "distance" and $F_{(8, 250)} = 2.14$, $p < 0.05$, for the factor "interaction"; 15 mM, $F_{(2, 260)} = 3.80$ $p < 0.05$, for the factor "treatment", $F_{(4, 260)} = 43.72$, $p < 0.0001$, for the factor "distance" and $F_{(8, 260)} = 4.71$, $p < 0.0001$, for the factor "interaction"; two-way ANOVA, Figure 4.6 E). Post-hoc analysis further revealed that the main difference was in proximal astrocytes located close to "astrocyte Alpha", which displayed significantly reduced frequencies of Ca^{2+} oscillations at $[K^+]_o$ above ceiling levels compared to control conditions (30 mM, 0.12±0.01 events per second at 0 µm, n=14; 15 mM, 0.12±0.01 events per second at 0 µm, n=15; $p < 0.0001$, two-way ANOVA with Tukey's post hoc test), suggesting a non-specific effect of TTX on nearby activated neurons.

Taken together, these results suggest that ACh has no effect on astrocytic K^+ homeostasis, and that the observed changes in Ca^{2+} signalling were likely due to some effect of TTX on astrocytic activity.

4.4 Discussion

To survive animals constantly shift their behavioural states, as occurs during the sleep-wake cycle, which involves global changes in neuronal oscillatory activity and synchronization across different brain areas (e.g. cortex, hippocampus, striatum, thalamus)[511]. Previous studies have demonstrated that neuromodulators, such as DA[512], ACh[513] or NE[514], affect neuronal membrane properties and excitability leading to altered network oscillations at multiple frequencies[515]. For instance, modulation of the cholinergic[516,517,518] or monoaminergic[465,519,520] signalling pathways has been reported to affect neural network oscillatory dynamics underlying behavioural shifts, as happens during different phases of sleep (i.e. REM *vs* NREM) or between sleep and arousal states. However, the neurophysiological processes leading to the transitions between global brain states remain poorly understood.

Neuromodulators effect on network oscillations has been suggested to be mediated via synaptic modulation of different neuronal subtypes equipped with long-range projections[463,515,521]. However, glial cells (i.e. astrocytes, oligodendrocytes, microglia), once assumed to be merely supporting cells, also express receptors for most neuromodulators[522,523,524], and therefore can mediate neuromodulatory processes affecting network oscillations. In line with this view, previous reports showed that impairments of the neuromodulatory pathways in astrocytes, induced by selective overexpression of transgenes *in vivo*, either affected the IP_3-mediated $[Ca^{2+}]_i$ increase from internal stores[58] or the subsequent Ca^{2+}-dependent vesicular release of gliotransmitters[71], modulate network oscillations at different frequencies depending on the behavioural state. Particularly, Foley *et al.* (2017)[58] observed that mice with attenuated IP_3-mediated Ca^{2+} signalling in astrocytes spent more time in REM sleep displaying enhanced theta oscillations compared to wild-type mice, which the authors attributed to cholinergic signalling in the hippocampus.

In awake mice, Lee *et al.* (2014)[71] found that inhibition of glutamate release in astrocytes resulted in decreased EEG gamma power (25-40 Hz) and cognitive deficits (i.e. recognition memory), suggesting that recruitment of astrocytes and the consequent release of glutamate from these cells is required for the maintenance of cortical gamma oscillations.

Nonetheless, we are still lacking evidence regarding the role each neuromodulator plays during each behavioural state, specifically in terms of the signalling pathways, receptors and target cells (i.e. neurons and glial cells) that become activated across different brain areas.

In the CNS, K^+ homeostasis is controlled by astrocytic K^+ clearance mechanisms, including net K^+ uptake and K^+ spatial buffering to distal areas through GJs[408]. During physiological neuronal activity, the rate of K^+ clearance can be affected by different factors, such as changes in temperature[525], waste products (i.e. ammonia)[526], extracellular levels of glutamate[450] or pH[527], which influence neuronal excitability[527], as well as the functionality of the astrocytic machinery[450,525,526,528]. Recently, Ding *et al.* (2016)[142] showed that application of a cocktail of neuromodulators to cortical brain slices, containing ACh, Histamine, NE, DA and Orexin, results in altered $[K^+]_o$ dynamics without involving the activity of neurons. Consequently, it is becoming increasingly evident that some neuromodulators can act in parallel on both neurons and astrocytes to fine-tune behavioural output, as previously suggested[142]. Accordingly, we hypothesized that different neuromodulators can modulate $[K^+]_o$ clearance by selectively activating different signalling pathways either directly (via astrocytes) or indirectly (via neurons) to adjust $[K^+]_o$ levels, as a tool to ultimately mediate the transitions between network oscillations associated with different brain states.

To validate this hypothesis, I have measured the K^+ clearance rate following local application of KCl at different concentrations in the presence of the neuromodulators 5-HT, DA, NE, Histamine and ACh (Carbachol). Results suggest that not all neuromodulators affect $[K^+]_o$ clearance to the same extent.

Among astrocytic K^+ clearance mechanisms, net K^+ uptake becomes activated following low local increases in $[K^+]_o$ (~3-12 mM), mostly affecting small astrocytic networks located within close proximity to the synaptic release site, and becomes saturated at $[K^+]_o$ above ceiling levels (>12 mM)[421,529]. In contrast, the K^+ spatial buffering process via GJ-mediated astrocytic networks is active when there is high accumulation of $[K^+]_o$[408] (above ceiling levels), reviewed by[305]. In that regard, neuromodulators that affect the clearance rate of low $[K^+]_o$ (~5 mM) independent of neuronal activity are likely to play a role in the modulation of astrocytic net K^+ uptake mechanisms, mediated via the NKA pump and $K_{ir}4.1$ channels[452,498,530], whereas neuromodulators that affect the clearance rate of high and excessive $[K^+]_o$ (15 mM and 30 mM respectively) are more prone to regulate the K^+ spatial buffering process through GJs[531,532].

Interestingly, previous studies suggested a correlation between astrocytic Ca^{2+} oscillations and $[K^+]_o$ clearance[51]. However, the exact molecular mechanisms instigating this association still need to be established. For this purpose, I have assessed the astrocytic Ca^{2+} signalling in the presence of the above-mentioned neuromodulators by selectively co-labelling astrocytes with the fluorescent dyes Fluo-4 AM and SR101. Astrocytic Ca^{2+} oscillations were classified as spontaneous, when occurring prior to stimulation with KCl puff (during the first 2 minutes), or evoked, if recorded within 10 seconds following local application of different KCl concentrations (5 mM, 15 mM and 30 mM).

While spontaneous Ca^{2+} oscillations provide information about intrinsic astrocytic function regardless of K^+ clearance mechanisms and neuronal input[371], changes in evoked Ca^{2+} activity, which is correlated with an increase in $[K^+]_o$ levels, provide a link between the K^+ clearance process and astrocytic Ca^{2+} signalling, as previously suggested[51].

4.4.1 The impact of 5-HT on astrocytic K^+ clearance and Ca^{2+} signalling

In the above-mentioned experiments, bath application of 5-HT decreased the K^+ clearance rate at excessive $[K^+]_o$ regardless of synaptic activity (Figure 4.2 A-B), suggesting that 5-HT directly modulates astrocytic K^+ spatial buffering via GJs. Consistently, 5-HT affected evoked Ca^{2+} oscillations in cortical astrocytes by increasing the average percentage of evoked astrocytes, as well as the average frequency of evoked Ca^{2+} responses only following local application of 30 mM KCl. In contrast, lower $[K^+]_o$, namely 15 mM and 5 mM, had no significant impact on the evoked Ca^{2+} activity (Figure 4.2 C-D). However, while the observed serotonergic effect on evoked Ca^{2+} signals at excessive $[K^+]_o$ was abolished after TTX application, the impact of 5-HT on the K^+ clearance rate was independent of neuronal activity. Consequently, I propose that under excessive $[K^+]_o$ regimes, 5-HT differentially activates both neuronal and astrocytic receptors to impact indirectly on astrocytic Ca^{2+} signalling and directly on K^+ spatial buffering, respectively. Moreover, the lack of impact on both the K^+ clearance rate and Ca^{2+} signalling at lower $[K^+]_o$ (Figure 4.2 B-D) suggests that 5-HT is not affecting the net K^+ uptake mechanism.

Accordingly, previous studies showed that 5-HT hyperpolarizes astrocytic membranes[378], which influences the K^+ spatial buffering process[348]. In particular, application of the Selective Serotonin Reuptake Inhibitor (SSRI) fluoxetine found to increase $[Ca^{2+}]_i$ and trigger the phosphorylation of the $ERK_{1/2}$ pathway[533], leading to inhibition of both $K_{ir}4.1$ in astrocytes[534] and Cx43-mediated GJ

coupling[535], which reduces Ca^{2+} waves propagation[378], thus providing a plausible explanation to the observed decrease in the K^+ clearance rate (Figure 4.2 A-B).

4.4.2 The impact of DA on astrocytic K^+ clearance and Ca^{2+} signalling

Among all the neuromodulators tested (i.e. 5-HT, DA, NE, Histamine, ACh), only DA significantly decreased the K^+ clearance rate at all $[K^+]_o$ tested (5 mM, 15 mM and 30 mM), independent of neuronal activity (Figure 4.3 A-B). Moreover, DA enhanced the evoked Ca^{2+} activity in astrocytes, by increasing the average percentage of evoked astrocytes, as well as the average frequency of evoked Ca^{2+} events following local application of 30 mM, 15 mM and 5 mM KCl. However, these results suggest that while the dopaminergic impact on the frequency of astrocytic Ca^{2+} signals involved indirect neuronal input at $[K^+]_o$ above ceiling levels (>12 mM), it directly affected astrocytic Ca^{2+} activity at low (5 mM) $[K^+]_o$, as it persisted after TTX application (Figure 4.3 C-D).

These data support previous reports indicating that DA blocks $K_{ir}4.1$ and $K_{ir}4.1/K_{ir}5.1$ heteromeric channels, and reduces aquaporin 4 (AQP-4) channel permeability via stimulation of D_2-like receptors, leading to Ca^{2+} release from internal stores and subsequent PKC activation[536,537]. Whereas K_{ir} channels take part during both net K^+ uptake (at low $[K^+]_o$) and K^+ spatial buffering processes (at high and excessive $[K^+]_o$ levels), AQP-4 channels only participate in the net K^+ uptake process (Appendix Table 3). Together, these data suggest that: *i)* DA directly affects multiple stages in astrocytic K^+ clearance mechanisms, including net K^+ uptake and K^+ spatial buffering; *ii*) DA directly activates astrocytic Ca^{2+} signalling at different $[K^+]_o$, resulting in the activation of larger astrocytic networks (Figure 4.3 C), but leads to a decrease of K^+ spatial buffering and overall decrease of the K^+ clearance rate, likely mediated via inhibition of the first

step required for this process (i.e. entrance of K^+ ions through $K_{ir}4.1$ channels)[536] (Figure 4.3 A-B); and *iii*) DA affects the temporal pattern of astrocytic Ca^{2+} signalling both directly (at physiological $[K^+]_o$) and indirectly (at high $[K^+]_o$) via the activity of neurons (Figure 4.3 C-D).

4.4.3 The impact of NE on astrocytic K^+ clearance and Ca^{2+} signalling

NE has been previously associated with modulation of astrocytic housekeeping roles, specifically enhancement of glutamate uptake via α_1-adrenergic receptors and increased glycogenesis mediated by β_1-adrenergic receptors[514] (Figure 1.2). Indeed, bath application of NE reduced the K^+ clearance rate following local application of high (15 mM) and excessive (30 mM) $[K^+]_o$ independent of synaptic activity (Figure 4.4 A-B), suggesting that NE directly modulates the K^+ spatial buffering process. Moreover, NE directly affected astrocytic Ca^{2+} activity depending on $[K^+]_o$, as evident from the increase in the average percentage of evoked astrocytes and their increased frequency of Ca^{2+} elevations following application of 30 mM KCl (Figure 4.4 C-E). In addition, NE decreased the average frequency of spontaneous Ca^{2+} signals (Figure 4.4 D) without affecting the average percentage of spontaneously active astrocytes (Figure 4.4 C), suggesting that NE can affect intrinsic Ca^{2+} activity regardless of $[K^+]_o$.

One plausible interpretation of these results is that NE has a direct yet complex effect on astrocytic $[Ca^{2+}]_i$ oscillations, in which at one level it decreases spontaneous Ca^{2+} activity regardless of $[K^+]_o$, thereby affecting glutamate uptake, and on another level it affects GJ-mediated communication required for the K^+ spatial buffering process via increase of $[Ca^{2+}]_i$ oscillations evoked by excessive $[K^+]_o$ accumulation. At lower (5 mM) $[K^+]_o$, NE had no significant impact on the evoked Ca^{2+} activity (Figure 4.4 C-E) nor on the K^+ clearance rate (Figure 4.4 B), which is in contrast to previous reports indicating that stimulation of β_1-adrenergic receptors enhance NKA pump[514] and

NKCC1 cotransporter[538] activities, thereby promoting astrocytic net K^+ uptake following small increases in $[K^+]_o$. However, NE may downregulate NKA pump activity at high or excessive $[K^+]_o$, as previously oberserved[498], which might explain why bath application of NE at ≥15 mM led to decreased K^+ clearance rates (Figure 4.4 B).

4.4.4 The impact of Histamine on astrocytic K^+ clearance and Ca^{2+} signalling

Bath application of Histamine resulted in reduced K^+ clearance rates at all $[K^+]_o$ tested (5-30 mM; Figure 4.5 A-B). However, while this effect was highly dependent on neuronal activity following application of low and high $[K^+]_o$, it was independent at excessive $[K^+]_o$, suggesting that Histamine directly modulates the astrocytic K^+ spatial buffering process. Regarding astrocytic Ca^{2+} activity, Histamine had no effect on spontaneous Ca^{2+} signalling (Figure 4.5 C-D), indicating that Histamine does not affect intrinsic Ca^{2+} activity in astrocytes. Despite increasing the average percentage of evoked astrocytes, as well as the average frequency of evoked Ca^{2+} oscillations for all $[K^+]_o$, this effect was driven by neurons only at excessive (30 mM) $[K^+]_o$, as it returned to normal levels after TTX application (Figure 4.5 C-D). Moreover, Histamine affected the spatiotemporal pattern of astrocytic Ca^{2+} signalling, which was $[K^+]_o$-dependent (Figure 4.5 E). According to these results, Histamine likely modulates the redistribution of K^+ ions to distal astrocytes (K^+ spatial buffering) up to ~100 μm and ~150 μm at high (15 mM) and excessive (30 mM) $[K^+]_o$ respectively, through activation of both neuronal and astrocytic receptors, whereas it might influence smaller networks composed of proximal astrocytes required during the net K^+ uptake process when there is low (5 mM) $[K^+]_o$ levels, specifically via astrocytic intermediaries.

Together, these results suggest that Histamine impacts on astrocytic K^+ clearance mechanisms via differential activation of both neuronal and astrocytic receptors.

Indeed, previous studies showed that activation of H_1 receptors in astrocytes triggers PKC, which in turn phosphorylates and blocks K_{ir} channels[539] involved in K^+ clearance mechanisms (Appendix Table 3). Furthermore, Histamine has been reported to reduce the expression levels of AQP-4 channels, thus playing a role in the net K^+ uptake process[540]. However, our results indicate that the impact of Histamine on the net K^+ uptake mechanism (<12 mM) was mediated indirectly by neurons (Figure 4.5 B), yet the evoked Ca^{2+} activity was not driven by neurons (Figure 4.5 C-D) and could be mediated via modulation of astrocytic voltage-gated Ca^{2+} channels (VGCCs)[541].

4.4.5 The impact of ACh on astrocytic K^+ clearance and Ca^{2+} signalling

Unlike other neuromodulators (i.e. 5-HT, DA, NE, Histamine), bath application of high concentrations of the cholinergic agonist Carbachol (100 μM) resulted in no significant alterations in the K^+ clearance rate for any of the $[K^+]_o$ tested (Figure 4.6 A-B). In line with these results, application of Carbachol had no significant effect on either the percentage nor the frequency of spontaneous or evoked Ca^{2+} elevations in cortical astrocytes (Figure 4.6 C-E), which suggests that ACh does not affect astrocytic K^+ clearance mechanisms. However, co-application of Carbachol and TTX led to an increase in the number of spontaneously active astrocytes and in the average frequency of spontaneous Ca^{2+} elevations, suggesting that neuronal activity under cholinergic influence suppresses spontaneous or intrinsic astrocytic Ca^{2+} signalling. Moreover, TTX led to a reduction of the average percentage of evoked astrocytes and affected the frequency of evoked Ca^{2+} signals in proximal astrocytes at excessive $[K^+]_o$ (30 mM; Figure 4.6 C-E), implying that the modulation of the neuronal activity by ACh is involved in astrocytic function at these $[K^+]_o$.

Accordingly, previous studies showed an indirect modulation of ACh on astrocytes by inducing depolarization of the astrocytic membrane via neuronal release of glutamate, which likely

enhances the spontaneous $[Ca^{2+}]_i$ activity both *in vitro*[338] and *in situ*[542,481]. Together, these results suggest that ACh is not involved in the modulation of astrocytic K^+ clearance mechanisms at any of the $[K^+]_o$ tested.

Overall, this chapter sheds light on the nature of the association between astrocytic Ca^{2+} signalling and K^+ homeostasis at different $[K^+]_o$ levels. Moreover, I provide evidence regarding the direct and indirect pathways in which neuromodulators affect astrocytic function within cortical networks, including the K^+ clearance rate and Ca^{2+} signalling. A key finding was that only some neuromodulators from the cocktail used by Ding *et al.* (2016)[142], namely 5-HT, NE, DA and Histamine, can affect astrocytic K^+ clearance mechanisms independent of neuronal activity, as application of TTX had no significant impact on the K^+ clearance time course. On the other hand, ACh may modulate network oscillations, as we and others previously reported[409] (Chapter 2), via direct activation of neuronal networks and not through modulation of astrocytic K^+ clearance mechanisms.

Since neuromodulators play a crucial role during different behaviours[463,464,514], the obtained results suggest that they exert their function by affecting both neurons and astrocytes via parallel pathways. Although the link between Ca^{2+} signalling and K^+ homeostasis is not well understood, the data presented in this thesis support the intriguing concept that astrocytes, by selectively modulating their K^+ clearance capacity in response to activation by different neuromodulators, have the potential to affect the excitability and oscillatory properties of individual neurons as a mechanism to recruit them into synchronized networks[305].

CHAPTER 5:

GENERAL DISCUSSION

"There exists a microscopic breed of brain beetle, commonly known as an 'idea'.
An idea desires only one thing: To catch the perfect brain wave."
—*Leah Broadby*

The need to understand how neuronal oscillations are formed and manipulated has increased substantially in importance in recent decades, as it has become more apparent that they are correlated with different behavioural states and altered in various brain diseases (e.g. epilepsy, PD; Chapter 1)[305,463]. However, the cellular and synaptic mechanisms involved in each network oscillation are not well understood.

In this thesis, I have investigated the potential role of cortical astrocytes in modulating neuronal network oscillations using K^+ clearance mechanisms. The overarching hypothesis was that astrocytes can act as "network managers" that modulate their K^+ clearance capabilities to regulate the excitability and synchronization of individual neurons into neuronal ensembles, thus mediating the **transitions** between network oscillations at different frequencies. To confirm this hypothesis, I have used several techniques, including electrophysiological recordings from both individual and networks of neurons, as well as $[K^+]_o$ measurements with K^+-selective microelectrodes along with Ca^{2+} and K^+ imaging, under different pharmacological manipulation.

The results in **Chapter 2** show that impairments in astrocytic K^+ clearance mechanisms lead to an increased excitability and a shift of the resonance frequency of individual neurons towards higher frequencies, underpinning the formation of high frequency network oscillations, particularly within the beta and gamma range. These results strongly suggest that astrocytes are capable of modulating both neuronal excitability and network oscillations by specifically manipulating $[K^+]_o$ levels. To further explore the bidirectional neuronal-astrocytic signalling pathways that govern the astrocytic K^+ clearance process, I measured the spatiotemporal dynamics of $[K^+]_o$ and $[K^+]_i$ in astrocytes using a combination of K^+-selective microelectrodes with fluorescent imaging of K^+ and Ca^{2+} probes. The results in **Chapter 3** indeed suggest that a high increase of $[K^+]_o$ is correlated with activation of larger astrocytic networks. Moreover, inhibition of different stages of the astrocytic K^+ clearance mechanisms results in distinctive spatiotemporal dynamics of both $[K^+]_o$ and $[K^+]_i$. **Chapter 4** provides conclusive evidence that different neuromodulators can directly affect astrocytes to modulate the K^+ clearance process, using a differential regulation of both neuronal and astrocytic receptors that result in alterations of the K^+ clearance rate and astrocytic Ca^{2+} signalling.

Overall, the findings gathered in this thesis support the view that astrocytes work in parallel with neurons and mediate their recruitment into neuronal ensembles that work in synchronization at multiple frequencies, thereby becoming the perfect candidates to gear the **transition** between behavioural states associated with those frequencies.

5.1 Astrocytic modulation of neuronal network oscillations

Behavioural states require temporal coordination of neuronal activity to integrate information in multiple brain areas (e.g. hippocampus, cortex, thalamus)[543,544,545].

This network coherence is efficiently achieved through the synchronous activity of network oscillations fluctuating at different frequencies[108,546], which is important for many physiological functions (e.g. attention, memory consolidation, sleep)[547,548,549], as shown in Table 1.1 (Chapter 1). Several mechanisms are known to be involved in the generation of neuronal oscillations in different brain areas (e.g. cellular excitability, dendritic structure, extracellular ions)[2,11], however the precise process that mediates the transition between the different oscillatory frequencies is unknown.

Despite being described at the same time as neurons in the 19th century[209], glial cells received very little attention, mainly due to a conceptual fixation about their role as non-excitable cells that only provide trophic and structural support to neurons[219,220]. Hence, during the past century, most studies focused on changes in the activity of neurons as the main effectors on brain waves[47,55,59,66,69,550,551]. Later advances in the field (e.g. electron microscopy, intracellular recordings)[369], facilitated the study of glial cells, including astrocytes, elucidating their crucial involvement in a variety of structural, metabolic and homeostatic roles in both health and disease[305].

Notably, the advent of Ca^{2+} imaging techniques allowed the discovery of bidirectional communication pathways between neurons and astrocytes at the synaptic level, as astrocytes were able to communicate with neurons with increases in $[Ca^{2+}]_i$ in response to neuronally-released neurotransmitters[552], leading to the well-established concept of tripartite synapses[244]. Since then, many research groups studied the versatility of astrocytic Ca^{2+} signalling during synaptic plasticity and transmission associated with different behavioural states (e.g. learning, memory), especially in the hippocampus[553,554,555], and to a lesser extent in the cortex[556,557].

In this study, I have investigated the interactions between neurons and astrocytes at the cellular level, which underlie the generation of cortical network oscillations and their behavioural correlates. The results from Chapter 4 show that there is a correlation between Ca^{2+} signalling and $[K^+]_o$ that depends on the distance at which astrocytes are located within the network. Accordingly, under normal aCSF conditions proximal astrocytes typically display higher frequencies of Ca^{2+} oscillations, compared to distal astrocytes at $[K^+]_o$ above ceiling levels (>12 mM), which facilitates the flow of K^+ ions via GJs to distal areas (K^+ spatial buffering)[450]. In contrast, the average frequencies of evoked Ca^{2+} oscillations are comparable between proximal and distal astrocytes following application of low (5 mM) $[K^+]_o$ levels, likely attributed to the fast activity of the NKA pump during net K^+ uptake mechanisms[452,498] (Figure 4.4 E).

Notably, I found that some neuromodulators can modulate astrocytic K^+ clearance mechanisms by altering the spatiotemporal pattern of Ca^{2+} oscillations either directly (via astrocytes) or indirectly (via neurons), and this modulation is $[K^+]_o$-dependent. Indeed, 5-HT and NE only affected astrocytic Ca^{2+} signalling at excessive (30 mM) $[K^+]_o$, however whereas the serotonergic effect was driven by neurons, NE directly affected astrocytic function through activation of astrocytic receptors. Moreover, DA, Histamine and ACh (Carbachol) exerted a differential regulation of neuronal and astrocytic receptors depending on $[K^+]_o$. At excessive (30 mM) $[K^+]_o$, the impact of DA, Histamine and ACh on evoked Ca^{2+} activity was highly dependent on neuronal activity, while both monoamines acted specifically via astrocytes when the levels of $[K^+]_o$ decreased.

Together these results suggest complex interactions between neurons and astrocytes through the release of different neuromodulators that allow the tight control of K^+ homeostasis within cortical networks.

5.1.1 The role of astrocytes as network managers of behavioural states

To maintain synchronization, the oscillatory properties of all neuronal membranes within a network should resonate over the same range of frequencies. This suggests that a single neuron's resonance frequency could be modulated to adapt to the activity of the neuronal network[558]. During the past years, several studies focused on investigating the role of astrocytic Ca^{2+} signalling as the underlying mechanism affecting neuronal intrinsic properties, synaptic transmission and network oscillations[472,473,556,559]. However, we and others have shown that changes in $[K^+]_o$ can also affect the excitability properties of neurons leading to altered neuronal oscillations at multiple frequencies[409] (Chapter 2).

5.1.1.1 The impact of K^+ clearance mechanisms on neuronal network oscillations

Astrocytes are key players in maintaining K^+ homeostasis in the CNS, which suggests that they have the potential to modulate intrinsic neuronal properties (i.e. resonance frequency) and as a result neuronal network oscillations by adjusting the levels of $[K^+]_o$. Interestingly, Wang *et al.* (2012)[304] suggested that the Ca^{2+}-dependent activation of the NKA pump to enhance $[K^+]_o$ uptake by astrocytes is a powerful tool that allows astrocytes to maintain homeostasis and further modulate synaptic transmission at the network level. In this study, I have extended Wang's hypothesis[304] postulating that modulation of astrocytic K^+ clearance mechanisms, specifically net K^+ uptake via $K_{ir}4.1$ channels and K^+ redistribution to distal areas through GJ-mediated networks (K^+ spatial buffering process), engages the transition between network oscillatory frequencies by affecting the neuron's RMP and their resonance frequency, which displays voltage- and K^+ current-dependence[560,561]. Results in Chapter 2 provide the first evidence that modulation of K^+ clearance mechanisms in cortical astrocytes impacts on the **resonance frequency** of individual neurons by extending the frequency range at which the soma and dendrites resonate.

The amplification of the oscillations magnitude at the frequencies involved in this oscillatory behaviour suggests that impairments of the K^+ clearance mechanisms have the potential to affect the synchronization of both local and distal neuronal populations, via net K^+ uptake and K^+ spatial buffering processes, respectively. In fact, the observed alterations at the cellular level correlated with changes in the **network activity** following blockade of astrocytic $K_{ir}4.1$ channels or reduced connectivity with GJ blockers. A key finding was the differential increase in oscillation power, which mainly affects high-frequency oscillations (>12 Hz; Chapter 2)[409], suggesting that astrocytes can modulate behavioural states occurring at these frequencies (e.g. attention, conscious perception; Table 1.1, Chapter 1).

Dye-coupling experiments showed that high $[K^+]_o$ enhances astrocytic GJ-mediated connectivity (Supplementary Figure S4, Chapter 2)[409], suggesting that an increase in $[K^+]_o$ leads to the recruitment of more astrocytes in order to facilitate the distribution of K^+ ions via K^+ spatial buffering[450]. These results, together with the observed reduced astrocytic connectivity after GJ blockade, indicate that astrocytic networks are plastic, and further support the hypothesis that K^+ facilitates its own buffering to restore brain homeostasis according to network activity[450]. This flexible configuration has been reported to endow GJ-connected astrocytes with the power to modulate not only synaptic activity within their spatial domain but potentially to affect the underlying synchronization of neuronal networks located at distal brain areas[409,559]. In that regard, a previous study suggested a role for increased $[K^+]_o$ and GJs in mediating fast network oscillations, as transient application of solutions containing K^+ evoked hippocampal oscillations within 30-80 Hz that were accompanied by increases in $[K^+]_o$, whereas application of GJ blockers reduced the gamma power[72].

Other groups showed that electrical coupling also influences membrane resonance leading to neuronal synchronization in response to oscillatory inputs to ultimately shape the network oscillation frequency involved in different brain states[562,563]. Moreover, Moca *et al*. (2014)[564] demonstrated that membrane resonance favours synchronization, while promoting the stability of high-frequency gamma oscillations in the visual cortex, and synchronous Ca^{2+} waves have been successfully imaged from extensive GJ-coupled astrocytic networks *in vivo* in response to changes in coordinated neuronal activity[565]. Together these studies suggest that astrocytes are capable of modulating neuronal network oscillations, as well as other physiological processes occurring over widespread brain regions (e.g. cerebral blood flow). Notably, these reports further support the observation that impairments in astrocytic K^+ clearance mechanisms resulting in excessive $[K^+]_o$ levels likely affect membrane resonance properties of individual cortical neurons leading to the amplification of fast hypersynchronous oscillatory activities within the beta and gamma range at the network level.

Recently, LaBerge and Kasevich (2017)[566] proposed that the dendritic structure also influences network oscillations, as computational models of cortical circuits showed that apical dendrites from pyramidal neurons in the cortex can produce oscillations within specific frequency ranges. This oscillatory behaviour allows them to coordinate the timing of spike signals from other connected neurons and engage them to oscillate within the same range of frequencies in order to efficiently process information. In addition, distinct subcellular compartments have been reported to differ in their resonant frequency properties[414], which is consistent with results from Chapter 2 showing that local application of high $[K^+]_o$ on apical dendrites is sufficient to increase both the resonance frequency and I_h currents (Figure 2.5).

These observations further support the hypothesis that alterations in the astrocytic K^+ clearance process can provide the underlaying mechanism needed for the transition in neuronal oscillatory behaviour (Figure 2.6). Accordingly, the dendritic compartmentalization of the resonance frequency may facilitate or favour the integration of signals propagating through it, hence actively affecting the neural code and contributing to the overall network output.

Because astrocytic networks have been previously shown to differ between different areas in the hippocampus[531], I performed additional experiments in two cortical areas, including the primary motor (M1) and somatosensory (S1) cortices. Connectivity experiments showed that astrocytes in M1 form smaller networks, composed of either directly or indirectly connected astrocytes loaded with biocytin for 12 or 30 minutes, respectively (Appendix Figure 3, Appendix Table 4). In addition, astrocytic networks from M1 also displayed different topology and increased R_{in} values compared to astrocytes located in S1 (Appendix Figure 3, Appendix Table 4).

Consistent with these results, Houades *et al.* (2008)[567] previously showed that astrocytic networks within the same cortical layer IV in S1 were shaped differently depending on their location inside or outside the barrel field. The different astrocytic topology between cortical areas is likely due to the fact that astrocytes can serve different functions, in particular by affecting the propagation of Ca^{2+} waves[374]. Indeed, cortical astrocytes show different Ca^{2+} activity (asynchronous *vs* synchronous) between layer I and layers II/III within S1[373]. Hence, the data presented support the view that the morphological and functional segregation of astrocytic networks could lead to differential regulation of local neuronal networks within a defined brain structure by coordinated subpopulations of astrocytes with distinct coupling properties, based on neuronal network orientation and activity demands, as previously suggested[567,568].

Together, these data suggest that modulation of the different phases of the astrocytic K^+ clearance process, either at the uptake level or spatial buffering through the astrocytic network, can serve as a tool used by astrocytes to modulate multiple behavioural states.

5.1.1.2 The impact of neuromodulators on K^+ clearance mechanisms

To elucidate the physiological effectors of astrocytic K^+ clearance mechanisms during different behaviours, I have investigated the influence of neuromodulators known to act on both neurons and astrocytes, including ACh[338,339,569,570], 5-HT[340], Histamine[341,467] , NE[342,343,468,469] and DA[344,470] (Figure 1.2). Notably, synaptic release of neuromodulators (e.g. NE, Histamine, ACh, DA) and subsequent gliotransmission by astrocytes have been found to mediate behavioural states (e.g. arousal), by altering membrane and excitability properties, as well as intracellular signalling pathways in both neurons and glial cells[142,483]. In addition, previous reports showed that neuromodulators can fine-tune I_h conductances underlying membrane resonance of individual neurons in the entorhinal cortex (i.e. ACh[571] and 5-HT[572] in layer II, DA in layer V[573]), as well as in the hippocampus (i.e. NE[574]), thus likely affecting the oscillatory behaviour of single neurons and network oscillations in different brain areas[575]. However, whether this was a direct effect of the neuromodulators on neuronal activity, or indirect via astrocytic modulation was never tested.

Results in Chapter 3 show that alterations in astrocytic mechanisms to clear $[K^+]_o$ at different stages lead to a decrease in the **K^+ clearance rate** (Figure 3.3). Similar to the effect of selective blockade of $K_{ir}4.1$ and GJ with $BaCl_2$ or Cx43 mimetic peptides respectively, application of different **neuromodulators** revealed that they can modulate astrocytic K^+ clearance mechanisms by affecting the K^+ clearance rate via differential regulation of neuronal and astrocytic receptors (Chapter 4).

These results, together with the observed impact of altered K^+ clearance on single neurons and network oscillations (Chapter 2), suggest that neuromodulators could affect the K^+ clearance rate by either acting directly on astrocytes, or indirectly via neuronal intermediaries to ultimately modulate the synchronization of neuronal network oscillations and their behavioural correlates. However, each neuromodulator exerts its effect differently on the astrocytic K^+ clearance process.

The cholinergic system

ACh is known to affect several brain waves within different frequencies that underlie a wide variety of behavioural states (Table 1.1, see also Chapter 1)[463,576]. These include slow oscillations (alpha and theta range) involved in working memory[97], which typically couple with faster oscillations to facilitate synchronization among neuronal ensembles across brain regions during attentional[577] and episodic memory[578] tasks. Indeed, activation of muscarinic ACh receptors modulates rapid synchronization of gamma oscillations, as well as long-term modifications of network dynamics in the cortex[579]. More recently, a modelling study showed that low levels of ACh correlated with slow oscillations during NREM sleep, whereas higher concentrations of ACh were associated with fast and asynchronous oscillations predominant in awake states[580], suggesting a dose-dependent influence of ACh on information processing within neuronal circuits that results in a wide spectrum of network oscillations. Regarding the role of ACh at the single-cell level, astrocytic Ca^{2+} transients released from internal stores following activation of muscarinic ACh receptors have been shown to modulate cortical oscillations in the theta range and REM sleep[58]. In the hippocampus, ACh has been reported to affect both neurons and astrocytes. While ACh led to excitation of hilar interneurons and thus slow GABAergic inhibition of dentate granule cells[581], it also activated astrocytic α7nAChR leading to fast $[Ca^{2+}]_i$ elevations and subsequent release of glutamate or D-serine, depending on the network state (wakefulness *vs* sleep, respectively)[508].

Intriguingly, disruption of glutamate release in astrocytes reduced the power of Carbachol-induced gamma oscillations involved in active cognitive functions (i.e. recognition memory)[71], suggesting that astrocytic-mediated gliotransmission is required for the maintenance of gamma rhythms, once thought to be exclusively dependent on neuronal activity[582,583,584].

In our experiments, bath application of Carbachol increased the power of oscillations across a wide spectrum of frequencies at the network level following local application of excessive $[K^+]_o$ (30 mM; Chapter 2)[409]. However, Carbachol had no significant impact on the K^+ clearance rate or the frequency and number of astrocytes eliciting $[Ca^{2+}]_i$ elevations following local application of various $[K^+]_o$ (Figure 4.6). These results suggest that, in the somatosensory cortex, ACh is not directly involved in modulating astrocytic K^+ clearance mechanisms, and therefore may affect network oscillations via neuronal pathways, as discussed above.

The monoaminergic system

Monoamines, including catecholamines (i.e. NE, DA), 5-HT and Histamine are involved in a broad spectrum of physiological functions (e.g. memory, emotion, arousal)[97,585,586], as well as in psychiatric and neurodegenerative disorders (e.g. PD, AD, schizophrenia, depression)[587,588,589,590]. Among monoamines, DA appears to be one of the oldest neurotransmitters found in early metazoans[591] and has long been known to influence cognitive function in health and disease[592,593]. Previous studies reported on a modulatory role of DA on both beta[594] and gamma[595] oscillations, as well as on phase-amplitude coupling between delta and gamma rhytms[596]. Interestingly, a recent study proposed the concept of "neuromodulatory band", comprising high-frequency oscillations within 19-38 Hz in the visual cortex that accurately correlated with DA levels during spontaneous neuronal activity, thereby establishing a direct link between alterations in this band with changes in the network state driven by DA[597].

However, studies performed under pathological conditions revealed that denervation of DA neurons in parkinsonian patients and animal models leads to excessive synchronization of beta oscillations that correlates with motor impairments[587,598,599]. Such controversies regarding the dopaminergic modulation of beta oscillations might rely on the distinction between physiology and pathology. In this sense, it has been postulated that chronic, but not acute DA depletion underlies exacerbated beta oscillations in PD mice models[600], suggesting that finding the right balance between DA levels is key for normal brain function. Furthermore, the disease state may trigger reactive cells and processes over large brain areas, thus affecting the excitation-to-inhibition activity, while the continuous absence of DA innervation may impinge physiological signalling cascades, likely involving other neuromodulators (i.e. NE, 5-HT)[601], therefore resulting in abnormal network oscillations. Accordingly, DA also acts through β-adrenergic receptors in the cortex leading to an increase in brain-derived neurotrophic factor (BDNF) levels[602] and possibly phosphorylation of AQP-4 via activation of PKC[537], whereas other studies found that D_2-like receptors colocalize with α7nACh receptors in both perisynaptic and perivascular astrocytic processes[603].

In that regard, our results from Chapter 3 indicate that focal photolysis of caged DA compounds decreased the K^+ clearance rate (Figure 4.3 A-B) independent of the activity of neurons and increased both the number of evoked astrocytes and the average frequency of evoked Ca^{2+} oscillations (Figures 4.3 C-D) following local application of various $[K^+]_o$ (5-30 mM). It is suggested that the observed decrease in the K^+ clearance rate is likely mediated via direct activation of astrocytic D_2-like receptors leading to Ca^{2+} release from internal stores and fast Ca^{2+} oscillations[595], which could potentially affect the K^+ clearance machinery by directly decreasing the open probability of K_{ir}4.1/5.1 channels and therefore their currents, as shown *in vitro*[536], and

thus enhance the network oscillatory activity especially in the beta and gamma range, as previously observed in cortical brain slices[409] (Chapter 2).

In the CNS, the serotonergic system consists of axonal projections originating from the raphe nuclei to almost every brain structure. 5-HT has been found to participate in cortical development[604] and in different behavioural states, including mood[605], impulse control[606], attention[607], motor functions[608] and cognition[609]. In the cortex, 5-HT has been reported to modulate slow oscillations (< 2 Hz) through 5-HT_{2A} receptors by promoting the initiation of Up states, as well as gamma rhythms by exerting opposite actions on 5-HT_{1A} and 5-HT_{2A} receptors of fast-spiking interneurons[610]. However, unlike other extensively studied neuromodulators, there is sparse evidence regarding the role of other types of 5-HT receptors and their expression by neurons and other non-neuronal cells.

Interestingly, cortical astrocytes also express 5-HT_2 receptors, whose activation drives IP_3-mediated Ca^{2+} signalling[611] together with inward K^+ currents[612]. Previous studies performed in cell cultures showed that high levels of 5-HT likely impact on astrocytic Ca^{2+} signals, by increasing the velocity and decreasing the propagation distance in the hippocampus[378], as well as on the K^+ clearance process, via inhibition of either $K_{ir}4.1$ channel currents[534], or Cx43-mediated GJs from cortical and striatal astrocytes[535]. This is consistent with the results from Chapter 4 showing that 5-HT reduces the K^+ clearance rate (Figure 4.2 A-B) and increases both the number of evoked astrocytes and the average frequency of evoked Ca^{2+} responses (Figure 4.2 C-D) following 30 mM KCl puffs. In addition, the serotonergic effect on evoked Ca^{2+} activity was neuronal dependent, suggesting that 5-HT works in parallel on both neurons (directly) and astrocytes (indirectly) to modulate network oscillations. As slow and fast oscillations coexist during natural sleep and anaesthesia states[10], I suggest that the serotonergic system plays a role in the modulation of these

brain sates by regulating excessive $[K^+]_o$ levels via astrocytic processes, together with direct activation of neuronal receptors, likely involving interactions with other neuromodulators across brain areas (i.e. DA)[590].

Another catecholamine that could be responsible for influencing network oscillations via K^+ clearance is NE, which is produced in the locus coeruleus that sends broad projections to other brain regions, including the cortex[613]. Intriguingly, the network dynamics in the locus coeruleus and consequently NE signalling have been reported to alternate between tonic and phasic periods, which allow switching between behavioural states, such as arousal, locomotion or focused attention, resulting in enhanced performance to important stimuli[614,615]. Previous reports suggested that NE alters the pattern of network activity by increasing the levels of proteins involved in synaptic plasticity and acquisition of long-term memories (e.g. BDNF)[586] and by mediating synaptic exclusion of Homer1a, required for the remodelling of AMPA receptors during the sleep-wake cycle[616]. Another study further showed that not only NE, but its collective action with other neuromodulators and neurotransmitters, including ACh and GABA, can influence thalamocortical slow oscillations resulting in transitions between vigilance and sleep stages[617], which contributes to both learning and memory consolidation. In addition, NE selectively tunes brain waves comprising theta and gamma frequency bands[618], as well as high-frequency oscillations (~20-80 Hz) that also play a role in memory functions, depending on the type of receptor being activated ($\alpha 1$ *vs* $\beta 1$), in both the hippocampus[619] and the cortex[620].

Other studies previously showed that NE can elicit fast Ca^{2+} transients and waves travelling through GJs that ultimately affect local network dynamics[375] and behaviour (e.g. memory consolidation, locomotion)[621,622], thereby suggesting that the widespread action of NE may serve as a mechanism to engage astrocytic networks across broad regions according to the network state.

In line with this view, previous reports showed that activation of β-adrenergic receptors on cortical astrocytes leads to adenylyl cyclase (AC) and PKA activation, thus resulting in a range of cellular effects (e.g. increased excitability)[623].

Activation of β-adrenergic receptors also promotes opening of VGCCs, which increases $[Ca^{2+}]_i$ in astrocytes[624] and enhances NKA pump activity, thereby suggesting that NE could optimize K^+ clearance at low $[K^+]_o$. However, results from Chapter 4 show that NE reduces the K^+ clearance rate at high and excessive $[K^+]_o$ (>12 mM, Figure 4.4 A-B), while increases the number of evoked astrocytes displaying $[Ca^{2+}]_i$ elevations independent of synaptic activity only following excessive $[K^+]_o$ (30 mM; Figure 4.4 C-D), which correlates with its effect on $[K^+]_o$ removal. As high or excessive $[K^+]_o$ levels have been reported to prevent NKA pump from mediating net K^+ uptake[498], I suggest that, under these conditions, specific activation of β-adrenergic receptors on astrocytes promotes the downregulation of the NKA pump activity and forces an increase in evoked $[Ca^{2+}]_i$ signals seeking astrocytic recruitment into the active network in order to restore $[K^+]_o$ to physiological levels. In turn, this astrocyte-specific modulation of Ca^{2+} activity likely affects the redistribution of $[K^+]_o$ via GJs, and consequently neuronal synchronization and network activity at multiple frequencies leading to switching between different behavioural states.

Histaminergic neurons originate in the tuberomammillary nucleus of the hypothalamus and innervate all brain regions. Histamine activity correlates with wakefulness and arousal, thus taking part in innate states[625]. Moreover, the histaminergic system has been shown to critically modulate learned behaviours and memory, by increasing neuronal excitability and facilitating synaptic transmission in the medial entorhinal cortex[541], which encodes the spatial representations in the brain. In a more recent study, the same group further revealed that Histamine enhances both theta and gamma oscillations leading to successful spatial recognition[626], but not novel object

recognition associated with other neuromodulators (i.e. ACh)[71]. These effects were achieved by differential activation of postsynaptic H_1 and presynaptic H_3 receptors to mediate neuronal depolarization via activation of PKC and inhibition of K_{ir} channels, or inhibition of spontaneous GABA release, respectively.

In our experiments, Histamine decreased the K^+ clearance rate (Figure 4.5 A-B) and increased the evoked Ca^{2+} activity in astrocytes (Figure 4.5 C-E) following all $[K^+]_o$ tested. As astrocytes also express histaminergic receptors[467], I propose that Histamine modulates astrocytic K^+ clearance mechanisms by differentially activating histaminergic receptors depending on $[K^+]_o$. On the one hand, Histamine may modulate net K^+ uptake and evoked Ca^{2+} oscillations following small (5 mM) $[K^+]_o$ elevations by specific activation of astrocytic H_2-receptors. On the other hand, I suggest that Histamine preferentially acts on both neuronal and astrocytic H_1 receptors to affect K^+ spatial buffering at high (15 mM) and excessive (30 mM) $[K^+]_o$, thereby leading to K_{ir} channel blockade and amplification of gamma oscillations.

Altogether these results suggest that neuromodulators act on both neurons and astrocytes in parallel to maximise their impact on synchronous oscillatory activities at different frequencies, making them suitable candidates for modulating network oscillations in the cortex. Moreover, I provide evidence that astrocytic modulation of neuronal activity is based not only on Ca^{2+} signalling, as originally proposed, but also on the regulation of $[K^+]_o$ removal through K^+ clearance mechanisms.

These results reveal another piece of the puzzle, displaying bidirectional communication pathways between neurons and astrocytes, and yield new information about potential mechanisms by which single neurons and astrocytes communicate to engage neurons into specific neuronal networks that are active during different behavioural states.

5.2 Conclusions and future directions

This project sheds light on the cellular effectors of the astrocytic K^+ clearance process in the cortex. Furthermore, the work carried out in this thesis serves as a proof of concept that neurons can impact on astrocytic Ca^{2+} signalling and K^+ clearance mechanisms via release of neuromodulators, especially monoamines, to fine-tune local cellular excitability properties, thus engaging neighbouring neurons into synchronized network oscillations associated with different behaviours.

As many of the medications for the treatment of neurological disorders target neuromodulatory tone[587], bridging the gap between astrocytic function and network oscillatory dynamics is essential to better understand the actual mechanisms of action. Accordingly, alterations in K^+ clearance mechanisms that are associated with deficient neuromodulator signalling pathways may serve as potential therapeutic targets for network disorders characterized by excitation-to-inhibition imbalance and abnormal synchronization, such as epilepsy, ALS or PD[305,627]. Therefore, finding agents that specifically target astrocytic K^+ clearance mechanisms could lead to alleviation of disease symptoms or progression. However, more research is needed to better comprehend how K^+ clearance mechanisms engage during different behaviours.

The present study provides insight on the modulatory role of specific neuromodulators on K^+ clearance mechanisms, including ACh, Histamine, NE, DA and 5-HT. However, due to technical constraints, some of the neuromodulators tested were bath applied, which hinders the interpretation of their spatiotemporal impact on different brain structures. Hence, future work in this area should focus on investigating the effects of neuromodulators locally within specifically targeted neuronal-astrocytic networks.

A more local approach to study neuronal release of neuromodulators and their impact on astrocytic networks is the use of caged compounds. Although photolysis of caged DA and caged 5-HT with UV light provided the spatiotemporal control needed for each neuromodulator to target independent astrocytic domains, more research is needed to better characterize the effects of these compounds on neuronal-astrocytic networks *in vivo*.

To overcome the limitation of current methods, recent advances in optical and bioengineering techniques, including the development of novel genetically-encoded fluorescent indicators and nanosensors in transgenic mice, circuit tracing tools and dynamic two-photon or three-dimensional imaging, offer opportunities to dissect the specific contributions of cellular interactions within specific microcircuits and to assess the distribution of extracellular and intracellular ions, thus providing better insights on the spatiotemporal dynamics of $[K^+]_o$ and their correlation with Ca^{2+} signalling[385,435,463,628]. For instance, "optogenetic tagging" has been successfully used for the identification of specific cellular subtypes with high spatiotemporal resolution. This genetic approach is based on the Cre-dependent expression of light-sensitive opsins (e.g. channelrhodopsin) in a given neuronal population, typically achieved through the use of virus delivery systems (e.g. rabies)[629,630,631]. Furthermore, other tools acting at molecular levels will enable the direct manipulation of different signalling pathways through the overexpression of genes and proteins that are specific to neuronal populations (e.g. GRK6 isoform for DA, GATA-2 transcription factor for 5-HT)[632,633].

Together, the combination of both cellular (electrophysiological and optical recordings) and molecular (genetic tagging and overexpression of proteins) approaches can help better characterize the effectors of the astrocytic K^+ clearance process and their targets at molecular, cellular, synaptic and network levels, and thus their behavioural correlates.

In line with the design of more physiological and localized experiments to examine the role of neuromodulators and astrocytes within specific neuronal networks, it would be interesting to assess whether endogenous increases in neuromodulator release from different neuronal populations located across brain structures are sufficient to affect astrocytic K^+ clearance mechanisms, leading to differential modulation of gliotransmission[379] and resonant frequency properties underlying different oscillations *in vivo*. In this regard, large-scale simultaneous optical recordings of neuronal and astrocytic networks across brain structures have the potential to achieve the spatiotemporal resolution for accurate analysis of the functional organization and interregional interactions of neuronal oscillations during particular behaviours, such as sleep, as originally suggested fifteen years ago[108]. Indeed, combinations of brain stimulation together with simultaneous recordings from large tagged cellular populations have the potential to reveal the direct effects of endogenous neuromodulator's release on astrocytic $[K^+]_o$ clearance function, thus unravelling physiological interactions across brain structures presumably implicated in different behaviours.

Finally, despite the proposed mechanisms of action for each neuromodulator on K^+ clearance mechanisms and membrane properties, we cannot rule out the existence of interactions between the above-mentioned neuromodulators and other molecules that were not tested in the present study (e.g. Orexin, D-serine, ATP/adenosine, glutamate)[142,634]. Likewise, it is possible that the observed effects were due to neuromodulators acting on different cell types (i.e. microglia, oligodendrocytes)[523,635]. Therefore, additional studies are required to complement the work presented in this thesis and provide answers to unexplored questions, regarding (1) the impact of convergent signalling pathways activated by different neuromodulators specifically on astrocytic K^+ clearance mechanisms and resonance frequency properties in different cortical layers, and (2) the contribution of other glial cell types, namely oligodendrocytes, to the observed alterations in

network oscillations, as they also express channels and receptors involved in $[K^+]_o$ clearance[636] (Appendix Table 3).

For this purpose, computational models based on biological data hold promise in fulfilling our experimental and theoretical knowledge about the differential regulation of neuromodulators on neuronal network activity by predicting their spatiotemporal actions within the CNS, which in turn will help design more specific and effective therapeutic strategies for mental illnesses in which these circuits are dysregulated[580,637,638].

REFERENCES

1. Schaul, N. The fundamental neural mechanisms of electroencephalography. *Electroencephalography and Clinical Neurophysiology* (1998). doi:10.1016/S0013-4694(97)00111-9
2. Buzsaki, G. Rhythms of the Brain. *Cycle* (2006). doi:10.1093/acprof
3. Sanchez-Vives, M. V & McCormick, D. A. Cellular and network mechanisms of rhythmic recurrent activity in neocortex. *Nat. Neurosci.* 3, 1027–34 (2000).
4. Cunningham, M. O. *et al.* Neuronal metabolism governs cortical network response state. *Proc. Natl. Acad. Sci.* (2006). doi:10.1073/pnas.0600604103
5. Nunez, P. L. Neocortical Dynamics and Human EEG Rhythms. *Oxford University Press*, 1995.
6. Cossart, R., Aronov, D. & Yuste, R. Attractor dynamics of network UP states in the neocortex. *Nature* 423, 283–8 (2003).
7. Fries, P. A mechanism for cognitive dynamics: neuronal communication through neuronal coherence. *Trends Cogn. Sci.* 9, 474–80 (2005).
8. Fries, P., Reynolds, J. H., Rorie, A. E. & Desimone, R. Modulation of oscillatory neuronal synchronization by selective visual attention. *Science* 291, 1560-3 (2001). doi:10.1126/science.1055465
9. Tallon-Baudry, C., Mandon, S., Freiwald, W. A. & Kreiter, A. K. Oscillatory synchrony in the monkey temporal lobe correlates with performance in a visual short-term memory task. *Cereb. Cortex* (2004). doi:10.1093/cercor/bhh031
10. Steriade, M. Grouping of brain rhythms in corticothalamic systems. *Neuroscience* 137, 1087–1106 (2006).
11. Penttonen, M. & Buzsáki, G. Natural logarithmic relationship between brain oscillators. *Thalamus and Related Systems* 2, 145–152 (2003).
12. Contreras, D. & Llinas, R. Voltage-sensitive dye imaging of neocortical spatiotemporal dynamics to afferent activation frequency. *J. Neurosci.* 21, 9403–9413 (2001).
13. He, B. J., Snyder, A. Z., Zempel, J. M., Smyth, M. D. & Raichle, M. E. Electrophysiological correlates of the brain's intrinsic large-scale functional architecture. *Proc. Natl. Acad. Sci.* (2008). doi:10.1073/pnas.0807010105
14. Brooks, D. C. Waves associated with eye movement in the awake and sleeping cat. *Electroencephalogr. Clin. Neurophysiol.* (1968). doi:10.1016/0013-4694(68)90042-4
15. Murthy, V. N. & Fetz, E. E. Coherent 25- to 35-Hz oscillations in the sensorimotor cortex of awake behaving monkeys. *Proc. Natl. Acad. Sci.* (1992). doi:10.1073/pnas.89.12.5670
16. Achermann, P. & Borbély, A. A. Low-frequency (< 1 Hz) oscillations in the human sleep electroencephalogram. *Neuroscience* (1997). doi:10.1016/S0306-4522(97)00186-3
17. Nir, Y. *et al.* Regional Slow Waves and Spindles in Human Sleep. *Neuron* (2011). doi:10.1016/j.neuron.2011.02.043
18. Skaggs, W. E. *et al.* EEG Sharp Waves and Sparse Ensemble Unit Activity in the Macaque Hippocampus. *J. Neurophysiol.* (2007). doi:10.1152/jn.00401.2007
19. Hughes, S. W. *et al.* Synchronized oscillations at α and θ frequencies in the lateral geniculate nucleus. *Neuron* (2004). doi:10.1016/S0896-6273(04)00191-6
20. Bereshpolova, Y., Amitai, Y., Gusev, A. G., Stoelzel, C. R. & Swadlow, H. A. Dendritic Backpropagation and the State of the Awake Neocortex. *J. Neurosci.* (2007).

doi:10.1523/JNEUROSCI.2218-07.2007
21. Peyrache, A., Battaglia, F. P. & Destexhe, A. Inhibition recruitment in prefrontal cortex during sleep spindles and gating of hippocampal inputs. *Proc. Natl. Acad. Sci.* (2011). doi:10.1073/pnas.1103612108
22. Watson, B. O. & Buzsáki, G. Sleep, memory & brain rhythms. *Daedalus* (2015). doi:10.1162/DAED_a_00318
23. Steriade, M., Dossi, R. C. & Nuñez, A. Network modulation of a slow intrinsic oscillation of cat thalamocortical neurons implicated in sleep delta waves: cortically induced synchronization and brainstem cholinergic suppression. *J. Neurosci.* (1991). doi:20026697
24. Buzsáki, G. Two-stage model of memory trace formation: A role for 'noisy' brain states. *Neuroscience* (1989). doi:10.1016/0306-4522(89)90423-5
25. Berger, H. Das Elektrenkephalogramm des Menschen. *Nov. Acta Leopoldina* 6, 173–309 (1938).
26. Chapman, C. A., Xu, Y., Haykin, S. & Racine, R. J. Beta-frequency (15-35 Hz) electroencephalogram activities elicited by toluene and electrical stimulation in the behaving rat. *Neuroscience* (1998). doi:10.1016/S0306-4522(98)00092-X
27. Timofeev, I. & Steriade, M. Fast (mainly 30-100 Hz) oscillations in the cat cerebellothalamic pathway and their synchronization with cortical potentials. *J. Physiol.* (1997). doi:10.1111/j.1469-7793.1997.153bf.x
28. Amzica, F., Nuñez, A. & Steriade, M. Delta frequency (1-4 Hz) oscillations of perigeniculate thalamic neurons and their modulation by light. *Neuroscience* (1992). doi:10.1016/0306-4522(92)90315-S
29. Leung, L. S. & Yim, C. Y. Rhythmic delta-frequency activities in the nucleus accumbens of anesthetized and freely moving rats. *Can. J. Physiol. Pharmacol.* (1993). doi:10.1139/y93-049
30. Pare, D., Collins, D. R. & Paré, D. Neuronal correlates of fear in the lateral amygdala: multiple extracellular recordings in conscious cats. *J. Neurosci.* (2000). doi:10.1523/JNEUROSCI.20-07-02701.2000
31. Buzsáki, G. Theta oscillations in the hippocampus. *Neuron* (2002). doi:10.1016/S0896-6273(02)00586-X
32. Mitchell, S. J. & Ranck, J. B. Generation of theta rhythm in medial entorhinal cortex of freely moving rats. *Brain Res.* (1980). doi:10.1016/0006-8993(80)90006-2
33. Leung, L. W. S. & Borst, J. G. G. Electrical activity of the cingulate cortex. I. Generating mechanisms and relations to behavior. *Brain Res.* (1987). doi:10.1016/0006-8993(87)91220-0
34. Pavlides, C., Greenstein, Y. J., Grudman, M. & Winson, J. Long-term potentiation in the dentate gyrus is induced preferentially on the positive phase of θ-rhythm. *Brain Res.* (1988). doi:10.1016/0006-8993(88)91499-0
35. Steriade, M. & Deschenes, M. The thalamus as a neuronal oscillator. *Brain Research Reviews* (1984). doi:10.1016/0165-0173(84)90017-1
36. Chatila, M., Milleret, C., Buser, P. & Rougeul, A. A 10 Hz 'alpha-like' rhythm in the visual cortex of the waking cat. *Electroencephalogr. Clin. Neurophysiol.* (1992). doi:10.1016/0013-4694(92)90147-A
37. Lopes da Silva, F. H., van Lierop, T. H. M. T., Schrijer, C. F. & Storm van Leeuwen, W. Organization of thalamic and cortical alpha rhythms: Spectra and coherences. *Electroencephalogr. Clin. Neurophysiol.* (1973). doi:10.1016/0013-4694(73)90216-2

38. Penttonen, M. *et al.* Ultra-slow oscillation (0.025 Hz) triggers hippocampal afterdischarges in Wistar rats. *Neuroscience* (1999). doi:10.1016/S0306-4522(99)00367-X
39. Feingold, J., Gibson, D. J., DePasquale, B. & Graybiel, A. M. Bursts of beta oscillation differentiate postperformance activity in the striatum and motor cortex of monkeys performing movement tasks. *Proc. Natl. Acad. Sci.* (2015). doi:10.1073/pnas.1517629112
40. Osinski, B. L., Kim, A., Xiao, W., Mehta, N. M. & Kay, L. M. Pharmacological manipulation of the olfactory bulb modulates beta oscillations: testing model predictions. *J. Neurophysiol.* (2018). doi:10.1152/jn.00090.2018
41. Maloney, K. J., Cape, E. G., Gotman, J. & Jones, B. E. High-frequency γ electroencephalogram activity in association with sleep-wake states and spontaneous behaviors in the rat. *Neuroscience* (1997). doi:10.1016/S0306-4522(96)00298-9
42. Eeckman, F. H. & Freeman, W. J. Correlations between unit firing and EEG in the rat olfactory system. *Brain Res.* (1990). doi:10.1016/0006-8993(90)91663-2
43. Buzsáki, G. *et al.* Hippocampal network patterns of activity in the mouse. *Neuroscience* (2003). doi:10.1016/S0306-4522(02)00669-3
44. McCormick, D. A. & Pape, H. C. Properties of a hyperpolarization-activated cation current and its role in rhythmic oscillation in thalamic relay neurones. *J. Physiol.* (1990). doi:10.1113/jphysiol.1990.sp018331
45. Soltesz, I. *et al.* Two inward currents and the transformation of low-frequency oscillations of rat and cat thalamocortical cells. *J. Physiol.* 441, 175-97 (1991). doi:10.1113/jphysiol.1991.sp018745
46. B. W. Connors, M. J. Gutnick, D. A. P. Electrophysiological properties of neocortical neurons in vitro. *J. Neurophysiol.* (1982). doi:10.1152/jn.1982.48.6.1302
47. Steriade, M., Nuñez, A. & Amzica, F. A novel slow (< 1 Hz) oscillation of neocortical neurons in vivo: depolarizing and hyperpolarizing components. *J. Neurosci.* (1993). doi:10.1523/JNEUROSCI.13-08-03252.1993
48. Carracedo, L. M. *et al.* A Neocortical Delta Rhythm Facilitates Reciprocal Interlaminar Interactions via Nested Theta Rhythms. *J. Neurosci.* 33, 10750-61 (2013). doi:10.1523/JNEUROSCI.0735-13.2013
49. Metherate, R., Ashe, J. H. & Kawaguchi, Y. Ionic flux contributions to neocortical slow waves and nucleus basalis-mediated activation: whole-cell recordings in vivo. *J. Neurosci.* (1993). doi:10.1523/jneurosci.4883-11.2012
50. Amzica, F., Neckelmann, D. and Steriade, M. Cortical neuron-glia interactions during spike-and-wave (SW) seizures. *Soc. Neurosci. Abstr.*, 23, 1688 (1997).
51. Amzica, F., Massimini, M. & Manfridi, A. Spatial buffering during slow and paroxysmal sleep oscillations in cortical networks of glial cells in vivo. *J. Neurosci.* 22, 1042–1053 (2002).
52. Kozachkov, L. & Michmizos, K. P. The Causal Role of Astrocytes in Slow-Wave Rhythmogenesis: A Computational Modelling Study. (2017).
53. Hangya, B., Borhegyi, Z., Szilagyi, N., Freund, T. F. & Varga, V. GABAergic Neurons of the Medial Septum Lead the Hippocampal Network during Theta Activity. *J. Neurosci.* (2009). doi:10.1523/JNEUROSCI.5665-08.2009
54. Freund, T. F. & Antal, M. GABA-containing neurons in the septum control inhibitory interneurons in the hippocampus. *Nature* (1988). doi:10.1038/336170a0
55. Vandecasteele, M. *et al.* Optogenetic activation of septal cholinergic neurons suppresses sharp wave ripples and enhances theta oscillations in the hippocampus. *Proc. Natl. Acad.*

Sci. (2014). doi:10.1073/pnas.1411233111
56. D'Angelo, E. *et al.* Theta-frequency bursting and resonance in cerebellar granule cells: experimental evidence and modeling of a slow K^+-dependent mechanism. *J. Neurosci.* (2001). doi:21/3/759 [pii]
57. Kamondi, A., Acsády, L., Wang, X. J. & Buzsáki, G. Theta oscillations in somata and dendrites of hippocampal pyramidal cells in vivo: Activity-dependent phase-precession of action potentials. *Hippocampus* (1998). doi:10.1002/(SICI)1098-1063(1998)8:3<244::AID-HIPO7>3.0.CO;2-J
58. Foley, J. *et al.* Astrocytic IP_3/Ca^{2+} Signaling Modulates Theta Rhythm and REM Sleep. *Front. Neural Circuits* (2017). doi:10.3389/fncir.2017.00003
59. Steriade, M. & Timofeev, I. Neuronal plasticity in thalamocortical networks during sleep and waking oscillations. *Neuron* (2003). doi:10.1016/S0896-6273(03)00065-5
60. Page, A. J., O'Donnell, T. A. & Blackshaw, L. A. Inhibition of mechanosensitivity in visceral primary afferents by GABAB receptors involves calcium and potassium channels. *Neuroscience* (2006). doi:10.1016/j.neuroscience.2005.09.016
61. Hughes, S. W. *et al.* Thalamic gap junctions control local neuronal synchrony and influence macroscopic oscillation amplitude during EEG alpha rhythms. *Front. Psychol.* (2011). doi:10.3389/fpsyg.2011.00193
62. Jedema, H. P. Corticotropin-Releasing Hormone Directly Activates Noradrenergic Neurons of the Locus Ceruleus Recorded In Vitro. *J. Neurosci.* (2004). doi:10.1523/JNEUROSCI.2830-04.2004
63. McCormick, D. A. Neurotransmitter actions in the thalamus and cerebral cortex and their role in neuromodulation of thalamocortical activity. *Prog. Neurobiol.* (1992). doi:10.1016/0301-0082(92)90012-4
64. Enoch, M. A. *et al.* Common genetic origins for EEG, alcoholism and anxiety: The role of CRH-BP. *PLoS One* (2008). doi:10.1371/journal.pone.0003620
65. Roopun, A. K. *et al.* A beta2-frequency (20-30 Hz) oscillation in nonsynaptic networks of somatosensory cortex. *Proc. Natl. Acad. Sci.* (2006). doi:10.1073/pnas.0607443103
66. Roopun. Cholinergic neuromodulation controls directed temporal communication in neocortex in vitro. *Front. Neural Circuits* (2010). doi:10.3389/fncir.2010.00008
67. Schmiedt, J. T. *et al.* Beta Oscillation Dynamics in Extrastriate Cortex after Removal of Primary Visual Cortex. *J. Neurosci.* (2014). doi:10.1523/JNEUROSCI.0509-14.2014
68. Whittington, M. A., Traub, R. D. & Jefferys, J. G. R. Synchronized oscillations in interneuron networks driven by metabotropic glutamate receptor activation. *Nature* (1995). doi:10.1038/373612a0
69. Fisahn, A., Pike, F. G., Buhl, E. H. & Paulsen, O. Cholinergic induction of network oscillations at 40 Hz in the hippocampus in vitro. *Nature* (1998). doi:10.1038/28179
70. Ainsworth, M. *et al.* Dual Gamma Rhythm Generators Control Interlaminar Synchrony in Auditory Cortex. *J. Neurosci.* (2011). doi:10.1523/JNEUROSCI.2209-11.2011
71. Lee, H. S. *et al.* Astrocytes contribute to gamma oscillations and recognition memory. *Proc. Natl. Acad. Sci.* 111, E3343-52 (2014).
72. LeBeau, F. E. N., Towers, S. K., Traub, R. D., Whittington, M. A. & Buhl, E. H. Fast network oscillations induced by potassium transients in the rat hippocampus in vitro. *J. Physiol.* (2002). doi:10.1113/jphysiol.2002.015933
73. Traub, R. D. *et al.* A possible role for gap junctions in generation of very fast EEG oscillations preceding the onset of, and perhaps initiating, seizures. *Epilepsia* (2001).

doi:10.1046/j.1528-1157.2001.26900.x
74. Wang & Buzsáki, G. Gamma oscillation by synaptic inhibition in a hippocampal interneuronal network model. *J. Neurosci.* (1996). doi:citeulike-article-id:134404
75. Walter, W. G. The location of cerebral tumors by electroencephalography. *Lancet* 8, 305–308 (1936).
76. Huber, R., Ghilardi, M. F., Massimini, M. & Tononi, G. Local sleep and learning. *Nature* (2004). doi:10.1038/nature02663
77. Başar-Eroglu, C., Başar, E., Demiralp, T. & Schürmann, M. P300-response: possible psychophysiological correlates in delta and theta frequency channels. A review. *Int. J. Psychophysiol.* (1992). doi:10.1016/0167-8760(92)90055-G
78. Basar, E. Brain function and oscillations, vol II: Integrative brain function. Neurophysiology and cognitive processes. *Springer, Berlin Heidelberg.* (1999). doi:10.1103/PhysRevA.90.013818
79. Hobson, J. A. The Dreaming Brain. *New York: Basic Books*, 1988.
80. Knyazev, G. G. Motivation, emotion, and their inhibitory control mirrored in brain oscillations. *Neuroscience and Biobehavioral Reviews* (2007). doi:10.1016/j.neubiorev.2006.10.004
81. Fernández, T. *et al.* EEG activation patterns during the performance of tasks involving different components of mental calculation. *Electroencephalogr. Clin. Neurophysiol.* (1995). doi:10.1016/0013-4694(94)00262-J
82. Harmony, T. *et al.* EEG delta activity: An indicator of attention to internal processing during performance of mental tasks. *Int. J. Psychophysiol.* (1996). doi:10.1016/S0167-8760(96)00053-0
83. Jouvet, M. Biogenic amines and the states of sleep. *Science* 163, 32-41 (1969). doi:10.1126/science.163.3862.32
84. Basar, E. Brain Function and Oscillations. I. Brain Oscillations: Principles and Approaches. *Springer, Berlin Heidelberg*, 1998.
85. Vanderwolf, C. H. Hippocampal electrical activity and voluntary movement in the rat. *Electroencephalogr. Clin. Neurophysiol.* (1969). doi:10.1016/0013-4694(69)90092-3
86. Magee, J. C. & Johnston, D. Synaptic activation of voltage-gated channels in the dendrites of hippocampal pyramidal neurons. *Science* 268, 301-4 (1995). doi:10.1126/science.7716525
87. Zhang, H. & Jacobs, J. Traveling Theta Waves in the Human Hippocampus. *J. Neurosci.* (2015). doi:10.1523/JNEUROSCI.5102-14.2015
88. Klimesch, W., Schimke, H. & Schwaiger, J. Episodic and semantic memory: an analysis in the EEG theta and alpha band. *Electroencephalogr. Clin. Neurophysiol.* (1994). doi:10.1016/0013-4694(94)90164-3
89. Halgren, E. *et al.* Laminar Profile of Spontaneous and Evoked Theta: Rhythmic Modulation of Cortical Processing During Word Integration HHS Public Access. *Neuropsychologia* (2015). doi:10.1016/j.neuropsychologia.2015.03.021
90. Pu, Y., Cornwell, B. R., Cheyne, D. & Johnson, B. W. The functional role of human right hippocampal/parahippocampal theta rhythm in environmental encoding during virtual spatial navigation. *Hum. Brain Mapp.* (2017). doi:10.1002/hbm.23458
91. Dorokhov, V. B. Alpha-bursts and K-complex: phasic activation pattern during spontaneous recovery of correct psychomotor performance at difference stages of drowsiness. *Zhurnal Vyss. Nervn. Deiatelnosti Im. I. P. Pavlov.* (2003).

92. Singer, W. Synchronization of Cortical Activity and its Putative Role in Information Processing and Learning. *Annu. Rev. Physiol.* (1993). doi:10.1146/annurev.physiol.55.1.349
93. Valera, F. J., Toro, A., Roy John, E. & Schwartz, E. L. Perceptual framing and cortical alpha rhythm. *Neuropsychologia* (1981). doi:10.1016/0028-3932(81)90005-1
94. Pfurtscheller, G., Neuper, C., Andrew, C. & Edlinger, G. Foot and hand area mu rhythms. *International Journal of Psychophysiology* 26, 121-35 (1997). doi:10.1016/S0167-8760(97)00760-5
95. Niedermeyer, E., Lopes da Silva, F. Electroencephalography: Basic Principles,Clinical Applications, and Related Fields. *Williams & Wilkins, Baltimore*, 2004.
96. Zoefel, B., Huster, R. J. & Herrmann, C. S. Neurofeedback training of the upper alpha frequency band in EEG improves cognitive performance. *Neuroimage* (2011). doi:10.1016/j.neuroimage.2010.08.078
97. Eckart, C., Woźniak-Kwaśniewska, A., Herweg, N. A., Fuentemilla, L. & Bunzeck, N. Acetylcholine modulates human working memory and subsequent familiarity based recognition via alpha oscillations. *Neuroimage* 137, 61-69 (2016). doi:10.1016/j.neuroimage.2016.05.049
98. Pfurtscheller, G., Stancák, A. & Neuper, C. Post-movement beta synchronization. A correlate of an idling motor area? *Electroencephalogr. Clin. Neurophysiol.* (1996). doi:10.1016/0013-4694(95)00258-8
99. Maier, A. *et al.* Divergence of fMRI and neural signals in V1 during perceptual suppression in the awake monkey. *Nat. Neurosci.* (2008). doi:10.1038/nn.2173
100. Wilke, M., Logothetis, N. K. & Leopold, D. A. Local field potential reflects perceptual suppression in monkey visual cortex. *Proc. Natl. Acad. Sci.* (2006). doi:10.1073/pnas.0604673103
101. Bosman, C. A. *et al.* Attentional Stimulus Selection through Selective Synchronization between Monkey Visual Areas. *Neuron* (2012). doi:10.1016/j.neuron.2012.06.037
102. Buschman, T. J. & Miller, E. K. Top-down versus bottom-up control of attention in the prefrontal and posterior parietal cortices. *Science* 315, 1860-2 (2007). doi:10.1126/science.1138071
103. Salazar, R. F., Dotson, N. M., Bressler, S. L. & Gray, C. M. Content-specific fronto-parietal synchronization during visual working memory. *Science* 338, 1097-100 (2012). doi:10.1126/science.1224000
104. Basar, E. EEG-Brain Dynamics. Relation Between EEG and Evoked Potentials. *Elsevier* (1980).
105. Canolty, R. T. *et al.* High gamma power is phase-locked to theta oscillations in human neocortex. *Science* 313, 1626-8 (2006). doi:10.1126/science.1128115
106. Chrobak, J. J. & Buzsáki, G. Gamma oscillations in the entorhinal cortex of the freely behaving rat. *J. Neurosci.* (1998). doi:0270-6474/97/180388-11$05.00/0
107. Alekseichuk, I., Turi, Z., Amador de Lara, G., Antal, A. & Paulus, W. Spatial Working Memory in Humans Depends on Theta and High Gamma Synchronization in the Prefrontal Cortex. *Curr. Biol.* (2016). doi:10.1016/j.cub.2016.04.035
108. Buzsáki, G. & Draguhn, A. Neuronal oscillations in cortical networks. *Science* (2004). doi:10.1126/science.1099745
109. Isomura, Y. *et al.* Integration and Segregation of Activity in Entorhinal-Hippocampal Subregions by Neocortical Slow Oscillations. *Neuron* 52, 871–882 (2006).

110. Jing, W. *et al.* EEG Bands of Wakeful Rest, Slow-Wave and Rapid-Eye-Movement Sleep at Different Brain Areas in Rats. *Front. Comput. Neurosci.* 10, 1–13 (2016).
111. Steriade, M. Impact of network activities on neuronal properties in corticothalamic systems. *J. Neurophysiol.* (2001). doi:10.1017/S1472928801000139
112. Fernández, T. *et al.* Event-related EEG oscillations to semantically unrelated words in normal and learning disabled children. *Brain Cogn.* (2012). doi:10.1016/j.bandc.2012.04.008
113. Klimesch, W. EEG alpha and theta oscillations reflect cognitive and memory performance: A review and analysis. *Brain Research Reviews* (1999). doi:10.1016/S0165-0173(98)00056-3
114. Huster, R. J., Enriquez-Geppert, S., Lavallee, C. F., Falkenstein, M. & Herrmann, C. S. Electroencephalography of response inhibition tasks: Functional networks and cognitive contributions. *International Journal of Psychophysiology* (2013). doi:10.1016/j.ijpsycho.2012.08.001
115. Schurmann, M. & Basar, E. Functional aspects of alpha oscillations in the EEG. *Int. J. Psychophysiol.* (2000). doi:10.1016/S0167-8760(00)00138-0
116. Jensen, O. & Mazaheri, A. Shaping Functional Architecture by Oscillatory Alpha Activity: Gating by Inhibition. *Front. Hum. Neurosci.* 4, 1–8 (2010).
117. Klimesch, W. Controlled Access To Stored Information. *Trends Cogn. Sci.* 16, 606–617 (2012).
118. Baker, S. N., Olivier, E. & Lemon, R. N. Coherent oscillations in monkey motor cortex and hand muscle EMG show task-dependent modulation. *J. Physiol.* (1997). doi:10.1111/j.1469-7793.1997.225bo.x
119. Brown, P. Abnormal oscillatory synchronisation in the motor system leads to impaired movement. *Current Opinion in Neurobiology* (2007). doi:10.1016/j.conb.2007.12.001
120. Neuper, C. & Pfurtscheller, G. Event-related dynamics of cortical rhythms: Frequency-specific features and functional correlates. *International Journal of Psychophysiology* (2001). doi:10.1016/S0167-8760(01)00178-7
121. Engel, A. K. & Fries, P. Beta-band oscillations — signalling the status quo? *Curr. Opin. Neurobiol.* 20, 156–165 (2010).
122. Pogosyan, A., Gaynor, L. D., Eusebio, A. & Brown, P. Boosting Cortical Activity at Beta-Band Frequencies Slows Movement in Humans. *Curr. Biol.* (2009). doi:10.1016/j.cub.2009.07.074
123. Gilbertson, T. Existing Motor State Is Favored at the Expense of New Movement during 13-35 Hz Oscillatory Synchrony in the Human Corticospinal System. *J. Neurosci.* (2005). doi:10.1523/JNEUROSCI.1762-05.2005
124. Llinás, R., Ribary, U., Contreras, D. & Pedroarena, G. The neuronal basis for consciousness. *Philosophical Transactions of the Royal Society B: Biological Sciences* (1998). doi:10.1098/rstb.1998.0336
125. Varela, F., Lachaux, J. P., Rodriguez, E. & Martinerie, J. The brainweb: Phase synchronization and large-scale integration. *Nat. Rev. Neurosci.* (2001). doi:10.1038/35067550
126. Merker, B. Cortical gamma oscillations: The functional key is activation, not cognition. *Neuroscience and Biobehavioral Reviews* (2013). doi:10.1016/j.neubiorev.2013.01.013
127. Fell, J. *et al.* Human memory formation is accompanied by rhinal-hippocampal coupling and decoupling. *Nat. Neurosci.* (2001). doi:10.1038/nn759

128. Lisman, J. E. & Idiart, M. A. P. Storage of 7 ± 2 short-term memories in oscillatory subcycles. *Science* 267, 1512-5 (1995). doi:10.1126/science.7878473
129. Hasselmo, M. E., Wyble, B. P. & Wallenstein, G. V. Encoding and retrieval of episodic memories: Role of cholinergic and GABAergic modulation in the hippocampus. *Hippocampus* (1996). doi:10.1002/(SICI)1098-1063(1996)6:6<693::AID-HIPO12>3.0.CO;2-W
130. Steriade, M., Gloor, P., Llinas, R. R., H., L. da S. F. & Mesulam, M. M. Basic mechanisms of cerebral rhytmic activities. *Electroencephalogr. Clin. Neurophysiol.* 481–508 (1990).
131. Bragin, A., Engel, J., Wilson, C. L., Fried, I. & Buzsáki, G. High-frequency oscillations in human brain. *Hippocampus* (1999). doi:10.1002/(SICI)1098-1063(1999)9:2<137::AID-HIPO5>3.0.CO;2-0
132. Curio, G. *et al.* Localization of evoked neuromagnetic 600 Hz activity in the cerebral somatosensory system. *Electroencephalogr. Clin. Neurophysiol.* (1994). doi:10.1016/0013-4694(94)90169-4
133. Maris, E., Fries, P. & van Ede, F. Diverse Phase Relations among Neuronal Rhythms and Their Potential Function. *Trends Neurosci.* 39, 86–99 (2016).
134. Liljenström, H. & Hasselmo, M. Acetylcholine and cortical oscillatory dynamics. *Comput. Neural Syst.* 523–530 (1993).
135. Steriade, M., McCormick, D. A. & Sejnowski, T. J. Thalamocortical oscillations in the sleeping and aroused brain. *Science* 262, 679-85 (1993). doi:10.1126/science.8235588
136. Tohidi, V. & Nadim, F. Membrane resonance in bursting pacemaker neurons of an oscillatory network is correlated with network frequency. *J. Neurosci.* 29, 6427–6435 (2009).
137. Yue, B. W. & Huguenard, J. R. The role of H-current in regulating strength and frequency of thalamic network oscillations. *Thalamus Relat. Syst.* (2001). doi:10.1016/S1472-9288(01)00009-7
138. Hutcheon, B. & Yarom, Y. Resonance, oscillation and the intrinsic frequency preferences of neurons. *Trends in Neurosciences* 23, 216–222 (2000).
139. Alonso, A. & Llinás, R. R. Subthreshold Na^+-dependent theta-like rhythmicity in stellate cells of entorhinal cortex layer II. *Nature* (1989). doi:10.1038/342175a0
140. Pike, F. G. *et al.* Distinct frequency preferences of different types of rat hippocampal neurones in response to oscillatory input currents. *J. Physiol.* (2000). doi:10.1111/j.1469-7793.2000.00205.x
141. Whittington, M. A. & Traub, R. D. Interneuron Diversity series: Inhibitory interneurons and network oscillations in vitro. *Trends in Neurosciences* 26, 676-82 (2003). doi:10.1016/j.tins.2003.09.016
142. Ding F, O'Donnell J, Xu Q, Kang N, Goldman N, N. M. Changes in the composition of brain interstitial ions control the sleep-wake cycle. *Science* 352, 550–5 (2016).
143. Penttonen, M., Kamondi, A., Acsády, L. & Buzsáki, G. Gamma frequency oscillation in the hippocampus of the rat: Intracellular analysis in vivo. *Eur. J. Neurosci.* (1998). doi:10.1046/j.1460-9568.1998.00096.x
144. Steriade M, B. G. Parallel activation of thalamic and cortical neurons by brainstem and basal forebrain cholinergic systems. *Brain cholinergic systems. Oxford University Press*, 3–64 (1990).

145. McCormick, D. A. & Prince, D. A. Acetylcholine induces burst firing in thalamic reticular neurones by activating a potassium conductance. *Nature* (1986). doi:10.1038/319402a0
146. Muir, J. L., Dunnett, S. B., Robbins, T. W. & Everitt, B. J. Attentional functions of the forebrain cholinergic systems: effects of intraventricular hemicholinium, physostigmine, basal forebrain lesions and intracortical grafts on a multiple-choice serial reaction time task. *Exp. Brain Res.* (1992). doi:10.1007/BF00229886
147. Sarter, M. & Bruno, J. P. Cognitive functions of cortical acetylcholine: Toward a unifying hypothesis. *Brain Research Reviews* (1997). doi:10.1016/S0165-0173(96)00009-4
148. Buzsaki, G. *et al.* Nucleus basalis and thalamic control of neocortical activity in the freely moving rat. *J. Neurosci.* (1988). doi:10.1523/JNEUROSCI.08-11-04007.1988
149. Traub, R. D., Whittington, M. A., Stanford, I. M. & Jefferys, J. G. R. A mechanism for generation of long-range synchronous fast oscillations in the cortex. *Nature* (1996). doi:10.1038/383621a0
150. Contreras, D. & Steriade, M. Cellular basis of EEG slow rhythms: corticothalamic relationships. *J. Neurosci.* (1995). doi:10.1021/jo502028g
151. Berger, H. Uber das Elektroenkephalogramm des Menschen. *Arch. fur Psychatrie* (1929).
152. Karbowsky, K. Hans Berger (1873–1941). *J Neurol* 249, 1130–1131 (2002).
153. Jasper, H. & Penfield, W. Electrocorticograms in man: Effect of voluntary movement upon the electrical activity of the precentral gyrus. *Arch. für Psychiatr. und Nervenkrankheiten* (1949). doi:10.1007/BF01062488
154. Crandall, P. H., Walter, R. D. & Rand, R. W. Clinical Applications of Studies on Stereotactically Implanted Electrodes in Temporal-Lobe Epilepsy. *J. Neurosurg.* 20, 827–840 (1963).
155. Csicsvari, J. Massively Parallel Recording of Unit and Local Field Potentials With Silicon-Based Electrodes. *J. Neurophysiol.* (2003). doi:10.1152/jn.00116.2003
156. Mazzoni, A., Logothetis, N. & Panzeri, S. The information content of Local Field Potentials: experiments and models. *arXiv Prepr. arXiv1206.0560* 1–32 (2012).
157. Mitzdorf, U. Current source-density method and application in cat cerebral cortex: investigation of evoked potentials and EEG phenomena. *Physiol. Rev.* (1985). doi:10.1152/physrev.1985.65.1.37
158. Gustafsson, B. Afterpotentials and transduction properties in different types of central neurones. *Arch. Ital. Biol.* (1984). doi:10.4449/AIB.V122I1.3213
159. Belitski, A. *et al.* Low-Frequency Local Field Potentials and Spikes in Primary Visual Cortex Convey Independent Visual Information. *J. Neurosci.* (2008). doi:10.1523/JNEUROSCI.0009-08.2008
160. Montemurro, M. A., Rasch, M. J., Murayama, Y., Logothetis, N. K. & Panzeri, S. Phase-of-Firing Coding of Natural Visual Stimuli in Primary Visual Cortex. *Curr. Biol.* (2008). doi:10.1016/j.cub.2008.02.023
161. Jessberger, J., Zhong, W., I, J. B. & Draguhn, A. Olfactory Bulb Field Potentials and Respiration in Sleep-Wake States of Mice. *Neural Plast* 2016, 4570831 (2016).
162. Constantinople, C. M. & Bruno, R. M. Deep cortical layers are activated directly by thalamus. *Science* 340, 1591–4 (2013).
163. Mazzoni, A., Panzeri, S., Logothetis, N. K. & Brunel, N. Encoding of naturalistic stimuli by local field potential spectra in networks of excitatory and inhibitory neurons. *PLoS Comput. Biol.* (2008). doi:10.1371/journal.pcbi.1000239

164. Dehghani, N., Bédard, C., Cash, S. S., Halgren, E. & Destexhe, A. Comparative power spectral analysis of simultaneous elecroencephalographic and magnetoencephalographic recordings in humans suggests non-resistive extracellular media. *J Comput Neurosci* 29, 405–421 (2010).
165. S, S. Magnetoencephalography. *Prog Clin Neurosci.* 26, 164–74 (2012).
166. Singh S, Antony A, T. N. Yield of magnetoencephalography in mesial temporal lobe epilepsy. *Epilepsia Abst 2081* (2010).
167. Boxerman, J. L. *et al.* The intravascular contribution to fmri signal change: monte carlo modeling and diffusion-weighted studies in vivo. *Magn. Reson. Med.* (1995). doi:10.1002/mrm.1910340103
168. Buxton, R. B. & Frank, L. R. A model for the coupling between cerebral blood flow and oxygen metabolism during neural stimulation. *J. Cereb. Blood Flow Metab.* (1997). doi:10.1097/00004647-199701000-00009
169. Ogawa, S. & Lee, T. M. Magnetic resonance imaging of blood vessels at high fields: In vivo and in vitro measurements and image simulation. *Magn. Reson. Med.* (1990). doi:10.1002/mrm.1910160103
170. Ogawa, S., Lee, T. M, Nayak, A. S. & Glynn, P. Oxygenation-sensitive contrast in magnetic resonance image of rodent brain at high magnetic fields. *Magn. Reson. Med.* (1990). doi:10.1002/mrm.1910140108
171. Ogawa, S., Lee, T. M., Kay, A. R. & Tank, D. W. Brain magnetic resonance imaging with contrast dependent on blood oxygenation. *Proc. Natl. Acad. Sci.* (1990). doi:10.1073/pnas.87.24.9868
172. Kuffler, S. W. Discharge patterns and functional organization of mammalian retina. *J. Neurophysiol.* (1953). doi:10.1152/jn.1953.16.1.37
173. Hubel, D. H. & Wiesel, T. N. Receptive fields and functional architecture in two nonstriate visual areas (18 and 19) of the cat. *J. Neurophysiol.* (1965). doi:10.1152/jn.1965.28.2.229
174. Greicius, M. D., Srivastava, G., Reiss, A. L. & Menon, V. Default-mode network activity distinguishes Alzheimer's disease from healthy aging: Evidence from functional MRI. *Proc. Natl. Acad. Sci.* (2004). doi:10.1073/pnas.0308627101
175. Damaraju, E. *et al.* Dynamic functional connectivity analysis reveals transient states of dysconnectivity in schizophrenia. *NeuroImage Clin.* (2014). doi:10.1016/j.nicl.2014.07.003
176. Rees, G., Friston, K. & Koch, C. A direct quantitative relationship between the functional properties of human and macaque V5. *Nat. Neurosci.* (2000). doi:10.1038/76673
177. Logothetis, N. K., Pauls, J., Augath, M., Trinath, T. & Oeltermann, A. Neurophysiological investigation of the basis of the fMRI signal. *Nature* (2001). doi:10.1038/35084005
178. Smith, A. J. *et al.* Cerebral energetics and spiking frequency: The neurophysiological basis of fMRI. *Proc. Natl. Acad. Sci.* (2002). doi:10.1073/pnas.132272199
179. Rasch, M. J., Gretton, A., Murayama, Y., Maass, W. & Logothetis, N. K. Inferring Spike Trains From Local Field Potentials. *J. Neurophysiol.* (2008). doi:10.1152/jn.00919.2007
180. Leopold, D. A., Murayama, Y. & Logothetis, N. K. Very slow activity fluctuations in monkey visual cortex: Implications for functional brain imaging. *Cereb. Cortex* (2003). doi:10.1093/cercor/13.4.422
181. Lecoq, J. *et al.* Visualizing mammalian brain area interactions by dual-axis two-photon calcium imaging. *Nat. Neurosci.* 17, 1825–1829 (2014).

182. Kim, C. K. *et al.* Simultaneous fast measurement of circuit dynamics at multiple sites across the mammalian brain. *Nat. Methods* 13, 325–8 (2016).
183. Waggoner, A.S., Grinvald, A. Mechanisms of rapid optical changes of potential sensitive dyes. *NY Acad. Sci.* 30, 217–241 (1977).
184. Gupta, R. K. *et al.* Improvements in optical methods for measuring rapid changes in membrane potential. *J. Membr. Biol.* (1981). doi:10.1007/BF01870975
185. Shoham, D. *et al.* Imaging cortical dynamics at high spatial and temporal resolution with novel blue voltage-sensitive dyes. *Neuron* (1999). doi:10.1016/S0896-6273(00)81027-2
186. Petersen, C. C. H. & Sakmann, B. Functionally Independent Columns of Rat Somatosensory Barrel Cortex Revealed with Voltage-Sensitive Dye Imaging. *J. Neurosci.* (2001). doi:10.1523/JNEUROSCI.21-21-08435.2001
187. Jin, W., Zhang, R. J. & Wu, J. Y. Voltage-sensitive dye imaging of population neuronal activity in cortical tissue. *J. Neurosci. Methods* 115, 13–27 (2002).
188. Laaris, N. & Keller, A. Functional Independence of Layer IV Barrels. *J Neurophysiol* (2002). doi:10.1152/jn.00512.2001
189. Carlson, G. C. & Coulter, D. A. In vitro functional imaging in brain slices using fast voltage- sensitive dye imaging combined with whole-cell patch recording. *Nat Protoc.* 148, 825–832 (2008).
190. Berger, T. *et al.* Combined Voltage and Calcium Epifluorescence Imaging In Vitro and In Vivo Reveals Subthreshold and Suprathreshold Dynamics of Mouse Barrel Cortex. *J. Neurophysiol.* 97, 3751–3762 (2007).
191. Michinori Kubota, Y. H. and J. H. Layer-specific short-term dynamics in network activity in the cerebral cortex. *Neuroreport* 17, 1107–1110 (2006).
192. Petersen, C. C. H., Grinvald, A. & Sakmann, B. Spatiotemporal dynamics of sensory responses in layer 2/3 of rat barrel cortex measured in vivo by voltage-sensitive dye imaging combined with whole-cell voltage recordings and neuron reconstructions. *J. Neurosci.* (2003). doi:10.1523/JNEUROSCI.23-04-01298.2003
193. Brown, C.E., Aminoltejari, K., Erb, H., Winship, I.R., Murphy, T. H. In Vivo Voltage-Sensitive Dye Imaging in Adult Mice Reveals That Somatosensory Maps Lost to Stroke Are Replaced over Weeks by New Structural and Functional Circuits with Prolonged Modes of Activation within Both the Peri-Infarct Zone and Distant Sites. *J. Neurosci.* 29, 1719–1734 (2009).
194. Spors, H. & Grinvald, A. Spatio-temporal dynamics of odor representations in the mammalian olfactory bulb. *Neuron* (2002). doi:10.1016/S0896-6273(02)00644-X
195. Orbach, H.S., Cohen, L. B. Optical monitoring of activity from many areas of the in vitro and in vivo salamander olfactory bulb: a new method for studying functional organization in the vertebrate central nervous system. *J. Neurosci.* 3, 2251–2262 (1983).
196. Tominaga, T., Kajiwara, R. & Tominaga, Y. VSD Imaging Method of Ex Vivo Brain Preparation. *J. Neurosci. Neuroengineering* 2, 211–219 (2013).
197. Kuhn, B., Denk, W. & Bruno, R. M. In vivo two-photon voltage-sensitive dye imaging reveals top-down control of cortical layers 1 and 2 during wakefulness. *Proc. Natl. Acad. Sci.* (2008). doi:10.1073/pnas.0802462105
198. Lippert, M. T., Takagaki, K., Xu, W., Huang, X. & Wu, J. Y. Methods for voltage-sensitive dye imaging of rat cortical activity with high signal-to-noise ratio. *J. Neurophysiol.* 98, 502–12 (2007).

199. Canepari, M. & Zecevic, D. Membrane potential imaging in the nervous system. (2010).
200. Cohen, L. B. & Salzberg, B. M. Optical measurement of membrane potential. *Reviews of Physiology, Biochemistry and Pharmacology* 83, (1978). doi:10.1007/3-540-08907-1_2
201. Peterka, D. S., Takahashi, H. & Yuste, R. Imaging Voltage in Neurons. *Neuron* 69, 9–21 (2011).
202. Hanslmayr, S., Matuschek, J. & Fellner, M. C. Entrainment of prefrontal beta oscillations induces an endogenous echo and impairs memory formation. *Curr. Biol.* (2014). doi:10.1016/j.cub.2014.03.007
203. Romei, V., Gross, J. & Thut, G. On the Role of Prestimulus Alpha Rhythms over Occipito-Parietal Areas in Visual Input Regulation: Correlation or Causation? *J. Neurosci.* (2010). doi:10.1523/JNEUROSCI.0160-10.2010
204. Fröhlich, F. & McCormick, D. A. Endogenous electric fields may guide neocortical network activity. *Neuron* (2010). doi:10.1016/j.neuron.2010.06.005
205. Neuling, T., Rach, S. & Herrmann, C. S. Orchestrating neuronal networks: sustained after-effects of transcranial alternating current stimulation depend upon brain states. *Front. Hum. Neurosci.* (2013). doi:10.3389/fnhum.2013.00161
206. Lindén, H. *et al.* Modeling the spatial reach of the LFP. *Neuron* 72, 859–872 (2011).
207. Tucker, D. M. Spatial sampling of head electrical fields: the geodesic sensor net. *Electroencephalogr. Clin. Neurophysiol.* (1993). doi:10.1016/0013-4694(93)90121-B
208. Ebersole, J. S. & Ebersole, S. M. Combining MEG and EEG source modeling in epilepsy evaluations. *Journal of Clinical Neurophysiology* (2010). doi:10.1097/WNP.0b013e318201ffc4
209. Dutrochet, M. H. Recherches anatomiques et physiologique sur la structure intime des animaux et des végétaux et sur leur motilité. *J. B. Baillière, Paris* (1824). doi:10.5962/bhl.title.117365
210. Remak, R. Vorlaüfige Mittheilung microscopischer Beobachtungen über den innern Bau der Cerebrospinalnerven und über die Entwicklung ihrer Formelemente. *Müllers Arch Anat Physiol wiss Med*, 145–161 (1836).
211. Virchow, R. Die Cellularpathologie in ihrer Begründung auf physiologische and pathologische Gewebelehre. *Berlin: Hirschwald.* (1858).
212. J, H. & F, M. Über die sogenannte Bindesubstanz der Centralorgane des Nervensystems. *Z Med* 34, 49–82 (1869).
213. Golgi, C. Sulla sostanza connettiva del cervello (nevroglia). *Rend. del R Inst. Lomb. di Sci. e Lett.* 3, 275–277 (1870).
214. Carl, W. Beiträge zur Kenntnis der normalen menschlichen Neuroglia. *Festschrift zum fünfzigjährigen Jubiläum des ärztlichen Vereins zu Frankfurt a.M.* 3, (1895).
215. Ramon y Cajal, S. Estructura de los centros nerviosos de las aves. *Rev Trimest Histol Norm Patol* 1, 305–315 (1888).
216. Ramon y Cajal, S. Contribucion al conocimiento de la neurologia del cerebro humano. *Trab. del Lab. Investig. Biol. la Univ. Madrid* XI, 255–315 (1913).
217. L, G. De viribus electricitatis in motu musculari commentarius. *Bol. Ex Typogr. Instituti Sci.* (1791).
218. G, V. Über den Verlauf und die letzten Enden der Nerven. *Nov. Acta Phys-Med Acad Leopoldina, Breslau* 18, 51–240 (1836).
219. Deiters, O. Untersuchungen über Gehirn und Rückenmark des Menschen und der Säugethiere. *Vieweg.* (1865).

220. C, G. Sulla fina struttura dei bulbi olfattori. *Riv sper Freniatr. Med Leg.* 1, 66–78 (1875).
221. Del, R.-H. P. Notas técnicas. Noticia de un nuevo y fácil método para la coloración de la neuroglia y del tejido conjuntivo. *Trab Lab Invest Biol Univ Madrid* XV, 367–378 (1917).
222. Allen, N. J. & Barres, B. a. Neuroscience: Glia - more than just brain glue. *Nature* 457, 675–677 (2009).
223. del Rio-Horgega, P. El "tercer elemento" de los centros nerviosos. I. La microglía en estado normal. *Bol Soc Esp Biol* (1919).
224. del Rio-Horgega, P. Microglia. *Cytology and cellular pathology of the nervous system. New York: Hoeber*, 482–534 (1932).
225. Cunningham, C. Microglia and neurodegeneration: The role of systemic inflammation. *Glia* 61, 71–90 (2013).
226. Soyon Hong, Victoria F Beja-Glasser, Bianca M Nfonoyim, Arnaud Frouin, Shaomin Li, Saranya Ramakrishnan, Katherine M Merry, Qiaoqiao Shi, Arnon Rosenthal, Ben A Barres, Cynthia A Lemere, Dennis J Selkoe and B. S. Complement and microglia mediate early synapse loss in Alzheimer mouse models. *Science* 352, 712-716 (2016). doi:10.1126/science.aad8373
227. Robertson, W. On a new method of obtaining a black reaction in certain tissue-elements of the central nervous system (platinum method). *Scott Med Surg J* 4, 23–30 (1899).
228. del Rio-Horgega, P. Son homologables la glía de escasas radiaciones y la célula de Schwann. *Boletín la Soc. Española Biol.* 10, 25–28 (1922).
229. Penfield, W. Oligodendroglia and its relation to classical neuroglia. *Brain* (1924). doi:10.1093/brain/47.4.430
230. Chang, K., Redmond, S. A., Chan, J. R., Francisco, S. & Francisco, S. Remodeling myelination: implications for mechanisms of neural plasticity. 19, 190–197 (2016).
231. Moll, N. M. *et al.* SOX17 is expressed in regenerating oligodendrocytes in experimental models of demyelination and in multiple sclerosis. *Glia* 61, 1659–1672 (2013).
232. Nishiyama, A., Watanabe, M., Yang, Z. & Bu, J. Identity, distribution, and development of polydendrocytes: NG2-expressing glial cells. *J. Neurocytol.* 31, 437–455 (2002).
233. Peters, A. A fourth type of neuroglial cell in the adult central nervous system. *J. Neurocytol.* (2004). doi:10.1023/B:NEUR.0000044195.64009.27
234. Nishiyama, A., Komitova, M., Suzuki, R. & Zhu, X. Polydendrocytes (NG2 cells): Multifunctional cells with lineage plasticity. *Nature Reviews Neuroscience* (2009). doi:10.1038/nrn2495
235. Lenhossek M von. Der feinere Bau des Nervensystems im Lichte neuester Forschung. *Berlin Fischer's Med. Buchhandlung.* (1893).
236. Golgi, C. Contribuzione alla fina anatomia degli organi centrali del sistema nervoso. *Riv. clin.* 11, 338–350 (1871).
237. Kölliker. Handbuch der Gewebelehre des Menschen. *Gewebelehre des Menschen.* (1889).
238. Andriezen, W. The neuroglia elements of the brain. *Br Med J* 2, 227–230 (1893).
239. Butt, A. M., Colquhoun, K. & Berry, M. Confocal imaging of glial cells in the intact rat optic nerve. *Glia* (1994). doi:10.1002/glia.440100410
240. Oberheim, N. A. *et al.* Uniquely Hominid Features of Adult Human Astrocytes. *J. Neurosci.* 29, 3276–3287 (2009).
241. Raine, C. S. On the association between perinodal astrocytic processes and the node of Ranvier in the C.N.S. *J. Neurocytol.* 13, 21–27 (1984).

242. Peters, A., Palay, S. L. & Webster, H. The fine structure of the nervous system. *Journal of Neuropathology & Experimental Neurology* (1991). doi:10.1001/archneur.1970.00480240094019
243. Ramon y Cajal, S. Histologie du Systeme Nerveux de l'Homme et des Vertebres. Maloine, Paris: 1911. Tome I. *Demography* (1909). doi:10.5962/bhl.title.48637
244. Araque, A., Parpura, V., Sanzgiri, R. P. & Haydon, P. G. Tripartite synapses: Glia, the unacknowledged partner. *Trends in Neurosciences* 22, 208–215 (1999).
245. Oberheim, N. A., Wang, X., Goldman, S. & Nedergaard, M. Astrocytic complexity distinguishes the human brain. *Trends Neurosci.* (2006). doi:10.1016/j.tins.2006.08.004
246. Bushong, E. a, Martone, M. E., Jones, Y. Z. & Ellisman, M. H. Protoplasmic astrocytes in CA1 stratum radiatum occupy separate anatomical domains. *J. Neurosci.* 22, 183–192 (2002).
247. Cameron, H. A., Woolley, C. S., McEwen, B. S. & Gould, E. Differentiation of newly born neurons and glia in the dentate gyrus of the adult rat. *Neuroscience* (1993). doi:10.1016/0306-4522(93)90335-D
248. Seri, B., García-Verdugo, J. M., Collado-Morente, L., McEwen, B. S. & Alvarez-Buylla, A. Cell types, lineage, and architecture of the germinal zone in the adult dentate gyrus. *J. Comp. Neurol.* (2004). doi:10.1002/cne.20288
249. Alvarez-Buylla, A. & Temple, S. Stem cells in the developing and adult nervous system. *J Neurobiol* 36, 105–10 (1998).
250. Malatesta, P., Hartfuss, E. & Götz, M. Isolation of radial glial cells by fluorescent-activated cell sorting reveals a neuronal lineage. *Development* 127, 5253-63 (2000). doi:10.1109/ISCC.2005.107
251. Rakic, P. Mode of cell migration to the superficial layers of fetal monkey neocortex. *J. Comp. Neurol.* (1972). doi:10.1002/cne.901450105
252. Kriegstein, A. R. & Noctor, S. C. Patterns of neuronal migration in the embryonic cortex. *Trends in Neurosciences* (2004). doi:10.1016/j.tins.2004.05.001
253. Noctor, S. C., Flint, A. C., Weissman, T. A., Dammerman, R. S. & Kriegstein, A. R. Neurons derived from radial glial cells establish radial units in neocortex. *Nature* (2001). doi:10.1038/35055553
254. Rakic, P. Neurons in rhesus monkey visual cortex: Systematic relation between time of origin and eventual disposition. *Science* 183, 425-7 (1974). doi:10.1126/science.183.4123.425
255. Rakic, P. Specification of cerebral cortical areas. *Science* 241, 170-6 (1988). doi:10.1126/science.3291116
256. Rakic, P. Evolution of the neocortex: A perspective from developmental biology. *Nature Reviews Neuroscience* (2009). doi:10.1038/nrn2719
257. Angevine, J. B. & Sidman, R. L. Autoradiographic study of cell migration during histogenesis of cerebral cortex in the mouse. *Nature* (1961). doi:10.1038/192766b0
258. Zecevic, N. & Rakic, P. Development of layer I neurons in the primate cerebral cortex. *J. Neurosci.* (2001). doi:21/15/5607 [pii]
259. Rakic, P. Pre- and post-developmental neurogenesis in primates. *Clinical Neuroscience Research* (2002). doi:10.1016/S1566-2772(02)00005-1
260. Levitt, P. & Rakic, P. Immunoperoxidase localization of glial fibrillary acidic protein in radial glial cells and astrocytes of the developing rhesus monkey brain. *J. Comp. Neurol.* (1980). doi:10.1002/cne.901930316

261. Schmechel, D. E. & Rakic, P. A golgi study of radial glial cells in developing monkey telencephalon: Morphogenesis and transformation into astrocytes. *Anat. Embryol. (Berl).* (1979). doi:10.1007/BF00300010
262. Newman, E. & Reichenbach, A. The Muller cell: A functional element of the retina. *Trends in Neurosciences* (1996). doi:10.1016/0166-2236(96)10040-0
263. Palay, S. L. & Chan-Palay, V. Cerebellar Cortex: cytology and organization. *Springer-Verlag* (1974). doi:10.1007/978-3-642-65581-4
264. Hatton, G. I. Pituicytes, glia and control of terminal secretion. *J Exp Biol* (1988).
265. Malatesta, P. *et al.* Neuronal or glial progeny: Regional differences in radial glia fate. *Neuron* (2003). doi:10.1016/S0896-6273(03)00116-8
266. Hewett, J. A. Determinants of regional and local diversity within the astroglial lineage of the normal central nervous system. *Journal of Neurochemistry* (2009). doi:10.1111/j.1471-4159.2009.06288.x
267. Levison, S. W. & Goldman, J. E. Both oligodendrocytes and astrocytes develop from progenitors in the subventricular zone of postnatal rat forebrain. *Neuron* (1993). doi:10.1016/0896-6273(93)90311-E
268. Doetsch, F., García-Verdugo, J. M. & Alvarez-Buylla, A. Cellular Composition and Three-Dimensional Organization of the Subventricular Germinal Zone in the Adult Mammalian Brain. *J. Neurosci.* (1997). doi:10.1523/JNEUROSCI.17-13-05046.1997
269. Zhu, X., Hill, R. A. & Nishiyama, A. NG2 cells generate oligodendrocytes and gray matter astrocytes in the spinal cord. *Neuron Glia Biol.* (2008). doi:10.1017/S1740925X09000015
270. Oberheim, N. A., Goldman, S. A. & Nedergaard, M. Heterogeneity of Astrocytic Form and Function. *Methods Mol Biol* 814, 23–45 (2012).
271. Butt, A. M., Colquhoun, K., Tutton, M. & Berry, M. Three-dimensional morphology of astrocytes and oligodendrocytes in the intact mouse optic nerve. *J. Neurocytol.* 23, 469–485 (1994).
272. Butt, A. M., Kiff, J., Hubbard, P. & Berry, M. Synantocytes: New functions for novel NG2 expressing glia. *J. Neurocytol.* 31, 551–65 (2002).
273. Awasaki, T., Lai, S.-L., Ito, K. & Lee, T. Organization and Postembryonic Development of Glial Cells in the Adult Central Brain of Drosophila. *J. Neurosci.* (2008). doi:10.1523/JNEUROSCI.4844-08.2008
274. Doherty, J., Logan, M. A., Tasdemir, O. E. & Freeman, M. R. Ensheathing Glia Function as Phagocytes in the Adult Drosophila Brain. *J. Neurosci.* (2009). doi:10.1523/JNEUROSCI.5951-08.2009
275. Bass, N. H., Hess, H. H., Pope, A. & Thalheimer, C. Quantitative cytoarchitectonic distribution of neurons, glia, and DNA in rat cerebral cortex. *J. Comp. Neurol.* (1971). doi:10.1002/cne.901430405
276. R, F. Quantitative share of the glia in development of the cortex. *Acta Anat* 20, 290–6 (1954).
277. Hawkins, A. & Olszewski, J. Glia/nerve cell index for cortex of the whale. *Science* 126, 76-7 (1957). doi:10.1126/science.126.3263.76
278. Karbowski, J. Global and regional brain metabolic scaling and its functional consequences. *BMC Biol.* (2007). doi:10.1186/1741-7007-5-18
279. Tower, D. B. Structural and functional organization of mammalian cerebral cortex: The correlation of neurone density with brain size. Cortical neurone density in the fin whale

(Balaenoptera Physalus L.) with a note on the cortical neurone density in the Indian elephan. *J. Comp. Neurol.* (1954). doi:10.1002/cne.901010103
280. Nissl, F. Nervenzellen und graue Substanz. *Muench Med Wehnschr* 1023–1060 (1898).
281. Glees, P. The biology of the neuroglia: a summary. in *Biology of neuroglia. Springfield, IL: Charles C Thomas* 234–242 (1958).
282. Hydén, H. The neuron. *The cell: biochemistry, physiology, morphology*. *New York: Academic Press* 215–323 (1960).
283. Attwell, D. & Laughlin, S. B. An energy budget for signaling in the grey matter of the brain. *Journal of Cerebral Blood Flow and Metabolism* (2001). doi:10.1097/00004647-200110000-00001
284. Zhang, K. & Sejnowski, T. J. A universal scaling law between gray matter and white matter of cerebral cortex. *Proc. Natl. Acad. Sci.* (2000). doi:10.1073/pnas.090504197
285. Herculano-Houzel, S., Mota, B. & Lent, R. Cellular scaling rules for rodent brains. *Proc. Natl. Acad. Sci.* (2006). doi:10.1073/pnas.0604911103
286. Herculano-Houzel, S., Collins, C. E., Wong, P. & Kaas, J. H. Cellular scaling rules for primate brains. *Proc. Natl. Acad. Sci.* (2007). doi:10.1073/pnas.0611396104
287. Terry, R. D., DeTeresa, R. & Hansen, L. A. Neocortical cell counts in normal human adult aging. *Ann. Neurol.* (1987). doi:10.1002/ana.410210603
288. Pelvig, D. P., Pakkenberg, H., Stark, A. K. & Pakkenberg, B. Neocortical glial cell numbers in human brains. *Neurobiol. Aging* 29, 1754–1762 (2008).
289. Glees, P. Neuroglia. Morphology and function. *Postgrad. Med. J.* (1955).
290. Herculano-Houzel, S. Isotropic Fractionator: A Simple, Rapid Method for the Quantification of Total Cell and Neuron Numbers in the Brain. *J. Neurosci.* (2005). doi:10.1523/JNEUROSCI.4526-04.2005
291. Nurnberger JI, G. M. The cell density of neural tissues: direct counting method and possible applications as a biologic referent. *Prog Neurobiol* 2, 100–128 (1957).
292. Repetto, I. E. *et al.* The Isotropic Fractionator as a Tool for Quantitative Analysis in Central Nervous System Diseases. *Front. Cell. Neurosci.* 10, 190 (2016). doi:10.3389/fncel.2016.00190
293. Azevedo, F. A. C. *et al.* Equal numbers of neuronal and nonneuronal cells make the human brain an isometrically scaled-up primate brain. *J. Comp. Neurol.* (2009). doi:10.1002/cne.21974
294. Blinkov, S. M. & Glezer, I. I. The Human Brain in Figures and Tables. *PsycCRITIQUES* (1968). doi:10.1037/0010366
295. Haug, H. History of neuromorphometry. *J. Neurosci. Methods* (1986). doi:10.1016/0165-0270(86)90110-X
296. Haug, H. Brain sizes, surfaces, and neuronal sizes of the cortex cerebri: A stereological investigation of man and his variability and a comparison with some mammals (primates, whales, marsupials, insectivores, and one elephant). *Am. J. Anat.* (1987). doi:10.1002/aja.1001800203
297. Herculano-Houzel, S. The glia/neuron ratio: How it varies uniformly across brain structures and species and what that means for brain physiology and evolution. *Glia* 62, 1377–1391 (2014).
298. Ribeiro PFM, Ventura-Antunes L, Gabi M, Mota B, Grinberg LT, F. J. & Ferretti-Rebustini REL, Leite REP, Jacob Filho W, H.-H. S. The human cerebral cortex is neither one nor many: Neuronal distribution reveals two quantitatively different zones in the gray

matter, three in the white matter, and explains local variations in cortical folding. *Front Neuroanat* 7, 28 (2013).
299. Herculano-Houzel, S. Scaling of brain metabolism with a fixed energy budget per neuron: Implications for neuronal activity, plasticity and evolution. *PLoS One* 6, e17524 (2011). doi:10.1371/journal.pone.0017514
300. Reichenbach, A. Glia:Neuron index: Review and hypothesis to account for different values in various mammals. *Glia* (1989). doi:10.1002/glia.440020202
301. Han, X. *et al.* Forebrain engraftment by human glial progenitor cells enhances synaptic plasticity and learning in adult mice. *Cell Stem Cell* (2013). doi:10.1016/j.stem.2012.12.015
302. Ramon y Cajal, S. Algunas conjeturas sobre el mecanismo anatomico de la ideacion, asociacion y atencion. *Imprenta y Libr. Nicolas Moya* 3–14 (1895).
303. Ramon y Cajal, S. Algo sobre la significación fisiológica de la neuroglia. *Rev. Trimest. Microgr.* 1, 3–47 (1897).
304. Wang F, Smith NA, Xu Q, Fujita T, Baba A, Matsuda T, Takano T, Bekar L, N. M. Astrocytes Modulate Neural Network Activity by Ca^{2+}-Dependent Uptake of Extracellular K^{+}. *Sci Signal* 5, (2012).
305. Bellot-Saez, A., Kékesi, O., Morley, J. W. & Buskila, Y. Astrocytic modulation of neuronal excitability through K^{+} spatial buffering. *Neurosci. Biobehav. Rev.* (2017). doi:10.1016/j.neubiorev.2017.03.002
306. Ullian, E. M., Sapperstein, S. K., Christopherson, K. S. & Barres, B. A. Control of synapse number by glia. *Science* 291, 657-61 (2001). doi:10.1126/science.291.5504.657
307. Magistretti, P. J. Neuron-glia metabolic coupling and plasticity. *J Exp Biol* 209, 2304–2311 (2006).
308. Buskila, Y. & Amitai, Y. Astrocytic iNOS-Dependent Enhancement of Synaptic Release in Mouse Neocortex. *J. Neurophysiol.* 103, 1322-8 (2010). doi:10.1152/jn.00676.2009
309. Fields, R. D. New Insights into Neuron-Glia Communication. *Science* 298, 556-62 (2002). doi:10.1126/science.298.5593.556
310. Suzuki, A. *et al.* Astrocyte-neuron lactate transport is required for long-term memory formation. *Cell* 44, 810-23 (2011). doi:10.1016/j.cell.2011.02.018
311. Pekny, M. & Pekna, M. Astrocyte intermediate filaments in CNS pathologies and regeneration. *J Pathol* 204, 428–437 (2004).
312. Ling, E. A., Paterson, J. A., Privat, A., Mori, S. & Leblond, C. P. Investigation of glial cells in semithin sections. I. Identification of glial cells in the brain of young rats. *J. Comp. Neurol.* (1973). doi:10.1002/cne.901490104
313. Doetsch, F., Caille, I., Lim, D. A., Garcia-Verdugo, J. M. & Alvarez-Buylla, A. Subventricular zone astrocytes are neural stem cells in the adult mammalian brain. *Cell* (1999). doi:10.1016/S0092-8674(00)80783-7
314. Eng LF, Gerstl B, V. J. A study of proteins in old multiple sclerosis plaques. *Trans Am Soc Neurochem.* 1–42 (1970).
315. Sofroniew, M. V. Molecular dissection of reactive astrogliosis and glial scar formation. *Trends Neurosci.* 32, 638–647 (2009).
316. Bush, T. G. *et al.* Fulminant jejuno-ileitis following ablation of enteric gila in adult transgenic mice. *Cell* (1998). doi:10.1016/S0092-8674(00)81571-8
317. Herrmann, J. E. *et al.* STAT3 is a Critical Regulator of Astrogliosis and Scar Formation after Spinal Cord Injury. *J. Neurosci.* (2008). doi:10.1523/JNEUROSCI.1709-08.2008

318. Bellot, A., Guivernau, B., Tajes, M. & Mun, F. J. The structure and function of actin cytoskeleton in mature glutamatergic dendritic spines. *Brain Res* 1573, 1–16 (2014).
319. Murk, K., Suarez, E. M. B., Cockbill, L. M. R., Banks, P. & Hanley, J. G. The antagonistic modulation of Arp2/3 activity by N-WASP , WAVE2 and PICK1 defines dynamic changes in astrocyte morphology. *J Cell Sci* 126, 3873–83 (2013).
320. Boukhelifa, M. *et al.* A critical role for palladin in astrocyte morphology and response to injury. *Mol Cell Neurosci* 23, 661–668 (2003).
321. Pekny, M. *et al.* Mice lacking glial fibrillary acidic protein display astrocytes devoid of intermediate filaments but develop and reproduce normally. *EMBO J* 14, 1590–1598 (1995).
322. Middeldorp, J. & Hol, E. M. GFAP in health and disease. *Prog. Neurobiol.* 93, 421–443 (2011).
323. Eddleston, M. & Mucke, L. Molecular profile of reactive astrocytes-Implications for their role in neurologic disease. *Neuroscience* (1993). doi:10.1016/0306-4522(93)90380-X
324. Wilhelmsson, U. *et al.* Redefining the concept of reactive astrocytes as cells that remain within their unique domains upon reaction to injury. *Proc. Natl. Acad. Sci.* 103, 17513-8 (2006). doi:10.1073/pnas.0602841103
325. Oberheim, N. A. *et al.* Loss of astrocytic domain organization in the epileptic brain. *J. Neurosci.* 28, 3264–76 (2008).
326. Garcia, A. D. R., Petrova, R., Eng, L. & Joyner, A. L. Sonic Hedgehog Regulates Discrete Populations of Astrocytes in the Adult Mouse Forebrain. *J. Neurosci.* 30, 13597-608 (2010). doi:10.1523/JNEUROSCI.0830-10.2010
327. Alexander, W. S. Progressive fibrinoid degeneration of fibrillary astrocytes associated with mental retardation in a hydrocephalic infant. *Brain* (1949). doi:10.1093/brain/72.3.373
328. Brenner, M. *et al.* Mutations in GFAP, encoding glial fibrillary acidic protein, are associated with Alexander disease. *Nat. Genet.* 27, 117-20 (2001). doi:10.1038/83679
329. Matyash, V. & Kettenmann, H. Heterogeneity in astrocyte morphology and physiology. *Brain Research Reviews* 63, 2–10 (2010).
330. Larsen, B. R. & MacAulay, N. Kir4.1-mediated spatial buffering of K^+: Experimental challenges in determination of its temporal and quantitative contribution to K^+ clearance in the brain. *Channels* 8, 544-550 (2014). doi:10.4161/19336950.2014.970448
331. Giaume, C. & Theis, M. Pharmacological and genetic approaches to study connexin-mediated channels in glial cells of the central nervous system. *Brain Res Rev* 63, 160–176 (2010).
332. Haydon, P. G. & Carmignoto, G. Astrocyte Control of Synaptic Transmission and Neurovascular Coupling. *Physiol Rev* 86, 1009–1031 (2006).
333. Lalo, U., Pankratov, Y., Kirchhoff, F., North, R. A. & Verkhratsky, A. NMDA Receptors Mediate Neuron-to-Glia Signaling in Mouse Cortical Astrocytes. *J. Neurosci.* 26, 2673–2683 (2006).
334. Tsuzuki, K. & Ishiuchi, S. GluR2 expressed by glial fibrillary acidic protein promoter decreases the number of neurons. *Front Biosci.* 13, 2784-96 (2008). doi:10.2741/2885
335. Wang, X. *et al.* Astrocytic Ca^{2+} signaling evoked by sensory stimulation in vivo. *Nat. Neurosci.* 9, 816–23 (2006).
336. Neary, J. T. *et al.* Mitogenic signaling by ATP/P2Y purinergic receptors in astrocytes: involvement of a calcium-independent protein kinase C, extracellular signal-regulated

protein kinase pathway distinct from the phosphatidylinositol-specific phospholipase C/calcium pathway. *J. Neurosci.* 19, 4211–4220 (1999).
337. Rosier, A., Arckens, L., Orban, G. A. & Vandesande, F. Immunocytochemical detection of astrocyte GABAA receptors in cat visual cortex. *J Histochem Cytochem* (1993).
338. Oikawa, H., Nakamichi, N., Kambe, Y., Ogura, M. & Yoneda, Y. An increase in intracellular free calcium ions by nicotinic acetylcholine receptors in a single cultured rat cortical astrocyte. *J. Neurosci. Res.* 79, 535-44 (2005). doi:10.1002/jnr.20398
339. Amar, M., Lucas-Meunier, E., Baux, G. & Fossier, P. Blockade of different muscarinic receptor subtypes changes the equilibrium between excitation and inhibition in rat visual cortex. *Neuroscience* 169, 1610–1620 (2010).
340. Hirst, W. D., Cheung, N. Y., Rattray, M., Price, G. W. & Wilkin, G. P. Cultured astrocytes express messenger RNA for multiple serotonin receptor subtypes, without functional coupling of 5-HT1 receptor subtypes to adenylyl cyclase. *Mol. Brain Res.* (1998). doi:10.1016/S0169-328X(98)00206-X
341. Jurič, D. M., Mele, T. & Čarman-Kržan, M. Involvement of histaminergic receptor mechanisms in the stimulation of NT-3 synthesis in astrocytes. *Neuropharmacology* 60, 1309-17 (2011). doi:10.1016/j.neuropharm.2011.01.019
342. Thorlin, T., Eriksson, P. S., Rönnbäck, L. & Hansson, E. Receptor-activated Ca^{2+} increases in vibrodissociated cortical astrocytes: A nonenzymatic method for acute isolation of astrocytes. *J. Neurosci. Res.* (1998). doi:10.1002/(SICI)1097-4547(19981101)54:3<390::AID-JNR10>3.0.CO;2-#
343. Quach, T. T., Duchemin, A. M., Rose, C. & Schwartz, J. C. [3H]glycogenolysis in brain slices mediated by β-adrenoceptors: Comparison of physiological response and [3H]dihydroalprenolol binding parameters. *Neuropharmacology* (1988). doi:10.1016/0028-3908(88)90185-2
344. Reuss, B. & Unsicker, K. Atypical neuroleptic drugs downregulate dopamine sensitivity in rat cortical and striatal astrocytes. *Mol. Cell. Neurosci.* 18, 197-209 (2001). doi:10.1006/mcne.2001.1017
345. Walz, W., Wuttke, W. & Hertz, L. Astrocytes in primary cultures: Membrane potential characteristics reveal exclusive potassium conductance and potassium accumulator properties. *Brain Res.* 292, 367–374 (1984).
346. McKhann, G. M., D'Ambrosio, R. & Janigro, D. Heterogeneity of astrocyte resting membrane potentials and intercellular coupling revealed by whole-cell and gramicidin-perforated patch recordings from cultured neocortical and hippocampal slice astrocytes. *J. Neurosci.* (1997). doi:MO1
347. Djukic, B., Casper, K. B., Philpot, B. D., Chin, L. & Mccarthy, K. D. Conditional Knock-Out of Kir 4.1 Leads to Glial Membrane Depolarization , Inhibition of Potassium and Glutamate Uptake, and Enhanced Short-Term Synaptic Potentiation. *J Neurosci* 27, 11354–11365 (2007).
348. Kucheryavykh, Y. V, Kucheryavykh, L. Y., Nichols, C. G., Maldonado, H. M. & Baksi, K. Downregulation of Kir4.1 Inward Rectifying Potassium Channel Subunits by RNAi Impairs Potassium Transfer and Glutamate Uptake by Cultured Cortical Astrocytes. *Glia* 281, 274–281 (2007).
349. Bordey, A. & Sontheimer, H. Properties of human glial cells associated with epileptic seizure foci. *Epilepsy Res.* 32, 286-303 (1998). doi:10.1016/S0920-1211(98)00059-X

350. Buono, R. J. *et al.* Association between variation in the human KCNJ10 potassium ion channel gene and seizure susceptibility. *Epilepsy Res.* 58, 175-83 (2004). doi:10.1016/j.eplepsyres.2004.02.003
351. Kaiser, M. *et al.* Progressive loss of a glial potassium channel (KCNJ10) in the spinal cord of the SOD1 (G93A) transgenic mouse model of amyotrophic lateral sclerosis. *J. Neurochem.* 99, 900-12 (2006). doi:10.1111/j.1471-4159.2006.04131.x
352. Wilcock, D. M., Vitek, M. P. & Colton, C. A. Vascular amyloid alters astrocytic water and potassium channels in mouse models and humans with Alzheimer's disease. *Neuroscience* 159, 1055-69 (2009). doi:10.1016/j.neuroscience.2009.01.023
353. Tong, X. *et al.* Astrocyte Kir4.1 ion channel deficits contribute to neuronal dysfunction in Huntington's disease model mice. *Nat. Neurosci.* 17, 694–703 (2014).
354. Ulbricht, E. *et al.* Proliferative gliosis causes mislocation and inactivation of inwardly rectifying K^+ (Kir) channels in rabbit retinal glial cells. *Exp. Eye Res.* (2008). doi:10.1016/j.exer.2007.11.002
355. Higashimori, H. & Sontheimer, H. Role of Kir4.1 channels in growth control of glia. *Glia* 55, 1668-79 (2007). doi:10.1002/glia.20574
356. Barres, B. A., Chun, L. L. & Corey, D. P. Calcium current in cortical astrocytes: induction by cAMP and neurotransmitters and permissive effect of serum factors. *J. Neurosci.* 9, 3169-75 (1989). doi:10.1523/JNEUROSCI.09-09-03169.1989
357. Carmignoto, G., Pasti, L. & Pozzan, T. On the role of voltage-dependent calcium channels in calcium signaling of astrocytes in situ. *J. Neurosci.* 18, 4637-45 (1998). doi:10.1523/JNEUROSCI.18-12-04637.1998
358. Bevan, S., Chiu, S. Y., Gray, P. T. A. & Ritchie, J. M. The presence of voltage-gated sodium, potassium and chloride channels in rat cultured astrocytes. *Proc. R. Soc. London - Biol. Sci.* (1985). doi:10.1098/rspb.1985.0063
359. Berger, T., Schnitzer, J., Orkand, P. M. & Kettenmann, H. Sodium and Calcium Currents in Glial Cells of the Mouse Corpus Callosum Slice. *Eur. J. Neurosci.* (1992). doi:10.1111/j.1460-9568.1992.tb00153.x
360. Black, J. A., Westenbroek, R., Ransom, B. R., Catterall, W. A. & Waxman, S. G. Type II sodium channels in spinal cord astrocytes in situ: Immunocytochemical observations. *Glia* (1994). doi:10.1002/glia.440120307
361. Steinhäuser, C., Kressin, K., Kuprijanova, E., Weber, M. & Seifert, G. Properties of voltage-activated Na^+ and K^+ currents in mouse hippocampal glial cells in situ and after acute isolation from tissue slices. *Pflügers Arch. Eur. J. Physiol.* 428, 610-20 (1994). doi:10.1007/BF00374585
362. Rose, C. R. & Verkhratsky, A. Principles of sodium homeostasis and sodium signalling in astroglia. *Glia* 64, 1611-27 (2016). doi:10.1002/glia.22964
363. Minelli, A. *et al.* Cellular and subcellular localization of Na^+-Ca^{2+}exchanger protein isoforms, NCX1, NCX2, and NCX3 in cerebral cortex and hippocampus of adult rat. *Cell Calcium* 41, 221-34 (2007). doi:10.1016/j.ceca.2006.06.004
364. Juhaszova, M. & Blaustein, M. P. Na^+ pump low and high ouabain affinity alpha subunit isoforms are differently distributed in cells. *Proc. Natl. Acad. Sci. U. S. A.* (1997). doi:10.1073/pnas.94.5.1800
365. Walz, W. & Hertz, L. Ouabain-sensitive and ouabain-resistant net uptake of potassium into astrocytes and neurons in primary cultures. *J. Neurochem.* 39, 70–7 (1982).

366. Kelly, T., Kafitz, K. W., Roderigo, C. & Rose, C. R. Ammonium-evoked alterations in intracellular sodium and pH reduce glial glutamate transport activity. *Glia* 57, 921-34 (2009). doi:10.1002/glia.20817
367. Walz, W. & Hertz, L. Intense furosemide-sensitive potassium accumulation in astrocytes in the presence of pathologically high extracellular potassium levels. *J. Cereb. Blood Flow Metab.* (1984). doi:10.1038/jcbfm.1984.42
368. Pál, I., Kardos, J., Dobolyi, Á. & Héja, L. Appearance of fast astrocytic component in voltage-sensitive dye imaging of neural activity. *Mol. Brain* 8, 35 (2015).
369. Cornell-Bell, A. H., Finkbeiner, S. M., Cooper, M. S. & Smith, S. J. Glutamate induces calcium waves in cultured astrocytes: Long-range glial signaling. *Science* 247, 470-3 (1990). doi:10.1126/science.1967852
370. Shigetomi, E., Kracun, S., Sofroniew, M. V. & Khakh, B. S. A genetically targeted optical sensor to monitor calcium signals in astrocyte processes. *Nat. Neurosci.* 13, 759-66 (2010). doi:10.1038/nn.2557
371. Nett, W. J., Oloff, S. H. & McCarthy, K. D. Hippocampal Astrocytes In Situ Exhibit Calcium Oscillations That Occur Independent of Neuronal Activity. *J. Neurophysiol.* 87, 528-37 (2002). doi:10.1152/jn.00268.2001
372. Zur Nieden, R. & Deitmer, J. W. The role of metabotropic glutamate receptors for the generation of calcium oscillations in rat hippocampal astrocytes in situ. *Cereb. Cortex* 16, 676-87 (2006). doi:10.1093/cercor/bhj013
373. Takata, N. & Hirase, H. Cortical layer 1 and layer 2/3 astrocytes exhibit distinct calcium dynamics in vivo. *PLoS One* 3, (2008).
374. Lallouette, J., De Pittà, M., Ben-Jacob, E. & Berry, H. Sparse short-distance connections enhance calcium wave propagation in a 3D model of astrocyte networks. *Front. Comput. Neurosci.* 8, 45 (2014).
375. Ding, F. *et al.* α1-Adrenergic receptors mediate coordinated Ca^{2+} signaling of cortical astrocytes in awake, behaving mice. *Cell Calcium* 54, 387-94 (2013). doi:10.1016/j.ceca.2013.09.001
376. Jung, S., Pfeiffer, F. & Deitmer, J. W. Histamine-induced calcium entry in rat cerebellar astrocytes: Evidence for capacitative and non-capacitative mechanisms. *J. Physiol.* (2000). doi:10.1111/j.1469-7793.2000.00549.x
377. Jennings, A. *et al.* Dopamine elevates and lowers astroglial Ca^{2+} through distinct pathways depending on local synaptic circuitry. *Glia* 65, 447-459 (2017). doi:10.1002/glia.23103
378. Blomstrand, F. *et al.* 5-Hydroxytryptamine and glutamate modulate velocity and extent of intercellular calcium signalling in hippocampal astroglial cells in primary cultures. *Doktorsavhandlingar vid Chalmers Tek. Hogsk.* (1999). doi:10.1016/S0306-4522(98)00351-0
379. Covelo, A. & Araque, A. Neuronal activity determines distinct gliotransmitter release from a single astrocyte. *Elife* 7, e32237 (2018). doi:10.7554/eLife.32237
380. Berridge, M. J. Rapid accumulation of inositol trisphosphate reveals that agonists hydrolyse polyphosphoinositides instead of phosphatidylinositol. *Biochem. J.* (1983). doi:10.1042/bj2120849
381. De Pittà, M., Goldberg, M., Volman, V., Berry, H. & Ben-Jacob, E. Glutamate regulation of calcium and IP_3 oscillating and pulsating dynamics in astrocytes. *J. Biol. Phys.* 35, 383-411 (2009). doi:10.1007/s10867-009-9155-y

382. Siekmann, I., Cao, P., Sneyd, J. & Crampin, E. J. Data-driven modelling of the inositol trisphosphate receptor (IPR) and its role in calcium induced calcium release (CICR). 1–23 (2015).
383. Mariotti, L., Losi, G., Sessolo, M., Marcon, I. & Carmignoto, G. The inhibitory neurotransmitter GABA evokes long-lasting Ca^{2+} oscillations in cortical astrocytes. *Glia* 64, 363-73 (2016). doi:10.1002/glia.22933
384. Mariotti, L. *et al.* Interneuron-specific signaling evokes distinctive somatostatin-mediated responses in adult cortical astrocytes. *Nat. Commun.* (2018). doi:10.1038/s41467-017-02642-6
385. Stobart, J. L. *et al.* Cortical Circuit Activity Evokes Rapid Astrocyte Calcium Signals on a Similar Timescale to Neurons. *Neuron* 98, 726-735.e4 (2018).
386. Muñoz, M. F., Puebla, M. & Figueroa, X. F. Control of the neurovascular coupling by nitric oxide-dependent regulation of astrocytic Ca^{2+} signaling. *Fron Cell Neurosci* 9, 59 (2015).
387. Filosa, J. A. *et al.* Local potassium signaling couples neuronal activity to vasodilation in the brain. *Nat. Neurosci.* 9, 1397-1403 (2006). doi:10.1038/nn1779
388. Igelhorst, B. A., Niederkinkhaus, V., Karus, C., Lange, M. D. & Dietzel, I. D. Regulation of neuronal excitability by release of proteins from glial cells. *Philos. Trans. R. Soc. B Biol. Sci.* 370, 20140194 (2015). doi:10.1098/rstb.2014.0194
389. Michelucci, A. *et al.* The Neurogenic Potential of Astrocytes Is Regulated by Inflammatory Signals. *Mol. Neurobiol.* 53, 3724-3739 (2016). doi:10.1007/s12035-015-9296-x
390. Perea, G. & Araque, A. Astrocytes potentiate transmitter release at single hippocampal synapses. *Science* 317, 1083-6 (2007). doi:10.1126/science.1144640
391. Navarrete, M. *et al.* Astrocytes mediate in vivo cholinergic-induced synaptic plasticity. *PLoS Biol.* 10, e1001259 (2012). doi:10.1371/journal.pbio.1001259
392. Henneberger, C., Papouin, T., Oliet, S. H. R. & Rusakov, D. A. Long-term potentiation depends on release of d-serine from astrocytes. *Nature* (2010). doi:10.1038/nature08673
393. Jourdain, P. *et al.* Glutamate exocytosis from astrocytes controls synaptic strength. *Nat. Neurosci.* 10, 331-9 (2007). doi:10.1038/nn1849
394. Wang, F. *et al.* Photolysis of Caged Ca^{2+} But Not Receptor-Mediated Ca^{2+} Signaling Triggers Astrocytic Glutamate Release. *J. Neurosci.* (2013). doi:10.1523/JNEUROSCI.2178-13.2013
395. Sardinha, V. M. *et al.* Astrocytic signaling supports hippocampal–prefrontal theta synchronization and cognitive function. *Glia* 65, 1944–1960 (2017).
396. Adar Adamsky, Adi Kol, Tirzah Kreisel, Adi Doron, Nofar Ozeri-Engelhard, Talia Melcer, Ron Refaeli, Henrike Horn, Limor Regev, Maya Groysman, Michael London, I. G. Astrocytic Activation Generates De Novo Neuronal Potentiation and Memory Enhancement. *Cell* 174, 59–71 (2018).
397. Fellin, T. *et al.* Neuronal synchrony mediated by astrocytic glutamate through activation of extrasynaptic NMDA receptors. *Neuron* 43, 729–743 (2004).
398. Bazargani, N. & Attwell, D. Astrocyte calcium signaling: The third wave. *Nature Neuroscience* (2016). doi:10.1038/nn.4201
399. Haas, B. *et al.* Activity-dependent ATP-waves in the mouse neocortex are independent from astrocytic calcium waves. *Cereb. Cortex* 16, 237–246 (2006).

400. Suadicani, S. O. P2X7 Receptors Mediate ATP Release and Amplification of Astrocytic Intercellular Ca^{2+} Signaling. *J. Neurosci.* (2006). doi:10.1523/JNEUROSCI.3902-05.2006
401. Pascual, O. *et al.* Astrocytic Purinergic Signaling Coordinates Synaptic Networks. *Science* 310, 113–116 (2005).
402. Lalo, U. *et al.* Exocytosis of ATP From Astrocytes Modulates Phasic and Tonic Inhibition in the Neocortex. *PLoS Biol.* 12, (2014).
403. Covelo, A. & Araque, A. Lateral regulation of synaptic transmission by astrocytes. *Neuroscience* 323, 62-6 (2016). doi:10.1016/j.neuroscience.2015.02.036
404. Pirttimaki, T. M. *et al.* Astrocyte-mediated neuronal synchronisation properties revealed by false gliotransmitter release. *J. Neurosci.* 37, 9859-9870 (2017). doi:10.1523/JNEUROSCI.2761-16.2017
405. Fiacco, T. A. *et al.* Selective Stimulation of Astrocyte Calcium In Situ Does Not Affect Neuronal Excitatory Synaptic Activity. *Neuron* 54, 611-26 (2007). doi:10.1016/j.neuron.2007.04.032
406. Petravicz, J., Fiacco, T. A. & McCarthy, K. D. Loss of IP_3 Receptor-Dependent Ca^{2+} Increases in Hippocampal Astrocytes Does Not Affect Baseline CA1 Pyramidal Neuron Synaptic Activity. *J. Neurosci.* 28, 4967-73 (2008). doi:10.1523/JNEUROSCI.5572-07.2008
407. Agulhon, C., Fiacco, T. A. & McCarthy, K. D. Hippocampal short- and long-term plasticity are not modulated by astrocyte Ca^{2+} signaling. *Science* 327, 1250-4 (2010). doi:10.1126/science.1184821
408. Kuffler SW, Nicholls JG, O. R. Effect of nerve impulses on the membrane potential of glial cells in the central nervous system of amphibia. *J Neurophysiol* 29, 788–806 (1966).
409. Bellot-Saez, A. *et al.* Astrocytic modulation of cortical oscillations. *Sci. Rep.* 8, 11565 (2018).
410. Kantevari, S., Buskila, Y. & Ellis-Davies, G. C. R. Synthesis and characterization of cell-permeant 6-nitrodibenzofuranyl-caged IP_3. *Photochem. Photobiol. Sci.* 11, 508 (2012).
411. Hirth, I. C., Britz, F. C. & Deitmer, J. W. G protein activation by uncaging of GTP-gamma-S in the leech giant glial cell. *J. Exp. Biol.* 210, 3771-9 (2007). doi:10.1242/jeb.008037
412. Van Zeijl, L. *et al.* Regulation of connexin43 gap junctional communication by phosphatidylinositol 4,5-bisphosphate. *J. Cell Biol.* 177, 881-91 (2007). doi:10.1083/jcb.200610144
413. Ashhad, S. & Narayanan, R. Active dendrites regulate the impact of gliotransmission on rat hippocampal pyramidal neurons. *Proc. Natl. Acad. Sci.* 113, E3280-9 (2016). doi:10.1073/pnas.1522180113
414. Narayana, R. & Johnston, D. Long-term potentiation in rat hippocampal neurons is accompanied by spatially widespread changes in intrinsic oscillatory dynamics and excitability. *Neuron* 56, 1061–1075 (2007).
415. Luthi, A. & McCormick, D. A. H-Current : Properties of a Neuronal and Network Pacemaker. *Neuron* 21, 9–12 (1998).
416. Lörincz, A., Notomi, T., Tamás, G., Shigemoto, R. & Nusser, Z. Polarized and compartment-dependent distribution of HCN1 in pyramidal cell dendrites. *Nat. Neurosci.* 5, 1185-93 (2002). doi:10.1038/nn962
417. Bazhenov, M., Timofeev, I., Steriade, M. & Sejnowski, T. J. Potassium Model for Slow (2-3 Hz) In Vivo Neocortical Paroxysmal Oscillations. *J. Neurophysiol.* 92, 1116-32

(2004). doi:10.1152/jn.00529.2003
418. Fröhlich, F., Bazhenov, M., Timofeev, I., Steriade, M. & Sejnowski, T. J. Slow state transitions of sustained neural oscillations by activity-dependent modulation of intrinsic excitability. *J. Neurosci.* 26, 6153–62 (2006).
419. Buskila, Y., Morley, J. W., Tapson, J. & van Schaik, A. The adaptation of spike backpropagation delays in cortical neurons. *Front. Cell. Neurosci.* 7, 192 (2013).
420. Sheets, P. L. *et al.* Corticospinal-specific HCN expression in mouse motor cortex : Ih-dependent synaptic integration as a candidate microcircuit mechanism involved in motor control. *J Neurophysiol* 2216–2231 (2011). doi:10.1152/jn.00232.2011.
421. Heinemann, U. & Dieter Lux, H. Ceiling of stimulus induced rises in extracellular potassium concentration in the cerebral cortex of cat. *Brain Res.* (1977). doi:10.1016/0006-8993(77)90903-9
422. Somjen, G. G. Ion regulation in the brain: implications for pathophysiology. *Neuroscientist* 8, 254–267 (2002).
423. Dufour, S., Dufour, P., Chever, O., Vallée, R. & Amzica, F. In vivo simultaneous intra- and extracellular potassium recordings using a micro-optrode. *J. Neurosci. Methods* 194, 206–217 (2011).
424. Gardner-Medwin, A. R. Analysis of potassium dynamics in mammalian brain tissue. *J. Physiol.* (1983). doi:10.1113/jphysiol.1983.sp014541
425. Kuffler SW, Nicholls JG, O. R. Physiological properties of glial cells in the central nervous system of amphibia. *J Neurophysiol*, 29, 768–787 (1966).
426. Lindner, E. & Gyurcsányi, R. E. Quality control criteria for solid-contact, solvent polymeric membrane ion-selective electrodes. *J. Solid State Electrochem.* 13, 51-68 (2009). doi:10.1007/s10008-008-0608-1
427. Coles, B. Y. J. A. & Orkand, R. K. Modification of potassium movement through the retina of the drone (Apis mellifera male) by glial uptake. *J. Physiol.* 340, 157–174 (1983).
428. Chester J. Karwoski, Eric A . Newman, Hiroshi Shimazaki, and L. M. P. Light-evoked Increases in Extracellular K^+ in the Plexiform Layers of Amphibian Retinas. *J. Gen. Physiol.* 86,189-213 (1985).
429. Hansen, A. J. Extracellular Potassium Concentration in Juvenile and Adult Rat Brain Cortex during Anoxia. *Acta Physiol. Scand.* 99, 412–20 (1977).
430. Moody, W. J., Kin, J., Futamachi, J. & Prince, D. A. Extracellular potassium activity during epileptogenesis. *Exp. Neurol.* 263, 248–263 (1974).
431. Enger, R. *et al.* Dynamics of Ionic Shifts in Cortical Spreading Depression. *Cereb. Cortex* 25, 4469-76 (2015). doi:10.1093/cercor/bhv054
432. Bazzigaluppi, P., Weisspapir, I., Stefanovic, B., Leybaert, L. & Carlen, P. L. Astrocytic gap junction blockade markedly increases extracellular potassium without causing seizures in the mouse neocortex. *Neurobiol. Dis.* (2017). doi:10.1016/j.nbd.2016.12.017
433. Stephan, J. *et al.* Kir4.1 Channels Mediate a Depolarization of Hippocampal Astrocytes Under Hyperammonemic Conditions In Situ. 978, 965–978 (2012).
434. Haack, N., Durry, S., Kafitz, K. W., Chesler, M. & Rose, C. Double-barreled and Concentric Microelectrodes for Measurement of Extracellular Ion Signals in Brain Tissue. *J. Vis. Exp.* (2015). doi:10.3791/53058
435. Wellbourne-Wood, J., Rimmele, T. S. & Chatton, J.Y. Imaging extracellular potassium dynamics in brain tissue using a potassium-sensitive nanosensor. *Neurophotonics* 4, 015002 (2017). doi:10.1117/1.NPh.4.1.015002

436. Voipio, J. & Pasternack, M. Ion-sensitive microelectrodes. *Membr. Technol.* 2002, 13 (2002).
437. Depauw, A. *et al.* A Highly Selective Potassium Sensor for the Detection of Potassium in Living Tissues. *Chemistry* 22, 14902–14911 (2016).
438. Rimmele, T. S. & Chatton, J. Y. A novel optical intracellular imaging approach for potassium dynamics in astrocytes. *PLoS One* 9, e109243 (2014).
439. Bazzigaluppi, P., Dufour, S. & Carlen, P. L. Wide field fluorescent imaging of extracellular spatiotemporal potassium dynamics in vivo. *Neuroimage* 104, 110–116 (2015).
440. Ammann D, C. P. Preparation and use of micro- and macroelectrodes for measurement of transmembrane potentials and ion activities. *Methods Enzymol.* (1989).
441. Haack, N. & Rose, C. R. Preparation , Calibration and Application of Potassium-Selective Microelectrodes. *Microelectrodes* 49, 87–105 (2014).
442. Deveau, J. S. T., Lindinger, M. I. & Grodzinski, B. An improved method for constructing and selectively silanizing double-barreled, neutral liquid-carrier, ion-selective microelectrodes. *Biol. Proced. Online* (2005). doi:10.1251/bpo103
443. Parks, G. J. On the Thickness of the Liquid Film formed by Condensation at the Surface of a Solid. (1903).
444. Munoz, J. L., Deyhimi, F. & Coles, J. A. Silanization of glass in the making of ion-sensitive microelectrodes. *J. Neurosci. Methods* (1983). doi:10.1016/0165-0270(83)90037-7
445. Walker, J. L. Ion Specific Liquid Ion Exchanger Microelectrodes. *Anal. Chem.* (1971). doi:10.1021/ac60298a039
446. Fedirko, N. Fabrication and Use of High-Speed, Concentric H^+- and Ca^{2+}-Selective Microelectrodes Suitable for In Vitro Extracellular Recording. *J. Neurophysiol.* (2006). doi:10.1152/jn.00258.2006
447. Nimmerjahn, A. & Helmchen, F. In vivo labeling of cortical astrocytes with sulforhodamine 101 (SR101). *Cold Spring Harb. Protoc.* 2012, 326-34 (2012). doi:10.1101/pdb.prot068155
448. Schindelin, J. *et al.* Fiji - an Open Source platform for biological image analysis. *Nat. Methods* 9, 676–682 (2013).
449. Jansen, L. A., Uhlmann, E. J., Crino, P. B., Gutmann, D. H. & Wong, M. Epileptogenesis and Reduced Inward Rectifier Potassium Current in Tuberous Sclerosis Complex-1 – Deficient Astrocytes. *Cultures* 46, 1871–1880 (2005).
450. Kristian Enkvist, M. O. & McCarthy, K. D. Astroglial Gap Junction Communication Is Increased by Treatment with Either Glutamate or High K^+ Concentration. *J. Neurochem.* (1994). doi:10.1046/j.1471-4159.1994.62020489.x
451. Rana, P. S. *et al.* Calibration and characterization of intracellular Asante Potassium Green probes, APG-2 and APG-4. *Anal. Biochem.* 567, 8-13 (2019). doi:10.1016/j.ab.2018.11.024
452. Larsen, B. R. *et al.* Contributions of the Na^+/K^+-ATPase, NKCC1, and Kir4.1 to hippocampal K^+ clearance and volume responses. *Glia* 62, 608–622 (2014).
453. Gardner-Medwin, A. R. A study of the mechanisms by which potassium moves through brain tissue in the rat. *J. Physiol.* (1983). doi:10.1113/jphysiol.1983.sp014539
454. Fick, A. On liquid diffusion. *J. Memb. Sci.* (1995). doi:10.1016/0376-7388(94)00230-V

455. Syková, E., Nicholson, C. & Sykova, Eva; Nicholson, C. Diffusion in brain extracellular space. *Physiol. Rev.* 88, 1277–1340 (2008).
456. Yossi Buskila, Orsolya Kékesi, Alba Bellot-Saez, Winston Seah, Tracey Berg, Michael Trpceski, J. J. Y. & L. O. Dynamic interplay between H-current and M-current controls motoneuron hyperexcitability in amyotrophic lateral sclerosis. *Cell Death Dis.* 10, (2019).
457. Kofuji, P. & Newman, E. A. Potassium buffering in the central nervous system. *Neuroscience* 129, 1045–1056 (2004).
458. Ballanyi, K., Grafe, P. & ten Bruggencate, G. Ion activities and potassium uptake mechanisms of glial cells in guinea-pig olfactory cortex slices. *J. Physiol.* 382, 159–74 (1987).
459. Andrew J. Whalen, Ying Xiao, Herve Kadji, Markus Dahlem, Bruce J. Gluckman, S. J. S. Control of Spreading Depression with Electrical Fields. *Sci. Rep.* 8, 8769 (2018).
460. Padmawar, P., Yao, X., Bloch, O., Manley, G. T. & Verkman, A. S. K^+ waves in brain cortex visualized using a long- wavelength K^+-sensing fluorescent indicator. *Nat. Methods.* 2, 825–828 (2005).
461. Bischof, H. *et al.* Novel genetically encoded fluorescent probes enable real-time detection of potassium in vitro and in vivo. *Nat. Commun.* 1–11 (2017). doi:10.1038/s41467-017-01615-z
462. Shen, Y., Wu, S., Rancic, V., Qian, Y. & Miyashita, S. Genetically encoded ratiometric indicators for potassium ion. *Commun. Biol.* 2, 18 (2018).
463. Lee, S. & Dan, Y. Neuromodulation of Brain States. *Neuron* 76, 209–222 (2012).
464. Saper, C. B., Scammell, T. E. & Lu, J. Hypothalamic regulation of sleep and circadian rhythms. *Nature* (2005). doi:10.1038/nature04284
465. Carter, M. E. *et al.* Tuning arousal with optogenetic modulation of locus coeruleus neurons. *Nat. Neurosci.* (2010). doi:10.1038/nn.2682
466. Yu, X., Franks, N. P. & Wisden, W. Sleep and Sedative States Induced by Targeting the Histamine and Noradrenergic Systems. *Front. Neural Circuits* 12, 4 (2018). doi:10.3389/fncir.2018.00004
467. N. Inagaki, H. Fukui, Y. Taguchi, N.P. Wang, A. Yamatodani, H. W. Characterization of histamine H1-receptors on astrocytes in primary culture: [3H]mepyramine binding studies. *Eur. J. Pharmacol.* 173, 43–51 (1989).
468. Bekar, L. K., He, W. & Nedergaard, M. Locus coeruleus alpha-adrenergic-mediated activation of cortical astrocytes in vivo. *Cereb. Cortex* 18, 2789–2795 (2008).
469. Morin, D., Sapena, R., Zini, R., Onteniente, B. & Tillement, J. P. Characterization of β-adrenergic receptors of freshly isolated astrocytes and neurons from rat brain. *Life Sci.* (1996). doi:10.1016/S0024-3205(96)00632-7
470. Khan, Z. U., Koulen, P., Rubinstein, M., Grandy, D. K. & Goldman-Rakic, P. S. An astroglia-linked dopamine D2-receptor action in prefrontal cortex. *Proc. Natl. Acad. Sci. U. S. A.* (2001). doi:10.1073/pnas.98.4.1964
471. Wei, X. *et al.* Dopamine D1 or D2 receptor-expressing neurons in the central nervous system. *Addict. Biol.* 23, 569-584 (2018). doi:10.1111/adb.12512
472. Poskanzer, K. E. & Yuste, R. Astrocytic regulation of cortical UP states. *Proc. Natl. Acad. Sci.* 108, 18453–18458 (2011).
473. Poskanzer, K. E. & Yuste, R. Astrocytes regulate cortical state switching in vivo. *Proc. Natl. Acad. Sci. U. S. A.* 2016, 1–10 (2016).

474. Fang, Q. *et al.* Histamine up-regulates astrocytic glutamate transporter 1 and protects neurons against ischemic injury. *Neuropharmacology* 77, 156-66 (2014). doi:10.1016/j.neuropharm.2013.06.012
475. Schnell, C., Negm, M., Driehaus, J., Scheller, A. & Hülsmann, S. Norepinephrine-induced calcium signaling in astrocytes in the respiratory network of the ventrolateral medulla. *Respir. Physiol. Neurobiol.* 226, 18-23 (2016). doi:10.1016/j.resp.2015.10.008
476. Nuriya, M., Takeuchi, M. & Yasui, M. Background norepinephrine primes astrocytic calcium responses to subsequent norepinephrine stimuli in the cerebral cortex. *Biochem. Biophys. Res. Commun.* 483, 732-738 (2017). doi:10.1016/j.bbrc.2016.12.073
477. Vaarmann, A., Gandhi, S. & Abramov, A. Y. Dopamine induces Ca^{2+} signaling in astrocytes through reactive oxygen species generated by monoamine oxidase. *J. Biol. Chem.* (2010). doi:10.1074/jbc.M110.111450
478. Bosson, A., Boisseau, S., Buisson, A., Savasta, M. & Albrieux, M. Disruption of dopaminergic transmission remodels tripartite synapse morphology and astrocytic calcium activity within substantia nigra pars reticulata. *Glia* (2015). doi:10.1002/glia.22777
479. Schipke, C. G., Heuser, I. & Peters, O. Antidepressants act on glial cells: SSRIs and serotonin elicit astrocyte calcium signaling in the mouse prefrontal cortex. *J. Psychiatr. Res.* (2011). doi:10.1016/j.jpsychires.2010.06.005
480. Sandén, N., Thorlin, T., Blomstrand, F., Persson, P. A. & Hansson, E. 5-Hydroxytryptamine(2B) receptors stimulate Ca^{2+} increases in cultured astrocytes from three different brain regions. *Neurochem. Int.* 36, 427-34 (2000). doi:10.1016/S0197-0186(99)00134-5
481. Araque, A., Martin, E. D., Perea, G., Arellano, J. I. & Buno, W. Synaptically Released Acetylcholine Evokes Ca^{2+} Elevations in Astrocytes in Hippocampal Slices. *J. Neurosci.* (2002). doi:20026212
482. Perea, G. Properties of Synaptically Evoked Astrocyte Calcium Signal Reveal Synaptic Information Processing by Astrocytes. *J. Neurosci.* 25, 2192-203 (2005). doi:10.1523/JNEUROSCI.3965-04.2005
483. Ma, Z., Stork, T., Bergles, D. E. & Freeman, M. R. Neuromodulators signal through astrocytes to alter neural circuit activity and behaviour. *Nature* 539, 428-432 (2016). doi:10.1038/nature20145
484. Bonhaus, D. W. *et al.* The pharmacology and distribution of human 5-hydroxytryptamine2B (5-HT2B) receptor gene products: comparison with 5-HT2A and 5-HT2C receptors. *Br. J. Pharmacol.* (1995). doi:10.1111/j.1476-5381.1995.tb14977.x
485. Azmitia, E. C., Gannon, P. J., Kheck, N. M. & Whitaker-Azmitia, P. M. Cellular localization of the 5-HT1A receptor in primate brain neurons and glial cells. *Neuropsychopharmacology* (1996). doi:10.1016/S0893-133X(96)80057-1
486. Carson, M. J., Thomas, E. A., Danielson, P. E. & Sutcliffe, J. G. The 5-HT(5A) serotonin receptor is expressed predominantly by astrocytes in which it inhibits cAMP accumulation: A mechanism for neuronal suppression of reactive astrocytes. *Glia* (1996). doi:10.1002/(SICI)1098-1136(199608)17:4<317::AID-GLIA6>3.0.CO;2-W
487. Maxishima, M. *et al.* Serotonin 2A receptor-like immunoreactivity is detected in astrocytes but not in oligodendrocytes of rat spinal cord. *Brain Res.* (2001). doi:10.1016/S0006-8993(00)03150-4
488. Mahé, C. *et al.* Functional expression of the serotonin 5-HT7 receptor in human glioblastoma cell lines. *Br. J. Pharmacol.* (2004). doi:10.1038/sj.bjp.0705936

489. Li, B., Zhang, S., Li, M., Hertz, L. & Peng, L. Serotonin increases ERK1/2 phosphorylation in astrocytes by stimulation of 5-HT2B and 5-HT2C receptors. *Neurochem. Int.* (2010). doi:10.1016/j.neuint.2010.04.017
490. Kong, E. K. C., Peng, L., Chen, Y., Yu, A. C. H. & Hertz, L. Up-regulation of 5-HT2Breceptor density and receptor-mediated glycogenolysis in mouse astrocytes by long-term fluoxetine administration. *Neurochem. Res.* (2002). doi:10.1023/A:1014862808126
491. Gantz, S. C., Levitt, E. S., Llamosas, N., Neve, K. A. & Williams, J. T. Depression of serotonin synaptic transmission by the dopamine Precursor L-DOPA. *Cell Rep.* 12, 944-54 (2015). doi:10.1016/j.celrep.2015.07.005
492. Zanassi, P., Paolillo, M., Montecucco, A., Avvedimento, E. V. & Schinelli, S. Pharmacological and molecular evidence for dopamine D1 receptor expression by striatal astrocytes in culture. *J. Neurosci. Res.* (1999). doi:10.1002/(SICI)1097-4547(19991115)58:4<544::AID-JNR7>3.0.CO;2-9
493. Castro, L. R. V. *et al.* Striatal neurones have a specific ability to respond to phasic dopamine release. *J. Physiol.* 591, 3197-214 (2013). doi:10.1113/jphysiol.2013.252197
494. Duffy, S. & MacVicar, B. a. Adrenergic calcium signaling in astrocyte networks within the hippocampal slice. *J. Neurosci.* (1995). doi:10.1523/JNEUROSCI.15-08-05535.1995
495. Carriba, P. *et al.* ATP and Noradrenaline Activate CREB in Astrocytes via Noncanonical Ca^{2+} and Cyclic AMP Independent Pathways. *Glia* 1344, 1330–1344 (2012).
496. Alexander, G. M., Grothusen, J. R., Gordon, S. W. & Schwartzman, R. J. Intracerebral microdialysis study of glutamate reuptake in awake, behaving rats. *Brain Res.* (1997). doi:10.1016/S0006-8993(97)00519-2
497. Xu, J. *et al.* Basic mechanism leading to stimulation of glycogenolysis by isoproterenol, EGF, elevated extracellular K^+ concentrations, or GABA. *Neurochem. Res.* 39, 661-7 (2014). doi:10.1007/s11064-014-1244-z
498. Hajek, I., Subbarao, K. V & Hertz, L. Acute and chronic effects of potassium and noradrenaline on Na^+, K^+-ATPase activity in cultured mouse neurons and astrocytes. *Neurochem Int* 28, 335–342 (1996).
499. Medrano, S., Gruenstein, E. & Dimlich, R. V. Histamine stimulates glycogenolysis in human astrocytoma cells by increasing intracellular free calcium. *Brain Res.* (1992).
500. Arbonés, L., Picatoste, F. & García, A. Histamine H1-receptors mediate phosphoinositide hydrolysis in astrocyte-enriched primary cultures. *Brain Res.* (1988). doi:10.1016/0006-8993(88)91554-5
501. Hill, S. J. Distribution, properties, and functional characteristics of three classes of histamine receptor. *Pharmacol Rev* (1990).
502. Mele, T. & Jurič, D. M. Identification and pharmacological characterization of the histamine H 3 receptor in cultured rat astrocytes. *Eur. J. Pharmacol.* 720, 198-204 (2013). doi:10.1016/j.ejphar.2013.10.028
503. Mariottini, C. *et al.* Activation of the histaminergic H3 receptor induces phosphorylation of the Akt/GSK-3β pathway in cultured cortical neurons and protects against neurotoxic insults. *J. Neurochem.* (2009). doi:10.1111/j.1471-4159.2009.06249.x
504. Jurič, D. M., Kržan, M. & Lipnik-Stangelj, M. Histamine and astrocyte function. *Pharmacol. Res.* 111, 774-783 (2016). doi:10.1016/j.phrs.2016.07.035
505. Hirase, H., Iwai, Y., Takata, N., Shinohara, Y. & Mishima, T. Volume transmission signalling via astrocytes. *Philosophical Transactions of the Royal Society B: Biological Sciences* 369, 20130604 (2014). doi:10.1098/rstb.2013.0604

506. Sharma, G. & Vijayaraghavan, S. Nicotinic cholinergic signaling in hippocampal astrocytes involves calcium-induced calcium release from intracellular stores. *Proc. Natl. Acad. Sci. U. S. A.* (2001). doi:10.1073/pnas.071540198
507. Kelly, J. F. *et al.* Amyloid beta-peptide disrupts carbachol-induced muscarinic cholinergic signal transduction in cortical neurons. *Proc. Natl. Acad. Sci. U. S. A.* (1996).
508. Papouin, T., Dunphy, J. M., Tolman, M., Dineley, K. T. & Haydon, P. G. Septal Cholinergic Neuromodulation Tunes the Astrocyte-Dependent Gating of Hippocampal NMDA Receptors to Wakefulness. *Neuron* 94, 840-854 (2017). doi:10.1016/j.neuron.2017.04.021
509. Takata, N. *et al.* Astrocyte Calcium Signaling Transforms Cholinergic Modulation to Cortical Plasticity In Vivo. *J. Neurosci.* 31, 18155–18165 (2011).
510. Hobson, J. A., Goldberg, M., Vivaldi, E. & Riew, D. Enhancement of desynchronized sleep signs after pontine microinjection of the muscarinic agonist bethanechol. *Brain Res.* (1983). doi:10.1016/0006-8993(83)90424-9
511. Gervasoni, D. Global Forebrain Dynamics Predict Rat Behavioral States and Their Transitions. *J. Neurosci.* 24, 11137-11147 (2004). doi:10.1523/jneurosci.3524-04.2004
512. Ito, H. & Schuman, E. Frequency-dependent gating of synaptic transmission and plasticity by dopamine. *Front. Neural Circuits* (2007). doi:10.3389/neuro.04/001.2007
513. Kirkwood, A., Rozas, C., Kirkwood, J., Perez, F. & Bear, M. F. Modulation of long-term synaptic depression in visual cortex by acetylcholine and norepinephrine. *J. Neurosci.* (1999).
514. O'Donnell, J., Zeppenfeld, D., McConnell, E., Pena, S. & Nedergaard, M. Norepinephrine: A neuromodulator that boosts the function of multiple cell types to optimize CNS performance. *Neurochemical Research* 37, 2496-512 (2012). doi:10.1007/s11064-012-0818-x
515. Constantinople, C. M. & Bruno, R. M. Effects and mechanisms of wakefulness on local cortical networks. *Neuron* 69, 1061-8 (2011). doi:10.1016/j.neuron.2011.02.040
516. Webster, H. H. & Jones, B. E. Neurotoxic lesions of the dorsolateral pontomesencephalic tegmentum-cholinergic cell area in the cat. II. Effects upon sleep-waking states. *Brain Res.* (1988). doi:10.1016/0006-8993(88)90471-4
517. Dort, C. J. Van *et al.* Optogenetic activation of cholinergic neurons in the PPT or LDT induces REM sleep. *Proc. Natl. Acad. Sci.* 112, 584-9 (2015). doi:10.1073/pnas.1423136112
518. Ni, K. M. *et al.* Selectively driving cholinergic fibers optically in the thalamic reticular nucleus promotes sleep. *Elife* (2016). doi:10.7554/eLife.10382
519. Monti, J. M. Involvement of histamine in the control of the waking state. *Life Sciences* (1993). doi:10.1016/0024-3205(93)90592-Q
520. Monti, J. M. & Jantos, H. The roles of dopamine and serotonin, and of their receptors, in regulating sleep and waking. *Progress in Brain Research* 172, 625-46 (2008). doi:10.1016/S0079-6123(08)00929-1
521. Rudy, B., Fishell, G., Lee, S., Zagha, E. & Hjerling-Leffler, J. The Largest Group of Superficial Neocortical GABAergic Interneurons Expresses Ionotropic Serotonin Receptors. *J. Neurosci.* (2010). doi:10.1523/jneurosci.1869-10.2010
522. Porter, J. T. & McCarthy, K. D. Astrocytic neurotransmitter receptors in situ and in vivo. *Progress in Neurobiology* (1997). doi:10.1016/S0301-0082(96)00068-8

523. Káradóttir, R. & Attwell, D. Neurotransmitter receptors in the life and death of oligodendrocytes. *Neuroscience* (2007). doi:10.1016/j.neuroscience.2006.08.070
524. Liu, H., Leak, R. K. & Hu, X. Neurotransmitter receptors on microglia. *Stroke and Vascular Neurology* (2016). doi:10.1136/svn-2016-000012
525. Ransom, C. B., Ransom, B. R. & Sontheimer, H. Activity-dependent extracellular K^+ accumulation in rat optic nerve: the role of glial and axonal Na^+ pumps. *J. Physiol.* (2000). doi:10.1111/j.1469-7793.2000.00427.x
526. Thrane, V. R. *et al.* Ammonia triggers neuronal disinhibition and seizures by impairing astrocyte potassium buffering. *Nat. Med.* 19, 1643-8 (2013). doi:10.1038/nm.3400
527. Ransom, B. Glial modulation of neural excitability mediated by extracellular pH: A hypothesis. *Prog. Brain Res.* (1992). doi:10.1016/S0079-6123(08)61737-9
528. Pellerin, L. & Magistretti, P. J. Glutamate Uptake Stimulates Na^+,K^+-ATPase Activity in Astrocytes via Activation of a Distinct Subunit Highly Sensitive to Ouabain. *J. Neurochem.* (2002). doi:10.1046/j.1471-4159.1997.69052132.x
529. Orkand, R. K. Introductory Remarks: glial-interstitial fluid exchange. *Neuronal Microenviron.* 481, 269–272 (1986).
530. Butt, A. M. & Kalsi, A. Inwardly rectifying potassium channels (Kir) in central nervous system glia: A special role for Kir4.1 in glial functions. *Journal of Cellular and Molecular Medicine* (2006). doi:10.1111/j.1582-4934.2006.tb00289.x
531. Wallraff, A., Heinemann, U., Theis, M., Willecke, K. & Steinha, C. The Impact of Astrocytic Gap Junctional Coupling on Potassium Buffering in the Hippocampus. *J Neurosci* 26, 5438–5447 (2006).
532. Pannasch, U. *et al.* Astroglial networks scale synaptic activity and plasticity. *Proc Natl Acad Sci U S A* 108, 8467–8472 (2011).
533. Li, B. *et al.* Fluoxetine-mediated 5-HT2B receptor stimulation in astrocytes causes EGF receptor transactivation and ERK phosphorylation. *Psychopharmacology (Berl).* 201, 443-58 (2008). doi:10.1007/s00213-008-1306-5
534. Ohno, Y., Hibino, H., Lossin, C., Inanobe, A. & Kurachi, Y. Inhibition of astroglial Kir4.1 channels by selective serotonin reuptake inhibitors. *Brain Res.* 1178, 44-51 (2007). doi:10.1016/j.brainres.2007.08.018
535. Jeanson, T. *et al.* Antidepressants Impact Connexin 43 Channel Functions in Astrocytes. *Front. Cell. Neurosci.* 9, 495 (2016). doi:10.3389/fncel.2015.00495
536. Zaika, O. L. *et al.* Direct inhibition of basolateral Kir4.1/5.1 and Kir4.1 channels in the cortical collecting duct by dopamine. *Am. J. Physiol. Physiol.* 305, F1277-F1287 (2013). doi:10.1152/ajprenal.00363.2013
537. Zelenina, M., Zelenin, S., Bondar, A. a, Brismar, H. & Aperia, A. Water permeability of aquaporin-4 is decreased by protein kinase C and dopamine. *Am. J. Physiol. Renal Physiol.* (2002). doi:10.1152/ajprenal.00260.2001
538. Song, D., Xu, J., Hertz, L. & Peng, L. Regulatory Volume Increase in Astrocytes Exposed to Hypertonic Medium Requires Stimulation and Glycogenolysis. *J. Neurosci. Res.* 93, 130–9 (2015).
539. Karle, C. A. *et al.* Human cardiac inwardly-rectifying K^+ channel Kir2.1b is inhibited by direct protein kinase C-dependent regulation in human isolated cardiomyocytes and in an expression system. *Circulation* (2002). doi:10.1161/01.CIR.0000029747.53262.5C
540. Carmosino, M. *et al.* Trafficking and phosphorylation dynamics of AQP4 in histamine-treated human gastric cells. *Biol. Cell* (2007). doi:10.1042/BC20060068

541. He, C. *et al.* Superficial Layer-Specific Histaminergic Modulation of Medial Entorhinal Cortex Required for Spatial Learning. *Cereb. Cortex* (2016). doi:10.1093/cercor/bhu322
542. Shelton, M. K. & McCarthy, K. D. Hippocampal astrocytes exhibit Ca^{2+}-elevating muscarinic cholinergic and histaminergic receptors in situ. *J. Neurochem.* (2000). doi:10.1046/j.1471-4159.2000.740555.x
543. Magee, J. C. & Johnston, D. A synaptically controlled, associative signal for Hebbian plasticity in hippocampal neurons. *Science* 275, 209-13 (1997). doi:10.1126/science.275.5297.209
544. See, J. Z., Atencio, C. A., Sohal, V. S. & Schreiner, C. E. Coordinated neuronal ensembles in primary auditory cortical columns. *Elife* (2018). doi:10.7554/eLife.35587
545. Viejo, G., Cortier, T. & Peyrache, A. Brain-state invariant thalamo-cortical coordination revealed by non-linear encoders. *PLoS Comput. Biol.* 14, e1006041 (2018). doi:10.1371/journal.pcbi.1006041
546. Castelo-Branco, M., Neuenschwander, S. & Singer, W. Synchronization of visual responses between the cortex, lateral geniculate nucleus, and retina in the anesthetized cat. *J. Neurosci.* (1998). doi:10.1523/JNEUROSCI.18-16-06395.1998
547. Marshall, L., Helgadóttir, H., Mölle, M. & Born, J. Boosting slow oscillations during sleep potentiates memory. *Nature* (2006). doi:10.1038/nature05278
548. Maingret, N., Girardeau, G., Todorova, R., Goutierre, M. & Zugaro, M. Hippocampo-cortical coupling mediates memory consolidation during sleep. *Nat. Neurosci.* 19, 959-64 (2016). doi:10.1038/nn.4304
549. Clayton, M. S., Yeung, N. & Cohen Kadosh, R. The roles of cortical oscillations in sustained attention. *Trends in Cognitive Sciences* (2015). doi:10.1016/j.tics.2015.02.004
550. Wei, Y., Krishnan, G. P. & Bazhenov, M. Synaptic Mechanisms of Memory Consolidation during Sleep Slow Oscillations. *J. Neurosci.* 36, 4231-47 (2016). doi:10.1523/JNEUROSCI.3648-15.2016
551. Helfrich, R. F. *et al.* Neural Mechanisms of Sustained Attention Are Rhythmic. *Neuron* 99, 854-865 (2018). doi:10.1016/j.neuron.2018.07.032
552. Peters A, P. S. An electron microscope study of the distribution and patterns of astroglial processes in the central nervous system. *J Anat* 419, (1965).
553. Perez-Alvarez, A., Navarrete, M., Covelo, A., Martin, E. D. & Araque, A. Structural and Functional Plasticity of Astrocyte Processes and Dendritic Spine Interactions. *J. Neurosci.* 34, 12738-44 (2014). doi:10.1523/JNEUROSCI.2401-14.2014
554. Panatier, A. *et al.* Astrocytes are endogenous regulators of basal transmission at central synapses. *Cell* 146, 785-98 (2011). doi:10.1016/j.cell.2011.07.022
555. Bernardinelli, Y. *et al.* Activity-dependent structural plasticity of perisynaptic astrocytic domains promotes excitatory synapse stability. *Curr. Biol.* 24, 1679-88 (2014). doi:10.1016/j.cub.2014.06.025
556. Min, R. & Nevian, T. Astrocyte signaling controls spike timing–dependent depression at neocortical synapses. *Nat. Neurosci.* 15, 746–753 (2012).
557. Halassa, M. M. *et al.* Astrocytic Modulation of Sleep Homeostasis and Cognitive Consequences of Sleep Loss. *Neuron* (2009). doi:10.1016/j.neuron.2008.11.024
558. Chen, Y., Li, X., Rotstein, H. G. & Nadim, F. Membrane potential resonance frequency directly influences network frequency through electrical coupling. *J. Neurophysiol.* 116, 1554-1563 (2016). doi:10.1152/jn.00361.2016

559. Szabó, Z. *et al.* Extensive astrocyte synchronization advances neuronal coupling in slow wave activity in vivo. *Sci. Rep.* (2017). doi:10.1038/s41598-017-06073-7
560. Gutfreund, Y., Yarom, Y. & Segev, I. Subthreshold oscillations and resonant frequency in guinea-pig cortical neurons: physiology and modelling. *J. Physiol.* 483, 621–640 (1995).
561. Yoshida, M., Giocomo, L. M., Boardman, I. & Hasselmo, M. E. Frequency of Subthreshold Oscillations at Different Membrane Potential Voltages in Neurons at Different Anatomical Positions on the Dorsoventral Axis in the Rat Medial Entorhinal Cortex. *J. Neurosci.* (2011). doi:10.1523/JNEUROSCI.1654-11.2011
562. Dugué, G. P. *et al.* Electrical Coupling Mediates Tunable Low-Frequency Oscillations and Resonance in the Cerebellar Golgi Cell Network. *Neuron* 61, 126-39 (2009). doi:10.1016/j.neuron.2008.11.028
563. Tchumatchenko, T. & Clopath, C. Oscillations emerging from noise-driven steady state in networks with electrical synapses and subthreshold resonance. *Nat. Commun.* (2014). doi:10.1038/ncomms6512
564. Moca, V. V., Nikolić, D., Singer, W. & Mureşan, R. C. Membrane resonance enables stable and robust gamma oscillations. *Cereb. Cortex* (2014). doi:10.1093/cercor/bhs293
565. Kuga, N., Sasaki, T., Takahara, Y., Matsuki, N. & Ikegaya, Y. Large-Scale Calcium Waves Traveling through Astrocytic Networks In Vivo. *J Neurosci* 31, 2607–2614 (2011).
566. LaBerge, D. & Kasevich, R. S. Neuroelectric Tuning of Cortical Oscillations by Apical Dendrites in Loop Circuits. *Front. Syst. Neurosci.* (2017). doi:10.3389/fnsys.2017.00037
567. Houades, V., Koulakoff, A., Ezan, P., Seif, I. & Giaume, C. Gap Junction-Mediated Astrocytic Networks in the Mouse Barrel Cortex. *J. Neurosci.* 28, 5207–5217 (2008).
568. Biology, N. G. & Kingdom, U. Shapes of astrocyte networks in the juvenile brain. *Neuron Glia Biol.* 2, 3–14 (2006).
569. Shen, J. X. & Yakel, J. L. Functional α7 nicotinic ACh receptors on astrocytes in rat hippocampal CA1 slices. *J. Mol. Neurosci.* (2012). doi:10.1007/s12031-012-9719-3
570. Dennis, S. H. *et al.* Activation of Muscarinic M1 Acetylcholine Receptors Induces Long-Term Potentiation in the Hippocampus. *Cereb. Cortex* (2016). doi:10.1093/cercor/bhv227
571. Heys, J. G. & Hasselmo, M. E. Neuromodulation of Ih in Layer II Medial Entorhinal Cortex Stellate Cells: A Voltage-Clamp Study. *J. Neurosci.* 32, 9066-72 (2012). doi:10.1523/JNEUROSCI.0868-12.2012
572. Ma, L., Shalinsky, M. H., Alonso, A. & Dickson, C. T. Effects of serotonin on the intrinsic membrane properties of layer II medial entorhinal cortex neurons. *Hippocampus* 17, 114-29 (2007). doi:10.1002/hipo.20250
573. Rosenkranz, J. A. Dopaminergic Regulation of Neuronal Excitability through Modulation of Ih in Layer V Entorhinal Cortex. *J. Neurosci.* 26, 3229-44 (2006). doi:10.1523/JNEUROSCI.4333-05.2006
574. Maccaferri, G. & McBain, C. J. The hyperpolarization-activated current (I(h)) and its contribution to pacemaker activity in rat CA1 hippocampal stratum oriens-alveus interneurones. *J. Physiol.* (1996). doi:10.1113/jphysiol.1996.sp021754
575. Tseng, H., Martinez, D. & Nadim, F. The frequency preference of neurons and synapses in a recurrent oscillatory network. *J. Neurosci.* 34, 12933–45 (2014).
576. Zagha, E. & McCormick, D. A. Neural control of brain state. *Current Opinion in Neurobiology* (2014). doi:10.1016/j.conb.2014.09.010
577. Howe, W. M. *et al.* Acetylcholine Release in Prefrontal Cortex Promotes Gamma Oscillations and Theta–Gamma Coupling during Cue Detection. *J. Neurosci.* (2017).

doi:10.1523/JNEUROSCI.2737-16.2017
578. Shirvalkar, P. R., Rapp, P. R. & Shapiro, M. L. Bidirectional changes to hippocampal theta-gamma comodulation predict memory for recent spatial episodes. *Proc. Natl. Acad. Sci.* (2010). doi:10.1073/pnas.0911184107
579. Rodriguez, R. Short- and Long-Term Effects of Cholinergic Modulation on Gamma Oscillations and Response Synchronization in the Visual Cortex. *J. Neurosci.* (2004). doi:10.1523/JNEUROSCI.1839-04.2004
580. Ramaswamy, S., Colangelo, C. & Markram, H. Data-Driven Modeling of Cholinergic Modulation of Neural Microcircuits: Bridging Neurons, Synapses and Network Activity. *Front. Neural Circuits* 12, 77 (2018). doi:10.3389/fncir.2018.00077
581. Pabst, M. *et al.* Astrocyte Intermediaries of Septal Cholinergic Modulation in the Hippocampus. *Neuron* (2016). doi:10.1016/j.neuron.2016.04.003
582. Traub, R. D. *et al.* A model of gamma-frequency network oscillations induced in the rat CA3 region by carbachol in vitro. *Eur. J. Neurosci.* (2000). doi:10.1046/j.1460-9568.2000.00300.x
583. Tiesinga, P. H. E. & José, J. V. Robust gamma oscillations in networks of inhibitory hippocampal interneurons. *Netw. Comput. Neural Syst.* (2000). doi:10.1088/0954-898X_11_1_301
584. Oren, I., Hájos, N. & Paulsen, O. Identification of the current generator underlying cholinergically induced gamma frequency field potential oscillations in the hippocampal CA3 region. *J. Physiol.* (2010). doi:10.1113/jphysiol.2009.180851
585. Lowry, C. A., Johnson, P. L., Hay-Schmidt, A., Mikkelsen, J. & Shekhar, A. Modulation of anxiety circuits by serotonergic systems. *Stress* 8, 233-46 (2005). doi:10.1080/10253890500492787
586. Cirelli, C. & Tononi, G. Differential expression of plasticity-related genes in waking and sleep and their regulation by the noradrenergic system. *J. Neurosci.* (2000). doi:20/24/9187 [pii]
587. Ray, N. J. *et al.* Local field potential beta activity in the subthalamic nucleus of patients with Parkinson's disease is associated with improvements in bradykinesia after dopamine and deep brain stimulation. *Exp. Neurol.* (2008). doi:10.1016/j.expneurol.2008.05.008
588. Panula, P. *et al.* Neuronal histamine deficit in Alzheimer's disease. *Neuroscience* (1997). doi:10.1016/S0306-4522(97)00353-9
589. Heneka, M. T. *et al.* Locus ceruleus controls Alzheimer's disease pathology by modulating microglial functions through norepinephrine. *Proc. Natl. Acad. Sci.* (2010). doi:10.1073/pnas.0909586107
590. De Deurwaerdère, P. & Di Giovanni, G. Serotonergic modulation of the activity of mesencephalic dopaminergic systems: Therapeutic implications. *Progress in Neurobiology* (2017). doi:10.1016/j.pneurobio.2016.03.004
591. Carlberg, M. & Anctil, M. Biogenic amines in coelenterates. *Comparative Biochemistry and Physiology. Part C: Comparative* (1993). doi:10.1016/0742-8413(93)90250-O
592. Winterer, G. & Weinberger, D. R. Genes, dopamine and cortical signal-to-noise ratio in schizophrenia. *Trends in Neurosciences* (2004). doi:10.1016/j.tins.2004.08.002
593. Puig, M. V., Rose, J., Schmidt, R. & Freund, N. Dopamine modulation of learning and memory in the prefrontal cortex: insights from studies in primates, rodents, and birds. *Front. Neural Circuits* (2014). doi:10.3389/fncir.2014.00093

594. Kononowicz, T. & van Rijn, H. Tonic and Phasic Dopamine Fluctuations as Reflected in Beta-power Predict Interval Timing Behavior. *Procedia - Soc. Behav. Sci.* (2014). doi:10.1016/j.sbspro.2014.02.313
595. Andersson, R. H. *et al.* Neuregulin and dopamine modulation of hippocampal gamma oscillations is dependent on dopamine D4 receptors. *Proc. Natl. Acad. Sci.* (2012). doi:10.1073/pnas.1201011109
596. Andino-Pavlovsky, V. *et al.* Dopamine Modulates Delta-Gamma Phase-Amplitude Coupling in the Prefrontal Cortex of Behaving Rats. *Front. Neural Circuits* (2017). doi:10.3389/fncir.2017.00029
597. Zaldivar, D., Goense, J., Lowe, S. C., Logothetis, N. K. & Panzeri, S. Dopamine Is Signaled by Mid-frequency Oscillations and Boosts Output Layers Visual Information in Visual Cortex. *Curr. Biol.* (2018). doi:10.1016/j.cub.2017.12.006
598. Degos, B., Deniau, J. M., Chavez, M. & Maurice, N. Chronic but not acute dopaminergic transmission interruption promotes a progressive increase in cortical beta frequency synchronization: Relationships to vigilance state and akinesia. *Cereb. Cortex* (2009). doi:10.1093/cercor/bhn199
599. Sharott, A. *et al.* Dopamine depletion increases the power and coherence of β-oscillations in the cerebral cortex and subthalamic nucleus of the awake rat. *Eur. J. Neurosci.* (2005). doi:10.1111/j.1460-9568.2005.03973.x
600. Mallet, N. *et al.* Disrupted Dopamine Transmission and the Emergence of Exaggerated Beta Oscillations in Subthalamic Nucleus and Cerebral Cortex. *J. Neurosci.* (2008). doi:10.1523/JNEUROSCI.0123-08.2008
601. Delaville, C., Navailles, S. & Benazzouz, A. Effects of noradrenaline and serotonin depletions on the neuronal activity of globus pallidus and substantia nigra pars reticulata in experimental parkinsonism. *Neuroscience* 202, 424-33 (2012). doi:10.1016/j.neuroscience.2011.11.024
602. Koppel, I. *et al.* Dopamine cross-reacts with adrenoreceptors in cortical astrocytes to induce BDNF expression, CREB signaling and morphological transformation. *Glia* 66, 206-216 (2018). doi:10.1002/glia.23238
603. Duffy, A. M. *et al.* Acetylcholine α7 nicotinic and dopamine D2 receptors are targeted to many of the same postsynaptic dendrites and astrocytes in the rodent prefrontal cortex. *Synapse* 65, 1350-1367 (2011). doi:10.1002/syn.20977
604. Vitalis, T., Cases, O., Passemard, S., Callebert, J. & Parnavelas, J. G. Embryonic depletion of serotonin affects cortical development. *Eur. J. Neurosci.* (2007). doi:10.1111/j.1460-9568.2007.05661.x
605. Carr, G. V. & Lucki, I. The role of serotonin receptor subtypes in treating depression: A review of animal studies. *Psychopharmacology* (2011). doi:10.1007/s00213-010-2097-z
606. Winstanley, C. A., Theobald, D. E. H., Dalley, J. W., Glennon, J. C. & Robbins, T. W. 5-HT2Aand 5-HT2Creceptor antagonists have opposing effects on a measure of impulsivity: Interactions with global 5-HT depletion. *Psychopharmacology (Berl).* 176, 376-85 (2004). doi:10.1007/s00213-004-1884-9
607. Scholes, K. E. *et al.* Acute serotonin and dopamine depletion improves attentional control: Findings from the Stroop task. *Neuropsychopharmacology* 32, 1600-10 (2007). doi:10.1038/sj.npp.1301262
608. El Oussini H, Scekic-Zahirovic J, Vercruysse P, Marques C, Dirrig-Grosch S, Dieterlé S, Picchiarelli G, Sinniger J, Rouaux C, D. L. Degeneration of serotonin neurons triggers

spasticity in amyotrophic lateral sclerosis. *Ann Neurol.* 82, 444–456 (2017).
609. Clarke, H. F., Dalley, J. W., Crofts, H. S., Robbins, T. W. & Roberts, A. C. Cognitive Inflexibility after Prefrontal Serotonin Depletion. *Science* 304, 878-80 (2004). doi:10.1126/science.1094987
610. Puig, M. V., Watakabe, A., Ushimaru, M., Yamamori, T. & Kawaguchi, Y. Serotonin Modulates Fast-Spiking Interneuron and Synchronous Activity in the Rat Prefrontal Cortex through 5-HT1A and 5-HT2A Receptors. *J. Neurosci.* 30, 2211-22 (2010). doi:10.1523/JNEUROSCI.3335-09.2010
611. Masson, J., Emerit, M. B., Hamon, M. & Darmon, M. Serotonergic signaling: Multiple effectors and pleiotropic effects. *Wiley Interdiscip. Rev. Membr. Transp. Signal.* (2012). doi:10.1002/wmts.50
612. Jalonen, T. O. *et al.* Serotonin induces inward potassium and calcium currents in rat cortical astrocytes. *Brain Res.* (1997). doi:10.1016/S0006-8993(97)00163-7
613. Séguéla, P., Watkins, K. C., Geffard, M. & Descarries, L. Noradrenaline axon terminals in adult rat neocortex: An immunocytochemical analysis in serial thin sections. *Neuroscience* (1990). doi:10.1016/0306-4522(90)90079-J
614. Aston-Jones G, B. F., Aston-Jones, G. & Bloom, F. E. Norepinephrine-containing locus coeruleus neurons in behaving rats exhibit pronounced responses to non-noxious environmental stimuli. *J. Neurosci.* (1981). doi:10.1523/jneurosci.4553-14.2015
615. Aston-Jones, G. & Cohen, J. D. An integrative theory of locus coeruleus-norepinephrine function: Adaptive Gain and Optimal Performance. *Annu. Rev. Neurosci.* (2005). doi:10.1146/annurev.neuro.28.061604.135709
616. Diering, G. H. *et al.* Homer1a drives homeostatic scaling-down of excitatory synapses during sleep. *Science* 355, 511-515 (2017). doi:10.1126/science.aai8355
617. Krishnan, G. P. *et al.* Cellular and neurochemical basis of sleep stages in the thalamocortical network. *Elife* (2016). doi:10.7554/eLife.18607
618. Walling, S. G., Brown, R. A. M., Milway, J. S., Earle, A. G. & Harley, C. W. Selective tuning of hippocampal oscillations by phasic locus coeruleus activation in awake male rats. *Hippocampus* (2011). doi:10.1002/hipo.20816
619. Haggerty, D. C., Glykos, V., Adams, N. E. & LeBeau, F. E. N. Bidirectional modulation of hippocampal gamma (20-80Hz) frequency activity in vitro via alpha(α)- and beta(β)-adrenergic receptors (AR). *Neuroscience* (2013). doi:10.1016/j.neuroscience.2013.08.028
620. Neves, R. M., van Keulen, S., Yang, M., Logothetis, N. K. & Eschenko, O. Locus Coeruleus phasic discharge is essential for stimulus-induced gamma oscillations in the prefrontal cortex. *J. Neurophysiol.* (2017). doi:10.1152/jn.00552.2017
621. Gao, V. *et al.* Astrocytic β_2-adrenergic receptors mediate hippocampal long-term memory consolidation. *Proc. Natl. Acad. Sci.* (2016). doi:10.1073/pnas.1605063113
622. Paukert, M. *et al.* Norepinephrine controls astroglial responsiveness to local circuit activity. *Neuron* 82, 1263-70 (2014). doi:10.1016/j.neuron.2014.04.038
623. Dunwiddie, T. Long-term increases in excitability in the CA1 region of rat hippocampus induced by beta-adrenergic stimulation: possible mediation by cAMP. *J. Neurosci.* 12, 506-17 (1992). doi:10.1016/j.ijhydene.2016.07.117
624. Gray, R. & Johnston, D. Noradrenaline and β-adrenoceptor agonists increase activity of voltage-dependent calcium channels in hippocampal neurons. *Nature* (1987). doi:10.1038/327620a0

625. Zha, X. & Xu, X. Dissecting the hypothalamic pathways that underlie innate behaviors. *Neurosci. Bull.* (2015). doi:10.1007/s12264-015-1564-2
626. Chen, Q. *et al.* Histamine Enhances Theta-Coupled Spiking and Gamma Oscillations in the Medial Entorhinal Cortex Consistent With Successful Spatial Recognition. *Cereb. Cortex* 28, 2439-2457 (2017). doi:10.1093/cercor/bhx145
627. Do-Ha, D., Buskila, Y. & Ooi, L. Impairments in Motor Neurons, Interneurons and Astrocytes Contribute to Hyperexcitability in ALS: Underlying Mechanisms and Paths to Therapy. *Molecular Neurobiology* (2018). doi:10.1007/s12035-017-0392-y
628. Bindocci, E. *et al.* Neuroscience: Three-dimensional Ca^{2+} imaging advances understanding of astrocyte biology. *Science* (2017). doi:10.1126/science.aai8185
629. Kvitsiani, D. *et al.* Distinct behavioural and network correlates of two interneuron types in prefrontal cortex. *Nature* (2013). doi:10.1038/nature12176
630. Roux, L., Stark, E., Sjulson, L. & Buzsáki, G. In vivo optogenetic identification and manipulation of GABAergic interneuron subtypes. *Current Opinion in Neurobiology* 26, 88-95 (2014). doi:10.1016/j.conb.2013.12.013
631. Osakada, F. *et al.* New rabies virus variants for monitoring and manipulating activity and gene expression in defined neural circuits. *Neuron* 71, 617-31 (2011). doi:10.1016/j.neuron.2011.07.005
632. Ahmed, M. R. *et al.* Overexpression of GRK6 rescues l-DOPA-induced signaling abnormalities in the dopamine-depleted striatum of hemiparkinsonian rats. *Exp. Neurol.* 266, 42-54 (2015). doi:10.1016/j.expneurol.2015.02.008
633. Nozawa, D. *et al.* GATA2-dependent and region-specific regulation of Gata2 transcription in the mouse midbrain. *Genes to Cells* (2009). doi:10.1111/j.1365-2443.2009.01289.x
634. Brown, R. E. *et al.* Convergent excitation of dorsal raphe serotonin neurons by multiple arousal systems (orexin/hypocretin, histamine and noradrenaline). *J. Neurosci.* (2002). doi:22/20/8850 [pii]
635. Maurer, S. V. & Williams, C. L. The cholinergic system modulates memory and hippocampal plasticity via its interactions with non-neuronal cells. *Frontiers in Immunology* (2017). doi:10.3389/fimmu.2017.01489
636. Menichella, D. M. *et al.* Genetic and Physiological Evidence That Oligodendrocyte Gap Junctions Contribute to Spatial Buffering of Potassium Released during Neuronal Activity. *J. Neurosci.* (2006). doi:10.1523/JNEUROSCI.0304-06.2006
637. Frank, M. J., Santamaria, A., O'Reilly, R. C. & Willcutt, E. Testing computational models of dopamine and noradrenaline dysfunction in attention deficit/hyperactivity disorder. *Neuropsychopharmacology* (2007). doi:10.1038/sj.npp.1301278
638. Shouno, O., Tachibana, Y., Nambu, A. & Doya, K. Computational Model of Recurrent Subthalamo-Pallidal Circuit for Generation of Parkinsonian Oscillations. *Front. Neuroanat.* 11, 21 (2017). doi:10.3389/fnana.2017.00021
639. Nielsen, S. *et al.* Specialized membrane domains for water transport in glial cells: high-resolution immunogold cytochemistry of aquaporin-4 in rat brain. *J. Neurosci.* (1997). doi:10.1523/JNEUROSCI.3404-07.2007
640. Nagelhus, E. a *et al.* Aquaporin-4 water channel protein in the rat retina and optic nerve: polarized expression in Müller cells and fibrous astrocytes. *J. Neurosci.* (1998). doi:10.1523/JNEUROSCI.18-07-02506.1998
641. Nagelhus, E. A. *et al.* Immunogold evidence suggests that coupling of K^+ siphoning and water transport in rat retinal Muller cells is mediated by a coenrichment of Kir4.1 and

AQP4 in specific membrane domains. *Glia* (1999). doi:10.1002/(SICI)1098-1136(199903)26:1<47::AID-GLIA5>3.0.CO;2-5
642. Strohschein, S. *et al.* Impact of aquaporin-4 channels on K^+ buffering and gap junction coupling in the hippocampus. *Glia* 59, 973-80 (2011). doi:10.1002/glia.21169
643. Binder, D. K., Yao, X., Verkman, A. S. & Manley, G. T. Increased seizure duration in mice lacking aquaporin-4 water channels. *Acta Neurochir. Suppl.* (2006). doi:10.1007/3-211-30714-1-80
644. Amiry-Moghaddam, M. *et al.* Delayed K^+ clearance associated with aquaporin-4 mislocalization: Phenotypic defects in brains of α-syntrophin-null mice. *Proc. Natl. Acad. Sci.* 100, 13615-20 (2003). doi:10.1073/pnas.2336064100
645. Olsen, M. L., Higashimori, H., Campbell, S. L., Hablitz, J. J. & Sontheimer, H. Functional expression of Kir4.1 channels in spinal cord astrocytes. *Glia* 53, 516-28 (2006). doi:10.1002/glia.20312
646. Hibino, H., Fujita, A., Iwai, K., Yamada, M. & Kurachi, Y. Differential assembly of inwardly rectifying K^+ channel subunits, Kir4.1 and Kir5.1, in brain astrocytes. *J. Biol. Chem.* (2004). doi:10.1074/jbc.M405985200
647. Kofuji, P. *et al.* Kir potassium channel subunit expression in retinal glial cells: implications for spatial potassium buffering. *Glia* (2002). doi:10.1002/glia.10112
648. Orkand, R. K. Extracellular potassium accumulation in the nervous system. *Fed Proc* 39, 1515–1518 (1980).
649. Schröder, W., Seifert, G., Hüttmann, K., Hinterkeuser, S. & Steinhäuser, C. AMPA receptor-mediated modulation of inward rectifier K^+ channels in astrocytes of mouse hippocampus. *Mol. Cell. Neurosci.* (2002). doi:10.1006/mcne.2001.1080
650. Prüss, H., Derst, C., Lommel, R. & Veh, R. W. Differential distribution of individual subunits of strongly inwardly rectifying potassium channels (Kir2 family) in rat brain. *Mol. Brain Res.* (2005). doi:10.1016/j.molbrainres.2005.05.006
651. Ishii, M. *et al.* Differential expression and distribution of Kir5.1 and Kir4.1 inwardly rectifying K^+ channels in retina. *Am. J. Physiol. Cell Physiol.* 285, C260-7 (2003). doi:10.1152/ajpcell.00560.2002
652. Brasko, C., Hawkins, V., De La Rocha, I. C. & Butt, A. M. Expression of Kir4.1 and Kir5.1 inwardly rectifying potassium channels in oligodendrocytes, the myelinating cells of the CNS. *Brain Struct. Funct.* (2017). doi:10.1007/s00429-016-1199-8
653. Thomzig, A. *et al.* Kir6.1 is the principal pore-forming subunit of astrocyte but not neuronal plasma membrane K-ATP channels. *Mol. Cell. Neurosci.* (2001). doi:10.1006/mcne.2001.1048
654. Skatchkov, S. N. *et al.* Kir subfamily in frog retina: Specific spatial distribution of Kir 6.1 in glial (Müller) cells. *Neuroreport* (2001). doi:10.1097/00001756-200105250-00028
655. Scemes, E., Suadicani, S. O. & Spray, D. C. Intercellular communication in spinal cord astrocytes: fine tuning between gap junctions and P2 nucleotide receptors in calcium wave propagation. *J. Neurosci.* (2000). doi:10.1038/jid.2014.371
656. Nagy, J. I., Ionescu, A. V., Lynn, B. D. & Rash, J. E. Connexin29 and connexin32 at oligodendrocyte and astrocyte gap junctions and in myelin of the mouse central nervous system. *J. Comp. Neurol.* (2003). doi:10.1002/cne.10797
657. Zahs, K. R., Kofuji, P., Meier, C. & Dermietzel, R. Connexin immunoreactivity in glial cells of the rat retina. *J. Comp. Neurol.* (2003). doi:10.1002/cne.10524

658. Tanaka, M. *et al.* Connexin43 and Bergmann glial gap junctions in cerebellar function. *Front. Neurosci.* 2, 225-233 (2008). doi:10.3389/neuro.01.038.2008
659. Rouach, N. *et al.* Gap junctions and connexin expression in the normal and pathological central nervous system. *Biol. Cell* (2002). doi:10.1016/S0248-4900(02)00016-3
660. Hofer, A. & Dermietzel, R. Visualization and functional blocking of gap junction hemichannels (connexons) with antibodies against external loop domains in astrocytes. *Glia* (1998). doi:10.1002/(SICI)1098-1136(199809)24:1<141::AID-GLIA13>3.0.CO;2-R
661. Nagy, J. I., Dudek, F. E. & Rash, J. E. Update on connexins and gap junctions in neurons and glia in the mammalian nervous system. in *Brain Research Reviews* (2004). doi:10.1016/j.brainresrev.2004.05.005
662. Martín-Vasallo, P. *et al.* Oligodendrocytes in brain and optic nerve express the β3 subunit isoform of Na,K-ATPase. *Glia* (2000). doi:10.1002/1098-1136(200009)31:3<206::AID-GLIA20>3.0.CO;2-1
663. Peng, L., Martín-Vasallo, P. & Sweadner, K. J. Isoforms of Na,K-ATPase alpha and beta subunits in the rat cerebellum and in granule cell cultures. *J. Neurosci.* (1997). doi:0270-6474/97/173488-15$05.00/0
664. Crambert, G. & Geering, K. FXYD Proteins: New Tissue-Specific Regulators of the Ubiquitous Na,K-ATPase. *Sci. Signal.* (2003). doi:10.1126/stke.2003.166.re1
665. Su, G., Haworth, R. a, Dempsey, R. J. & Sun, D. Regulation of Na^+-K^+-Cl^- cotransporter in primary astrocytes by dibutyryl cAMP and high $[K^+]_o$. *Am. J. Physiol. Cell Physiol.* 279, C1710-21 (2000).
666. Wang, H., Yan, Y., Kintner, D. B., Lytle, C. & Sun, D. GABA-mediated trophic effect on oligodendrocytes requires Na-K-2Cl cotransport activity. *J. Neurophysiol.* (2003). doi:10.1152/jn.01174.2002
667. Kanaka, C. *et al.* The differential expression patterns of messenger RNAs encoding K-Cl cotransporters (KCC1,2) and Na-K-2Cl cotransporter (NKCC1) in the rat nervous system. *Neuroscience* (2001). doi:10.1016/S0306-4522(01)00149-X
668. Dzhala, V. I. *et al.* NKCC1 transporter facilitates seizures in the developing brain. *Nat. Med.* (2005). doi:10.1038/nm1301

APPENDIX: Tables

K^+ electrode	Stimulus	Amplitude (mM)	#Rise time (sec)	#Decay time (sec)
Single-barrelled	30 mM KCl	4.23±0.92	4.27±0.48	30.7±2.85
	15 mM KCl	3.03±1.03	3.44±0.92	24.8±12.4
Double-barrelled (1 µm)	30 mM KCl	8.34±0.33	1.37±0.18	26.3±4.01
	15 mM KCl	4.59±0.66	2.00±0.12	22.0±7.54
Double-barrelled (1 µm)*	30 mM KCl	15.3±1.05	0.28±0.01	3.08±0.13
	15 mM KCl	6.67±0.81	0.22±0.01	2.45±0.13
Double-barrelled (3 µm)	30 mM KCl	6.12±0.74	3.49±0.28	51.4±4.78
	15 mM KCl	4.42±0.87	4.22±0.53	34.8±7.36

Table 1. Measurement of different properties of K^+ transients with different types of K^+-selective microelectrodes under normal physiological conditions. Data is reported as mean ± S.E.M. #20-80 % rise time, 80-20 % decay time. **Double-barrelled K^+-selective microelectrode with 1 µm tips after optimization*

$[K^+]_o$	Condition	Clearance rate (mM/sec)	Amplitude (mM)	#Rise time (sec)	#Peak area (mMxsec)
30 mM	aCSF	2.02±0.14	9.19±0.65	0.40±0.03	1.91±0.10
	$BaCl_2$	0.66±0.07	9.00±0.69	0.40±0.03	2.51±0.13
	Gap-26/27	0.71±0.08	9.16±0.74	0.41±0.03	2.21±0.14
15 mM	aCSF	1.09±0.09	4.38±0.34	0.34±0.02	1.01±0.05
	$BaCl_2$	0.71±0.04	4.45±0.34	0.36±0.01	1.42±0.09
	Gap-26/27	0.81±0.08	4.45±0.44	0.36±0.03	1.18±0.08
5 mM	aCSF	0.56±0.05	1.38±0.11	0.27±0.01	0.30±0.02
	$BaCl_2$	0.28±0.01	1.32±0.13	0.29±0.02	0.37±0.02
	Gap-26/27	0.49±0.05	1.34±0.09	0.28±0.02	0.28±0.02

Table 2. The impact of altered astrocytic K^+ clearance on the K^+ clearance rate. Data is reported as mean ± S.E.M. #10-90 % rise time, top 10 % peak area.

Component	Cellular expression	Active $[K^+]_o$	K^+ clearance mechanism	Brain area
AQP-4 channel	Astrocyte[639] Ependymal cell[639] Müller cell[640,641]	Low and High $[K^+]_o$[642]	Net K^+ uptake[642,643] K^+ spatial buffering[639,644] K^+ siphoning[641]	Cerebellum[639] Supraoptic nucleus[639] Thalamus[639] Retina[640,641] Neocortex[639,643] Hippocampus[644]
K_{ir} channels: **K_{ir}4.1** ***ATP-dependent***	Astrocyte[347,348,645,646] Müller cell[641,647] Oligodendrocyte[530] Bergmann cell[530]	Low, High and Excessive $[K^+]_o$[530,647,648]	Net K^+ uptake[530] K^+ spatial buffering[648] K^+ siphoning[641,647]	Retina[641,647] Hippocampus[347, 646] Neocortex[348] Spinal cord[645] Olfactory bulb[646] Thalamus[646]
K_{ir}2.1 ***Classical inwardly rectifying***	Astrocyte[649] Müller cell[647] Oligodendrocyte[530] Bergmann cell[530] Neuron[530,650]	Low, High and Excessive $[K^+]_o$[530,647,648]	Net K^+ uptake[647,530] K^+ siphoning[647]	Hippocampus[649] Retina[647] Cerebellum[530] Neocortex[650] Olfactory bulb[650] Thalamus[650] Basal ganglia[650]
K_{ir}5.1 ***Other***	Astrocyte[646] Müller cell[651] Oligodendrocyte[652]	Low, High and Excessive $[K^+]_o$[530,647,648]	Net K^+ uptake[530] K^+ siphoning[651]	Retina[651] Neocortex[646] Olfactory bulb[646]
K_{ir}6.1 ***ATP-sensitive***	Astrocyte[530,653] Müller cell[654] Oligodendrocyte[530] Bergmann cell[653] Neuron[530]	High and Excessive $[K^+]_o$[653]	K^+ spatial buffering[653]	Hippocampus[653] Neocortex[653] Cerebellum[653] Retina[654]
Gap junctions: **Cx43**	Astrocyte[531,567,655,656] Müller cell[657] Bergmann cell[658] Ependymal cell[659]	High and Excessive $[K^+]_o$[531, 532]	K^+ spatial buffering[531]	Hippocampus[531,532] Neocortex[567] Cerebellum[658,660] Spinal cord[655] Brain stem[378] Hypothalamus[378,656] Retina[657] Thalamus[656]
Cx30	Astrocyte[531,567,655,656]	High and Excessive$[K^+]_o$ [531, 532]	K^+ spatial buffering[531]	Hippocampus[531,532] Neocortex[567,656] Spinal cord[655]
Cx47 ***OCx47:ACx43***	Oligodendrocyte[636, 656,661]	High and Excessive $[K^+]_o$[636]	K^+ spatial buffering[636]	Spinal cord[636,661] Neocortex[661] Hippocampus[661] Cerebellum[661] Brainstem[661]
Cx32 ***OCx32:ACx30***	Oligodendrocyte[636, 656,659] Neuron[659]	High and Excessive $[K^+]_o$[636]	K^+ spatial buffering[636]	Neocortex[656] Hypothalamus[656] Thalamus[656] Spinal cord[636]

NKA pump	Astrocyte[452,498] Müller cell[262] Oligodendrocyte[662] Bergmann cell[663] Neuron[664]	Low and High $[K^+]_o$[452,529,498]	Net K^+ uptake [262, 452,498,529] K^+ siphoning[262]	Neocortex[498,662] Spinal cord[498] Hippocampus[452] Retina[262] Cerebellum[663]
NKCC1 cotransporter	Astrocyte[345,452,665] Oligodendrocyte[666] Bergmann cell[667] Neuron[668]	High $[K^+]_o$[345,452, 529,665]	Net K^+ uptake[345,452, 529,665]	Neocortex[345,665,668] Hippocampus[452] Spinal cord[666] Cerebellum[667]

Table 3. The differential involvement of distinct astrocytic channels, pumps and cotransporters in K^+ clearance mechanisms depending on $[K^+]_o$. Low $[K^+]_o$ refers to <5 mM, High $[K^+]_o$ refers to 5-12 mM, Excessive $[K^+]_o$ refers to >12 mM.

Time (min)	Area	R_{in} (MΩ)	RMP (mV)	#Coupled	X/Y ratio
30	S1	32.2±8.9	-76.6±1.5	56.0±6.1	1.8±0.2
12	S1	14.9±3.0	-76.6±1.7	19.8±1.8	1.4±0.1
30	M1	64.4±7.3	-78.6±1.5	32.1±2.7	1.0±0.1
12	M1	36.8±8.9	-72.8±1.1	11.4±1.9	0.9±0.1

Table 4. Astrocytic networks differ between cortical areas under normal physiological conditions. Data is reported as mean ± S.E.M. #Number of biocytin-coupled astrocytes. *R_{in}, input resistance; RMP, resting membrane potential*

Appendix: Figures

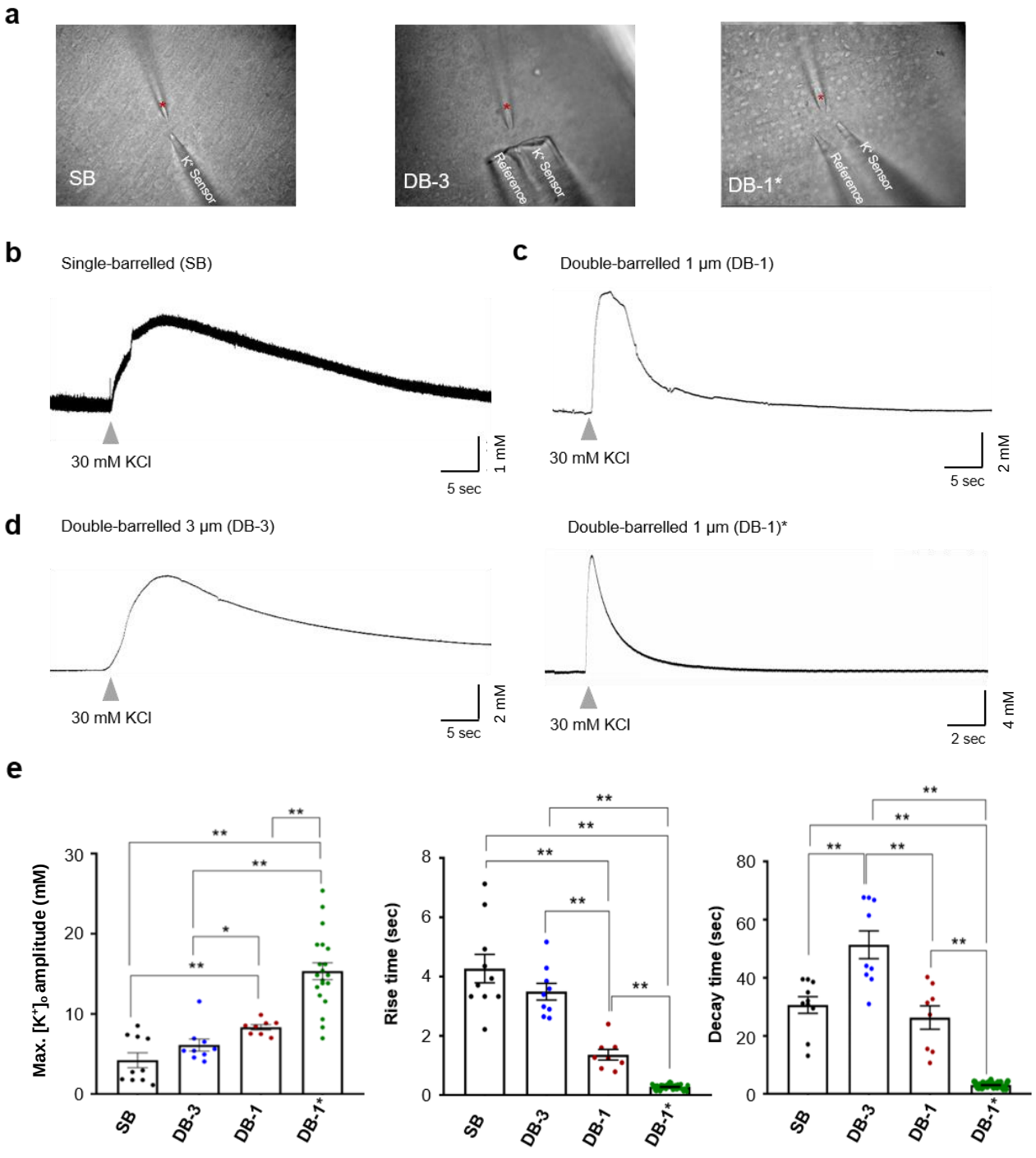

Figure 1. Comparison between different types of K^+-selective microelectrode measurements in cortical slices.

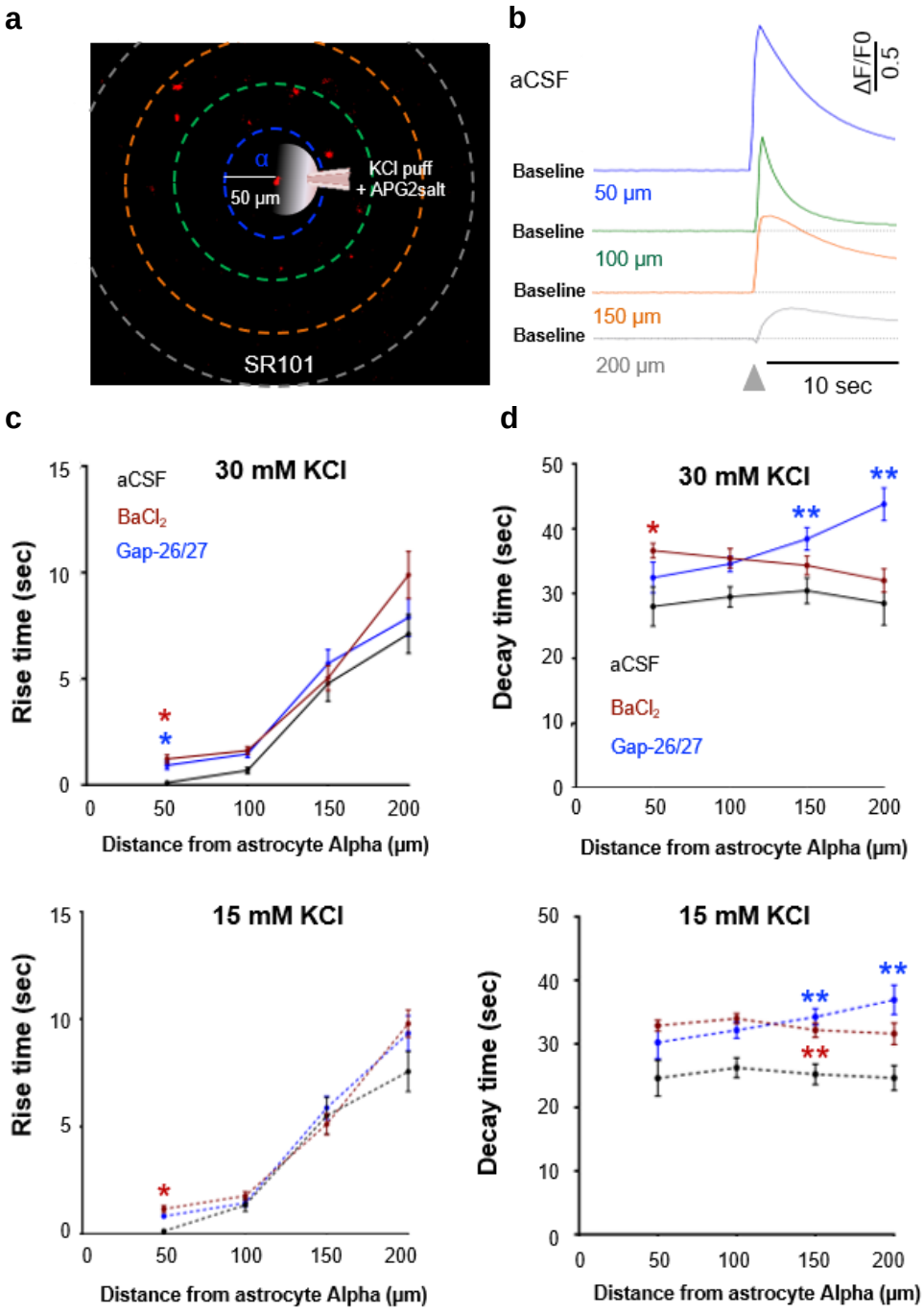

Figure 2. Imaging $[K^+]_o$ dynamics.

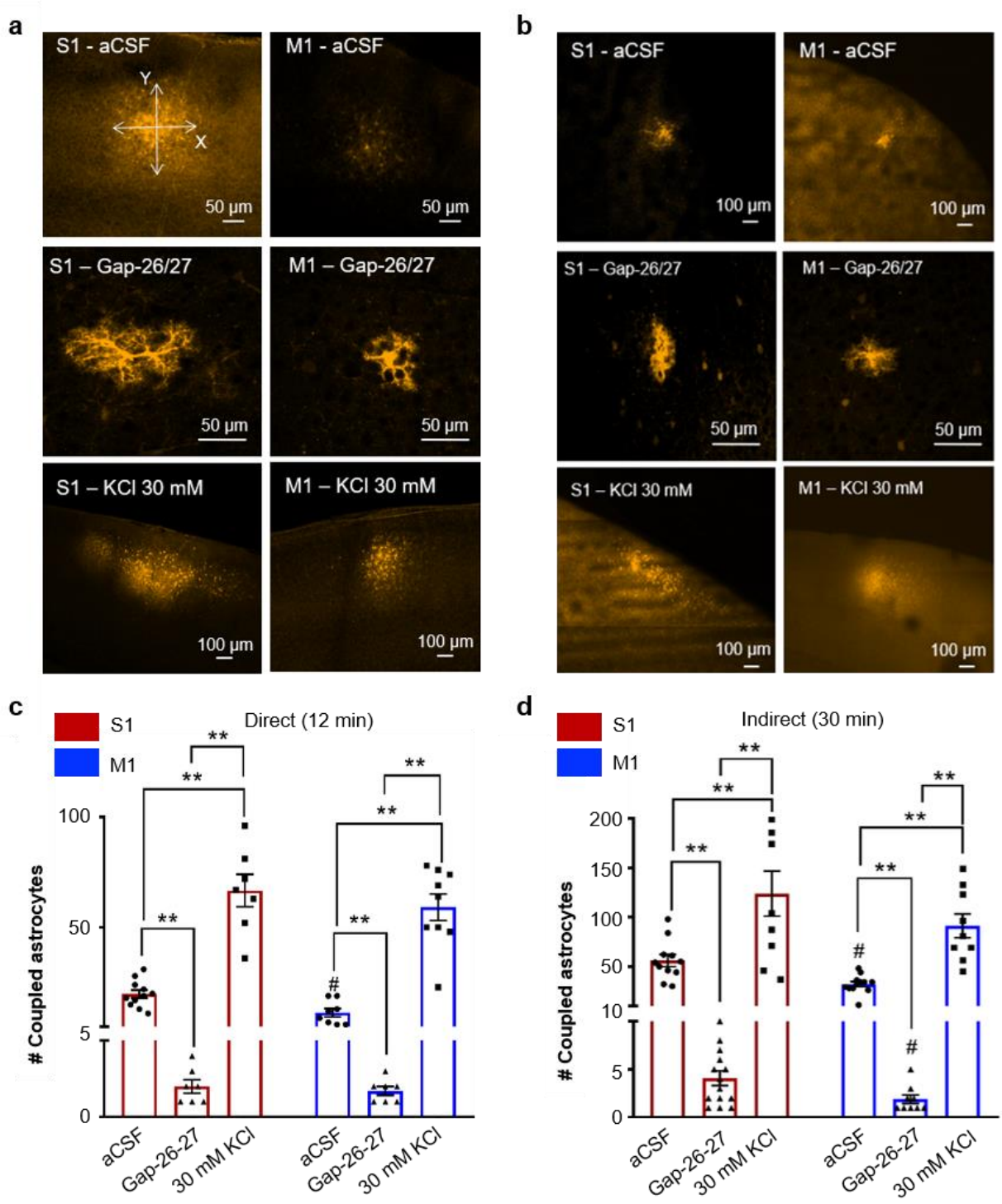

Figure 3. Astrocytes from the motor cortex form smaller networks compared to astrocytes from the somatosensory cortex.

Appendix: Figure legends

Figure 1. Comparison between different types of K^+-selective microelectrode measurements in cortical slices. a) DIC images showing the experimental setup for $[K^+]_o$ recordings using single-barrelled K^+-selective microelectrodes (SB, left), double-barrelled K^+-selective microelectrodes with 3 µm tips (DB-3, middle) and optimized double-barrelled K^+-selective microelectrodes with 1 µm tips (DB-1*, right) following KCl puffs (red asterisk). b-d) Sample traces of $[K^+]_o$ recordings depicting changes in the K^+ clearance time course recorded with SB microelectrodes (b), DB-1 microelectrodes (c) before (top) and after (bottom) optimization, and DB-3 microelectrodes (d), following local application of 30 mM KCl (indicated by arrow) under normal aCSF conditions. e) Quantitative analysis of the impact of local application of 30 mM KCl puffs on the K^+ transients' amplitude (in mM, left), 20-80 % rise time (in seconds, middle) and 80-20 % decay time (in seconds, right), recorded with SB (black; n=10 recordings), DB-3 (blue; n=9 recordings), DB-1 (red; n=8 recordings) and DB-1* (green; n=30 recordings) microelectrodes under normal aCSF conditions. Note the faster rise and decay times recorded with DB-1* microelectrodes after optimization compared to suboptimal electrodes. Data is reported as mean ± SEM. **p < 0.05; **p < 0.01; unpaired student t-test*

Figure 2. Imaging $[K^+]_o$ dynamics. a) Fluorescence image showing SR101 stained astrocytes. Puffs containing KCl at various concentrations and APG-2 salt are applied close to "astrocyte Alpha" (blue), defined as distance 0 µm. b) Sample traces of K^+ transients imaged with APG-2 salt fluorescent dye in the extracellular space showing changes from baseline ΔF/F0 fluorescence levels following local application of 30 mM KCl puffs (arrow) under normal aCSF conditions at various distances (colour-coded in a). c-d) Quantitative analysis of the impact of 30 mM (top, continuous line) and 15 mM (bottom, dashed line) KCl puffs on the K^+ transients' rise time (c) and decay time (d) under normal aCSF (30 mM, n=8 recordings; 15 mM, n=9 recordings), 100 µM $BaCl_2$ (30 mM, n=10 recordings; 15 mM, n=8 recordings) and Gap-26/27 (30 mM, n=10 recordings; 15 mM, n=9 recordings) conditions. Data is reported as mean ± SEM. **p < 0.05; **p < 0.0001; two-way ANOVA*

Figure 3. Astrocytes from the motor cortex form smaller networks compared to astrocytes from the somatosensory cortex. a-b) Confocal images (20x objective top, bottom; 40x objective middle) showing direct (12 minutes, a) or indirect (30 minutes, b) networks of biocytin-stained astrocytes in layer II/III of the somatosensory (S1, left) or motor (M1, right) cortices under normal aCSF (top), Gap-26/27 (middle) or following local application of 30 mM KCl (bottom) conditions. Top left inset – arrows indicate y and x axis to measure X/Y ratios. c-d) Astrocytes loaded for 12 min (c; S1 – aCSF n=11, Gap-26/27 n=7, 30 mM KCl n=7; M1 – aCSF n=8, Gap-26/27 n=7, 30 KCl mM n=9) and 30 min (d; S1 – aCSF n=11, Gap-26/27 n=14, 30 mM KCl n=9; M1 – aCSF n=12, Gap-26/27 n=9, 30 mM KCl n=9) from M1 (blue) are less connected compared to astrocytes from S1 (red) in normal aCSF. Astrocytic coupling is significantly reduced after incubation with Gap-26/27 (middle) and increased after local application of 30 mM KCl (bottom) in both S1 (red) and M1 (blue) cortical areas. Data is reported as mean ± SEM. Asterisks represent significance levels between different conditions within the same area (S1 or M1). Pound signs represent significance levels between different areas (S1 *vs* M1) at the same condition. *#p < 0.01; **p < 0.01; unpaired student t-test*